Neuronally Derived Extracellular Vesicles as Biomarkers for Parkinson's Disease



Shijun Yan

Christ Church College

Nuffield Department of Clinical Neurosciences

University of Oxford

A thesis submitted for the degree of

Doctor of Philosophy in Clinical Neurosciences

Trinity 2025

Declaration

This thesis is the result of my own work, except where explicitly stated otherwise. It includes material adapted from three co-first-authored publications, as listed in Section 9.1, and a manuscript currently under review. It incorporates modified excerpts and figures from manuscripts published during the course of my DPhil in Open Access journals. Where required, permissions from co-authors and publishers were obtained.

I confirm that I am the primary contributor to the design, execution, analysis, and interpretation of the experimental work presented, and that I authored all reproduced text and figures. Collaborative contributions are clearly acknowledged in the relevant chapters. No part of this thesis has been submitted for any other degree at the University of Oxford or elsewhere. Full citations are provided in the respective chapter footnotes, and original publications are referenced in the bibliography.

Acknowledgement

I would like to express my heartfelt gratitude to all those who have supported me throughout my doctoral journey. First and foremost, I am deeply thankful to my supervisor, Professor George Tofaris. His constant support, high standards, and thoughtful guidance have shaped not only the direction of my research but also my development as an independent scientist. From academic mentorship to generous support in scholarship applications, his encouragement and belief in my potential have meant a great deal to me. I am especially grateful for his dedication and commitment throughout this challenging yet rewarding period.

I would also like to thank the members of the Tofaris Lab for fostering such a supportive and friendly environment. In particular, I am sincerely grateful to Dr. Cheng Jiang, who mentored me closely in the early stages of my DPhil. His practical training and thoughtful advice helped shape my approach to research. My thanks also go to Drs. Anis Sahoo and Suman Dutta for their invaluable help with experiments and many stimulating discussions, as well as to all past and present lab members for their camaraderie and support.

I gratefully acknowledge the financial support from the Weston Foundation, the Goodger and Schorstein Scholarships awarded by the Medical Sciences Division, University of Oxford, and the Chinese Government Award for Outstanding Self-financed Students Abroad from the China Scholarship Council. Their generous support enabled me to fully dedicate myself to my research.

I would also like to thank Professor Jason Davis for his role as my co-supervisor and for our collaboration. My sincere thanks go to the clinical collaborators and institutions whose contributions were vital to this work. I am particularly thankful to Professor Michele Hu from University of Oxford; Dr. Tanja Zerenner from University of Bristol; Wenjing Zhang from The Chinese University of Hong Kong, Shenzhen; Dr. Bowen Shu and Xinying Li from Southern

Medical University; Dr. Michael Sommerauer and Aline Seger from the University of Cologne, Professor Wolfgang Oertel and Janzen Annette from Philipps-University Marburg, as well as the team at the Parkinson's Progression Markers Initiative. I am also deeply grateful to all the clinicians and nurses involved in sample collection and patient assessments, and above all, to the individuals who generously donated their samples for research, this work would not have been possible without you.

On a personal note, I owe my deepest thanks to my family for their unconditional love, encouragement, and support throughout this long journey. I am especially grateful to my mother, whose strength, patience, and unwavering faith in me have been a guiding force through every challenge. My heartfelt thanks also go to my dear friends Dmitry Zenko and Jade Marsh, whose kindness, humour, and friendship have made the difficult times easier.

This thesis is the result of the generosity, support, and shared commitment of many people. I am deeply indebted to everyone who has contributed to making this DPhil journey a rich experience filled with growth, challenges, and enduring relationships. I shall always carry their support with gratitude for years to come. Thank you all.

Abstract

Neuronally Derived Extracellular Vesicles as Biomarkers for Parkinson's Disease

Shijun Yan, Christ Church College, Doctor of Philosophy, Trinity 2025

Parkinson's disease (PD) is a neurodegenerative disorder with a prolonged prodromal phase, often marked by non-motor symptoms such as isolated rapid eye movement sleep behaviour disorder (iRBD), which confers increased risk of phenoconversion. However, the absence of reliable biomarkers limits effective risk stratification and early pathological detection. Neuronally derived extracellular vesicles (nEVs), isolated from peripheral biofluids, offer a minimally invasive approach to accessing central nervous system pathology. Yet, variability in isolation protocols and analytical approaches has hindered their clinical applicability. This thesis investigates the potential of nEVs for the early PD detection and stratification. Methodological optimisation resolved confounders in nEV isolation, validated L1CAM-based immunocapture, and established refined protocols for α-synuclein quantification. Based on this framework, elevated serum nEV α-synuclein was demonstrated in individuals at risk of PD, and its integration with prodromal markers improved stratification precision. Complementing these findings, a novel microfluidic single-EV detection platform was developed, revealing membrane-associated α-synuclein on nEVs as an early-stage biomarker. Furthermore, non-EV proteins including serum phosphorylated tau-217 (p-tau217) and neurofilament light chain (NfL) were explored, demonstrating that p-tau217, but not NfL, is a useful biomarker of cognitive impairment in iRBD that informs phenoconversion risk. Collectively, these findings establish nEV as a multidimensional biomarker, integrating methodological standardisation with pathophysiological insights. By coupling optimised isolation protocols with targeted biomarker panels and advanced detection technologies, this thesis advances a translational diagnostic framework for PD, enabling risk profiling, early detection, and objective monitoring.

Table of Contents

1. INTRODUCTION 1

1.1 PARKINSON'S DISEASE 1

1.1.1 Epidemiology of PD 1

1.1.2 Pathology of PD 2

1.1.3 Clinical presentation of PD 5

1.1.4 Prodromal PD 7

1.1.5 Clinical diagnosis of PD 9

1.2 EXTRACELLULAR VESICLES 10

1.2.1 Biogenesis of EVs 10

1.2.2 Biological composition of EVs 13

1.2.3 Roles of EVs in the CNS 14

1.2.3.1 Neuronally derived EVs 14

1.2.3.2 EV-mediated neuron-glia communication 15

1.2.3.3 EV-mediated protein transfer 15

1.2.4 The role of EVs in PD 16

1.2.4.1 α-Synuclein transmission via EVs 16

1.2.4.2 Lysosomal dysfunction and EV trafficking 17

1.2.4.3 Potential protective functions of EVs in PD 18

1.2.4.4 Therapeutic potential of EVs in PD 19

1.2.5 EV isolation techniques 19

1.2.5.1 Differential ultracentrifugation 19

1.2.5.2 Density gradient ultracentrifugation 20

1.2.5.3 Immunoprecipitation 20

1.2.5.4 Ultrafiltration 21

1.2.5.5 Size exclusion chromatography 21

1.2.5.6 Microfluidic platforms 22

1.2.5.7 Polyethylene glycol precipitation 23

1.2.5.8 Commercial kits 23

1.3 BIOMARKERS IN PD 25

1.3.1 Biofluid-based biomarkers 26

1.3.1.1 CSF biomarkers 26

1.3.1.2 Blood-based biomarkers 27

1.3.1.3 Other biofluid and tissue biomarkers 28

1.3.2 EV-based biomarkers 29

1.3.2.1 nEV biomarkers 29
1.3.2.2 Other EV biomarkers 32
1.4 EV-BASED PROTEIN BIOMARKER DETECTION TECHNOLOGIES 33
1.4.1 Conventional immunoassays 33
1.4.2 Meso Scale Discovery 34
1.4.3 Proximity extension assay 34
1.4.4 Single-molecule array 35
1.4.5 Microfluidic platforms 36
1.4.6 Super-resolution microscopy 37
1.4.7 Nano-flow cytometry 37
1.5 THESIS AIMS AND OBJECTIVES 39
2. MATERIAL AND METHODS 39
2.1 KEY RESOURCES TABLE 39
2.2 HUMAN SAMPLES 46
2.2.1 Serum sample acquisition 46
2.2.2 Serum processing 46
2.2.3 Clinical assessments 46
2.3 EV ISOLATION 47
2.3.1 Capto Core multimodal chromatography 47
2.3.2 Ultracentrifugation 48
2.3.3 Immunocapture of EVs from serum 48
2.4 EV CHARACTERISATION 49
2.4.1 EV protein extraction 49
2.4.2 Immunoblotting 49
2.4.3 Nanoparticle tracking analysis 50
2.4.4 Transmission electron microscopy 50
2.5 PROTEIN MEASUREMENTS 51
2.6 STATISTICAL ANALYSIS 52
3. METHODOLOGICAL CONSIDERATIONS IN NEURONAL EV ISOLATION FOR α-SYNUCLEIN BIOMARKERS 55
3.1 INTRODUCTION 55
3.1.1 Limitations in blood EV-associated α-synuclein biomarkers 55
3.1.2 L1CAM and nEV biomarkers 55
3.1.3 Need for methodological standardisation 56

3.2 AIMS AND OBJECTIVES 57
3.3 MATERIAL AND METHODS 57
3.3.1 Clinical samples 57
3.3.2 Capto Core multimodal chromatography 58
3.3.3 Immunoprecipitation 58
3.3.4 Ultrafiltration 58
3.3.5 MSD electrochemiluminescence 59
3.4 RESULTS 59
3.4.1 Isolation of EVs from the bulk of human serum proteins 59
3.4.2 Association between α-synuclein and L1EVs 62
3.4.3 ATP1A3 is not detected on serum EVs 65
3.5 DISCUSSION 67
3.5.1 Isolation of EVs from serum using Capto Core multimodal chromatography 67
3.5.2 L1CAM as a marker for EV isolation 68
3.5.3 ATP1A3 is not associated with serum EVs 68
3.5.4 Limitations and future directions 69
3.5.5 Conclusion 69
3.6 SUPPLEMENTARY INFORMATION 70

4. NEURONALLY DERIVED EV α-SYNUCLEIN AS A SERUM BIOMARKER FOR INDIVIDUALS AT RISK OF DEVELOPING PD 72

4.1 INTRODUCTION 72
4.1.1 Prodromal PD and the need for early-stage biomarkers 72
4.1.2 nEV as a source of biomarkers 73
4.2 AIMS AND OBJECTIVES 73
4.3 MATERIAL AND METHODS 74
4.3.1 Study design 74
4.3.2 L1EV immunocapture and protein measurements 77
4.4 RESULTS 78
4.4.1 Demographic characteristics 78
4.4.2 α-Synuclein in serum L1EV is elevated in iRBD subjects across single-centre cohorts 81
4.4.3 Serum L1EV α-synuclein levels differentiate those with probable prodromal PD from subjects with minimal risk in a multicentre cohort 82
4.4.4 L1EV α-synuclein is increased in subjects with specific additional prodromal markers within at-risk groups and may precede dopaminergic neurodegeneration 85

4.4.5 L1EV α-synuclein differentiates those at-risk of developing PD from healthy control populations irrespective of initial diagnosis 90
4.4.6 Association of serum L1EV α-synuclein levels with CSF pathology and phenoconversion 93
4.4.7 Serum L1EV α-synuclein is increased in *LRRK2*^{G2019S} non-manifest carriers with additional prodromal markers and *LRRK2*^{G2019S} PD with CSF pathology 97
4.5 DISCUSSION 100
4.5.1 L1EV α-synuclein as a biomarker for subjects at risk of developing PD 100
4.5.2 Performance of L1EV α-synuclein in phenoconversion and subgroup stratification 101
4.5.3 Correlation of L1EV α-synuclein with CSF SAA 102
4.5.4 Potential mechanisms underlying increased L1EV α-synuclein 103
4.5.5 Limitations and future directions 104
4.5.6 Conclusion 105
4.6 SUPPLEMENTARY INFORMATION 106
5. SINGLE EV DETECTION ASSAY IDENTIFIES MEMBRANE-ASSOCIATED α-SYNUCLEIN AS AN EARLY-STAGE BIOMARKER IN PD 116
5.1 INTRODUCTION 116
5.1.1 EVs as biomarkers for PD 116
5.1.2 Microfluidic-based EV analysis 116
5.2 AIMS AND OBJECTIVES 117
5.3 MATERIAL AND METHODS 119
5.3.1 Clinical samples 119
5.3.2 Cell line cultures 119
5.3.3 Generation of human iPSC-derived midbrain dopaminergic neurons 120
5.3.4 EV isolation from serum 119
5.3.5 EV isolation from CM 122
5.3.6 Labelling of EV-bead immunocomplexes for surface marker analysis 123
5.3.7 Microfluidic chip design and fabrication 123
5.3.8 Droplet generation 124
5.3.9 Fluorescence image acquisition 125
5.3.10 Image analysis 125
5.3.11 Nano-flow cytometry 126
5.3.12 Direct Stochastic Optical Reconstruction Microscopy 126
5.3.13 MSD electrochemiluminescence 127
5.3.14 Molecular cloning and lentivirus production 128

5.3.15 Lentiviral transduction of SH-SY5Y cells and cell fractionation 128
5.3.16 Immunofluorescence staining 130
5.4 RESULTS 128
5.4.1 Development of the microfluidic digital immunoassay for single EV detection 130
5.4.2 The assay enables parallel quantification of distinct EV subpopulations 135
5.4.3 Identification of α-synuclein as a serum EV membrane-associated protein 139
5.4.4 α-Synuclein L1EV membrane-association increases under pathological conditions 143
5.4.5 Serum L1EV membrane-associated α-synuclein is increased in individuals with iRBD or PD compared to healthy controls 148
5.5 DISCUSSION 152
5.5.1 Droplet-based assay for precise multiplexed quantification of EV membrane proteins 152
5.5.2 α-Synuclein is a L1EV membrane-associated protein 153
5.5.3 α-Synuclein and L1EV membrane association increases under pathological conditions 155
5.5.4 L1EV membrane associated α-synuclein is an improved biomarker for early PD diagnostics 155
5.5.5 Limitations and future directions 156
5.5.6 Conclusion 156
5.6 SUPPLEMENTARY INFORMATION 157

6. SERUM P-TAU217 PREDICTS COGNITIVE IMPAIRMENT IN IRBD 166

6.1 INTRODUCTION 166
6.1.1 Co-pathologies and cognitive decline in iRBD 166
6.1.2 Serum NfL as a biomarker for diffuse neurodegeneration 166
6.1.3 Multimodal biomarker strategies in prodromal PD 167
6.2 AIMS AND OBJECTIVES 167
6.3 MATERIAL AND METHODS 168
6.3.1 Study design 168
6.3.2 Biomarker measurements 169
6.4 RESULTS 169
6.4.1 Demographic characteristics 169
6.4.2 Serum p-tau217 is a better predictor of cognitive and motor impairment than NfL in individuals with iRBD 172
6.4.3 Serum p-tau217 predicts phenoconversion to PD with cognitive impairment or DLB 177
6.4.4 Time to event analysis 179
6.5 DISCUSSION 180
6.5.1 Serum p-tau217 reflects early cognitive and motor changes in iRBD 180

6.5.2 Serum p-tau217 stratifies cognitive risk in iRBD 181
6.5.3 Serum NfL identifies rapidly progressive iRBD trajectories 182
6.5.4 Limitations and Future Directions 182
6.5.5 Conclusion 182
6.6 SUPPLEMENTARY INFORMATION 183

7. DISCUSSION AND CONCLUSIONS 191

7.1 SUMMARY OF KEY FINDINGS 191
7.2 BROADER IMPLICATIONS AND APPLICATIONS 192
7.3 FUTURE PROSPECTS FOR CLINICAL TRANSLATION 194
7.4 CONCLUDING REMARKS 196

8. REFERENCES 198

9. APPENDIX 216

9.1 MANUSCRIPTS ACCEPTED FOR PUBLICATION 216
9.2 ATTENDED CONFERENCES 217

List of Figures

Figure 1.1: Formation of Lewy body 4
Figure 1.2: Clinical symptoms and time course of PD progression 7
Figure 1.3: Biogenesis and structural composition of EVs 12
Figure 1.4: EVs in α-synuclein homeostasis and lysosomal dysfunction in PD 18
Figure 1.5: Schematic workflow of nEV-based diagnostics 30
Figure 3.1: Isolation of EVs from serum using Capto Core multimodal chromatography 61
Figure 3.2: α-Synuclein concentration in total EVs isolated from serum by Capto Core multimodal chromatography 62
Figure 3.3: Validation of L1CAM as a marker for EV isolation 64
Figure 3.4: Schematic of anti-L1CAM immunocapture from serum 65
Figure 3.5: ATP1A3 is not associated with serum EVs 66
Figure 4.1: Study selection criteria and design for derivation and validation groups 76
Figure 4.2: L1EV α-synuclein levels across batches 77
Figure 4.3: Correlation between L1EV α-synuclein and age 78
Figure 4.4: L1EV α-synuclein levels in the derivation and validation groups 84
Figure 4.5: L1EV α-synuclein measurements in *GBA1*^{N409S} gene carriers 87
Figure 4.6: L1EV α-synuclein measurements in at-risk subjects with available DaT SPECT 89
Figure 4.7: L1EV α-synuclein levels are increased in at-risk individuals with positive LR of developing PD 93
Figure 4.8: L1EV α-synuclein levels and CSF SAA or phenoconversion 95
Figure 4.9: Kaplan-Meier survival curves for phenoconversion to PD or DLB as stratified by L1EV α-synuclein 96
Figure 4.10: Correlation between serum L1EV α-synuclein and CSF total α-synuclein 97
Figure 4.11: L1EV α-synuclein measurements in *LRRK2*^{G2019S} non-manifest gene carriers and *LRRK2*^{G2019S} PD subjects 100
Figure S4.1: L1EV α-synuclein levels in Marburg and Cologne cohorts 106
Figure S4.2: L1EV α-synuclein levels in prodromal groups with available DaT SPECT 109
Figure S4.3: Correlation between L1EV α-synuclein levels and cognitive or motor scores 109

Figure S4.4: Comparison of L1EV α-synuclein levels between current and historic controls ... 111
Figure S4.5: L1EV-associated syntenin-1 levels in each condition 113
Figure S4.6: L1EV α-synuclein measurements in prodromal groups with available SAA 114
Figure 5.1: Graphic abstract 118
Figure 5.2: Droplet-based microfluidic EV digital immunoassay 132
Figure 5.3: Quantification of bead-to-droplet ratio according to Poisson distribution 133
Figure 5.4: Time course of fluorescent signal generation through the microdroplet-confined enzymatic reaction 134
Figure 5.5: Single serum EVs are captured on anti-L1CAM antibodies-coated beads 135
Figure 5.6: Confirmation of EV isolation from serum 135
Figure 5.7: Singleplex and multiplex EV membrane protein detection 138
Figure 5.8: Identification of α-synuclein as a serum EV membrane-associated protein 142
Figure 5.9: Confirmation of EV isolation from conditioned media 145
Figure 5.10: L1EV membrane-associated α-synuclein is increased under pathological conditions 146
Figure 5.11: L1EV membrane-associated α-synuclein is increased in iPSC-derived *SNCA*^{TRIP} dopaminergic neurons 148
Figure 5.12: Serum L1EV membrane-associated α-synuclein is increased in individuals with iRBD or PD 151
Figure 5.13: Reproducibility of the assay in detecting L1EV membrane-associated α-synuclein 152
Figure S5.1: Detailed mask design of the microfluidic chip 157
Figure S5.2: Robust droplet generation by syringe-vacuum-driven microfluidic device 158
Figure S5.3: NanoFCM analysis of membrane-associated CD9 and CD81 expression on single serum EVs 159
Figure S5.4: Representative images of α-synuclein detection on L1EVs using the droplet assay at various EV concentrations 160
Figure S5.5: Detection of α-synuclein and CD9 on serum L1EVs 163
Figure S5.6: Detection of L1EV membrane-associated α-synuclein and CD81 under pathological conditions 164
Figure 6.1: Study selection criteria and design 169
Figure 6.2: Serum and EV-associated p-tau217 levels in AD and healthy controls 176

Figure 6.3: Serum p-tau217 and NfL in iRBD with additional prodromal markers 177
Figure 6.4: Serum p-tau217 and NfL levels in individuals with iRBD who phenoconverted 178
Figure 6.5: Kaplan-Meier survival curves for phenoconversion to PD-MCI or DLB as stratified by serum p-tau217 180
Figure S6.1: Validation of the MSD p-tau217 assay 183
Figure S6.2: Serum p-tau217 and NfL levels in iRBD stratified by likelihood ratio of prodromal PD 184
Figure S6.3: Serum p-tau217 and NfL levels in iRBD with additional prodromal marker ... 185
Figure S6.4: Correlation between serum p-tau217 and NfL levels, and logistic regression analysis of their performance in distinguishing phenoconversion to PD-MCI or DLB from PD with normal cognition 186
Figure S6.5: Kaplan-Meier survival curves for phenoconversion to PD-MCI or DLB with subjects stratified by NfL 188
Figure S6.6: Kaplan-Meier survival curves for phenoconversion to DLB with subjects stratified by p-tau217 using non-phenoconverters without MCI as the reference group 189

List of Tables

Table 1.1: Comparation of EV isolation techniques 24
Table 1.2: Comparative analysis of EV protein detection technologies 38
Table 2.1: Key resources table 39
Table S3.1: Summary of EV-associated α-synuclein studies 70
Table 4.1: Demographic characteristics of individual cohort 79
Table 4.2: Influence of age or gender on L1EV α-synuclein 80
Table 4.3: ROC analyses in the derivation and validation groups 85
Table 4.4: Difference in L1EV α-synuclein levels between *GBA1*^{N409S} gene carriers with and without additional prodromal markers 86
Table 4.5: Association between L1EV α-synuclein and prodromal markers in iRBD 88
Table 4.6: Summary of prodromal markers in each cohort 92
Table 4.7: Demographic characteristics of subjects with *LRRK2*^{G2019S} from PPMI cohort 99
Table S4.1: Summary of prodromal markers in the PPMI cohort 107
Table S4.2: Correlation analyses in each cohort 110
Table S4.3: ROC analyses for stratifying at-risk subjects 112
Table 5.1: iPSC clones used in this study 120
Table 5.2: Demographic characteristics 149
Table S5.1: Performance of the assay in detecting serum L1EV membrane-associated α-synuclein and CD81 161
Table S5.2: Comparison of current microfluidic assays for EV protein detection 162
Table 6.1: Demographic, clinical, and biomarker characteristics of the iRBD cohorts 171
Table 6.2: Association between serum p-tau217 levels and prodromal markers in iRBD 174
Table 6.3: Association between serum NfL levels and prodromal markers in iRBD 175
Table S6.1: ROC analyses of p-tau217 in the iRBD subgroup comparisons 186
Table S6.2: Cox regression for time to phenoconversion to PD-MCI or DLB 187
Table S6.3: Mutually adjusted Cox regression for time to phenoconversion to PD-MCI or DLB 187

List of Abbreviations

µg	Microgram
µL	Microlitre
Aβ	Amyloid beta
AD	Alzheimer's disease
Alix	AlG-2 interacting protein X
ATP1A3	ATPase Na^+/K^+ transporting subunit alpha 3
AUC	Area under the Receiver Operating Characteristic curve
AutoCAD	Automatic Computer Aided Design
BSA	Bovine serum albumin
CBD	Corticobasal degeneration
CI	Confidence interval
CM	Conditioned medium
CN	Cognitive normal
CNS	Central nervous system
CSF	Cerebrospinal fluid
DaT SPECT	Dopamine transporter single photon emission computed tomography
DGUC	Density gradient ultracentrifugation
DLB	Dementia with Lewy bodies
DLD	Deterministic lateral displacement
DNA-PAINT	DNA Points Accumulation for Imaging in Nanoscale Topography
dSTORM	Direct Stochastic Optical Reconstruction Microscopy
ELISA	Enzyme-linked immunosorbent assay
EpCAM	Epithelial cell adhesion molecule
ESCRT	Endosomal sorting complex required for transport
EV	Extracellular vesicle
FBS	Fetal bovine serum
FDG	Fluorescein Di-β-D-Galactopyranoside
GAP43	Growth-associated protein 43
GBA1	Glucocerebrosidase beta 1
GFAP	Glial fibrillary acidic protein
HC	Healthy control

HR	Hazard ratio
IL	Interleukin
ILV	Intraluminal vesicles
IP	Immunoprecipitation
iPSC	Induced pluripotent stem cell
IQR	Interquartile range
iRBD	Isolated RBD
ISEV	International Society for Extracellular Vesicles
ISO	Isogenic
L1CAM	L1 cell adhesion molecule
L1EV	L1CAM-positive extracellular vesicle
LOD	Limit of detection
LOQ	Limit of quantification
LR	Likelihood ratio
LRRK2	Leucine-rich repeat kinase 2
MCI	Mild cognitive impairment
MDS	Movement Disorder Society
MES	2-morpholinoethanesulfonic acid
miRNA	Micro RNA
mL	Millilitre
MoCA	Montreal Cognitive Assessment
MRI	Magnetic Resonance Imaging
MSD	Meso Scale Discovery
MVB	Multivesicular body
NA	Non-applicable
NCAM1	Neural cell adhesion molecule 1
nEV	Neuronally derived extracellular vesicle
NfL	Neurofilament light chain
NLGN3	Neuroligin 3
NLRP3	NOD-like receptor protein 3
NMC	Non-manifest carrier
NTA	Nanoparticle tracking analysis
NTC	Non-transduced control
OH	Orthostatic hypotension

pCBMA	Poly(carboxybetaine methacrylate)
PD	Parkinson’s disease
PDD	Parkinson’s disease dementia
PDMS	Polydimethylsiloxane
PEA	Proximity extension assay
PEG	Polyethylene glycol
pg	Picogram
PPMI	Parkinson’s Progression Markers Initiative
PS	Phosphatidylserine
PSG	Polysomnography
PSP	Progressive supranuclear palsy
pS129	Phosphorylated at Serine129
p-tau	Phosphorylated tau
RBD	Rapid eye movement sleep behaviour disorder
RBDSQ	Rapid eye movement Sleep Behaviour Disorder Screening Questionnaire
REM	Rapid eye movement
RIPA	Radioimmunoprecipitation assay
ROC	Receiver operating characteristic
SAA	Seed amplification assay
SβG	Streptavidin-β-galactosidase
SCOPA-AUT	Scale for Outcomes in Parkinson's disease for Autonomic symptoms
SD	Standard deviation
SEC	Size exclusion chromatography
SNpc	Substantia nigra pars compacta
STORBE	Strengthening the Reporting of Observational Studies in Epidemiology
TEM	Transmission electron microscopy
TNF	Tumour necrosis factor
TRIP	Triplication
TSG101	Tumour Susceptibility 101
Tetra Trio	Tetraspanin Trio
UC	Ultracentrifugation
UF	Ultrafiltration
UPDRS	Unified Parkinson’s Disease Rating Scale
UPSIT	University of Pennsylvania Smell Identification Test

Chapter 1

Introduction

1. Introduction

1.1 Parkinson's disease

Parkinson's disease (PD) is a progressive neurodegenerative disorder characterized by the loss of dopaminergic neurons in the substantia nigra pars compacta (SNpc) and pathological aggregation of misfolded α-synuclein into Lewy bodies. As of 2023, it is estimated that over 8.5 million individuals worldwide are affected by PD, with prevalence projected to nearly double by 2040 due to global population ageing.[1] Clinically, PD is associated with both motor and non-motor symptoms, the latter frequently preceding motor onset by years. The disease imposes a substantial socio-economic burden, with annual costs in the United States exceeding $50 billion, driven by direct medical expenditures and indirect costs such as caregiver burden.[2] The absence of disease-modifying therapies underscores the need for reliable biomarkers to detect early pathological changes and stratify at-risk individuals.

1.1.1 Epidemiology of PD

PD is the second most common neurodegenerative disease, with the incidence of PD rising exponentially with age, peaking at 1-3% of individuals aged ≥ 80 years.[3] However, 3–5% of patients present with early-onset PD (diagnosis < 40 years),[4] often linked to monogenic mutations such as *Parkin* (*PARK2*).[5] Geospatial variation in prevalence is notable, with age-standardised prevalence by country varying more than five times.[6,7] This disparity is partly driven by genetic susceptibility, including high-penetrance mutations such as leucine-rich repeat kinase 2 (*LRRK2*) and glucocerebrosidase (*GBA1*). The $LRRK2^{G2019S}$ variant accounts for 30 – 40% of familial PD cases in Ashkenazi Jewish and North African Arab populations,[8,9] while the $GBA1^{N409S}$ mutation increases PD risk 5- to 10-fold in Ashkenazi Jews.[10]

The persistent male predominance in PD (male-to-female ratio of ~1.4) may relate to the neuroprotective properties of oestrogen, which modulate mitochondrial function and dopamine metabolism.[11] Occupational exposures, such as trichloroethylene[12] and manganese,[13] disproportionately affect males in certain industries, while postmenopausal women exhibit increased risk, suggesting a role for hormonal modulation.[14] Conversely, lifestyle factors such as caffeine intake[15] and cigarette smoking[16] are associated with reduced risk.

1.1.2 Pathology of PD

The pathological hallmarks of PD include loss of dopaminergic neurons in the SNpc and the formation of Lewy bodies composed of aggregated α-synuclein.[17] Although nigrostriatal degeneration underlies the classical motor symptoms,[18] α-synuclein pathology extends to extranigral regions, including the locus coeruleus and olfactory bulb, thereby contributing to non-motor symptoms such as autonomic dysfunction and hyposmia.[19]

Emerging evidence further supports a distinction between "body-first" and "brain-first" subtypes of PD, suggesting that α-synuclein pathology may originate either in peripheral autonomic structures, such as the enteric nervous system and cardiac sympathetic nerves, or centrally in the olfactory bulb and brainstem, depending on disease subtype.[20] This systemic distribution of pathology aligns with the early non-motor symptoms and supports the view of PD as a multisystem disorder involving both central and peripheral nervous systems.

Understanding the molecular basis of α-synuclein aggregation is critical to explaining how such widespread pathology arises. α-Synuclein is a presynaptic protein implicated in synaptic vesicle trafficking and neurotransmitter release. Under pathological conditions, it undergoes conformational changes from native monomers to β-sheet-rich fibrils, initiating a hierarchical aggregation process comprising soluble oligomers, protofibrils, and mature amyloid fibrils (**Figure 1.1**).[17] Notably, although less structurally stable, oligomeric

intermediates are considered more neurotoxic due to their membrane-permeabilising potential and dynamic β-sheet-enriched conformations. This conformational transformation is central to its pathogenicity, leading to cellular toxicity, membrane disruption, vesicle clustering, and mitochondrial dysfunction.[21] Increasing evidence also supports a "prion-like" mechanism of propagation,[22] in which misfolded α-synuclein is transmitted between cells via templated misfolding and internalisation, possibly through extracellular vesicles (EVs)[23] or endocytosis.[24]

Genetic mutations in the *SNCA* gene (encoding α-synuclein), such as A53T and A30P, are linked to familial forms of PD and promote α-synuclein aggregation, likely by altering its conformation, fibrillisation kinetics, or its affinity for lipid membranes.[25-27] The interaction with lipid bilayers is particularly significant, as membrane-bound α-synuclein adopts an α-helical structure that may facilitate aggregation upon membrane detachment or structural disruption. These mutations may disrupt the equilibrium between membrane-bound helical states and cytosolic conformers, increasing the availability of aggregation-prone species. Therefore, α-synuclein and lipid interface is thought to modulate not only fibril formation but also the generation of toxic oligomeric species.[28]

Phosphorylation at serine 129 (pS129) is one of the most prominent post-translational modifications observed in Lewy pathology.[29] While earlier studies proposed that pS129 may stabilise aggregates or promote fibril formation,[30] more recent evidence suggests that it is more likely a downstream consequence of aggregation rather than its initiating factor.[31] Nevertheless, the high abundance of pS129-immunoreactive α-synuclein in pathological inclusions has made it a widely used marker of Lewy pathology in post-mortem and biofluid studies.[29,32]

Importantly, pS129-α-synuclein has been shown to display altered membrane binding properties, potentially influencing its intracellular trafficking and aggregation propensity.[33] Membrane-associated kinases have been implicated in pS129 phosphorylation, linking this modification directly to membrane-associated dynamics.[34] This suggests a bidirectional

relationship in which membrane interactions modulate post-translational modifications, and conversely, modifications such as pS129 may influence aggregation kinetics by altering lipid-protein interactions. Thus, pS129 is not merely a pathological marker but may also serve as a regulatory element within the aggregation cascade.

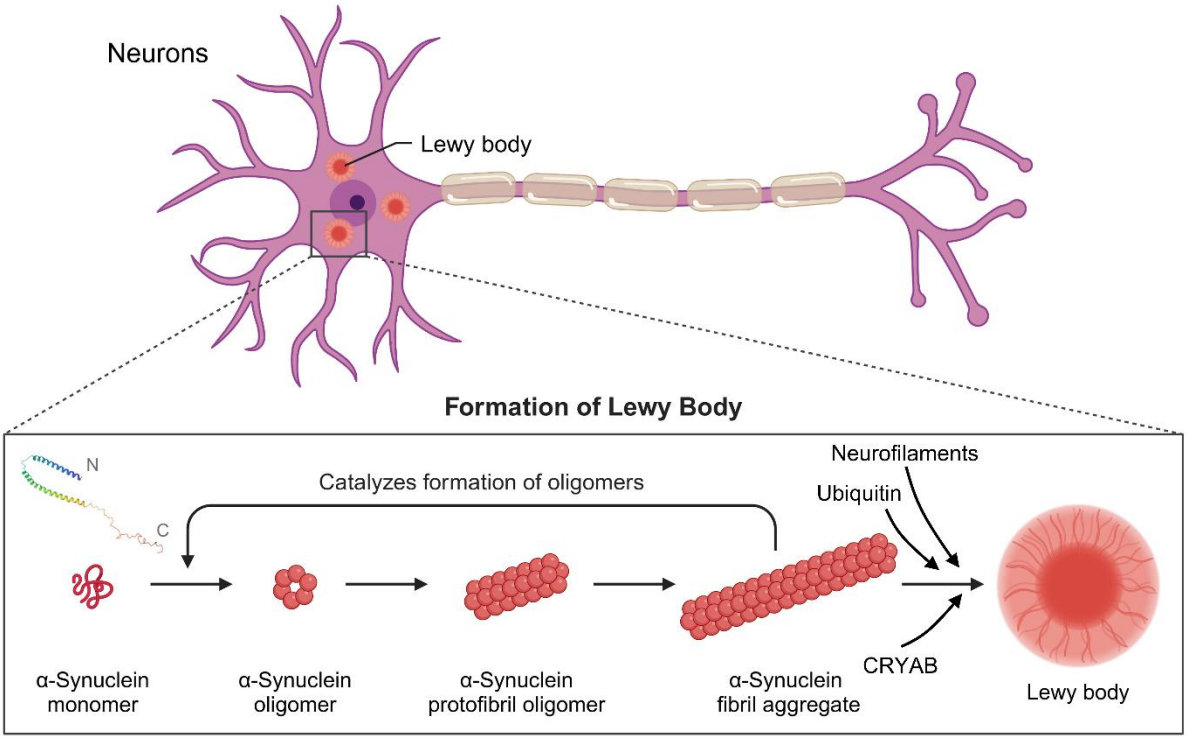


Figure 1.1: Formation of Lewy body. The progression of α-synuclein monomers into oligomers, which subsequently assemble with other proteinaceous components to form the Lewy body, the pathological hallmark of PD. Abbreviations: C = carboxyl terminus; N = amino terminus; CRYAB = crystallin alpha B.

Mitochondrial dysfunction and oxidative stress are central to the pathogenesis of PD. Dopaminergic neurons are particularly vulnerable to mitochondrial damage due to their high reliance on oxidative phosphorylation and limited antioxidant defences.[35,36] Mutations in *PINK1*[37] and *Parkin*[36] impair mitophagy, leading to the accumulation of dysfunctional mitochondria and overproduction of reactive oxygen species.[38] Environmental toxins such as MPTP recapitulate PD-like pathology by inhibiting complex I activity.[39]

Neuroinflammation is increasingly recognised as a key contributor to PD progression Activated microglia release pro-inflammatory cytokines such as tumour necrosis factor (TNF)-α, partly via NOD-like receptor protein 3 (NLRP3) inflammasome activation, which not only

exacerbates oxidative stress but also promotes α-synuclein aggregation.[40,41] Astrocytes also contribute to this inflammatory milieu by secreting complement proteins such as C3a, enhancing synaptic pruning and neuronal loss. Chronic neuroinflammation may thus form a feed-forward loop that sustains neuronal injury and spread of pathological α-synuclein.[42,43]

The interplay between α-synuclein pathology, mitochondrial impairment, and neuroinflammation establishes a vicious cycle of neurodegeneration. For instance, α-synuclein oligomers impair mitochondrial complex I activity,[44] thereby increasing reactive oxygen species production, which in turn promotes further α-synuclein oxidation and aggregation. This cycle underscores the complexity of PD pathophysiology and highlights the need for therapeutic strategies targeting multiple pathways.

1.1.3 Clinical presentation of PD

PD manifests as a complex multisystem disorder, characterised by heterogeneous motor and non-motor symptoms that evolve alongside the progressive spread of α-synuclein pathology across neural networks (**Figure 1.2**). The spatiotemporal progression of Lewy pathology follows a largely predictable pattern, as described by Braak staging.[45] In the early stages (Braak 1 and 2), pathology affects the olfactory bulb and the dorsal motor nucleus of the vagus, correlating with prodromal symptoms such as hyposmia and constipation.[46] Mid-stage pathology (Braak 3 and 4) extends to the SNpc and locus coeruleus, aligning with the emergence of motor features and rapid eye movement (REM) sleep behaviour disorder (RBD).[47] In the late stages (Braak 5 and 6), cortical involvement contributes to cognitive decline, hallucinations, and dementia.[48]

The cardinal motor features including bradykinesia, rigidity, and resting tremor. Bradykinesia, the diagnostic *sine qua non*, manifests as reduced movement amplitude and slowness, often accompanied by facial hypomimia and gait abnormalities such as shuffling and

festination.[49] Rigidity, typically asymmetric in early stages, presents as uniform resistance to passive movement due to increased muscle tone. Although resting tremor is present in approximately 70% of newly diagnosed patients, its absence does not exclude the diagnosis, reflecting the phenotypic diversity of PD.[50,51] Postural instability, a late-stage feature, is associated with noradrenergic locus coeruleus degeneration and correlates with frequent falls and accelerated cognitive decline.[52]

Non-motor symptoms often precede motor onset by up to two decades, providing a critical window for early diagnosis. These include RBD, olfactory dysfunction, depression, cognitive deficit, hallucinosis, and complex behavioural disorders.[53] RBD, characterised by dream enactment due to loss of pontine atonia during REM sleep, shows ~85% specificity for subsequent α-synucleinopathies and remains the strongest prodromal predictor.[54] Autonomic dysfunction, including orthostatic hypotension (OH), gastroparesis, and urinary urgency, is thought to reflect pathology in the intermediolateral column and dorsal vagal nucleus,[55] while depression correlates with serotonergic raphe nuclei degeneration.[56] Notably, approximately 30% of PD patients develop PD dementia (PDD) within 10 years, driven by cortical Lewy body accumulation in synergy with Alzheimer-type co-pathology.[57]

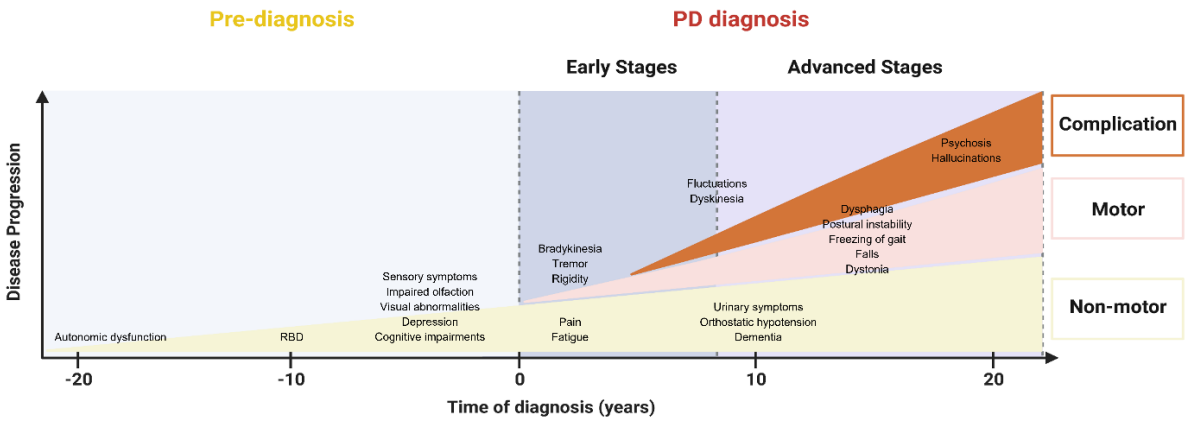


Figure 1.2: Clinical symptoms and time course of PD progression. PD is typically diagnosed at the onset of motor symptoms (time 0 years). However, a prodromal phase may precede diagnosis by more than 20 years and is characterised by non-motor features such as REM sleep behaviour disorder (RBD) and hyposmia. As the disease progresses, additional non-motor symptoms emerge, including cognitive impairment, mood disturbances, and autonomic dysfunction. Axial motor impairments, such as postural instability, frequent falls, and freezing of gait, tend to become more prominent in later stages. Long-term dopaminergic therapy can lead to complications including motor fluctuations, dyskinesia, and psychosis, which further contribute to cumulative disability.

1.1.4 Prodromal PD

Prodromal disease refers to the stage during which early neurodegenerative changes and symptoms occur in the absence of overt motor features sufficient for clinical diagnosis. This phase, which may span years to decades, reflects an interplay between genetic susceptibility, environmental exposures, and early neuropathological changes. The Movement Disorder Society (MDS) research criteria for prodromal PD provides a probabilistic model that integrates both risk factors and prodromal markers for individualised risk stratification.[58,59]

Risk markers include both non-modifiable and modifiable factors. Monogenic mutations (e.g. *SNCA, LRRK2, GBA1*) account for 10-15% of cases. Among these, *GBA1* variants confer the highest odds ratio for idiopathic PD, increasing risk by 5- to 10-fold, depending on variant severity.[60] Similarly, *LRRK2* mutations, such as G2019S, are implicated in the dysregulation of vesicular trafficking, lysosomal stress sensing, and neuroinflammation, leading to a higher risk of phenoconversion.[5] Polygenic risk scores, derived from genome-wide association studies, identified cumulative susceptibility in 90 loci, including *SNCA* and *VPS35*,

allowing risk estimation at the population level.[61] Furthermore, environmental exposures may synergise with genetic risk to accelerate neurodegeneration via mitochondrial dysfunction and oxidative stress.[62]

Prodromal markers reflect early neuropathological involvement. Video polysomnography (PSG) confirmed isolated RBD (iRBD) remains the most robust predictor, with over 80% of individuals converting to PD or related synucleinopathies within 12 years.[54] Hyposmia, detectable using tools such as University of Pennsylvania Smell Identification Test (UPSIT), precedes motor onset by 5-10 years and aligns with Braak stage 1 pathology in the olfactory bulb.[63] Subtle motor signs, such as reduced finger dexterity, can be detected through quantitative motor assessments such as MDS-Unified Parkinson's Disease Rating Scale (MDS-UPDRS).[64,65] Autonomic dysfunction, particularly OH and constipation, correlates with α-synuclein burden in the dorsal motor nucleus of the vagus.[55] Among imaging biomarkers, dopamine transporter single-photon emission computed tomography (DaT SPECT) detects presynaptic dopaminergic terminal loss in the striatum up to 7 years before diagnosis, and is considered the second strongest prodromal marker after iRBD in longitudinal studies.[59] Substantia nigra hyperechogenicity observed via transcranial sonography may further enhance specificity when used alongside iRBD.[66]

The prodromal PD criteria assign likelihood ratios (LRs) to each of these markers based on prospective cohort data, enabling probabilistic diagnosis of prodromal PD (i.e. ≥ 80% prodromal PD probability).[59] However, challenges remain in validating emerging biomarkers and standardising risk thresholds across diverse populations. Future efforts will require multimodal approaches that integrate multi-omics, imaging, and digital phenotyping to refine predictive models for identifying at-risk individuals.

1.1.5 Clinical diagnosis of PD

Despite decades of clinical experience, the diagnosis of PD remains clinically challenging due to overlapping clinical features with other neurodegenerative conditions and the lack of definitive diagnostic tests or biomarkers. Classical diagnostic frameworks, such as the UK Parkinson's Disease Society Brain Bank criteria, prioritise motor signs including bradykinesia alongside rigidity, tremor, or postural instability.[67] More recent MDS criteria incorporate supportive non-motor features, thereby enhancing diagnostic reproducibility and clinical applicability.[68]

Nevertheless, autopsy-confirmed series demonstrate that diagnostic sensitivity remains suboptimal, especially in the early stages. Only 58% of patients are correctly diagnosed within 3 years of symptom onset,[69,70] and misdiagnosis rates reach 22.4% due to phenotypic overlap with atypical parkinsonian syndromes such as MSA, progressive supranuclear palsy (PSP), corticobasal degeneration (CBD), despite their distinct underlying pathologies.[71] This inadequacy is further complicated by the finding that over 50% of nigrostriatal dopaminergic terminals are lost before overt motor symptoms emerge, highlighting the pathological latency of the disease.[72]

Emerging digital phenotyping tools, including wearable sensors capable of detecting asymmetrical movement or subtle bradykinesia, have been shown to outperform clinical examination in identifying prodromal disease, with reported sensitivity approaching 85%.[73] Meanwhile, machine learning models that integrate demographic data, hospital records, clinical assessment, and polygenic risk scores have demonstrated promising predictive power, achieving an area under the receiver operating characteristic (ROC) curve (AUC) of 0.94. However, further validation in diverse populations is still required.[74]

While these tools mark important progress, there remains an urgent need for objective, scalable, and minimally invasive molecular biomarkers to detect disease pathology during the

prodromal and preclinical stages. Among emerging strategies, EV-based approaches offer particular promise, given their ability to carry central nervous system (CNS)-derived molecular cargo and their accessibility through peripheral biofluids.

1.2 Extracellular vesicles

EVs are membrane-bound nanoparticles secreted by virtually all cell types, serving as dynamic mediators of intercellular communication, waste disposal, and disease propagation through their capacity to transfer proteins, nucleic acids, and lipids between cells. The International Society for Extracellular Vesicles (ISEV) classifies EVs based on their biogenesis pathways into exosomes (30 – 150 nm, of endosomal origin), microvesicles (100 – 1,000 nm, derived from plasma membrane budding), and apoptotic bodies (> 1,000 nm, formed during apoptosis).[75] However, due to overlapping physical characteristics and hybrid vesicle populations, multimodal validation strategies are required to distinguish EV subtypes in isolation workflows.

The discovery of EVs has reshaped our understanding of cellular physiology and disease mechanisms. In neurodegenerative disorders such as PD, neuronally derived EVs (nEVs) not only propagate pathological α-synuclein between neurons but also serve as a promising source of disease-specific biomarkers for early diagnosis.[76] This section outlines the biogenesis, molecular composition, and functional roles of EVs, with an focus on their relevance in PD and the methodological advances supporting their clinical application.

1.2.1 Biogenesis of EVs

The formation of EVs is driven by distinct cellular mechanisms that underlie their heterogeneity (**Figure 1.3**). Exosomes originate via the endosomal pathway, where inward budding of early endosomal membranes generates intraluminal vesicles (ILVs) within multivesicular bodies (MVBs). This process is primarily regulated by the endosomal sorting

complexes required for transport (ESCRT), which include four main complexes (ESCRT-0 to -III) and accessory proteins such as tumor susceptibility gene 101 (TSG101) and AlG-2 interacting protein X (Alix). These proteins direct the sorting of ubiquitinated cargo (e.g. tetraspanin CD63, CD81) into ILVs.[77] In parallel, ceramide generation mediated by neutral sphingomyelinase 2 contributes to membrane curvature to ILV budding, highlighting the interplay between protein machinery and lipid metabolism in exosome biogenesis.[78]

Microvesicles form via calcium-dependent outward budding of the plasma membrane. This process involves scramblases (e.g. TMEM16F), which redistribute phospholipids and expose phosphatidylserine (PS) on the vesicle surface. Budding is further supported by RhoA/ROCK-regulated actomyosin contraction, which generates the mechanical force required for vesicle shedding.

Apoptotic bodies emerge during programmed cell death via caspase-mediated cleavage of cytoskeletal regulators such as ROCK1, resulting in extensive membrane blebbing and encapsulation of cellular debris.[79] These vesicles contain nuclear fragments, organelles, and other cellular debris, and typically express surface PS to signal phagocytic clearance.

Recent evidence has highlighted the existence of hybrid or intermediate EV populations, which complicate the traditional classification scheme.[80] For instance, stress-induced EVs may display both exosomal (e.g. CD9+) and microvesicular (e.g. PS+) signatures, complicating isolation workflows.[81] This necessitates the use of multimodal isolation and characterisation approaches. As outlined in the MISEV 2023 guidelines, orthogonal validation combining physical, molecular, and functional criteria is essential to address this complexity, particularly when studying disease-associated EV subpopulations in complex biofluids.[75,82]

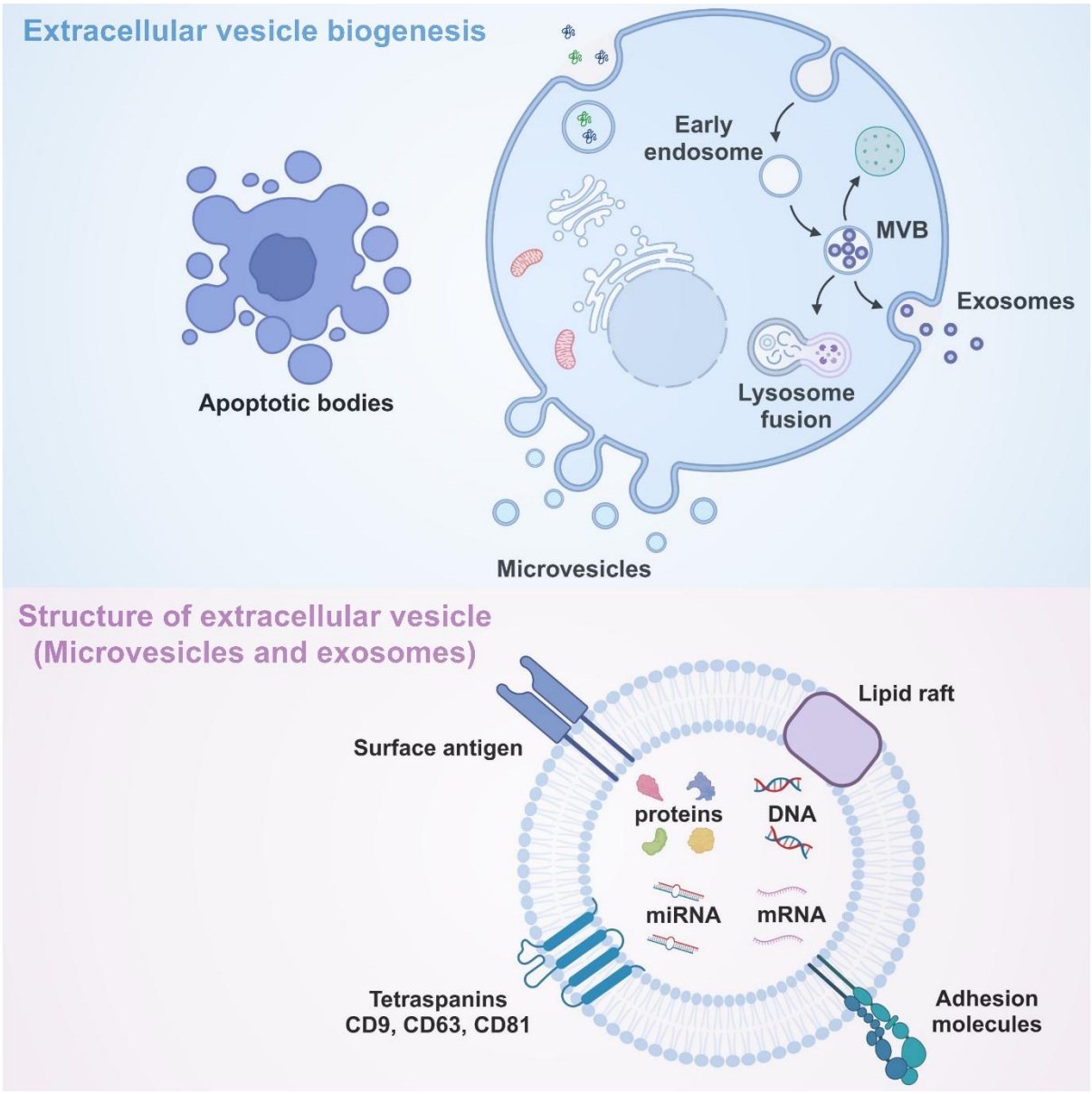


Figure 1.3: Biogenesis and structural composition of EVs. Exosomes are generated via inward budding within late endosomes and are released upon fusion of multivesicular bodies (MVBs) with the plasma membrane. Microvesicles form through direct outward budding from the plasma membrane. Additional EV subtypes, including ectosomes, membrane particles, exosome-like vesicles, and apoptotic bodies—differ in size, composition, and biogenesis pathway. All EVs are enclosed by a phospholipid bilayer that preserves cargo integrity and facilitates selective transfer of molecular contents. The membrane is enriched in tetraspanins (CD9, CD63, CD81), adhesion molecules, and lipid raft-associated proteins, which contribute to EV targeting and uptake. Encapsulated cargos include cytosolic proteins and nucleic acids such as DNA, messenger RNAs, microRNAs, long non-coding RNAs, and circular RNAs, all of which may modulate recipient cell function and participate in disease-related signalling.

1.2.2 Biological composition of EVs

EVs encapsulate a complex molecular cargo reflective of their cellular origin, including proteins, lipids, nucleic acids, and metabolites. These constituents mediate intercellular communication and contribute to both physiological regulation and disease progression.

The protein composition of EVs includes both housekeeping molecules alongside cell-type-specific markers. Tetraspanins (CD9, CD63, CD81) form stable membrane microdomains that facilitate selective cargo sorting and interaction with recipient cells. These proteins co-localise with ESCRT components, including TSG101 and Alix, as well as chaperones such as HSP70 and HSP90, which support vesicle integrity during systemic circulation.[83] Cell-type-specific markers enable subtype enrichment. For instance, L1 cell adhesion molecule (L1CAM) is commonly used for the isolation of nEVs from peripheral biofluids, while epithelial cell adhesion molecule (EpCAM) aids the isolation of tumour-derived EVs, enabling their application in non-invasive cancer diagnostics.[84] Additional constituents include glycolytic enzymes (e.g. GAPDH, pyruvate kinase),[85] which sustain metabolic activity, and cytoskeletal proteins (e.g. actin, tubulin), which preserve vesicular structure.[86]

The EV lipid bilayer is enriched in cholesterol, sphingomyelin, and PS, forming lipid rafts that stabilize membrane curvature and mediate receptor clustering. Cholesterol-rich domains stabilise tetraspanin clustering, while externalised PS signals for TREM2-dependent microglial phagocytosis in the CNS.[87] In disease states such as Alzheimer's disease (AD), EVs derived from brain exhibit altered lipid composition, including ceramide accumulation and glycerophospholipid reduction, suggesting their value as pathophysiological biomarkers.[88]

EVs also serve as carriers of diverse nucleic acids. Messenger RNAs, microRNAs (miRNAs), long non-coding RNAs, and fragments of nuclear or mitochondrial DNA are selectively packaged into EVs via sorting machinery involving RNA-binding proteins such as YBX1 and hnRNPA2B1.[89] For example, nEVs-mediated transfer of miR-132 has been shown

to regulate synaptic plasticity, while α-synuclein messenger RNA transported by EVs may facilitate protein misfolding and aggregation in recipient neurons.[76] Both mitochondrial and nuclear DNA fragments within EVs have been associated with immune activation or horizontal gene transfer.[90]

Metabolomic analyses have demonstrated that EVs are enriched in glycolytic intermediates, including citrate and lactate, as well as neurotransmitters such as glutamate. These cargoes support metabolic signalling and intercellular energy balance. For example, nEVs containing citrate have been implicated in modulating ATP synthesis at synapses.[91] Notably, recent studies in AD brain-derived EVs have revealed disease-specific alterations in their metabolomic profiles, further supporting their potential as early-stage biomarkers.[92]

1.2.3 Roles of EVs in the CNS

EVs are increasingly recognised as pivotal mediators of intercellular signalling in the CNS, contributing to both physiological regulation and the propagation of neuropathology. Originating from diverse neural cell types, including neurons, astrocytes, oligodendrocytes, and microglia, EVs encapsulate molecular cargo reflective of their cellular origin and facilitate dynamic neuro-glial communication under both homeostatic and pathological conditions.

1.2.3.1 Neuronally derived EVs

nEVs represent a discrete EV subpopulation reflective of neuronal activity and health. These vesicles encapsulate neuron-specific cargo, including synaptic proteins (e.g. PSD-95, synaptophysin), regulatory miRNAs (e.g. miR-132, miR-134), and disease-specific cargo (e.g. α-synuclein, tau). Their composition makes them sensitive indicators of neuronal integrity and dysfunction, particularly in neurodegenerative disorders. Notably, their ability to cross the blood-brain barrier and enter systemic circulation positions them as promising, accessible

biomarkers for CNS diseases including PD.[93-96] Furthermore, nEVs mediate synaptic modulation, inflammatory crosstalk, and the intercellular transfer of misfolded proteins.

1.2.3.2 EV-mediated neuron-glia communication

Under physiological conditions, EVs facilitate neuro-glial communication essential for synaptic plasticity, metabolic coupling, and immune homeostasis. Oligodendrocyte-derived EVs enriched in miR-219 and miR-338 promote myelination and axonal integrity.[97] Loss of these miRNAs in demyelination models impairs axonal nodal clustering, suggesting a role for EVs in axonal homeostasis.[98]

Astrocyte-derived EVs exhibit functional plasticity. Under homeostatic conditions, they package and transfer neuroprotective proteins such as αB-crystallin and prion protein, supporting neuronal viability and synaptic repair. In contrast, under neuroinflammatory conditions, these EVs can encapsulate pro-inflammatory mediators, including interleukin (IL)-1β, which exacerbate microglial activation and synaptic degeneration.[99]

Microglia-derived EVs also serve as bidirectional modulators of neuroinflammation, engaging in homeostatic synapse modulation or propagating inflammatory cues depending on activation status. Resting microglia release EVs that promote synaptic pruning, whereas activated microglia secrete EVs enriched with inflammatory signals that drive neurodegenerative processes, as seen in early stages of PD and AD.[100]

1.2.3.3 EV-mediated protein transfer

In disease context, EVs have been implicated in the intercellular transmission of misfolded proteins. In AD, nEVs isolated from brain tissues[101] have been shown to carry phosphorylated tau (p-tau) and amyloid-β (Aβ) oligomers, promoting tau hyperphosphorylation and accelerating amyloid plaque accumulation.[102] These findings are

corroborated by nEV isolated from both CSF[103] and plasma[104], facilitating their internalisation by recipient neurons and initiating templated aggregation cascades.[105]

Beyond tau and Aβ, other neurodegeneration-associated proteins such as TDP-43 and SOD1 have been identified within EVs isolated from plasma and Amyotrophic lateral sclerosis models,[106] suggesting a broader role for EVs in neurodegenerative proteinopathies. These findings suggest that EVs function not only as by-products of cellular dysfunction but also as active mediators of disease propagation in a protein- and disease-specific manner.

1.2.4 The role of EVs in PD

Beyond their physiological functions, EVs are increasingly implicated in the pathogenesis of PD. Their roles encompass the propagation of pathogenic α-synuclein, regulation of inflammatory responses, and involvement in lysosomal dysfunction.

1.2.4.1 α-Synuclein transmission via EVs

Compared to free α-synuclein, EV-associated forms exhibit enhanced stability, broader biodistribution, and partial protection from immune surveillance, which may facilitate long-range transmission across neural and peripheral tissues.[107] Accumulating evidence have demonstrated that α-synuclein is selectively incorporated into nEVs via ESCRT-I and flotillin-dependent pathways,[76] shielding it from lysosomal degradation and enabling uptake by vulnerable recipient neurons through heparan sulfate proteoglycan-mediated endocytosis.[108] Once internalised, EV-associated α-synuclein has been shown to promote aggregation[109] and trigger apoptotic pathways,[110] supporting a potential mechanism for the prion-like spread of pathology in PD.

In vitro, α-synuclein preformed fibrils induce the release of nEV from *SNCA* A53T induced pluripotent stem cells (iPSCs)-derived dopaminergic neurons, thereby accelerating Lewy body pathology.[23] Similarly, EVs derived from mouse neuroblastoma cells provide

catalytic environments for nucleation of α-synuclein aggregation.[111] In vivo, intrastriatal injection of nEVs isolated from CSF of PD patient leads to nigrostriatal α-synuclein accumulation, motor deficits, and dopaminergic neuron loss in mice.[23]

1.2.4.2 Lysosomal dysfunction and EV trafficking

Pathogenic mutations in the *GBA1* (e.g. p.L444P, p.N370S) impair lysosomal glucocerebrosidase activity, leading to intracellular α-synuclein accumulation and enhanced packaging into EVs (**Figure 1.4**).[112] These EVs, when released, contribute to intercellular propagation and promote microglial activation through TLR2-mediated mechanisms, triggering NLRP3 inflammasome activation and increased IL-1β release.[113] The resulting immune activation induces the transformation of astrocytes into a neurotoxic A1 phenotype, characterised by the release of complement component C3. C3 binds to C3a receptors on dopaminergic neurons, impairing synaptic function and accelerating neuronal loss.[114] This pathogenic cascade underscores the interplay between lysosomal dysfunction and EV-mediated inflammation in PD pathogenesis.

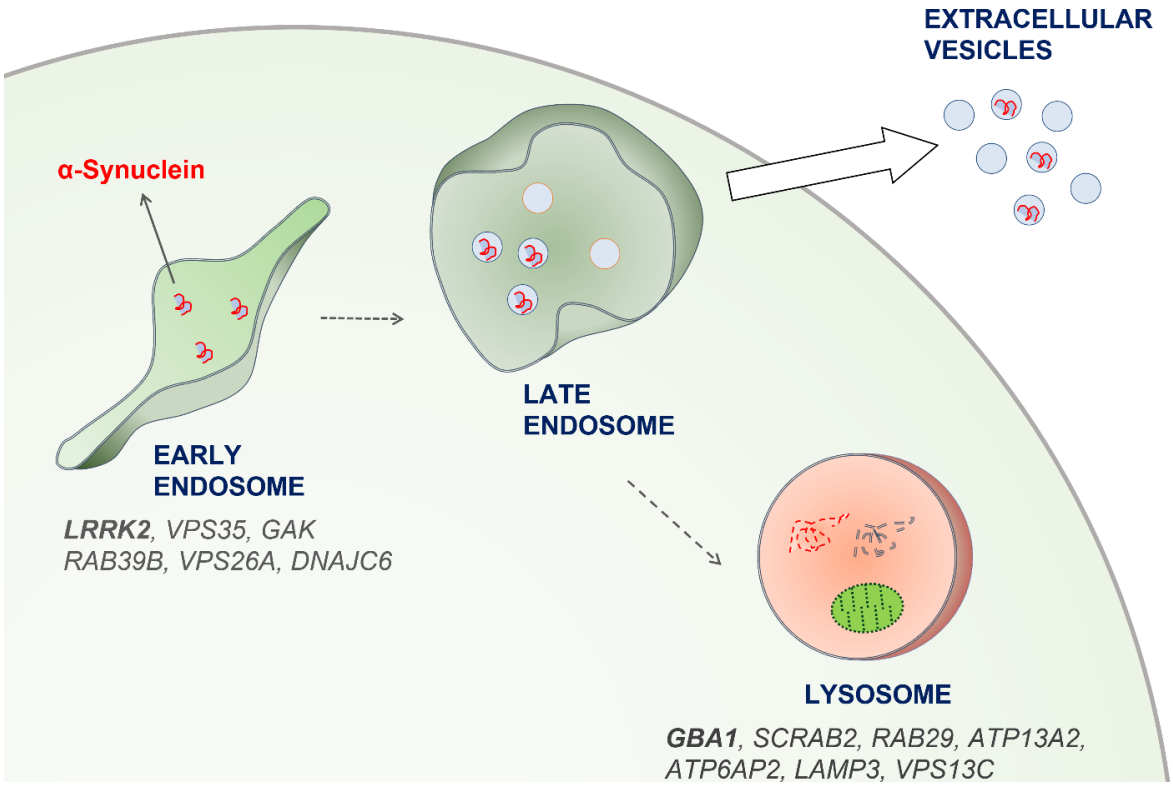


Figure 1.4: EVs in α-synuclein homeostasis and lysosomal dysfunction in PD. PD-linked genetic mutations impair lysosomal function, compromising the intracellular degradation of α-synuclein. In the context of lysosomal inhibition, α-synuclein is redirected into multivesicular bodies and released via EVs, particularly nEVs. This pathway suggests a compensatory mechanism for α-synuclein clearance and highlights the role of EVs in the pathological redistribution and propagation of α-synuclein.

1.2.4.3 Potential protective functions of EVs in PD

While much attention has focused on the pathological role of EVs in facilitating α-synuclein transmission, growing evidence suggests that EVs may also exert context-dependent neuroprotective effects. Under lysosomal stress or proteostatic dysfunction, EV-mediated export of α-synuclein may serve as a compensatory mechanism to reduce intracellular burden and mitigate cytotoxicity.[115] In dopaminergic neurons, EV release is upregulated under mitochondrial dysfunction, potentially acting as a route of metabolic unloading or damage-associated signalling.[116] Moreover, stem cell-derived EVs have demonstrated the ability to attenuate oxidative stress, reduce neuroinflammation, and promote neuronal survival in toxin- and proteinopathy-based PD models. These effects are attributed to the delivery of anti-inflammatory miRNAs, neurotrophic factors, and mitochondrial regulators.[117]

Collectively, these findings suggest that EVs function not only as pathological conveyors but also as intracellular clearance mechanisms and vehicles for neuroprotective signalling. The dual role of EVs highlights the importance of cargo characterisation and microenvironmental context in defining their functional impact in PD.

1.2.4.4 Therapeutic potential of EVs in PD

Given their endogenous biocompatibility and cell-targeting capacity, EVs are increasingly explored as therapeutic vectors. In PD models, intranasal administration of stem cell-derived EVs has been shown to ameliorate motor symptoms and rescue nigrostriatal neurons.[118] Engineered designer EVs loaded with therapeutic catalase messenger RNA or anti-α-synuclein short hairpin RNA have been shown to reduce neurotoxicity and neuroinflammation in 6-hydroxydopamine and fibril-induced PD mouse models.[119,120] These findings underscore the feasibility of EV-based interventions, although challenges remain in standardising cargo loading, delivery efficiency, and safety profiling for clinical translation.

1.2.5 EV isolation techniques

Efficient and reproducible isolation of EVs remains a technical prerequisite for both basic research and translational applications. Given the molecular and biophysical heterogeneity of EV subtypes, isolation methods must achieve a balance between yield, purity, scalability, and downstream compatibility for applications such as proteomic and transcriptomic analysis, and clinical biomarker validation. This section outlines the principles, strengths, and limitations of current EV isolation strategies (**Table 1.1**).

1.2.5.1 Differential ultracentrifugation

Differential ultracentrifugation (UC) remains the most established technique for EV isolation. It separates particles based on their size and density through stepwise increases in

centrifugal force. Typical workflows begin with low-speed centrifugation (300 ×g) to remove cells and debris, followed by higher-speed spins (2,000 – 10,000 ×g) to pellet cell debris and large vesicles, culminating in UC at ≥ 100,000 ×g to sediment exosomes and small EVs.[121]

Although cost-effective and scalable, UC often co-pellets non-EV contaminants such as lipoproteins and protein aggregates. Moreover, high shear forces may disrupt EV structure, resulting in reduced yields of intact EVs compared to size-exclusion chromatography (SEC).[122] The viscosity of input fluids (e.g. serum, plasma) significantly influences recovery, with more viscous matrices requiring extended spin durations at elevated speeds, which further heightens the risk of contamination.[123,124]

1.2.5.2 Density gradient ultracentrifugation

Density gradient UC (DGUC) separates EVs by buoyant density using discontinuous or continuous gradients formed from iodixanol or sucrose gradients. EVs typically partition at 1.10 – 1.14 g/mL, distinguishable from protein aggregates and nucleoproteins (1.18 g/mL). This method yields high-purity EVs than differential UC and is particularly valuable in downstream analyses demanding minimal background interference.[125]

Notably, studies using OptiPrep™ gradients showed efficient depletion of microvesicles and contaminating plasma proteins,[126] revealing unique transcriptomic signatures not captured by simpler protocols.[124] However, its resolution is limited when EVs overlap in size and density with non-EV entities such as viral particles.[127] It is also labour-intensive and low-throughput, which constrains its scalability for clinical applications.

1.2.5.3 Immunoprecipitation

Immunoprecipitation (IP) isolates EVs by capturing surface markers using antibodies conjugated to immunobeads. Most commonly, tetraspanins (total EVs) such as CD63, CD9, or cell type-specific antigens like L1CAM (nEVs) are targeted. This method offers high

specificity for isolating defined EV subpopulations from complex biofluids, enabling downstream analyses such as proteomics, miRNA profiling, or disease biomarker validation.

Recent studies have demonstrated that IP-based isolation achieves superior purity and selectivity, especially valuable for CNS-derived EVs in plasma or CSF. For instance, IP against L1CAM has been widely used for isolating nEVs from blood or CSF, achieving improved sensitivity than bulk EV isolation techniques.[128] In comparative studies, although IP may yield lower total particle counts than UC, it offers significantly higher signal-to-noise ratios and biomarker detection efficiency.[129]

However, limitations include reduced yield, dependence on antibody specificity, and potential for epitope masking or loss under certain buffer conditions. Additionally, method optimisation is often required to ensure reproducibility across laboratories. Despite this, its ability to selectively enrich specific EV subtypes renders IP a powerful tool for translational EV research, particularly when precision outweighs bulk recovery.

1.2.5.4 Ultrafiltration

Ultrafiltration (UF) employs membranes with defined molecular weight cut-offs to concentrate EVs while allowing soluble proteins to pass through. For instance, tangential flow filtration enables rapid EV enrichment from large-volume biofluids (e.g. ascites, CSF), achieving recovery rates > 90% with minimal membrane clogging.[130]

When combined with SEC, UF has proven high-fidelity EV recovery from biofluids such as CSF and plasma. While scalable and time-efficient, UF often retains soluble contaminants, including apolipoproteins such as ApoA1 and ApoB100, which can interfere with downstream analyses.[131]

1.2.5.5 Size exclusion chromatography

SEC utilises porous matrices (e.g. Sepharose CL-4B) to fractionate particles based on hydrodynamic radius. Larger particles such as chylomicrons and cell debris elute earlier,

followed by EVs, while soluble proteins (<30 kDa) in later fractions.[132] SEC preserves EV structure and is particularly effective in removing albumin and immunoglobulin contaminants, yielding high-purity EVs suitable for downstream applications such as proteomic and transcriptomic analyses.[133] These features make SEC a competitive alternative to contamination-prone isolation techniques in α-synuclein biomarker studies.

Recent approaches combining SEC with fluorescence-activated sorting platforms, such as EVQuant using quantum dot-labelled anti-CD63 antibodies, have enhanced both resolution and recovery.[134] However, its scalability remains limited, especially for viscous or high-volume samples, as column clogging and sample dilution necessitate pre-filtration and post-isolation concentration steps. In contrast, Capto Core multimodal chromatography, which uses porous beads with inert outer shells and ligand-activated cores to selectively retain small contaminants, enables high-throughput and scalable purification of EVs. This technique improves purity and yield compared to SEC alone,[135] while also minimising clogging and dilution, making it well suited for integration into standardised downstream workflows.

1.2.5.6 Microfluidic platforms

Microfluidic platforms represent a transformative advance in EV isolation, offering high precision, integration, and miniaturisation. These platforms exploit principles such as immunoaffinity capture, acoustofluidics, and deterministic lateral displacement (DLD) to selectively isolate EVs from microlitre-scale samples.

Techniques such as ExoChip, which utilises anti-CD63-functionalised polydimethylsiloxane (PDMS) microchannels to selectively capture EVs directly from plasma, enables downstream on-chip quantification of EV-associated RNA.[136] In parallel, magnetic bead-based microfluidic platforms offer an alternative approach. For instance, alternating magnetic field approaches support the dynamic mixing of antibody-coated magnetic beads with

serum samples within 3D-printed microfluidic chips, enabling EV isolation from < 50 μL of serum in 30 min.[137]

Acoustic and DLD-based platforms further enhance size-specific resolution while preserving EV integrity, as they avoid mechanical stress.[138,139] Hybrid systems combining continuous-flow microfluidics and immunoaffinity enrichment (e.g. magnetic beads coated with anti-EpCAM) offer high specificity and are particularly attractive for clinical and high-throughput diagnostic applications.[140]

However, a persistent limitation remains the lack of standardisation across laboratories, which hampers reproducibility and hinders complicates inter-platform comparisons. Despite this, microfluidic platforms hold promise in clinical EV isolation, particularly where sample volumes are limited or rapid processing is required.

1.2.5.7 Polyethylene glycol precipitation

Polyethylene glycol (PEG) precipitation induces EV aggregation by osmotic exclusion, enabling their sedimentation at relatively low centrifugal speeds. It offers simplicity, cost-effectiveness, and scalability, making it attractive for large-scale screening studies and biobanking applications.

However, PEG lacks specificity and often co-precipitates lipoproteins, protein aggregates, and polymer residues.[141] Additionally, PEG may distort vesicle morphology, complicating downstream characterisation using transmission electron microscopy (TEM) or nanoparticle tracking analysis (NTA).[142] Hence, PEG is better suited as a pre-concentration step rather than a primary isolation technique.

1.2.5.8 Commercial kits

Commercial kits offer convenient, standardised protocols for EV isolation, typically employing polymeric precipitation or membrane affinity methods. These kits can separate EVs from a range of biofluids, including cell culture supernatants, serum, plasma, and CSF.

Products like ExoQuick-TC™ (System Biosciences) and Total Exosome Isolation Reagent (Invitrogen) are widely used in translational research.

While advantageous for their speed and minimal equipment requirements, these kits often compromise on purity.[126] Contamination by serum proteins (e.g. albumin, IgG) and residual polymers may interfere with both quantitative and qualitative analyses. Therefore, such kits are more appropriate for exploratory studies or resource-limited settings, rather than for high-resolution EV applications.

Method	**Purity**	**Yield**	**Resolution**	**Time**	**Scalability**	**Automation**	**Cost**
Differential UC	Medium	Medium	Low	High	Medium	Low	Low
DGUC	High	Low – medium	Medium	High	Low	Low	Medium
IP	High	Low	High	Medium	Medium	Medium – high	High
UF	Low	High	Low	Medium	Medium	Medium	Medium
SEC	Medium	Medium	Low– medium	Medium	Medium	Medium	Medium
Microfluidic platforms	High	Low – medium	Low – high	Low	Low – medium	High	High
PEG	Low	High	Low	Low	High	Medium	Low
ExoQuick	Low	Medium	Low	Low	High	High	Medium

Table 1.1：Comparation of EV isolation techniques. Abbreviations: UC = ultracentrifugation; DGUC = density gradient UC; IP = immunoprecipitation; UF = ultrafiltration; SEC = size exclusion chromatography; PEG = polyethylene glycol.

1.3 Biomarkers in PD

The identification and validation of biomarkers are essential for advancing early diagnosis, monitoring disease progression, and refining patient stratification in PD. Traditional clinical diagnosis focuses on motor phenotyping, is inherently subjective and typically relies on late-stage manifestations, underscoring the need for objective, molecularly informed tools. Although non-motor symptoms, including RBD, hyposmia, and constipation have been validated as important prodromal indicators, their individual predictive value remains limited, and the utility of composite prodromal criteria is constrained by the partial independence and variable expression of these markers.[59]

Biomarkers serve multiple, complementary purposes across the disease spectrum. At the diagnostic level, they improve the differentiation of PD from atypical parkinsonian syndromes, particularly in early or clinically ambiguous presentations. Prognostically, they enable the prediction of disease trajectory, including motor deterioration, cognitive impairment, and phenotype evolution. In the prodromal or preclinical phase, predictive biomarkers facilitate the identification of at-risk individuals, opening a window for early intervention. Moreover, longitudinal biomarkers offer a means to track disease progression or therapeutic response over time, and molecular stratification biomarkers support the delineation of biologically defined subgroups, guiding personalised interventions and enriching clinical trial design. Collectively, these roles highlight the need for biomarkers that are not only disease-specific and sensitive, but also reproducible, scalable, and minimally invasive, ideally accessible from peripheral biofluids.

Current biomarker development spans clinical, genetic, imaging, and biofluid-based modalities. Among these, approaches based on nEVs isolated from biofluids have attracted particular interest owing to their capacity to provide minimally invasive access to CNS-derived molecular cargo via peripheral biofluids. This is especially relevant in PD, where underlying

pathology precedes overt symptom onset by years and often remains undetectable by conventional diagnostic tools.

Recent advances in ultrasensitive analytical platforms, such as seed amplification assay (SAA), Meso Scale Discovery (MSD) assays, single-molecule array (Simoa) platforms, microfluidic devices, and high-resolution proteomics have greatly expanded the biomarker landscape. These platforms allow the quantification of key disease-relevant proteins, including α-synuclein, tau, and DJ-1, as well as miRNAs and lipids, from minute volumes of biofluid samples. Importantly, these analytes can be measured either in unprocessed biofluids or following selective enrichment for nEVs. This section outlines current developments in biochemical biomarkers for PD, with particular emphasis on the emerging diagnostic and prognostic value of EV-associated biomarkers.

1.3.1 Biofluid-based biomarkers

1.3.1.1 CSF biomarkers

CSF offers a proximal readout of CNS pathology and has yielded several promising biomarkers. CSF total α-synuclein levels are typically reduced in PD patients,[143] while oligomeric and phosphorylated forms are often increased.[144] These changes align with PD pathology, where α-synuclein is sequestered into aggregates whereas misfolded oligomers accumulate. However, their diagnostic utility remains limited due to overlap with other neurodegenerative disorders.[145]

Combinatorial panels integrating α-synuclein, tau, Aβ, and inflammatory markers (e.g. YKL-40) have improved discriminatory accuracy.[146,147] Neurofilament light chain (NfL), a marker of axonal degeneration, although not specific to PD, aids in distinguishing PD from atypical parkinsonian syndromes.[148,149]

A major breakthrough has been the development of α-synuclein SAA, including real-time quaking-induced conversion and protein misfolding cyclic amplification, which detect misfolded α-synuclein aggregates based on their ability to seed fibril formation *in vitro*.[150] These assays have demonstrated excellent diagnostic performance with reported sensitivity and specificity > 85% for detecting synucleinopathies.[151-155] Recent multicentre validation in the Parkinson's Progression Markers Initiative (PPMI) cohort demonstrated 87.7% sensitivity and 96.3% specificity, with even higher accuracy in sporadic cases with olfactory deficits.[155] Moreover, SAA has been shown to detect α-synuclein pathology in prodromal individuals,[156] marking a potential shift towards preclinical diagnosis. Owing to their exceptional performance and biological relevance, these assays are now increasingly considered biochemical gold standards for *in vivo* detection of Lewy body pathology.

However, their broader clinical application is limited by invasiveness of CSF sampling and resource-intensive nature of the assays. Furthermore, diagnostic performance is reduced in certain PD subgroups, such as genetic or olfaction-intact PD,[155] possibly due to the lack of Lewy body formation.[157-159] These limitations highlight the need for more accessible biomarkers and fibril-agnostic detection methodologies.

1.3.1.2 Blood-based biomarkers

Despite challenges posed by peripheral dilution and protein contamination, blood-based biomarkers offer unmatched accessibility for repeated sampling and large-scale screening. Total α-synuclein in plasma or serum has been extensively studied, but findings remain inconsistent due to its abundance in red blood cells and vulnerability to haemolysis, which can confound measurements.[160] Assays targeting pathological species of α-synuclein, such as oligomeric α-synuclein or phosphorylated α-synuclein have demonstrated improved specificity and shown promise for early detection.[161-163]

NfL[164] and glial fibrillary acidic protein (GFAP),[165] are emerging as useful complementary biomarkers. Elevated serum NfL levels have been associated with faster motor deterioration and cognitive decline,[166,167] and shown utility in differentiating PD from atypical parkinsonian syndromes such as PSP and MSA,[168] although its diagnostic sensitivity remains modest.[169] GFAP, a marker of astrocytic reactivity, has been linked to cognitive impairment and phenoconversion from mild cognitive impairment (MCI) to PDD.[170]

Beyond protein markers, circulating miRNAs such as miR-24-3p, miR-146a-5p, and miR-19b-3p have demonstrated differential expression in PD. Although results vary across studies, meta-analyses suggest composite miRNA panels may achieve diagnostic sensitivity and specificity > 80%.[171]

Nevertheless, the development of reliable blood-based biomarkers remains constrained by several factors, including biological variability, preanalytical confounds (e.g. haemolysis), and limited specificity for CNS pathology. As such, rigorous standardisation of protocols and integration with complementary modalities, such as imaging or EV-based biomarkers, will be essential to enhance diagnostic precision and reproducibility.

1.3.1.3 Other biofluid and tissue biomarkers

Given that PD pathology is not confined to the brain, researchers have examined peripheral tissues (e.g. gut, skin) and other biofluids for accessible biomarkers of α-synucleinopathy. Skin biopsies detecting pS129-α-synuclein in dermal nerves have demonstrated > 90% accuracy, offering a minimally invasive diagnostic option for *in vivo* confirmation of Lewy pathology.[172,173] Complementary SAA applied to skin tissue has also shown similarly high diagnostic value,[174] including in prodromal cases.[175]

The gastrointestinal tract, implicated in the "body-first" subtype of PD, has been explored via colonic biopsies. While early studies reported promising α-synuclein immunoreactivity in mucosal tissues,[176-179] subsequent work revealed variable sensitivity

(ranging from 55 to 100%) and questionable specificity, as α-synuclein aggregates can also be detected in age-matched controls and patients with other neurodegenerative conditions.[55,180] Thus, this method is not currently suitable for clinical application.

Other tissues such as the olfactory mucosa and submandibular glands, are now being explored using SAA, with preliminary evidence supporting their utility for early detection.[181,182] In parallel, non-invasive biofluids such as saliva and urine are under evaluation, Although saliva total α-synuclein has shown inconsistent results,[183] the oligomeric form[183] and saliva SAA[184] have shown improved diagnostic performance. In urine, metabolic biomarkers such as kynurenine[185] ornithine,[186] and sebum lipid signature,[187] have also demonstrated potential value.

While these approaches offer intriguing insights into disease biology and novel avenues for biomarker development, none have yet achieved the technical maturity and reproducibility of CSF- or blood-based assays. Further assay refinement and large-scale validation will be required for their clinical translation.

1.3.2 EV-based biomarkers

1.3.2.1 nEV biomarkers

nEVs isolated from peripheral biofluids using neuron-specific surface markers offer a minimally invasive platform for investigating CNS pathology in PD (**Figure 1.5**). Traditional immunocapture methods have relied on L1CAM (also known as CD171) to isolate nEVs from blood or CSF. However, a recent study has questioned whether L1CAM is exclusively EV-bound or predominantly present in a soluble form in circulation.[188] This distinction has important implications, as non-vesicular L1CAM may confound interpretation of nEV-associated analytes such as α-synuclein. Therefore, while L1CAM-based immunocapture remains widely adopted, results derived from L1CAM+ EVs (L1EVs) must be cautiously

interpreted and ideally supported by orthogonal EV characterisation approaches. Nevertheless the consensus, including extensive investigations from our group,[189] is that a small fraction of L1CAM is present on EVs.

To improve neuronal specificity and recovery, alternative or complementary surface markers have been explored, including GluR2/3,[190] neuroligin 3 (NLGN3),[191,192] ATPase Na+/K+ transporting subunit alpha 3 (ATP1A3),[193] and growth-associated protein 43 (GAP43).[191,192] For example, nEVs immunocaptured with anti-NLGN3 and anti-GAP43 antibodies from plasma showed enhanced greater enrichment for neuronal transcripts and lipids compared to L1EVs.[192] Similarly, ATP1A3 has shown utility in isolating nEVs from induced human neuron, brain tissue, CSF, and plasma, with ATP1A3+ EVs exhibiting superior synaptic protein content compared to neural cell adhesion molecule 1 (NCAM1)+ or L1EVs.[193] Nevertheless, the low abundance of neuron-specific surface proteins in circulation poses significant challenges for consistent nEV recovery.

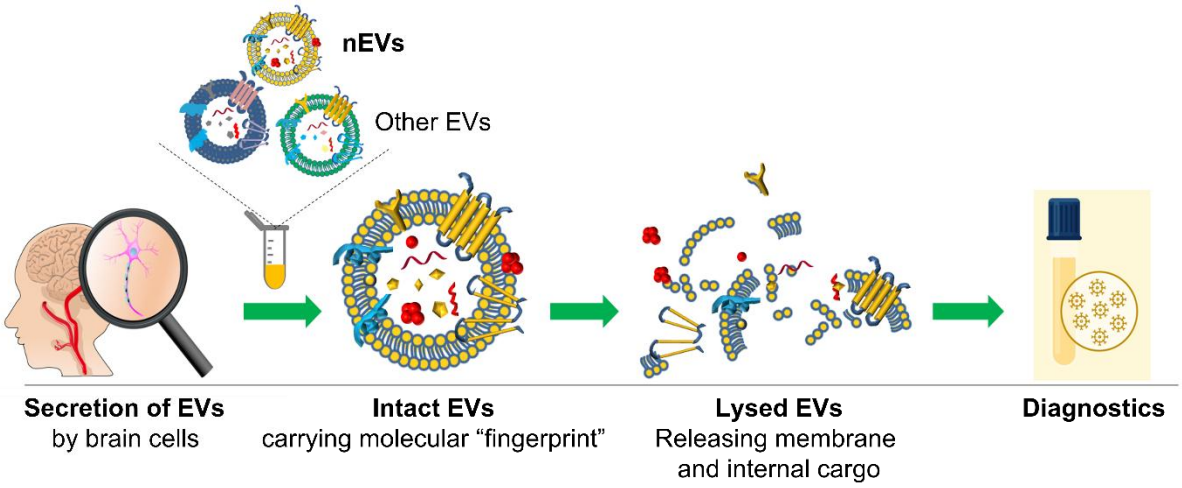


Figure 1.5: Schematic workflow of nEV-based diagnostics. nEVs enter circulation and can be selectively immunocaptured using neuron-enriched antigens such as L1CAM. The isolated nEVs are then lysed for downstream diagnostic applications, enabling the analysis of neuronal biomarkers relevant to PD.

In PD, EV-based diagnostics have focused on α-synuclein quantification within nEVs. Shi et al. first reported increased α-synuclein in plasma L1EVs in PD patients, with levels correlating with disease severity.[194] This finding was subsequently replicated in multicentre

studies from our group, where elevated serum L1EV α-synuclein distinguished PD from not only from healthy controls, but also atypical parkinsonian syndromes such as MSA, and tauopathies such as PSP and CBD, with AUCs > 0.85.[94,95] When combined with clusterin, a protein elevated in tauopathies, the differential accuracy of PD from MSA improved to 91%.[94] Importantly, these results were validated across multiple independent cohorts and laboratories, supporting the reproducibility of nEV α-synuclein as a biomarker.[195,196]

Nevertheless, it is important to acknowledge that α-synuclein is not exclusively pathological and may be present in nEVs from healthy individuals. Under normal physiological conditions, α-synuclein is actively expressed in presynaptic terminals, where it regulates synaptic vesicle recycling and neurotransmitter release, thereby supporting neuronal homeostasis.[197] As such, low levels of α-synuclein, especially its monomeric forms, are expected in nEVs, even in healthy controls, reflecting its physiological secretion and role in intercellular communication. This background expression presents a challenge for biomarker interpretation, as elevated total α-synuclein levels in nEVs may not necessarily reflect pathological processes. Accordingly, although L1EV α-synuclein has demonstrated diagnostic utility, focusing on pathological species, such as oligomeric or phosphorylated α-synuclein, which more accurately reflect pathological aggregation and Lewy body formation, may further enhance its diagnostic precision. This underscores the importance of rigorous pre-analytical standardisation and the use of analytical platforms capable of conformer-specific detection.

The integration of SAA into nEV-based diagnostics represents a notable advancement. Kluge et al. successfully amplified misfolded α-synuclein from plasma-derived nEVs, achieving high sensitivity and specificity in both prodromal[198] and clinical PD.[199] Although the reproducibility of this approach has been questioned,[200] this integration offers a promising minimally invasive approach for the molecular confirmation of Lewy body pathology.

Despite their potential, nEV biomarkers face several persistent technical constraints that may limit their translational potential. The inherently low abundance of nEVs in peripheral circulation complicates efforts to achieve sufficient yield and purity, particularly when targeting low-copy biomarkers. Moreover, when isolating nEVs from complex matrices such as serum, abundant background proteins such as albumin and immunoglobulins can exceed nEV cargo by several orders of magnitude.[201] Even with rigorous purification, trace contaminants may distort downstream readouts due to the minute abundance of targeted proteins in purified nEV fractions. These background signals are highly dependent on isolation technique, buffer composition, input volume, and detection techniques.

To realise the full potential of nEVs in PD diagnostics, rigorous standardisation, high-yield purification methods, and orthogonal analytical validation are essential. Advances in microfluidics and single-EV detection platforms may ultimately offer the throughput, specificity, and reproducibility required for clinical implementation.

1.3.2.2 Other EV biomarkers

In addition to pathological proteins, EVs encapsulate inflammatory mediators, offering insights into neuroinflammatory cascades in PD. For instance, plasma EV cytokine levels (e.g. pro-IL-1β, TNF-α) are elevated in PD and associated with cognitive deficit, supporting a role of neuroinflammation in the pathogenesis of PDD.[202]

Proteomic analyses of urinary EVs have identified SNAP23 and calbindin as novel biomarkers for distinguishing PD from controls, with reported AUCs > 0.8.[203] Phosphorylated LRRK2 (Ser1292) in urinary EVs has also emerged as a candidate biomarker, correlating with clinical severity and may stratify *LRRK2*-linked PD.[204] Other candidate biomarkers include DJ-1, an antioxidant protein,[205] and tau,[206] although current evidence remains preliminary and requires further validation in large cohorts.

EV-associated miRNAs have also shown promise as PD biomarkers.[207] Studies have demonstrated that CSF EV-associated miR-409-3p and miR-513 can discriminate PD patients from controls with excellent accuracy (AUC = 0.99).[208] Similarly, in plasma-derived EVs, miR-331-5p and miR-505 have shown strong diagnostic utility (AUC > 0.85).[209]

Despite encouraging findings, EV-based biomarkers face technical limitations including batch effects, RNA degradation, and lack of consensus on cargo normalisation. Nevertheless, their accessibility from peripheral fluids, combined with the capacity to track longitudinal changes, positions EVs as compelling candidates for early detection, disease stratification, and treatment monitoring.

1.4 EV-based protein biomarker detection technologies

The accurate detection of EV-associated proteins is critical for translating biomarkers into clinical practice. However, the low abundance and heterogeneity of EVs, particularly rare nEVs circulating in peripheral fluids, pose considerable analytical challenges. Traditional methods often lack the sensitivity to detect EV cargo, necessitating the development of advanced technologies that can resolve EV heterogeneity and quantify low-abundance targets. This section reviews major EV protein detection platforms, their respective merits, limitations, and application in neurodegenerative disease biomarker research, particularly in PD.

1.4.1 Conventional immunoassays

Traditional immunoassays like enzyme-linked immunosorbent assay (ELISA) and Western blot have been widely used to quantify EV proteins. These methods remain useful in validating EV isolation quality, profiling bulk EV markers (e.g. CD63, CD9, ALIX), and conducting proof-of-principle analyses. However, their limited sensitivity restricts utility in detecting low-abundance EV biomarkers such as serum L1EV α-synuclein, in which the concentrations lie in the low picogram range. Moreover, bulk assays cannot differentiate EV-

encapsulated proteins from co-isolated soluble contaminants, which may confound interpretation unless rigorous purification is applied.

Nonetheless, these assays remain valuable in optimised contexts, such as when applied to larger input volumes, or when quantifying abundant EV proteins. However, their limitations have prompted a shift towards high-sensitivity platforms better suited to the small sample volumes and low analyte concentrations characteristic of EV-based diagnostics.

1.4.2 Meso Scale Discovery

MSD assays employ electrochemiluminescence technology to provide higher sensitivity (in the low pg/mL range or below) and broader dynamic range (4 – 5 logs) than conventional ELISA. By employing biotinylated and ruthenium-labelled antibodies, as well as multi-array 96-well plates, MSD allows detection of multiple analytes (up to 10 per well) from small sample volumes (typically 25 – 50 μL).

In EV biomarker applications, MSD has been adapted to profile multiple markers simultaneously on either intact EVs or EV lysates. For instance, MSD has been applied on serum L1EVs for the quantification of total α-synuclein.[94,195,210] Moreover, it has been extended to detect EV-associated pS129-α-synuclein, a species not reliably measurable using conventional ELISA.[94,211]

However, MSD remains a bulk assay and cannot differentiate vesicular contents from co-isolated contaminants. Although it offers improved sensitivity, the requirement for specialised plates, dedicated MSD SECTOR instrument, and proprietary reagents poses cost and accessibility challenges.

1.4.3 Proximity extension assay

Proximity extension assay (PEA), exemplified by the Olink platform, offers sub-pg/mL sensitivity and high-throughput multiplexed detection. It employs antibody pairs conjugated to

oligonucleotides that generate a unique DNA sequence upon proximity binding to the same protein. This sequence is then amplified via quantitative polymerase chain reaction or next-generation sequencing, enabling sensitive detection of hundreds to thousands of analytes from sample volumes below 5 μL.

PEA has been successfully used in EV applications,[212] including the profiling of over 5000 proteins in CSF EVs, which revealed CNS-enriched signatures and identified novel biomarker candidates.[213] Similarly, studies of plasma nEVs in AD have reported altered levels of neurology-related and inflammatory proteins.[214]

However, PEA provides relative quantification (normalized protein expression) rather than an absolute concentration. Interpretation thus relies on comparison across well-matched samples. Moreover, its dependence on validated antibody pairs restricts detection to pre-defined proteins, alongside the need for proprietary kits and specialised instrumentation, limits its accessibility. As with all bulk assays, free protein contamination can compromise EV specificity without rigorous upstream enrichment.

1.4.4 Single-molecule array

Simoa is a digital immunoassay that detects proteins at the single-molecule level by counting individual enzyme-labelled immunocomplexes dispersed in femtolitre-sized microwells. Each target protein binds to capture antibodies immobilised on a bead, is tagged with a detection antibody and enzyme, and is then distributed into microwells. Only beads carrying the target protein generate signal,[215] allowing quantification at sub-fg/mL sensitivity, which is 1000-fold more sensitive than ELISA.[216]

In EV research, Simoa has facilitated the detection of rare pathogenic proteins in plasma-derived nEVs.[217] For example, the technique has been combined with a protease protection strategy to specifically measure intra-vesicular α-synuclein, revealing an

enrichment of pS129-α-synuclein inside plasma nEVs.[218] Simoa has also been used to measure other neurodegeneration-related proteins, such as tau, in both plasma and CSF EVs.[219]

Despite its superior sensitivity and moderate throughput (96 samples per run), Simoa has limited multiplexing capacity (typically ≤ 4 analytes), is costly (~$500 per test), and requires large sample input (> 50 µL per analyte). Moreover, like other bulk assays, it depends on rigorous EV isolation to ensure signal specificity.

1.4.5 Microfluidic platforms

Microfluidic platforms miniaturise and integrate EV isolation, labelling, and detection into a single chip-based device. These technologies are particularly advantageous in settings requiring high sensitivity, multiplexing, and small input volumes. Immunoaffinity-based microfluidic systems such as ExoSearch have enabled detection of tumour markers (e.g. EpCAM, CD24) in EVs isolated from < 30 µL of plasma, with diagnostic performance comparable to conventional platforms.[140]

More recently, droplet-based microfluidics have enabled single-EV analysis at ultrahigh throughput, facilitating the detection of rare EV subpopulations in complex biofluids.[220-223] These systems use bead-based EV capture, *in situ* labelling, and droplet compartmentalisation to quantify protein content with a limit of detection (LOD) of ~100 EVs/µL.[221] These systems offer ultrasensitive, multiplexed EV detection in complex medium, facilitating the potential for diverse clinical diagnostics.

However, current platforms typically offer single-sample throughput and allow only limited multiplexing (1 – 4 analytes). Additionally, they often require customised engineering, including surface functionalization and microfabrication. As most platforms are still in prototype stage and not standardised or commercially available, their immediate scalability for large cohorts or clinical adoption is limited.

1.4.6 Super-resolution microscopy

Super-resolution techniques, such as direct Stochastic Optical Reconstruction Microscopy (dSTORM) and DNA Point Accumulation for Imaging in Nanoscale Topography (DNA-PAINT), enable visualization and co-localisation of protein markers on individual EVs at nanometre resolution.

These methods have revealed spatial distributions of EV surface markers. For example, dSTORM imaging identified ATP1A3 as a marker for isolating nEVs and showed increased colocalisation with Aβ on the EVs isolated from plasma of AD patients, providing insights into nEV biomarker discovery.[193] DNA-PAINT has also been applied to profile EV surface proteins, using barcoded DNA strands to multiplex up to 10 markers per EV.[224] Such capabilities make them uniquely powerful tools for detailed single-EV biomarker profiling, complementing bulk approaches.

Although highly informative, these methods are low-throughput, time-intensive, and reliant on specialised expertise and equipment. Imaging hundreds of EVs can take hours, and quantitative readouts are often limited to relative frequencies. Moreover, sample preparation must preserve epitopes and vesicle morphology, while analysis requires advanced image processing expertise. Therefore, they are best suited for detailed molecular characterisation and biomarker validation, rather than high-throughput screening.

1.4.7 Nano-flow cytometry

Nano-flow cytometry (NanoFCM) extends flow cytometry to EV-sized particles (40–200 nm), enabling simultaneous analysis of EV size, concentration, and fluorescence-tagged surface markers. Unlike bulk proteomics, it provides single-vesicle resolution and allows rapid profiling of thousands of EVs from small volumes without prior isolation.[225]

A recent study applied NanoFCM to profile multiple tau protein variants on EVs in 10 µL of AD plasma, achieving excellent diagnostic accuracy (AUC = 0.99).[226] Similar strategies could be applied to PD biomarker (e.g. co-staining of L1CAM with different α-synuclein species) to evaluate the distribution of α-synuclein species across EV subpopulations.

However, its multiplexing capability remains constrained by available fluorescence channels, and distinguishing EVs from background particles (e.g. protein aggregates, lipoproteins) requires stringent gating and calibration. Additionally, instrumentation remains relatively specialised, limiting widespread access.

Technology	**Sensitivity (LOD)**	**Multiplexing capacity**	**Throughput**	**Key Advantages**	**Limitations**
Western blot	1-10 ng/mL	Low (1-4 targets/blot)	Low (up to 20 samples/run)	Standardized protocols, low cost	Semi-quantification, low sensitivity, long hands-on time
ELISA	1-100 pg/mL	Low (singleplex)	Medium (96 samples/run)	Standardized protocols, cost-effective	Limited multiplexing, low sensitivity
MSD	~0.1-10 pg/mL	High (up to 10-plex/well)	Medium–High (96 samples × 10 analytes/run)	High sensitivity, low sample volume	Bulk measurement, specialised instrument, high cost
PEA	Sub-pg/mL	Very high (up to 3072-plex panels)	Very high (384 samples × 3072 analytes/run)	Ultrasensitive, ultrahigh multiplexing, minimal volume	Relative quantification, specialised instrument, high cost

Simoa	Sub-fg/mL	Medium (up to 4-plex)	Medium (96 samples × 4 analytes/run)	Ultrasensitive, wide dynamic range	Limited multiplexing, specialised instrument, high cost
Microfluidic platforms	0.001 -10 pg/mL (platform-dependent)	Low to Medium (platform-dependent)	Low (usually 1 sample/run)	Integration of EV capture and detection, single-EV resolution, minimal volume	Complex fabrication, not standardised, scalability
Super-resolution microscopy	Single molecule	Low (1-3 targets/ session)	Very low (10^2-10^4 EVs/sample)	Nanoscale spatial resolution, single-EV resolution	Relative quantification, highly specialised equipment and analysis, lengthy acquisition
NanoFCM	Single EV detection	Medium (Up to 6-plex, fluorescent channel-dependent)	Low (10^4-10^5 EVs/run)	Simultaneous size and protein analyses, no need for prior EV isolation	Relative quantification, highly specialised equipment, calibration

Table 1.2: Comparative analysis of EV protein detection technologies. Abbreviations: LOD = limit of detection; MSD = Meso Scale Discovery; PEA = proximity extension assay; Simoa = single molecule array; dSTORM = direct Stochastic Optical Reconstruction Microscopy; NanoFCM = nanoscale flow cytometry.

1.5 Thesis aims and objectives

PD diagnosis currently relies on the manifestation of motor symptoms, which typically emerge only after significant dopaminergic neuron loss. This diagnostic latency underscores the urgent need for biomarkers capable of detecting early pathological changes, stratifying at-risk individuals, and monitoring disease progression. EVs, particularly nEVs, have emerged as

promising minimally invasive biomarkers. nEVs carry neuron-specific cargo, remain stable in peripheral fluids, and can provide molecular insight into CNS pathology. However, challenges persist, including the specific isolation of nEVs from serum, methodological standardisation across laboratories, and detection of disease-relevant α-synuclein at low abundance.

This thesis aims to bridge these gaps by integrating advanced EV isolation methods, multicentre clinical validation, and novel microfluidic technologies to establish L1EVs as a clinically useful and biologically informative biomarker source in PD. The work is structured around four key objectives:

1. **Optimisation of serum nEV isolation for α-synuclein biomarkers**
    - Develop a robust Capto Core multimodal chromatography protocol to separate EVs from serum contaminants.
    - Validate L1CAM as a reliable marker for nEV isolation.
    - Quantify α-synuclein levels in both free and EV-associated fractions obtained through multimodal chromatography.
2. **Identification of serum L1EV α-synuclein as a biomarker for individuals at risk of developing PD**
    - Assess the diagnostic accuracy of serum L1EV α-synuclein in identifying high-risk individuals, including those with iRBD, hyposmia, and *GBA1* mutation carriers.
    - Validate assay performance and reproducibility across multicentric cohorts.
    - Investigate correlations between L1EV α-synuclein levels, dopaminergic neurodegeneration, CSF α-synuclein SAA results, and clinical progression.
    - Examine the performance of L1EV α-synuclein as a biomarker in *LRRK2* non-manifest carriers (NMC) and *LRRK2* PD patients.

3. **Development of a droplet-based microfluidic platform for single-EV membrane-associated protein detection**
    - Develop a droplet-based microfluidic assay for high-throughput, single-EV detection of membrane-associated proteins.
    - Demonstrate the pathological relevance of EV surface α-synuclein using cellular models, including neuroblastoma cells expressing PD-associated α-synuclein mutants and iPSC-derived dopaminergic neurons.
    - Evaluate the clinical utility of this platform in differentiating prodromal and clinical PD patients from healthy controls.
4. **Investigation of serum p-tau 217 and NfL as predictive biomarkers for cognitive decline and phenoconversion**
    - Assess whether serum p-tau217 and NfL reflect early cognitive and motor dysfunction in iRBD and stratifies risk for progression to PD-MCI or DLB.
    - Compare the predictive performance of serum p-tau217 and NfL for disease conversion and assess whether their combination improves prognostic accuracy.
    - Determine the relationship between biomarker levels and specific clinical features.

By fulfilling these objectives, this thesis provides critical insights into the clinical relevance of nEVs in PD. Through the integration of advanced isolation protocols, clinical validation, and innovative detection technologies, it establishes a translational framework for the deployment of blood-based EV biomarkers, particularly L1CAM+ nEVs, as minimally invasive tools for early-stage diagnosis, risk stratification, and longitudinal disease surveillance.

Chapter 2

Material and Methods

2. Material and methods

2.1 Key resources table

REAGENT or RESOURCE	SOURCE	IDENTIFIER
Antibodies		
Anti-CD9 antibody (MM2/57)	Millipore	Cat# CBL162; RRID:AB_2075914
Anti-CD171 (L1CAM) antibody (UJ127)	Thermo Fisher Scientific	Cat# MA5-14140; RRID:AB_10979034
Anti-α-synuclein antibody (Syn1)	BD Biosciences	Cat# 610787; RRID:AB_398108
Anti-ATP1A3 antibody (XVIF9-G10)	Thermo Fisher Scientific	Cat# MA3-915; RRID:AB_2274447
Anti-CD56 (NCAM) antibody	Thermo Fisher Scientific	Cat# MA5-11563; RRID:AB_10985168
Biotin anti-CD81 antibody (M38)	Abcam	Cat# ab239238; RRID:AB_3665509
Biotin anti-CD11b antibody (ICRF44)	Thermo Fisher Scientific	Cat# 13-0118-82; RRID:AB_466368
Biotin anti-CD171 (L1CAM) antibody (UJ127)	Thermo Fisher Scientific	Cat# MA5-14137; RRID:AB_10990347
Biotin anti-CD56 (NCAM) antibody	Thermo Fisher Scientific	Cat# 13-0567-82; RRID:AB_10596499
Biotin anti-α-synuclein antibody (LB509)	BioLegend	Cat# 807710; RRID:AB_2832855

Biotin anti-α-synuclein aggregated antibody (A17183A)	BioLegend	Cat# 864906; RRID:AB_2832869
Anti-Syntenin1 antibody (EPR8102)	Abcam	Cat# ab236071; RRID:AB_3675524
Anti-SDCBP (syntenin-1) antibody	Abnova	Cat# PAB7132; RRID:AB_1580423
Anti-CD81 antibody (EPR4244)	Abcam	Cat# ab109201; RRID:AB_10866464
Anti-CD63 antibody (Ts63)	Thermo Fisher Scientific	Cat# 10628D; RRID:AB_2532983
Anti-Flotillin-1 antibody	BD Biosciences	Cat# 610820; RRID:AB_398139
Anti-α-synuclein (phospho S129) antibody	Abcam	Cat# ab51253; RRID:AB_869973
Anti-Calnexin antibody	Abcam	Cat# ab22595; RRID:AB_2069006
Anti-GAPDH antibody	Abcam	Cat# ab9485; RRID:AB_307275
Anti-Tubulin β 3 (Tuj1) antibody	BioLegend	Cat# 801201; RRID:AB_2313773
Goat anti-mouse IgG (H+L) secondary antibody, HRP	Thermo Fisher Scientific	Cat# 31430; RRID:AB_228307
Goat anti-rabbit IgG (H+L) secondary antibody, HRP	Thermo Fisher Scientific	Cat# 31460; RRID:AB_228341

Alexa Fluor 647 anti-CD9 antibody	EXBIO Praha	Cat# A6-208-T100; RRID:AB_10733480
FITC anti-CD81 antibody	Thermo Fisher Scientific	Cat# A15753; RRID:AB_2534533
Anti-α-synuclein antibody (MJFR1)	Abcam	Cat# ab138501; RRID:AB_2537217
Anti-aggregated-α-synuclein antibody (5G4)	Millipore	Cat# MABN389; RRID:AB_2716647
Anti-CD171 (L1CAM) antibody (5G3)	Thermo Fisher Scientific	Cat# 14-1719-82; RRID:AB_891383
Anti-Tetraspanin Trio antibody	ONI (EV profiler kit 2)	Cat# 800-00113
Anti-MAP2 antibody	Abcam	Cat# ab5392; RRID:AB_2138153
Goat anti-mouse IgG (H+L) secondary antibody, Alexa Fluor 568	Thermo Fisher Scientific	Cat# A-11004; RRID:AB_2534072
Goat anti-chicken IgY (H+L) secondary antibody, Alexa Fluor 647	Thermo Fisher Scientific	Cat# A-21449; RRID:AB_2535866
Bacterial and virus strains		
pLV-eGFP	Gift from Pantelis Tsoulfas	RRID:Addgene_36083
psPAX2	Gift from Didier Trono	RRID:Addgene_12260
pMD2.G	Gift from Didier Trono	RRID:Addgene_12259
Biological samples		
Human serum samples	This study	NA
Chemicals, peptides, and recombinant proteins		
LDN193189 hydrochloride	Sigma	Cat# SML0559

A83-01	Tocris	Cat# 2939
Recombinant mouse sonic hedgehog/Shh (C25II)	R&D Systems	Cat# 464-SH-200
Purmorphamine	Tocris	Cat# 4551
Recombinant human FGF-8a protein	Tocris	Cat# 4745-F8
CHIR 99021	Tocris	Cat# 4423
Human/mouse/rat BDNF recombinant protein	PeproTech	Cat# 450-02
Human GDNF recombinant protein	PeproTech	Cat# 450-10
Human TGF-beta 3 recombinant protein	Thermo Fisher Scientific	Cat# PHG9305
DAPT	Tocris	Cat# 2634
L-Ascorbic acid	Sigma	Cat# A4403
Dibutyryl cAMP sodium salt	Sigma	Cat# AD0627
Mouse laminin	Sigma	Cat# L2020
MES hydrate	Sigma	Cat# M8250
N-(3-Dimethylaminopropyl)-N′-ethylcarbodiimide hydrochloride (EDC)	Sigma	Cat# 03450
N-Hydroxysuccinimide (NHS)	Sigma	Cat# 130672
TWEEN® 20	Sigma	Cat# P7949
Streptavidin β-galactosidase (SβG) conjugate	Thermo Fisher Scientific	Cat# S931
Mineral oil	Sigma	Cat# M5904
Triton™ X-100	Sigma	Cat# T8787
Fluorescein Di-β-D-Galactopyranoside (FDG)	Thermo Fisher Scientific	Cat# F1179

Glycine	Sigma	Cat# G7126
Tris buffer	Sigma	Cat# 648314
Paraformaldehyde	Sigma	Cat# 158127
2% uranyl acetate solution	Electron Microscopy Sciences	Cat# 22400-2
Polybrene®	Santa Cruz Biotechnology	Cat# sc-134220
Critical commercial assays		
Pierce™ BCA Protein Assay Kit	Thermo Fisher Scientific	Cat# 23225
U-PLEX human α-synuclein kit	Meso Scale Discovery	Cat# K151WKK-2
R-PLEX human CD81 (EV Antibody Set	Meso Scale Discovery	Cat# F215N-3
S-PLEX Human Tau (pT217) assay	Meso Scale Discovery	Cat# K151APFS-2
R-PLEX Human Neurofilament L Antibody Set	Meso Scale Discovery	Cat# F217X-3
MSD GOLD 96-well Small Spot Streptavidin SECTOR Plate	Meso Scale Discovery	Cat# L45SA-1
U-PLEX development pack, 96-well 2-assay sector plate	Meso Scale Discovery	Cat# K15227N-2
Experimental models: Cell lines		
Human induced pluripotent stem cells (iPSCs)	This study	NA
SH-SY5Y	ATCC	RRID:CVCL_0019
Software and algorithms		
AutoCAD	Autodesk	https://www.autodesk.com/products/autocad/; RRID:SCR_021072

NIS-Elements	Nikon	https://www.nikoninstruments.com/Products/Software/; RRID:SCR_014329
Fiji Image J	GNU General Public License	https://imagej.net/software/fiji/; RRID: SCR_002285
CODI	ONI	https://alto.codi.bio/
GraphPad Prism	GraphPad Software	http://www.graphpad.com/; RRID:SCR_002798
SPSS	IBM	http://www-01.ibm.com/software/uk/analytics/spss/; RRID:SCR_002865
Biorender	Biorender	www.biorender.com/; RRID:SCR_018361
Other		
poly(carboxybetaine methacrylate) (pCBMA) beads	This study	NA
mTeSR™1	Stem Cell Technologies	Cat# 85857
Versene solution	Thermo Fisher Scientific	Cat# 15040066
Geltrex™ LDEV-free reduced growth factor basement membrane matrix	Thermo Fisher Scientific	Cat# A1413202
DMEM - high glucose	Sigma	Cat# D5671
Fetal Bovine Serum (FBS)	Sigma	Cat# F7524
MEM Non-Essential Amino Acids Solution (100X)	Thermo Fisher Scientific	Cat# 11140050

GlutaMAX™ Supplement	Thermo Fisher Scientific	Cat# 35050061
Antibiotic-Antimycotic (100X)	Thermo Fisher Scientific	Cat# 15240062
TrypLE™ Express Enzyme (1X), phenol red	Thermo Fisher Scientific	Cat# 12605036
Halt™ protease and phosphatase inhibitor cocktail	Thermo Fisher Scientific	Cat# 78444
Encapsulated superparamagnetic microspheres polymer-COOH (Blue)	Bangs Laboratories	Cat# MEGB002
Encapsulated superparamagnetic microspheres polymer-COOH (Red)	Bangs Laboratories	Cat# MEFR002
Bovine serum albumin (BSA)	Sigma	Cat# A7030
EZ-Link™ Micro Sulfo-NHS-LC-Biotinylation Kit	Thermo Fisher Scientific	Cat# 21935
MSD gold Sulfo-tag-NHS-Ester conjugation pack	Meso Scale Discovery	Cat# R31AA-1
SU-8 3025 Permanent negative epoxy photoresist	Kayaku	Cat# SU-8 3025
SYLGARD™ 184 Silicone Elastomer Kit	Dow-Corning	Cat# PDMS184
RIPA lysis and extraction buffer	Thermo Fisher Scientific	Cat# 89901
Amersham ECL prime western blotting detection reagent	Cytiva	Cat# RPN2232
HBSS	Thermo Fisher Scientific	Cat# 88284
Alexa Fluor® 647Conjugation Kit (Fast) - Lightning-Link®	Abcam	Cat# 269823

Alexa Fluor® 488 Conjugation Kit (Fast) - Lightning-Link®	Abcam	Cat# 236553
NEBuilder® HiFi DNA Assembly Master Mix	New England Biolabs	Cat# E2621S

Table 2.1: Key resources table. Summary of key resources and reagents used in this thesis.

2.2 Human samples

2.2.1 Serum sample acquisition

Blood samples from all centres were collected during the patient assessment. Serum was isolated, aliquoted, and frozen at -80°C until further use. Written informed consent was obtained from all participants, and the procedures adhered to the Declaration of Helsinki and were approved by the respective ethics committees at each site. All samples were sent on dry ice, processed in a blinded manner at Oxford, and underwent only one freeze-thaw cycle.

2.2.2 Serum processing

For EV isolation, a three-step sequential spin (300 ×g for 10 min, 2,000 ×g for 20 min, and 10,000 ×g for 30 min) was used to remove cellular debris, proteins aggregates, and fatty material in the serum. The supernatant (i.e. precleared serum) was transferred to protein low-binding tubes (0030108450, Eppendorf) for subsequent EV isolation.

2.2.3 Clinical assessments

All subjects were assessed clinically as part of on-going research programmes, including the updated prodromal MDS criteria[59] using MDS-UPDRS-I and -III, Scale for Outcomes in Parkinson's disease for Autonomic Symptoms (SCOPA-AUT), and Montreal Cognitive Assessment (MoCA). All iRBD were confirmed by video-assisted PSG. Possible RBD was defined based on RBD screening questionnaire (RBDSQ) score ≥ 5. Subthreshold

parkinsonism was confirmed based on MDS-UPDRS-III > 6 excluding postural and action tremor. Constipation, excessive daytime somnolence, symptomatic OH, urinary dysfunction, and depression were defined by MDS-UPDRS-I. Erectile dysfunction was determined based on SCOPA-AUT. Cognitive deficit was defined as MoCA score < 26. Hyposmia was defined as identification scores < 10th centile (score < 10 for age >55 years and < 13 for those aged between 36-55) on Sniffin' Sticks test, in the Oxford and Cologne cohorts; as a threshold/discrimination/identification (TDI) score ≤26 in the Marburg cohort,[227] and as a ≤ 15th percentile score on the University of Pennsylvania Smell Identification Test (UPSIT), corrected for age and sex, in the PPMI cohort. DaT SPECT imaging was acquired using standard protocol. Classification of DaT SPECT imaging as normal or abnormal was based on the descriptive reports by expert nuclear medicine radiologists, who were blinded to all clinical data other than age and sex, or on previously described quantitative measures. The age- and sex-adjusted LR for prodromal PD was calculated using the updated MDS research criteria.[59] This was conducted by multiplying all available LR for each of the prodromal marker as recommended by the MDS task force. Total LR was then combined with estimated age-adjusted probability to calculate the final post-test probability for each individual. A positive LR was defined as a probability of having prodromal PD ≥ 80%.

2.3 EV isolation

2.3.1 Capto Core multimodal chromatography

One mL of precleared serum or conditioned media (CM) was loaded onto a HiScreen Capto Core 700 prepacked filtration column (17548115, Cytiva). This column utilizes bead-based multimodal chromatography, in which an inert outer shell excludes macromolecules above ~700 kDa, while an active octylamine-functionalised core binds smaller contaminants through combined hydrophobic and electrostatic interactions. The column has a bed height of

150 mm and a volume of 4.7 mL. Elution was performed using PBS at a flow rate of 1 mL/min, with ten 1-mL fractions collected. Bound impurities are removed from the beads using a cleaning-in-place program with washing in 23.5mL of 1M NaOH in 30% isopropanol, followed by 23.5 mL of distilled water.

2.3.2 Ultracentrifugation

Samples were centrifugated using a SW60Ti rotor (L-100 XP, Beckman Coulter) at 120,000 ×g for 2 h. The supernatant (i.e. EV-depleted serum) was collected and the pellets (i.e. EV enriched fraction) were resuspended in PBS containing protease and phosphatase inhibitor cocktail, then stored at -80℃ until further use.

2.3.3 Immunocapture of EVs from serum

Immunocapture of specific EVs was performed using our previously developed and extensively validated direct immunocapture assay with minor modifications.[94,95] Briefly, 0.25 mL of precleared serum or 1 mL of chromatography fractioned serum was mixed with anti-L1CAM (MA5-14140, Thermo Fisher Scientific), anti-CD9 (CBL162, Millipore), anti-ATP1A3 (MA3-915, Thermo Fisher Scientific), or anti-NCAM1 antibodies (MA5-11563, Thermo Fisher Scientific) antibodies pre-conjugated to poly(carboxybetaine methacrylate) (pCBMA)-coated beads that were generated to reduce non-specific adsorption.[228] The immunobeads were incubated with samples at 4°C overnight on a rotating mixer. Bead-EVs complexes were then collected by magnetic separation and washed sequentially with 0.05% Tween-20 in PBS, followed by PBS alone. EVs were extracted in batches with disease and control samples distributed across each batch, followed by sample blinding.

2.4 EV characterisation

2.4.1 EV protein extraction

EVs isolated using UC or immunocapture were lysed in ice-cold radioimmunoprecipitation assay (RIPA) buffer supplemented with protease and phosphatase inhibitor cocktail. The lysates were collected after incubation for 30 min at room temperature with vigorous shaking at 1,000 RPM. Protein concentrations were measured with a BCA assay (23225, Thermo Fisher Scientific).

Each of the fraction obtained from multimodal chromatography was loaded onto an Amicon Ultra-0.5 centrifugal filter unit with Ultracel-10 membrane (UFC501096, Millipore) and concentrated to a final volume of 10 µL by repeated centrifugation at 14,000 ×g. The concentrate was then collected and processed for protein extraction and subsequently subjected to immunoblotting or MSD assays.

For EV protein quantification using the MSD assays, EVs were lysed in 1% triton X-100 in PBS containing protease and phosphatase inhibitor cocktail. Lysates were collected after incubation for 30 min at room temperature with vigorous shaking at 1,000 RPM.

2.4.2 Immunoblotting

The denatured and reduced samples were resolved by sodium dodecyl sulfatepolyacrylamide-polyacrylamide gel electrophoresis using NuPAGE 4 to 12% bis-tris gels and transferred to nitrocellulose membrane using the iBlot 2 Gel Transfer system (IB21001, Thermo Fisher Scientific). The membranes were incubated with primary antibodies overnight at 4°C. The following primary antibodies were used: anti-CD81 (1:1000, ab109201, Abcam), anti-CD63 (1:1000, 10628D, Thermo Fisher Scientific), anti-CD9 (1:1000, CBL162, Millipore), anti-Flotillin-1 (1:1000, 610820, BD Biosciences), anti-Syntenin1 (1:500, ab236071, Abcam), anti-L1CAM (1:1000, MA5-14140, Thermo Fisher Scientific), anti-

ATP1A3 (1:1000, MA3-915, Thermo Fisher Scientific), anti-α-synuclein (1:1000, 610787, BD Biosciences), anti-pS129-α-synuclein (1:2000, ab51253, Abcam), anti-Calnexin (1:2000, ab22595, Abcam), anti-GAPDH (1:2000, ab9485, Abcam), and anti-Tuj1 (1:10000, 801201, BioLegend). The relevant protein bands were detected using horseradish peroxidase-conjugated goat anti-mouse IgG (1:5000, 31430, Thermo Fisher Scientific) or horseradish peroxidase-conjugated goat anti-rabbit IgG (1:5000, 31460, Thermo Fisher Scientific), followed by Amersham enhanced chemiluminescence prime detection reagent (RPN2232, Cytiva). Blots were imaged on a Bio-Rad ChemiDoc imaging system.

2.4.3 Nanoparticle tracking analysis

To measure EV concentrations, EV preparations were serially diluted in PBS (1:100 to 1:20,000) to bring the concentration of EVs within the operating dynamic range of NTA. The appropriate dilution was injected into the NTA observation chamber using a syringe. Videos capturing the Brownian motion of particles were recorded to determine the number and size distribution of particles. NTA was conducted using the NS300 nanoparticle analyser (NanoSight). Camera settings were maintained between levels 8 – 12 with automatic adjustments for all post-acquisition parameters except for the detection threshold, which was set at 5. For each sample, three 30-second videos were recorded with a 5-second intermission, using the script control function.

2.4.4 Transmission electron microscopy

TEM was used to examine the shape, size, and morphology of EVs. Specifically, EVs isolated from serum or CM using either anti-CD9 or anti-L1CAM-coated beads were eluted by adding 25 µL of glycine solution (100 mM, pH 2.8; G7126, Sigma) to the beads, followed by gentle shaking at 300 RPM for 30 min at room temperature. After incubation, the eluate was neutralised by adding 25 µL of pH 8.0 Tris buffer (648314, Sigma), then fixed with 2 µL of 4 %

paraformaldehyde. Then, 10 µL of resultant eluent samples was applied to freshly glow-discharged carbon formvar 400 mesh copper grids (D400FC, Electron Microscopy Sciences) and incubated for 50 min. Grids were blotted with filter paper from the side and stained with 2% uranyl acetate (22400-2, Electron Microscopy Sciences) for 10 seconds. Excess stain was removed by blotting and grids were air-dried. Imaging was performed on a TEM (JEM-1400Flash, JEOL) operated at 120 kV using a Gatan Rio CMOS camera.

2.5 Protein measurements

Electrochemiluminescence was performed in 96-well MSD R-Plex or U-Plex plates (K15227N-2, MSD). Antibody pairs for α-synuclein were provided by MSD and pre-conjugated with biotin and ruthenium tags (K1515NR-2, MSD). For capture, the assay utilises the rabbit monoclonal antibody MJFR1 (Abcam) which binds to α-synuclein amino acids 118 – 123 with similar binding to monomeric or aggregated forms of α-synuclein.[229] For detection, a MSD proprietary mouse monoclonal antibody was used. This antibody pair has been cross-validated for the detection of total plasma α-synuclein against other immunoassay platforms.[230] The MJFR1 antibody was previously validated by our group for the detection of serum L1EV α-synuclein using electrochemical assays.[228]

Antibody pairs for CD81 were also supplied by MSD and pre-conjugated with biotin and ruthenium tags (K1515NR-2, MSD). For the detection of syntenin-1, an additive-free goat polyclonal anti-syntenin-1 antibody (PAB7132, Abnova) conjugated with biotin using a biotinylation kit (21935, Thermo Fisher Scientific), while a rabbit monoclonal anti-syntenin-1 antibody (ab236071, Abcam) conjugated with ruthenium using sulfo-tag conjugation kit (R31AA-1, MSD) for detection.

2.6 Statistical analysis

For multiple comparisons, I performed non-parametric statistical testing where the data were not normally distributed: Kruskal-Wallis one-way analysis of variance with the Dunn test for post hoc comparison between individual pairings when there were three or more independent groups and Mann-Whitney U test when there were only two independent groups. For normally distributed data, comparisons between two groups were analysed using Student's two-tailed t-test; comparisons among three or more groups were performed with ordinary one-way ANOVA. Data from different groups were analysed using ROC analysis with 95% confidence intervals (CIs; 2.5% to 97.5%). The optimum threshold was determined by the Youden index, i.e. the value associated with the maximal value of sensitivity + specificity − 1. The age- and sex-adjusted LR for prodromal PD was calculated using the updated MDS research criteria.[59] Within each cohort, Student's t-test or one-way ANOVA was used to compare age, and Pearson $\chi 2$ to compare sex frequency between groups. Biomarkers concentrations were log-transformed to improve the distribution in group comparisons for assessing demographic differences in biomarkers across study populations using linear regression models. Linear regression models adjusted for age and sex were used to assess associations between biomarkers and available prodromal markers. Logistic regression adjusted for age and sex was performed to determine the optimal biomarker combination for subgroup discrimination. Correlations between biomarkers and clinical measures were calculated using Pearson correlation when data were normally distributed or Spearman correlation when data were not normally distributed, age and sex adjusted partial correlation was performed when applicable. To study associations between biomarkers and risk of phenoconversion, Cox regression was performed. Biomarkers were first considered individually while adjusting for age at time of sampling and sex. Secondly, multivariable regression was fitted adjusting for age and sex, and mutually adjusting biomarkers for each

other. Kaplan-Meier curves were plotted stratifying individuals according to biomarker levels using derived cut-offs or quartiles. Hazard ratios (HR) with respect to the reference group were derived using Cox regression, Schoenfeld residuals were assessed to check the proportional hazards assumption. Values with $P < 0.05$ were regarded as significant. The robust regression and outlier removal method was applied to test for outliers in the measurements. Statistical analyses were performed using SPSS version 29.0 (IBM), Prism version 10.2.3 (GraphPad), and R version 4.1.1 (R Foundation).

Chapter 3

Methodological considerations in neuronal EV isolation for α-synuclein biomarkers

Adapted from Yan et al. *Brain 2023;* 146(11): e95-e97

3. Methodological considerations in neuronal EV isolation for α-synuclein biomarkers

3.1 Introduction

3.1.1 Limitations in blood EV-associated α-synuclein biomarkers

Peripheral biofluids such as serum and plasma offer a clinically scalable substrate for biomarker discovery in PD. However, despite extensive interest, the quantification of total α-synuclein in unfractionated blood has yielded conflicting results across studies.[160] This inconsistency is largely due to the fact that the vast majority of blood α-synuclein exists in a free form, mainly derived from peripheral sources such as red blood cells, rather than reflecting CNS pathology.[231] As a result, measurements of total plasma or serum α-synuclein lack diagnostic specificity and are confounded by sample handling artefacts such as haemolysis.

A particular challenge in EV biomarker research is the isolation of neuronally derived molecules from complex peripheral fluids. In this context, α-synuclein presents an important analytical problem. Free α-synuclein is prone to aggregation and non-specific binding to various surfaces, including magnetic beads and polymers such as PEG, which are often used in EV isolation kits such as ExoQuick. Therefore, the use of ExoQuick in studies of EV-associated α-synuclein is likely to confound the results due to non-specific precipitation of free circulating α-synuclein monomers and/or oligomers. Thus, refining EV isolation strategies is essential to accurately differentiate EV-associated from free α-synuclein in blood.

3.1.2 L1CAM and nEV biomarkers

To address these limitations, the field has increasingly focused on the enrichment of nEVs from biofluids using immunocapture methods targeting the neuronal antigen L1CAM.

L1CAM is predominantly expressed in neurons and has been widely adopted as a surrogate marker for neuronal origin in EV studies. Immunocapture using anti-L1CAM antibodies enables selective enrichment of nEVs from bulk EV populations, providing an opportunity to study neuronally derived biomarkers like α-synuclein.[232]

Nevertheless, the specificity of L1CAM as an EV marker has been contested.[188] Despite this, evidence from multiple independent groups,[194,196,210,233-235] including our work,[93-95] has demonstrated that EVs can be isolated using anti-L1CAM antibodies,[94,228] and that α-synuclein levels measured from L1EVs can reliably distinguish PD from both healthy controls and MSA.[94,95] Alternative nEV markers, such as ATP1A3[193] and NCAM1,[236] have been proposed, yet they remain less well-characterised and are not yet broadly adopted.

3.1.3 Need for methodological standardisation

Despite accumulating evidence supporting the utility of serum and plasma L1EV α-synuclein as a biomarker for PD, methodological discrepancies undermines inter-study comparability. Differences in isolation methods, detection platforms, and handling protocols can yield divergent quantitative results. Of particular concern is the widespread use of polymer-based precipitation kits, which, while convenient, may introduce significant background noise. For instance, a study employing ExoQuick reported substantially higher L1EV α-synuclein concentrations (2000 – 3500 pg/mL),[237] which is substantially higher than the threshold value (∼10 – 15 pg/mL) that was previously shown to separate PD from healthy controls by our group and others.[94,95,194,233] Notably, studies using ExoQuick in EV isolation from serum or plasma are inconsistent in absolute L1EV α-synuclein concentrations and reported relatively high levels (**Table S3.1**).[210,235,237]

To enhance the specificity and reproducibility of the EV isolation, our group previously developed pCBMA-coated magnetic beads, which resist non-specific binding of abundant

serum proteins, including free α-synuclein.[228] In this study, I further refined the approach by incorporating Capto Core multimodal chromatography, which combines size-exclusion properties with internal binding of small contaminants, offering a gentle and effective method for separating EVs from soluble contaminants while preserving EV structure and composition. This integration offers a cleaner substrate for downstream analyses and provides a more selective strategy for isolating nEVs, thereby enabling more reliable quantification of EV-associated α-synuclein.

3.2 Aims and objectives

The overarching aim of this work is to establish a standardised workflow for isolating EVs from human serum and to investigate the association between L1EVs and α-synuclein cargo. This methodological foundation is critical for enabling accurate quantification of EV-based biomarkers in PD research. The specific objectives are to:

1. Optimise serum EV isolation using Capto Core multimodal chromatography, ensuring effective separation of EVs from abundant soluble protein contaminants.
2. Validate L1CAM and ATP1A3 as reliable markers for EV isolation by assessing their associations with generic EV proteins.
3. Quantify both free and EV-associated α-synuclein across eluted fractions to determine its enrichment in EV-associated versus free-floating protein pools.

3.3 Material and methods

3.3.1 Clinical samples

Blood samples from the Oxford Discovery cohort were collected during the patient assessment, and the serum from healthy individuals (n = 20) was isolated, aliquoted and frozen at -80°C until further use.

3.3.2 Capto Core multimodal chromatography

One mL of precleared serum was loaded onto a HiScreen Capto Core 700 prepacked filtration column (17548115, Cytiva). This column This column uses multimodal chromatography beads with an inert shell for size exclusion and a ligand-activated core that captures smaller contaminants via combined hydrophobic and electrostatic interactions. The column has a bed height of 150 mm and a volume of 4.7 mL. Elution was performed using PBS at a flow rate of 1 mL/min, with ten 1-mL collected. A cleaning-in-place program with washing in 23.5 mL of 1 M NaOH in 30% isopropanol, followed by 23.5 mL of distilled water was performed between uses.

3.3.3 Immunoprecipitation

Immunoprecipitation was performed using anti-L1CAM (MA5-14140, Thermo Fisher Scientific), anti-CD9 (CBL162, Millipore), anti-ATP1A3 (MA3-915, Thermo Fisher Scientific), or anti-NCAM1 antibodies (MA5-11563, Thermo Fisher Scientific) pre-conjugated to pCBMA-coated beads that were generated to reduce non-specific adsorption. The immunobeads were mixed with 1 mL of each tested fraction and incubated at 4°C overnight on a rotating mixer. The immunocomplexes were then collected by magnetic separation and washed sequentially with 0.05% Tween-20 in PBS, followed by PBS alone. The isolates were then collected and processed for NTA, TEM, or protein analysis by immunoblotting or MSD-based quantification.

3.3.4 Ultrafiltration

Each of the fraction was loaded onto an Amicon Ultra-0.5 centrifugal filter unit with Ultracel-10 membrane (UFC501096, Millipore) and concentrated to a final volume of 10 μL by repeated centrifugation at 14,000 ×g. The concentrate was collected and processed for protein extraction, followed by immunoblotting or MSD assays.

3.3.5 MSD electrochemiluminescence

Proteins in each eluted chromatography fraction, or L1EVs immunocaptured from EV-enriched F3 and F4, were extracted in PBS containing 1% Triton X-100, supplemented with protease and phosphatase inhibitor cocktail. α-Synuclein and CD81 levels were quantified using MSD proprietary antibody pairs (α-synuclein: K151WKK-2; CD81: K1515NR-2, MSD) in U-PLEX plates (K15227N-2, MSD).

3.4 Results

3.4.1 Isolation of EVs from the bulk of human serum proteins

I first asked whether EVs can be separated from the bulk of human serum proteins using Capto Core multimodal chromatography. To this end, Cheng Jiang (a former member of the lab) and I used a HiScreen Capto Core 700 column to separate EVs from the bulk of human serum proteins. Based on the UV spectra that measured total protein abundance, I identified a small early-elution peak, followed by a second larger peak corresponding to abundant free proteins in serum from healthy individuals (**Figure 3.1A**). Ten separate fractions (F) spanning across these two peaks (F1 to F10) were collected (**Figure 3.1B**). The stacked spectra were obtained from $n = 10$ different healthy control samples, demonstrating the high reproducibility of the fractionation process (**Figure 3.2A**). Each of these fractions were subjected to total protein measurement and UF for immunoblotting. As shown in **Figure 3.2A**, the protein abundance in each fraction was consistent with the UV spectra. I then asked whether any of these fractions are enriched in EVs based on NTA. I found that F2 to F5 were enriched in nanoparticles, with no particles detected in subsequent fractions (**Figure 3.2B**).

To further define the molecular profile of EVs detected in F2 to F5, I performed immunoblotting for CD9, a generic EV surface marker, and syntenin-1, an internal EV cargo

protein and the best available marker for exosomes, which are endosome-derived EVs. I found that based on immunoblotting, CD9 and syntenin-1 bands were enriched in F3 and F4 but not in the later fractions (**Figure 3.2C**). Thus, multimodal chromatography using the HiScreen Capto Core 700 column successfully separated EVs from the bulk of free serum proteins, with EVs eluting primarily in F3 and F4. Under these conditions, I found that most α-synuclein in serum was detected in a free form in late fractions (peaking at ~4,000 pg/mL in F7), as shown in **Figure 3.2D**. Importantly, a small amount of α-synuclein was eluted in F3 and F4, and levels in theses EV-enriched fractions were highly consistent across biological replicates (43.46 ± 19.99 pg/mL serum), despite considerable variability in the free α-synuclein in fractions F5 – F8 (4716.47 ± 4973.63 pg/ mL serum), which may reflect haemolysis or contamination from other peripheral sources. Similar results have previously been reported in plasma.[196] Parallel measurements of CD81 using the MSD assay, which is more sensitive than immunoblotting, identified this generic EV marker mostly in F3 and F4, in line with the earlier findings using immunoblotting for CD9 and syntenin-1. Thus, α-synuclein levels in the EV-enriched fractions, which include both neuronal (L1EVs) and non-neuronal EVs, are much lower than free α-synuclein in serum.

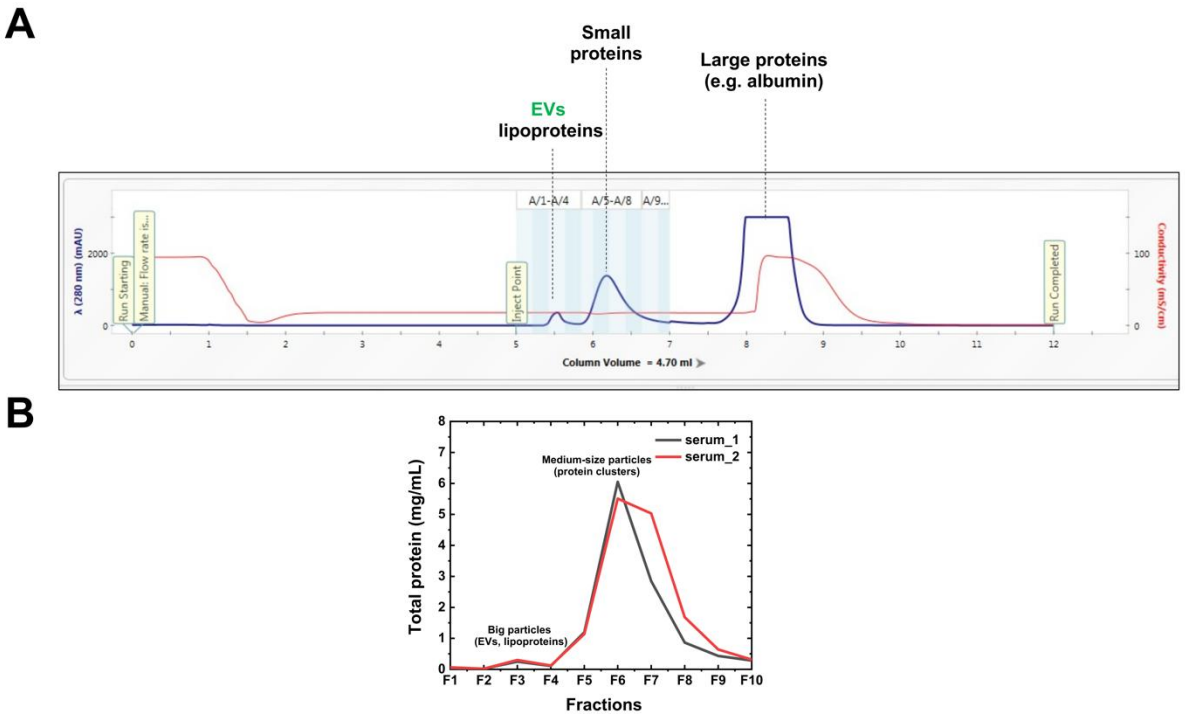


Figure 3.1: Isolation of EVs from serum using Capto Core multimodal chromatography. (**A**) The representative spectrum shows three major peaks corresponding to components eluted from human serum. The first peak reflects large particles, including EVs and lipoproteins. The second peak represents medium-sized components, which includes proteins such as L1CAM and α-synuclein. The final saturated peak corresponds to highly abundant large proteins such as albumin. (**B**) Quantification of total protein content in F1 to F10 measured from serum of n = 2 healthy individuals were tested. Experiments in panel **B** were performed by Cheng Jiang.

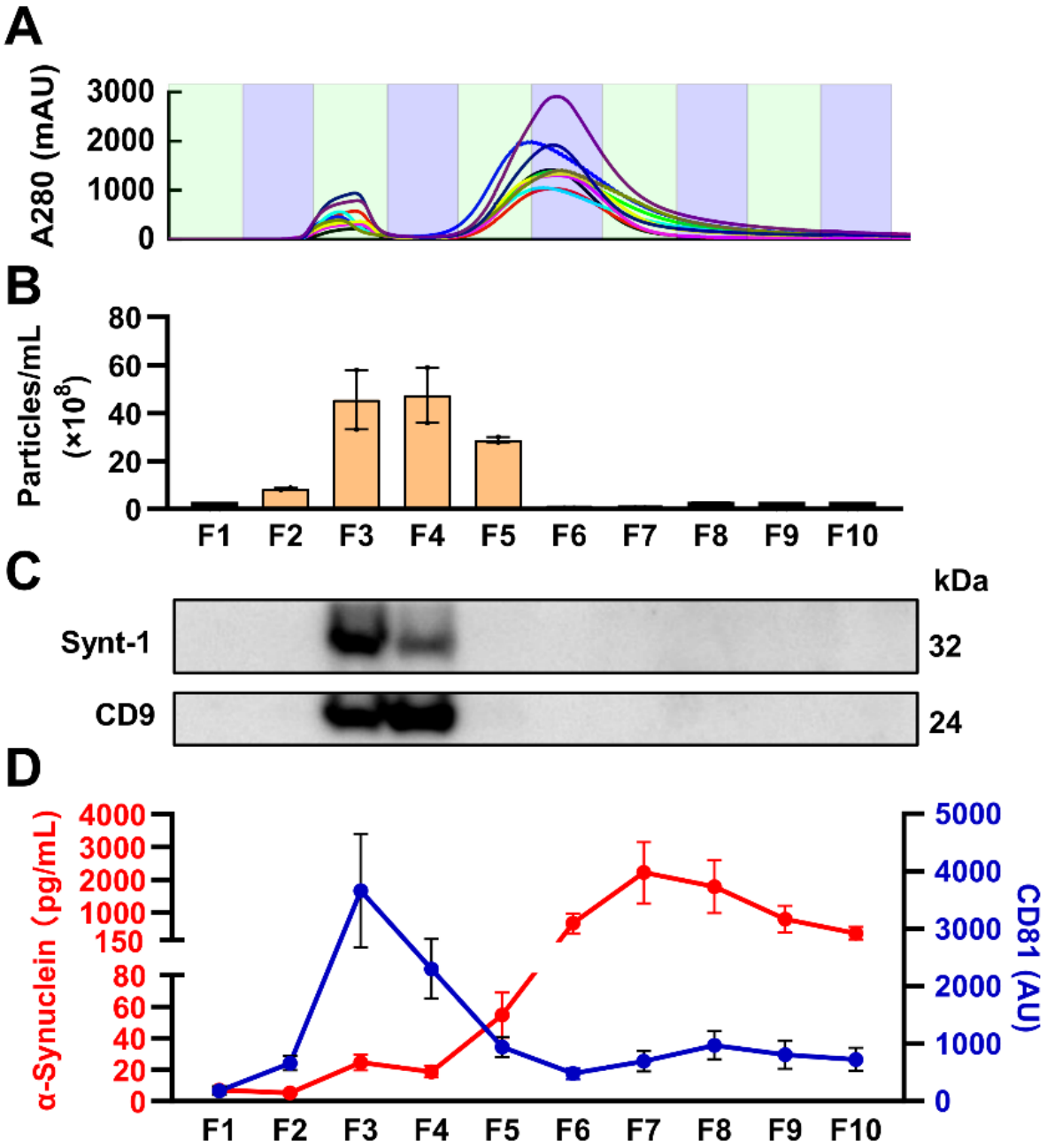


Figure 3.2: α-Synuclein concentration in total EVs isolated from serum by Capto Core multimodal chromatography. (**A**) Chromatography spectra of 10 eluted fractions (F) from 1 mL of serum. (**B**) The number of particles were measured in each fraction using nanoparticle tracking analysis. (**C**) Immunoblotting for syntenin-1 (Synt-1) and CD9 in each fraction after total protein concentration using ultrafiltration. (**D**) Profiling of each unprocessed fraction with duplexed MSD assay demonstrates that CD81 is detected in early fractions, which also contain very low levels of α-synuclein (< 50 pg/mL), whereas later fractions are enriched in free α-synuclein (up to ~3000 pg/mL). Experiments in panels **A** and **C** were performed by Cheng Jiang.

3.4.2 Association between α-synuclein and L1EVs

To assess whether full-length L1CAM is associated with EVs, I performed

immunocapture using anti-L1CAM-coated pCBMA beads followed by immunoblotting in each fraction from F2 to F7 spanning the two major chromatography peaks. I found that full-length L1CAM (220 kDa) was detected following anti-L1CAM immunocapture in all tested fractions and was predominantly present in its free form (**Figure 3.3A**). However, in F3 and F4, it was isolated in association with CD9 and syntenin-1 (**Figure 3.3A**). These data suggest that L1CAM can be immunocaptured both as a free molecule in later fractions and as an EV-associated form mostly in EV-enriched F3 and F4.

The presence of L1EVs was further confirmed by negative-staining TEM, demonstrating that the isolated particles had the typical cup-shaped morphology of EVs and measured ~100 nm (**Figure 3.3B**). Based on NTA, a typical peak size was detected at ~110 nm (**Figure 3.3C**) and the total number of eluted L1EVs (i.e. area under the curve in **Figure 3.3C**) was calculated to constitute ~8 % of total serum EVs from the corresponding fractions (F2 – F4), assuming elution efficiency was complete. This finding is within the range (< 10%) of the previously estimate from our lab using immunoblotting.[228] Under these conditions, anti-L1CAM immunocapture from pooled fractions F2 – F4, followed by α-synuclein measurements using the MSD assay, revealed that L1EV-associated α-synuclein was 13.33 ± 4.45 pg/mL of serum based on four healthy individuals each tested in duplicate (**Figure 3.3D**). This is in line with our previous estimates of α-synuclein concentration in serum L1EVs from healthy controls.[94,95,228]

Collectively, these findings demonstrate that L1CAM is present both as an EV membrane-associated protein and in a free, soluble form in the circulation (**Figure 3.4**). Although majority of L1CAM is present in a free form, it is important to acknowledge the small but valuable fraction that is associated with EVs.

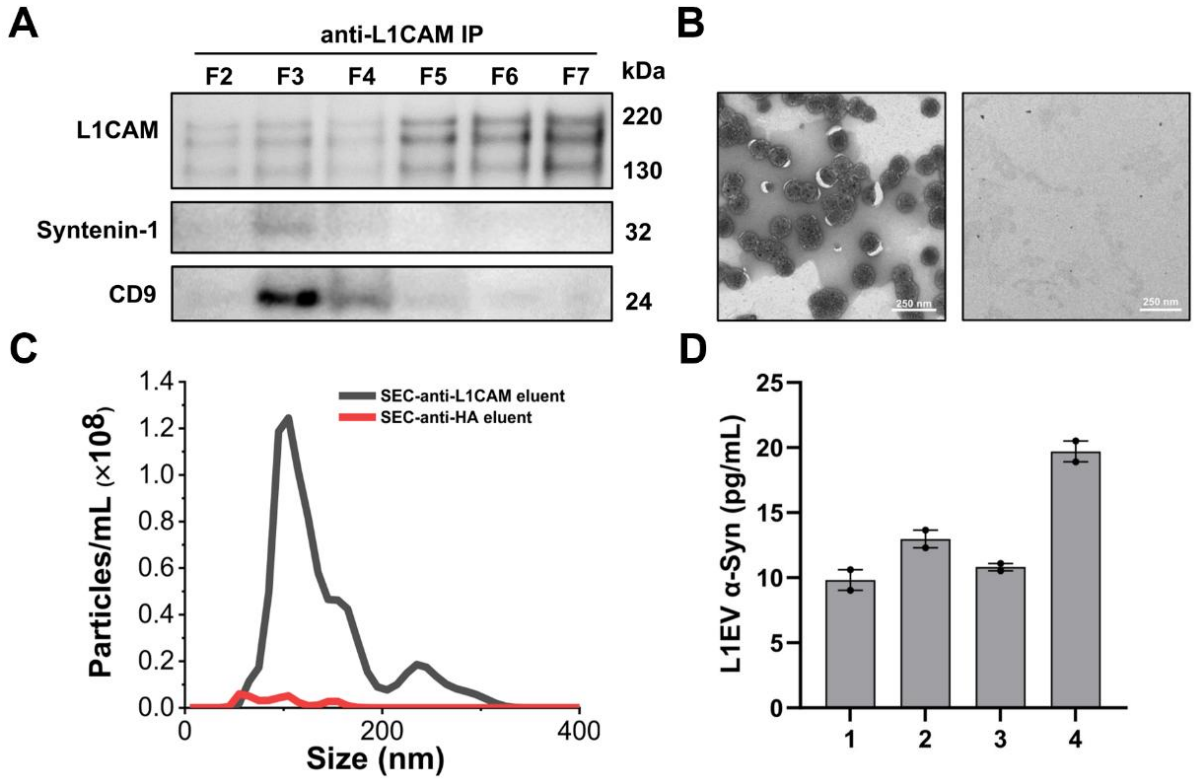


Figure 3.3: Validation of L1CAM as a marker for EV isolation. (**A**) Immunocapture using anti-L1CAM antibodies from fractions F2 to F7 covering the two identified peaks on chromatography spectra shows that full-length L1CAM was present in all fractions but only co-immunoprecipitated with EV proteins syntenin-1 and CD9 in F3 and F4, as shown by immunoblotting. (**B**) L1EVs immunocaptured from pooled F2 to F4 visualized with transmission electron microscopy (*left*), while no EVs were detected in anti-HA control (*right*). (**C**) Nanoparticle tracking analysis of EVs eluted following anti-L1CAM immunocapture from pooled F2 to F4. (**D**) α-Synuclein concentration in the EV subpopulation immunocaptured with anti-L1CAM antibodies from pooled F2 to F4 (*n* = 4 healthy volunteers tested, two replicates for each individual). Experiments in panels **B** and **C** were performed by Cheng Jiang.

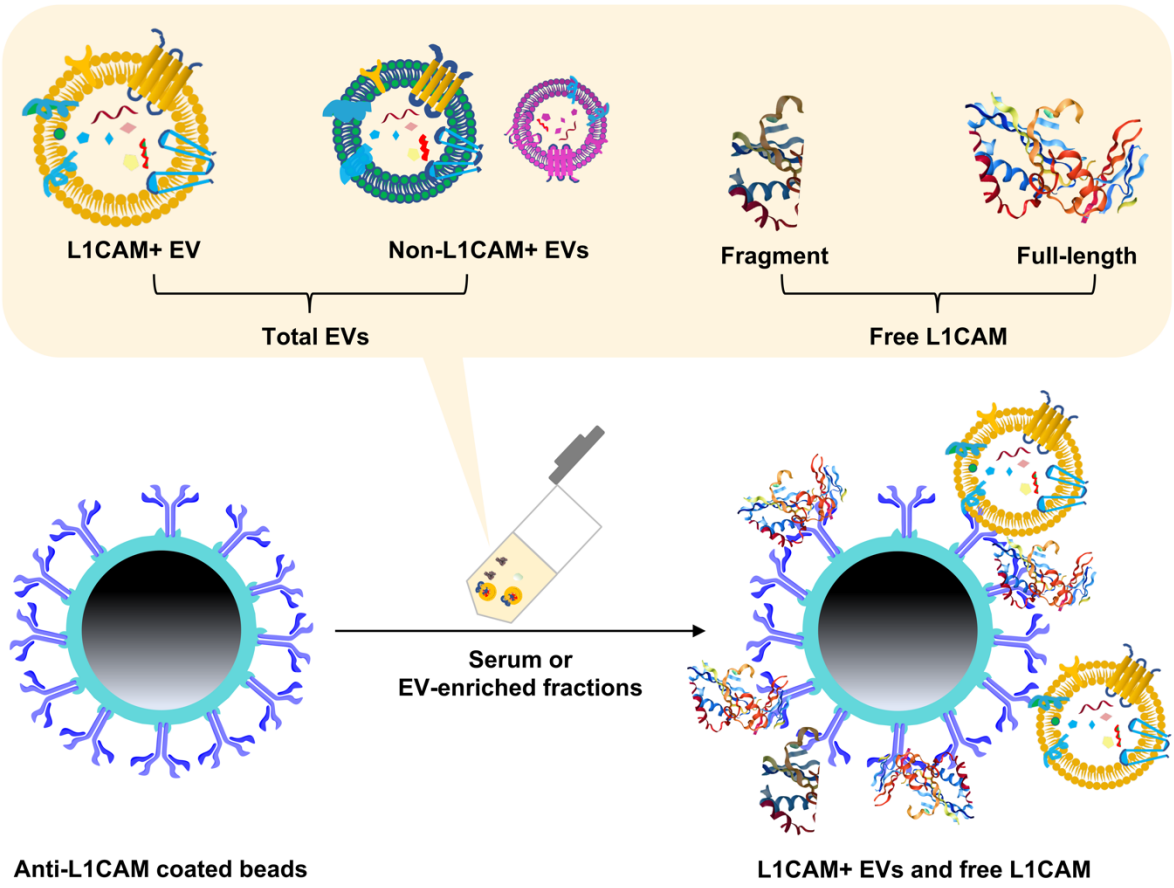


Figure 3.4: Schematic of anti-L1CAM immunocapture from serum. Full-length L1CAM is more abundant in serum as a free molecule, while a small fraction is also associated with EVs. This illustration was created by Cheng Jiang.

3.4.3 ATP1A3 is not detected on serum EVs

To investigate whether ATP1A3 can serve as reliable marker for isolating EVs from serum, each fraction was concentrated using UF, followed by immunoblotting. ATP1A3 was detectable only in the later, free protein-enriched fractions (F5 – F10) and was absent in the EV-enriched fractions (F2 – F4), as shown in **Figure 3.5A**. To further confirm this finding, I performed immunocapture with anti-CD9, anti-ATP1A3, anti-L1CAM, or anti-NCAM1 antibodies from pooled F3 and F4. Immunoblotting demonstrated the enrichment of EV markers (Flotillin 1, CD63, CD9, and CD81) in the CD9+, L1CAM+, and NCAM1+ immunoprecipitates, whereas no such enrichment was observed in ATP1A3+ immunoprecipitates (**Figure 3.5B**), suggesting that ATP1A3 is not present on the surface of

serum EVs, despite its association with L1EVs and NCAM1+ EVs. As expected, α-synuclein was undetectable by immunoblotting across all conditions, consistent with my earlier findings that its concentration in serum EVs lies below the detection limit of this method (**Figure 3.5B**).

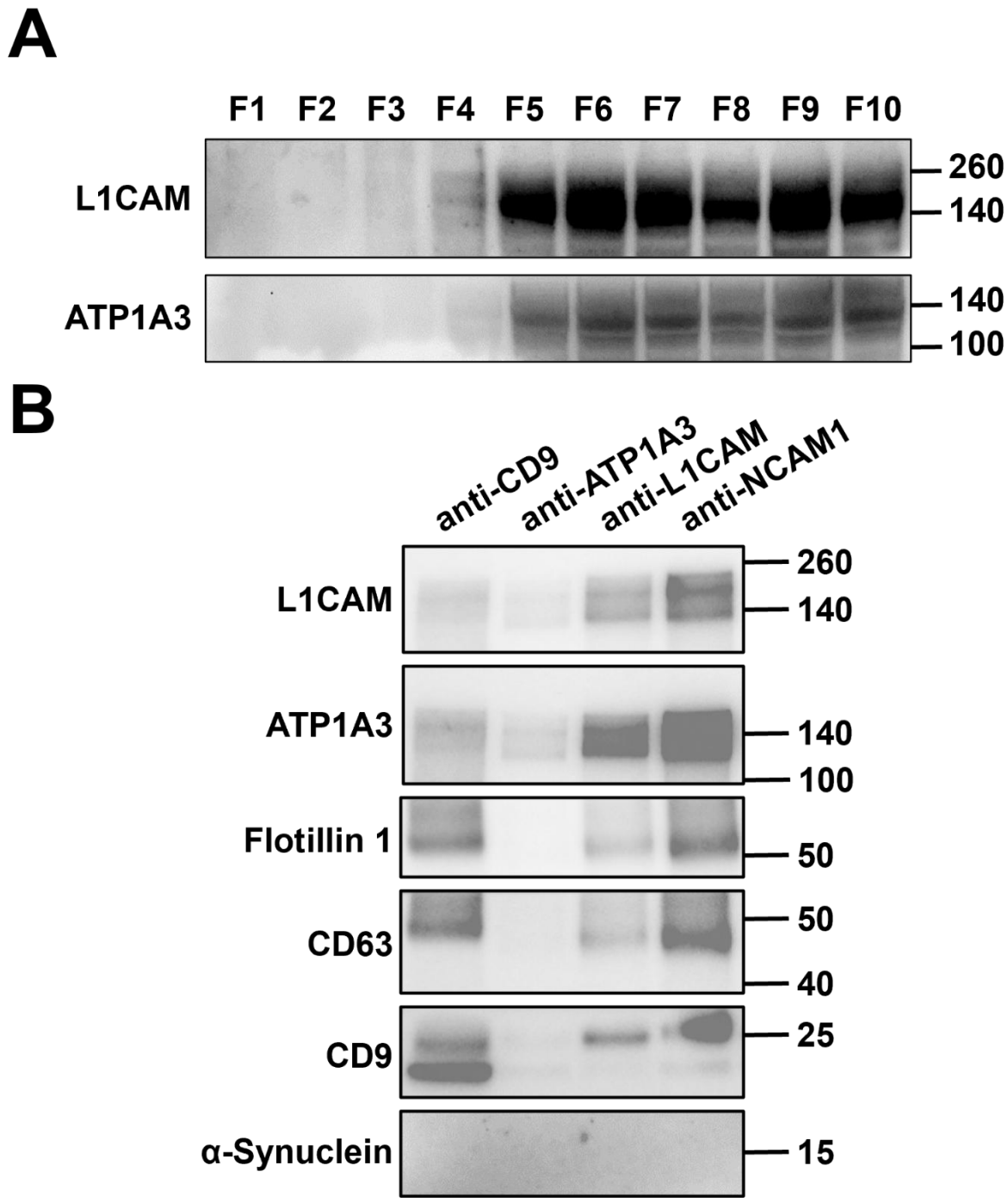


Figure 3.5: ATP1A3 is not associated with serum EVs. (**A**) Immunoblotting for neuronal markers L1CAM, ATP1A3 in each fraction. (**B**) Immunocapture using anti-CD9, anti-ATP1A3, anti-L1CAM, or anti-NCAM1 antibodies from pooled F3 and F4, followed by immunoblotting.

3.5 Discussion

3.5.1 Isolation of EVs from serum using Capto Core multimodal chromatography

In this study, I established a refined workflow for isolating EVs from human serum. Capto Core multimodal chromatography demonstrated robust capacity to isolate EVs from serum proteins, with early-eluting fractions (F3 and F4) showing consistent enrichment of canonical EV markers (CD9, syntenin-1, CD81) and a distinct size distribution peaked at ~110 nm, confirming the purity and specificity of the isolated EVs. In contrast, late fractions contained abundant free proteins, including the majority of circulating α-synuclein. These results align with prior plasma studies using similar methodologies,[196] highlighting Capto Core multimodal chromatography as a reproducible technique for serum EV isolation.

The selective removal of non-EV particles by Capto Core multimodal chromatography prior to IP provides a cleaner background for biomarker quantification. Notably, α-synuclein was found in both free and EV-associated forms, but with a striking disparity. While the vast majority (> 90%) was free, EV-associated α-synuclein constituted a small, but consistent fraction (~43 pg/mL serum). The low inter-individual variability observed in EV-associated α-synuclein, in contrast to the high variance in free protein levels likely due to haemolysis, underscores its potential reliability as a biomarker substrate.

The presence of α-synuclein in EV-enriched fractions raises important questions about its packaging and release mechanisms. While the functional significance of EV α-synuclein remains to be fully elucidated, it may represent a route by which neurons release α-synuclein into circulation and play a role in the intercellular transmission of pathology, potentially through interactions with EV membrane proteins or lipid rafts,[238] contributing to the spread of α-synuclein pathology.[239]

3.5.2 L1CAM as a marker for EV isolation

While full-length L1CAM (220 kDa) was primarily detected in a free form, a small fraction was found in F3 and F4, co-eluting with EV markers, suggesting the presence of an EV-associated form. The substantial amount of free L1CAM detected may reflect its known release into circulation as a soluble protein, either via proteolytic cleavage or alternative splicing, both of which have been previously reported.[240] This highlights a key challenge in using L1CAM as an EV marker, as the free form can confound EV-specific analyses if not adequately separated. While the specificity of L1CAM as a definitive nEV marker remains under investigation, these findings demonstrate its practical value in serum EV immunocapture workflows, particularly when a pre-enrichment step is used to reduce contamination from free L1CAM and improve specificity for its EV-associated form.

The estimated ~8% contribution of L1EVs to total serum EVs corresponds well with prior estimates of 5 – 10% from orthogonal EV characterisation methods.[228,236] Importantly, α-synuclein was detected in L1EVs at a concentration of ~13 pg/mL in healthy individuals, representing a small but significant fraction (~ 30%) of total EV-associated α-synuclein. This finding aligns with previously reported levels in healthy controls,[94,95] and supports the current reliance on L1CAM as a reliable, if imperfect, proxy for nEVs in peripheral fluids.

3.5.3 ATP1A3 is not associated with serum EVs

In contrast to promising data suggesting ATP1A3 as a nEV marker in plasma and CSF,[193] this study did not support its use for EV isolation from serum. ATP1A3 was only detected in later, free protein-enriched fractions and was absent from EV-enriched fractions. Moreover, IP using anti-ATP1A3 antibodies failed to recover generic EV markers, suggesting ATP1A3 is not EV-associated under native serum conditions. This absence may reflect the inter-laboratory inconsistency or the limitations of the detection methods, emphasising the need

for exploring other candidate nEVs markers and applying orthogonal validation strategies across laboratories.

3.5.4 Limitations and future directions

While this work provides valuable insights into the association between α-synuclein and L1EVs, several limitations must be acknowledged. First, EV-associated α-synuclein levels reported here may not be comprehensive due to the modest yield of Capto Core multimodal chromatography. Second, the current analysis was restricted to healthy donors. Whether disease-related changes in L1EV α-synuclein can be robustly detected remains to be evaluated in Chapter 4. Lastly, efforts to refine nEV immunocapture should continue. Although L1CAM remains the most widely used nEV marker in serum, multi-marker isolation strategies or novel microfluidic profiling may offer enhanced specificity and utility.

3.5.5 Conclusion

In summary, this work demonstrates a reproducible Capto Core multimodal chromatography-based workflow for serum EV isolation and provides new insights into the association between α-synuclein and EVs. The presence of α-synuclein in L1EVs, albeit in low concentrations, holds diagnostic potential in PD. These findings lay the methodological foundation for subsequent translational studies and support the broader goal of developing scalable, blood-based biomarkers for synucleinopathies.

3.6 Supplementary information

Authors	Matrix	EV isolation method	α-Synuclein measurement method	HC (n)	EV α-synuclein concentration	PD (n)	EV α-synuclein concentration
Dutta et al.[210]	Serum and plasma	ExoQuick + L1CAM IP	MSD	50	58±55 pg/mL	51	107±124 pg/mL
Blommer et al.[237]	Plasma	ExoQuick + L1CAM IP	MSD	49	3099.9±2986 pg/mL	224	2665.9±3194 pg/mL
Si et al.[241]	Serum	ExoQuick + L1CAM IP	ELISA	18	0.27±0.16 pg/mL	38	0.21 pg/mL
Zhao et al.[235]	Plasma	ExoQuick + L1CAM IP	ELISA	40	6.50±1.17 ng/mg EV protein	39	7.75±2.74 ng/mg EV protein
Chung et al.[242]	Plasma	exoEasy Maxi kit	IMR	46	74.5±4.3 fg/mL	116	56.0±3.7 fg/mL
Jiang et al.[94]	Serum	Direct L1CAM IP	MSD	144	12.71±5.93 pg/mL	230	27.44±18.82 pg/mL
Jiang et al.[95]	Serum	Direct L1CAM IP	MSD	47	10.8±4.5 pg/mL	60	22.5±4.8 pg/mL
Yan et al.[189]	Serum	Direct L1CAM IP	MSD	140	12.60±6.68 pg/mL	50	26.55±33.24 pg/mL
Shi et al.[194]	Plasma	Direct L1CAM IP	Luminex assay	215	~12 pg/mL	267	~25 pg/mL
Niu et al.[234]	Plasma	Direct L1CAM IP	MSD	21	649.1±582.9 pg/mL	53	2392±2150 pg/mL
Cerri et al.[233]	Plasma	UC	ELISA	33	12.3 pg/mL	39	25.2 pg/mL
Stuendl et al.[196]	Plasma	SEC	MSD	50	8.083 ± 0.540 pg	94	12.660 ± 0.828 pg

Table S3.1: Summary of EV-associated α-synuclein studies. The reported concentrations of EV-associated α-synuclein vary substantially across studies depending on the isolation and detection techniques employed. Abbreviations: HC = healthy control; PD = Parkinson's disease; IP = immunoprecipitation; UC = ultracentrifugation; SEC = size exclusion chromatography; MSD = Meso Scale Discovery; IMR = immunomagnetic reduction.

Chapter 4

Neuronally derived EV α-synuclein as a serum biomarker for individuals at risk of developing PD

Adapted from Yan et al. *JAMA Neurology* 2024; 81(1):59-68

4. Neuronally derived EV α-synuclein as a serum biomarker for individuals at risk of developing PD

4.1 Introduction

4.1.1 Prodromal PD and the need for early-stage biomarkers

PD is the most common movement disorder, characterised by a long prodromal phase, which starts several years before the clinical presentation with the classic motor symptoms. A number of non-motor symptoms such as RBD, olfactory loss, or autonomic dysfunction can manifest during the prodromal phase and are associated with higher risk of phenoconversion to PD.[59] iRBD is the strongest predictor of α-synucleinopathy, with > 80% of subjects converting to PD, DLB, or MSA within 12 years.[54] Subjects with heterozygous mutations in the *GBA1* gene are another recognised at-risk group, with a ~6 – 10% risk of developing PD by the age of 70,[60] which is much lower than the respective risk for iRBD. Identification of those individuals with the highest risk of phenoconversion is crucial for the assessment of future disease-modifying therapies within reasonable timescales.

Because symptoms broadly correlate with the evolution of α-synuclein pathology, accurate measurements of neuronally derived α-synuclein in at-risk individuals could aid the identification of those likely to convert to PD. However, current diagnostic methods mainly rely on clinical assessments of motor symptoms, which appear late in the disease course. This highlights the urgent need for biomarkers that can detect PD pathology in the early stages, preferably from an easily accessible biosample such as blood.

4.1.2 nEV as a source of biomarkers

EVs derived from tissues affected by disease have emerged as a rich source of biomarkers, because they carry molecular cargo reflective of their cell of origin.[189,243] As discussed in Section 1.3.2.1, nEV are valuable in PD as they transport disease related proteins into the circulation. Immunocapture of presumed neuronally-derived L1EVs has been applied to a number of neurological diseases as a proxy biomarker of brain pathology.[232] Our previous work in multiple cohorts showed that α-synuclein is elevated in L1EVs isolated from serum of patients with PD, PDD, or neuropathologically confirmed DLB and in a single cohort of subjects with PSG-confirmed iRBD but not in other parkinsonian sydromes.[94,95] This finding is consistent with the view that L1EV-associated α-synuclein levels are higher in PD patients based on several studies from our and other laboratories.[94,95,194,210,234,244] Unlike other studies,[194] our work did not identify any correlation between L1EV α-synuclein with PD severity based on motor or cognitive assessments, but instead observed stably elevated levels of L1EV α-synuclein with disease progression.[94] The latter parallels, in the opposite direction, measurements of total α-synuclein in CSF, which is decreased early in disease, remains stably low with disease progression and does not correlate with clinical severity.[245,246] Despite this extensive literature, the precise relevance of L1EVs associated α-synuclein in identifying individuals at risk of developing PD remains unresolved.

4.2 Aims and objectives

The study aims to determine whether serum L1EV-associated α-synuclein can identify subjects in the prodromal phase of α-synucleinopathies, particularly those at high risk of developing PD. Early identification of such individuals prior to phenoconversion is critical for timely intervention and for stratifying subjects in disease-modifying trials. The specific objectives are to:

1. Assess the clinical relevance of serum L1EV-associated α-synuclein in at-risk individuals, including those with iRBD, hyposmia, pathogenic *GBA1*^{N409S} or *LRRK2*^{G2019S} mutations, using large, well-characterised multicentre cohorts.
2. Examine associations between serum L1EV-associated α-synuclein and prodromal markers, and determine reproducibility across independent, multicentre cohorts.
3. Investigate the performance of this blood-based test in relation to established pathological markers, including dopaminergic neurodegeneration on DaT SPECT, CSF α-synuclein SAA, and phenoconversion to PD or DLB.

4.3 Material and methods

4.3.1 Study design

This is a retrospective cross-sectional study of four cohorts that followed the Strengthening the Reporting of Observational Studies in Epidemiology (STORBE) guidelines. The study profile for both derivation and validation groups is shown in **Figure 4.1**. The biomarker was first tested across homogeneous single-centre iRBD cohorts, with Oxford Discovery as the derivation group. The identified cut-off (derived threshold) for differentiating iRBD from healthy controls was assessed in the combined Marburg and Cologne cohorts as the first validation group. Inclusion criteria for iRBD were confirmation by video-assisted PSG and availability of serum sample. Subjects were excluded if a secondary cause for RBD was present. Oxford iRBD participants (n = 97) were recruited from the Discovery cohort of the Oxford Parkinson's Disease Centre.[247,248] Marburg iRBD participants (n = 51) were recruited nationwide from the German RBD registry project and annually followed for at least 4 years at Marburg by the same neurologist.[249] iRBD participants from Cologne (n = 24) were identified from the general population using a structured screening process after providing written informed consent.[250] Healthy controls from Oxford (n = 73), Marburg (n = 29), and

Cologne (*n* = 18) without significant comorbidities or relevant family history were included as reference groups. The threshold derived from the Oxford Discovery cohort was further assessed in the second validation group consisting of subjects with variable risk from the PPMI cohort. Inclusion criteria for PPMI were availability of serum sample and assessments for prodromal PD. These subjects were recruited across sites in the USA, Europe, or Israel (https://www.ppmi-info.org/) and included non-manifest *GBA1*^{N409S} gene carriers (*n* = 146), subjects with hyposmia (*n* = 20) or PSG confirmed iRBD (*n* = 27). Healthy controls without relevant comorbidities and family history (*n* = 20), *GBA1*^{N409S} PD (*n* = 21) and sporadic PD (*n* = 50) were included as reference groups. Subgroup analyses within each prodromal condition were performed to determine the performance of the test when more than one prodromal marker was present. The probability of having prodromal PD was estimated across cohorts and subjects were analysed blinded to the phenotype. Serum samples were matched to the clinical assessments. L1EVs were isolated and their α-synuclein and syntenin-1 levels were measured in batches without noticeable batch effects (**Figure 4.2**). Where such results were available, I also assessed the association between serum L1EV α-synuclein levels and CSF total α-synuclein levels, or CSF α-synuclein SAA results, or eventual phenoconversion.

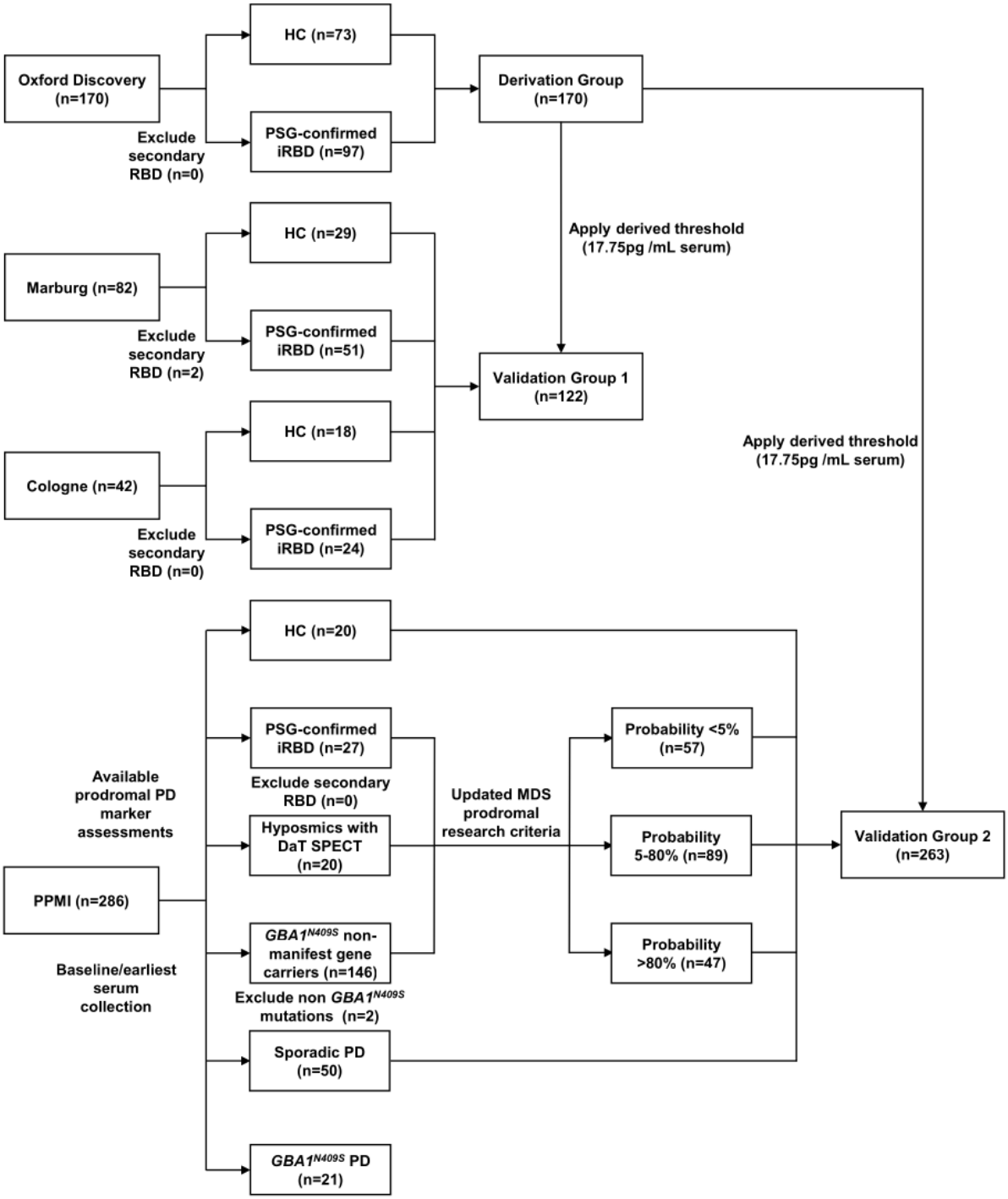


Figure 4.1: Study selection criteria and design for derivation and validation groups.

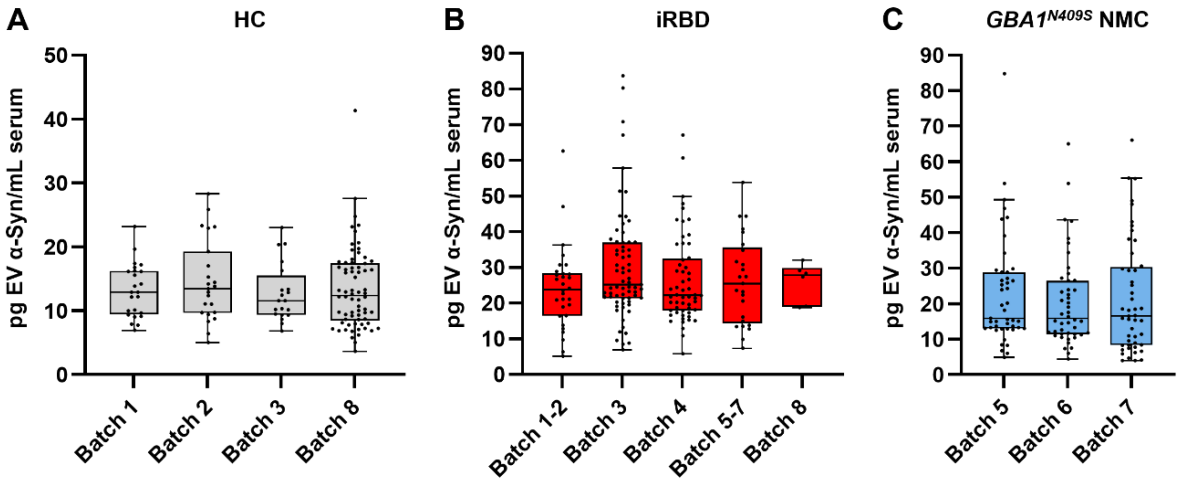


Figure 4.2: L1EV α-synuclein levels across batches. The samples were processed by operators who were blinded to the diagnosis. Following sample processing and unblinding, L1EV α-synuclein levels were compared across batches in (**A**) healthy controls (HC), (**B**) iRBD subjects, and (**C**) *GBA1*^{N409S} non-manifest gene carriers (NMC). Batch 1, 2, and 4 = Oxford plate 3; Batch 3 = Marburg and Cologne; Batch 5 = PPMI plate 1; Batch 6 = PPMI plate 2; Batch 7 = PPMI Batch 8 = Oxford, Marburg, Cologne, and PPMI. The midline of the box plots indicates the median, and the box indicates the 25th and 75th percentiles. Outliers and whiskers were plotted using the Tukey method. Statistical significance was determined by Kruskal-Wallis test.

4.3.2 L1EV immunocapture and protein measurements

Blood samples from all the centres were collected during patient assessments, the serum was isolated, aliquoted, and frozen at -80°C until further use. All samples were sent on dry ice and processed in a blinded fashion at Oxford. All samples were visually inspected before analysis, and haemolysed samples were excluded. Immunocapture of L1EVs was performed using our previously developed and extensively validated direct immunocapture approach, applied to 250 µL of precleared serum.[94,95] Electrochemiluminescence detection was performed in 96-well MSD U-PLEX plates. Antibody pairs for α-synuclein were supplied by MSD and were pre-conjugated with biotin and ruthenium labels. For syntenin-1 detection, an additive-free goat polyclonal anti-syntenin-1 antibody (PAB7132, Abnova) conjugated with biotin was used for capture, while a rabbit monoclonal anti-syntenin-1 antibody (ab236071, Abcam) conjugated with ruthenium served as the detection antibody.

4.4 Results

4.4.1 Demographic characteristics

Among the 576 participants included, the mean [SD] age was 64.30 [8.27] years, 394 [68.4%] were male and 182 were female [31.6%], as summarised in **Table 4.1**. In the derivation group (Oxford Discovery), 170 subjects (mean [SD] age, 64.18 [9.88] years; 156 [91.8%] male and 14 [8.2%] female) were included. In the first validation group (Marburg + Cologne), 122 subjects (mean [SD] age, 65.19 [8.18] years; 91[74.6%] male, 31 [25.4%] female) were included. In the second validation group (PPMI), 263 subjects (mean [SD] age, 63.78 [7.30] years; 134 [51.0%] male, 129 [49.0%] female) were included. No significant effect of age or gender on L1EV α-synuclein levels was observed across prodromal groups, as summarised in **Table 4.2** and **Figure 4.3**.

	Characteristic	HC [a]	iRBD	*GBA1*^{N409S} NMC	Hyposmics	P-value	Sporadic PD	*GBA1*^{N409S} PD
Oxford Discovery	No of individuals	73	97	NA	NA	NA	NA	NA
	Gender, No. (%)							
	Female	9 (12.3)	5 (5.2)	NA	NA	0.09	NA	NA
	Male	64 (87.7)	92 (94.8)	NA	NA		NA	NA
	Age, mean (SD), y	63.47 (12.19)	64.57 (8.38)	NA	NA	0.56	NA	NA
	MoCA, mean (SD)	26.54 (2.21)	26.05 (2.55)	NA	NA	0.26	NA	NA
	L1EV α-Syn, median (IQR), pg/mL	12.89 (7.09)	23.11 (12.03)	NA	NA	<0.0001	NA	NA
Marburg	No of individuals	29	51	NA	NA	NA	NA	NA
	Gender, No. (%)							
	Female	10 (34.5)	3 (5.9)	NA	NA	<0.0001	NA	NA
	Male	19 (65.5)	48 (94.1)	NA	NA		NA	NA
	Age, mean (SD), y	58.32 (8.24)	67.79 (7.03)	NA	NA	<0.0001	NA	NA
	MoCA, mean (SD)	28.17 (2.14)	27.41 (2.19)	NA	NA	0.43	NA	NA
	L1EV α-Syn, median (IQR), pg/mL	11.55 (4.31)	29.06 (15.08)	NA	NA	<0.0001	NA	NA
Cologne	No of individuals	18	24	NA	NA	NA	NA	NA
	Gender, No. (%)							
	Female	15 (83.3)	3 (13.6)	NA	NA	<0.0001	NA	NA
	Male	3 (16.7)	21 (86.4)	NA	NA		NA	NA
	Age, mean (SD), y	66.69 (7.03)	66.90 (6.81)	NA	NA	0.92	NA	NA
	MoCA, mean (SD)	27.61 (2.45)	27.21 (1.84)	NA	NA	0.55	NA	NA
	L1EV α-Syn, median (IQR), pg/mL	10.84 (9.31)	21.39 (16.41)	NA	NA	0.002	NA	NA
PPMI	No of individuals	20	27	146	20	NA	50	21
	Gender, No. (%)							
	Female	9 (45.0)	5 (18.5)	91 (62.3)	4 (20.0)	<0.0001	20 (40.0)	8 (38.1)
	Male	11 (55.0)	22 (81.5)	55 (37.7)	16 (80.0)		30 (60.0)	13 (61.9)

	Age, mean (SD), y	61.27 (10.66)	68.13 (5.44)	62.47 (6.74)	70.59 (6.61)	<0.0001	63.55 (6.07)	66.47 (7.19)
	MoCA, mean (SD)	28.00 (1.30)	26.37 (3.71)	26.94 (2.34)	27.10 (1.86)	0.21	26.48 (2.21)	26.14 (3.04)
	L1EV α-Syn, median (IQR), pg/mL	15.61 (8.35)	24.52 (19.93)	16.08 (16.14)	20.51 (24.18)	0<0.0001	26.55 (33.24)	26.94 (27.44)

Table 4.1: Demographic characteristics of individual cohort. Data are number (%), mean (SD) or median (IQR). Abbreviations: iRBD = isolated REM sleep behaviour disorder; GBA1 = glucocerebrosidase; NMC = non-manifest carrier; PD = Parkinson's Disease; MoCA = Montreal Cognitive Assessment; L1EV = L1CAM positive extracellular vesicles; α-Syn = α-Synuclein. Within each cohort, I used t-test or one way ANOVA to compare age and MoCA, Mann-Whitney U test or Kruskal-Wallis one-way analysis of variance to compare L1EV α-Syn, and Pearson χ^2 test to compare gender frequency between groups.

[a] MoCA was not available in 40 controls.

iRBD (*n* = 199)				***GBA1*^{N409S} NMC (*n* = 146)**			**Hyposmics (*n* = 20)**			**HC (*n* = 127)**		
Variable	**β**	**SE**	**P-value**	**β**	**SE**	**P-value**	**β**	**SE**	**P-value**	**β**	**SE**	**P-value**
Intercept	1.209	0.136	<0.001	1.202	0.276	<0.001	0.896	0.774	0.262	1.141	0.107	<0.001
Age	0.003	0.002	0.17	0.001	0.004	0.80	0.007	0.011	0.513	-0.0001	0.002	0.93
Gender [Female]	-0.023	0.058	0.70	0.028	0.061	0.64	-0.021	0.140	0.884	-0.042	0.039	0.29
Model R-square	0.011			0.002			0.027			0.010		
Model p-value	0.37			0.86			0.79			0.57		

Table 4.2: Influence of age or gender on L1EV α-synuclein. Multiple linear regression within each group, including iRBD, *GBA1*^{N409S} non-manifest carrier (NMC), hyposmics, and healthy control (HC), did not reveal an association between L1EV α-synuclein and age or gender using the equation: log (L1EV α-synuclein) = β_0 + (β_1 × Age) + (β_2 × Gender) + ε.

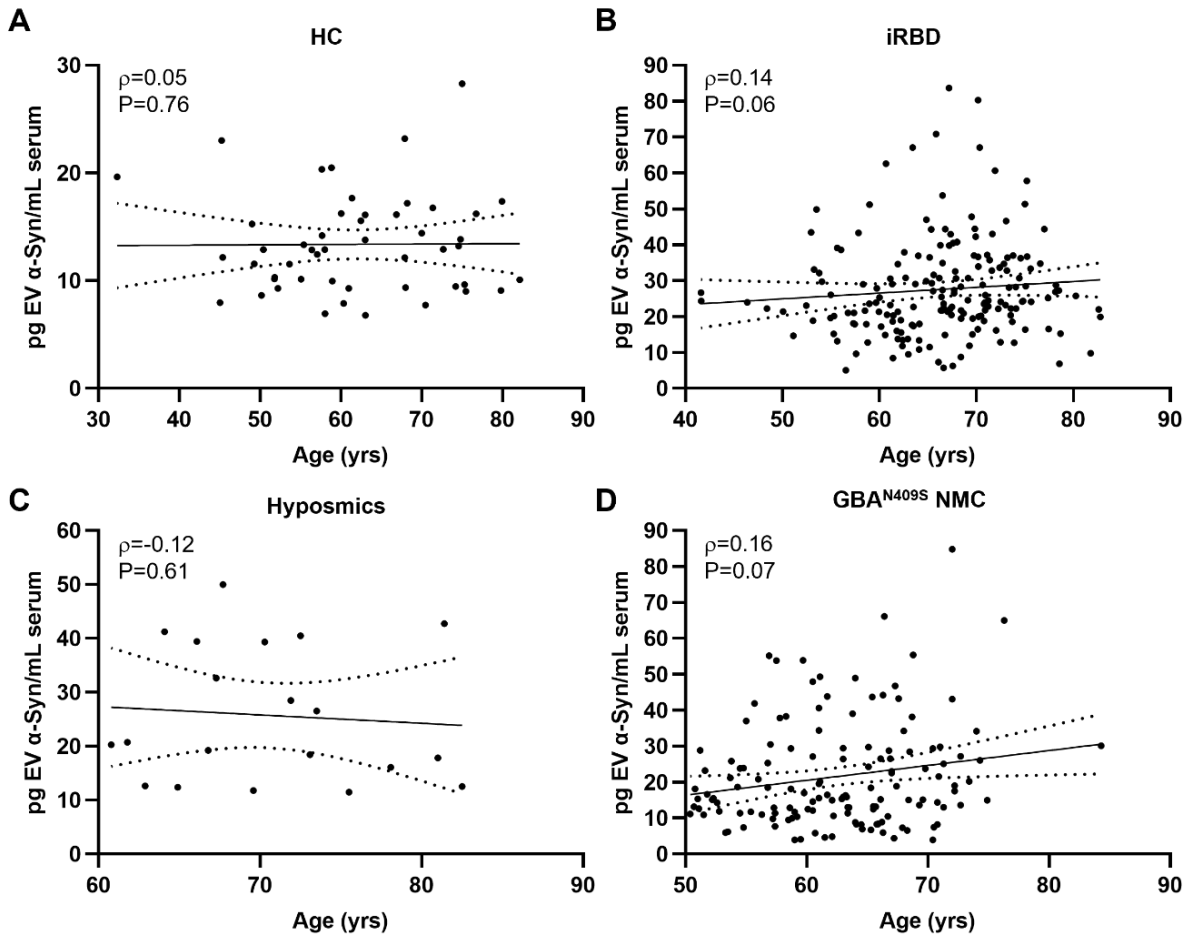


Figure 4.3: Correlation between L1EV α-synuclein and age. There was no significant correlation between L1EV α-synuclein levels and age at sampling in any of the four groups: (**A**) healthy control (HC), (**B**) iRBD, (**C**) hyposmics, and (**D**) *GBA1*^{N409S} non-manifest carrier (NMC). Least squares regression line with 95% CI was plotted, and Spearman coefficient with corresponding P values were reported for each group.

4.4.2 α-Synuclein in serum L1EV is elevated in iRBD subjects across single-centre cohorts

I first studied deeply phenotyped subjects with iRBD in order to determine whether L1EV α-synuclein is increased in this prodromal group who have the highest risk of converting to PD or DLB compared to controls. I confirmed (data shown as median ± IQR) that L1EV α-synuclein is elevated in the Oxford Discovery iRBD cohort that our group previously studied[94] by analysing serum samples from *n* = 97 iRBD subjects and *n* = 73 controls. I found consistent L1EV α-synuclein levels in iRBD (23.11 ± 12.03 pg/mL) compared to what have been previously reported for a subgroup of this cohort (*n* = 56; 22.17 ± 14.31 pg/mL),[94] which were

increased compared to controls (12.89 ± 7.09 pg/mL; $P < 0.0001$), as shown in **Figure 4.4A**. I further confirmed this finding in iRBD subjects from Marburg and Cologne (combined $n = 75$ iRBD and $n = 47$ controls), as shown in **Figure 4.4B**. These analyses showed that L1EV α-synuclein at a threshold of 17.75 pg/mL (derived from Oxford Discovery) exhibited a consistent performance in the independent iRBD group (Marburg + Cologne), as shown in **Figure 4.4C**, and for each of these cohorts in **Figure S4.1**. In the derivation group, the AUC = 0.85 (95% CI, 0.79 – 0.91), with sensitivity of 0.77 (95% CI, 0.68 – 0.85) and specificity of 0.82 (95% CI, 0.72 – 0.89). In the validation group, AUC = 0.91 (95% CI, 0.86 – 0.96), with sensitivity of 0.87 (95% CI, 0.78 – 0.93) and specificity of 0.82 (95% CI, 0.69 – 0.91). Overall, there was a ~2-fold increase in L1EV α-synuclein levels across the iRBD subjects (24.21 ± 13.75 pg/mL) compared to the controls (12.20 ± 7.39 pg/mL), with an AUC of 0.88 (95% CI, 0.84 – 0.92).

4.4.3 Serum L1EV α-synuclein levels differentiate those with probable prodromal PD from subjects with minimal risk in a multicentre cohort

Having established the consistency of the biomarker in a fairly homogeneous group of high-risk subjects, I investigated the broader applicability of the derived threshold from Oxford Discovery to a multicentre cohort (PPMI) consisting of a heterogenous group with variable risk of developing PD or related dementia. This group included *GBA1*^{N409S} gene carriers ($n = 146$), subjects with hyposmia ($n = 20$) or iRBD ($n = 27$). Healthy controls ($n = 20$) and sporadic PD patients ($n = 50$) from PPMI were included as negative and positive reference groups, respectively. For this analysis, I calculated their age- and sex-adjusted probability of having prodromal PD using the updated MDS prodromal research criteria.[59] These subjects were stratified into those with < 5% probability ($n = 57$), those with 5 – 80% probability ($n = 89$), and those with a positive lifetime risk which is defined as ≥ 80% probability ($n = 47$), as shown

in **Table S4.1**. I found that subjects with ≥ 80% probability of having prodromal PD exhibited increased L1EV α-synuclein levels (27.93 ± 23.80 pg/mL), similar to sporadic PD patients (26.55 ± 33.24 pg/mL), whereas subjects with < 5% probability of having prodromal PD exhibited L1EV α-synuclein levels (12.98 ± 10.32 pg/mL) similar to healthy controls (15.61 ± 8.35 pg/mL). L1EV α-synuclein levels in subjects with 5 – 80% probability of having prodromal PD (18.13 ± 16.33 pg/mL) were intermediate between subjects with ≥ 80% and subjects with < 5% probability of having prodromal PD or healthy controls (**Figure 4.4D**). By applying the threshold derived from the Oxford Discovery cohort (17.75 pg/mL), I found that subjects with ≥ 80% probability of having prodromal PD were differentiated from those with < 5% risk, with an AUC of 0.80 (95% CI, 0.71 – 0.89), sensitivity of 0.74 (95% CI, 0.60 – 0.84), and specificity of 0.67 (95% CI, 0.53 – 0.79), and from controls with an AUC of 0.80 (95% CI, 0.69 – 0.91), sensitivity of 0.74 (95% CI, 0.60 – 0.84), and specificity of 0.80 (95% CI, 0.58 – 0.92), as shown in **Figure 4.4E**. Similarly, patients with sporadic PD were differentiated from those with < 5% risk with an AUC of 0.81 (95% CI, 0.72 – 0.89), and from controls with an AUC of 0.81 (95% CI, 0.70 – 0.92). The optimal sensitivity and specificity for each subgroup is shown in **Table 4.3**.

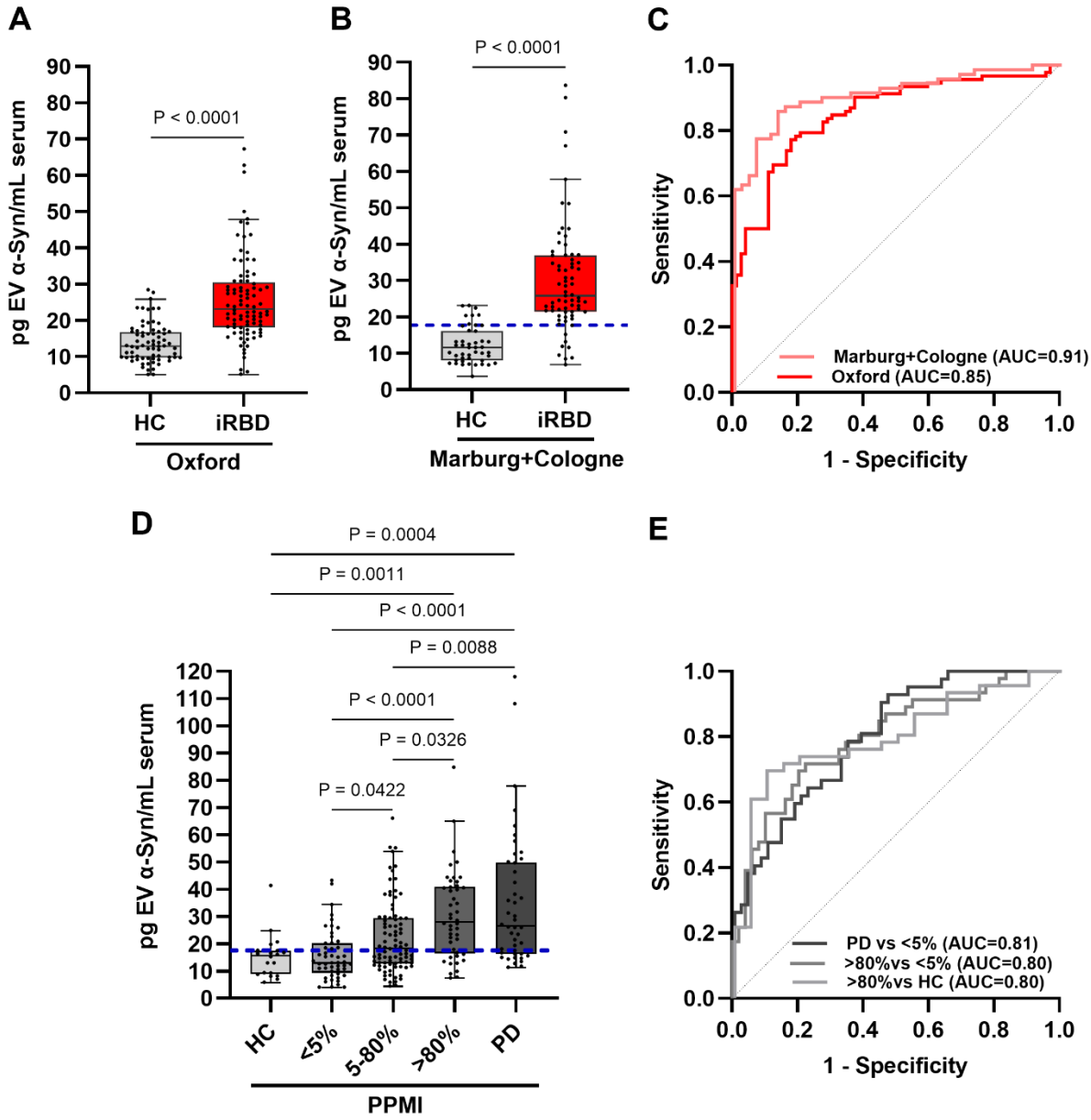


Figure 4.4: L1EV α-synuclein levels in the derivation and validation groups. Boxplots showing the distribution of L1EV α-synuclein in (**A**) the derivation group (Oxford Discovery iRBD cohort) and (**B**) the first validation group (Marburg and Cologne iRBD cohorts) when compared to controls. The derived threshold of 17.75 pg/mL (dotted blue line) was applied to the first validation group, showing the consistency of the biomarker across iRBD cohorts. (**C**) Corresponding ROC curves for the derivation and validation iRBD groups. (**D**) The derived threshold of 17.75 pg/mL (dotted blue line) also distinguished subjects with ≥ 80% probability of having prodromal PD who exhibited increased L1EV α-synuclein levels compared to those with minimal or intermediate risk in the second validation group (PPMI cohort). Healthy controls and sporadic PD were included as reference groups. (**E**) Corresponding ROC curves for the differentiation of subjects with sporadic PD or ≥ 80% probability of having prodromal PD from healthy controls or those with < 5% probability of having prodromal PD. The midline of the box plots indicates the median, and the box indicates the 25th and 75th percentiles. Outliers and whiskers were plotted using the Tukey method. Statistical significance was determined by Mann-Whitney (panels **A** and **B**) or Kruskal-Wallis test (panel **D**).

	AUC (95% CI)	Threshold (pg/mL) [a]	Sensitivity (95% CI)	Specificity (95% CI)
Oxford Discovery				
iRBD vs HC	0.85 (0.79 – 0.91)	17.75 [b]	0.77 (0.68 – 0.85)	0.82 (0.72 – 0.89)
Marburg + Cologne				
iRBD vs HC	0.91 (0.86 – 0.96)	18.41	0.86 (0.76-0.92)	0.87 (0.74 – 0.94)
PPMI				
PD vs < 5% risk	0.81 (0.72 – 0.89)	16.02	0.79 (0.64 – 0.88)	0.65 (0.51 – 0.77)
≥ 80% vs < 5% risk	0.80 (0.71 – 0.89)	20.35	0.72 (0.57 – 0.83)	0.78 (0.64 – 0.87)
5 – 80% vs < 5% risk	0.65 (0.56 – 0.75)	13.19	0.71 (0.61 – 0.80)	0.53 (0.39 – 0.66)
PD vs HC	0.81 (0.70 – 0.92)	21.00	0.61 (0.47 – 0.75)	0.90 (0.70 – 0.98)
≥ 80% risk vs HC	0.80 (0.69 – 0.91)	21.09	0.70(0.55 – 0.81)	0.90 (0.70 – 0.98)
5 – 80% risk vs HC	0.65 (0.52 – 0.77)	17.52	0.52 (0.41 – 0.62)	0.80 (0.58 – 0.92)
≥ 80% vs 5 – 80% risk	0.67 (0.57 – 0.77)	21.39	0.70 (0.55 – 0.81)	0.60 (0.49 – 0.69)

Table 4.3: ROC analyses in the derivation and validation groups. Abbreviations: iRBD = isolated REM sleep behaviour disorder; AUC = area under the receiver operating characteristic curve.

[a] Optimal threshold was determined by the Youden's index for each comparison and the respective sensitivity and specificity were reported.

[b] This threshold was used for validation across cohorts as detailed in **Figure 4.4**.

4.4.4 L1EV α-synuclein is increased in subjects with specific additional prodromal markers within at-risk groups and may precede dopaminergic neurodegeneration

The overall estimated risk of lifelong phenoconversion for *GBA1*^{N409S} gene carriers to PD is 6 – 10% by the age of 70.[60,251] Therefore, *GBA1*^{N409S} gene carriers may be at the earliest end of the prodromal phase. To investigate the value of L1EV α-synuclein in the stratification of this group, I identified those *GBA1*^{N409S} gene carriers who exhibited any prodromal markers based on the MDS research criteria[59] beyond their genetic status. A *GBA1*^{N409S} PD group was included for reference. *GBA1*^{N409S} gene carriers with constipation (n = 41; 21.21 ± 25.17 pg/mL;

P = 0.01), urinary dysfunction (*n* = 53; 20.37 ± 16.74 pg/mL; *P* = 0.02), based on MDS-UPDRS-I, subthreshold parkinsonism based on MDS-UPDRS-III > 6 excluding postural or action tremor (*n* = 12; 27.26 ± 23.26 pg/mL; *P* = 0.02) or cognitive deficit based on MoCA < 26 (*n* = 33; 18.13 ± 16.61 pg/mL; *P* = 0.03) exhibited higher L1EV α-synuclein levels (**Table 4.4** and **Figure 4.5**).

***GBA1*^{N409S} PM+ vs. *GBA1*^{N409S} PM-**		
	Median difference (pg/mL)	**P-value**
Prodromal marker		
Constipation	6.18	0.01
Subthreshold parkinsonism	12.23	0.02
Urinary dysfunction	5.34	0.02
Cognitive deficit	3.09	0.03
RBDSQ	1.98	0.06
EDS	1.77	0.06
DaT SPECT	9.50	0.07
Depression (± anxiety)	3.61	0.07
Symptomatic OH	0.81	0.09
Erectile dysfunction (in men)	0.19	0.18
Hyposmia	-2.04	0.89

Table 4.4: Difference in L1EV α-synuclein levels between *GBA1*^{N409S} gene carriers with and without additional prodromal markers. Mann-Whitney test was used to compare L1EV α-synuclein levels between two groups. Abbreviations: PM+ = *GBA1*^{N409S} non-manifest carrier (NCM) with the indicated prodromal marker; PM- = *GBA1*^{N409S} NMC without any additional prodromal markers; RBDSQ = REM Sleep Behaviour Disorder Screening Questionnaire; DAT SPECT = dopamine transporter single-photon emission computed tomography; EDS = excessive daytime somnolence; OH = orthostatic hypotension.

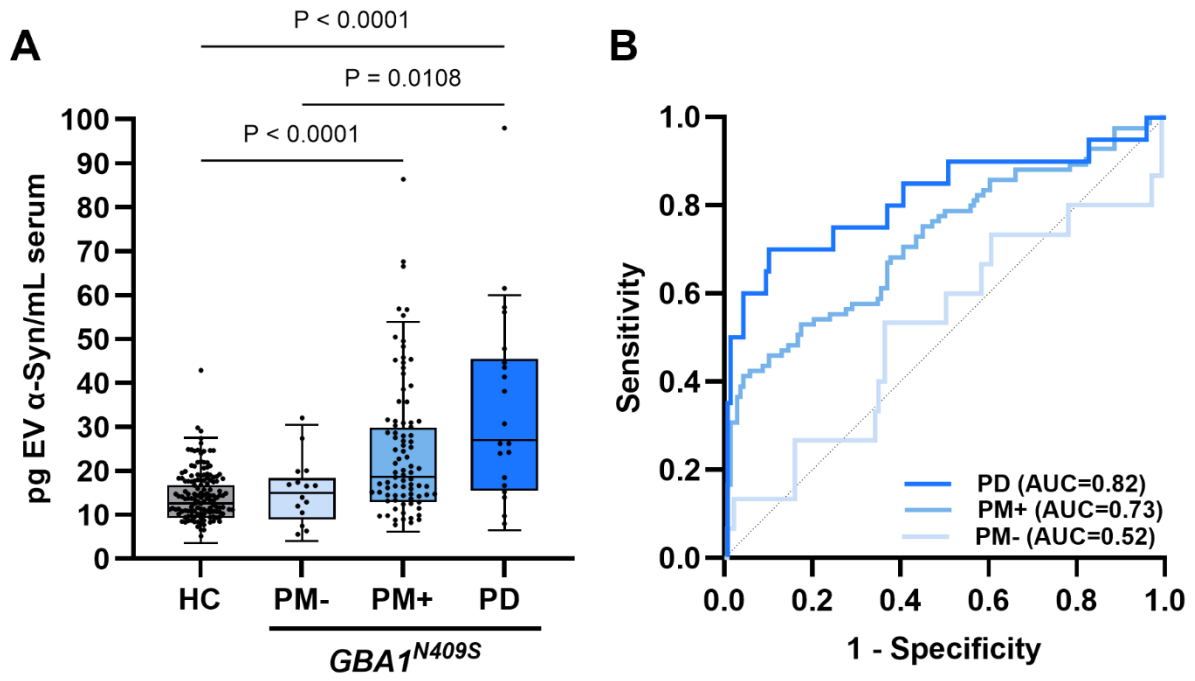


Figure 4.5: L1EV α-synuclein measurements in *GBA1*^{N409S} gene carriers. (**A**) Boxplot of L1EV α-synuclein measurements for healthy control (HC), *GBA1*^{N409S} non-manifest carriers (NMC) without additional prodromal makers (PM-), *GBA1*^{N409S} NMC with any of the following markers (PM+): constipation, urinary dysfunction, subthreshold parkinsonism, or cognitive deficit, and *GBA1*^{N409S} PD patients. (**B**) ROC curves for the differentiation of PM+, PM-, or *GBA1*^{N409S} PD from HC. The midline of the box plots indicates the median, and the box indicates the 25th and 75th percentiles. Outliers and whiskers were plotted using the Tukey method. Statistical significance was determined by Kruskal-Wallis test.

I then asked which prodromal markers are associated with L1EV α-synuclein levels in iRBD subjects with available relevant assessments (n = 127). Because iRBD conveys a much higher risk of prodromal PD than *GBA1* gene mutations, all of the subjects with iRBD had additional prodromal markers. To identify the main contributors in this group, I performed multiple linear regression analysis and found that hyposmia (β = 0.178 [SE = 0.065]; P = 0.007) and cognitive deficit (β = 0.116 [SE = 0.052]; P = 0.03) exhibited the strongest associations with higher L1EV α-synuclein levels (**Table 4.5**).

iRBD (*n* = 127)			
Variable	**β**	**SE**	**P-value**
Intercept	1.288	0.2525	<0.001
Age	-1.70×10^{-4}	0.004	0.97
Sex [Female]	-0.025	0.098	0.80
Constipation [Yes]	-0.062	0.054	0.25
Subthreshold parkinsonism [Positive]	0.107	0.076	0.16
Urinary dysfunction [Yes]	-0.033	0.054	0.55
Cognitive deficit [Yes]	0.116	0.052	0.03
DaT SPECT [Abnormal]	-0.018	0.051	0.73
Depression [Yes]	0.039	0.058	0.50
Symptomatic OH [Yes]	0.050	0.058	0.39
Olfaction [Abnormal]	0.178	0.065	0.007
Model R-square	0.11		
Model p-value	0.17		

Table 4.5: Association between L1EV α-synuclein and prodromal markers in iRBD. Multiple linear regression modelling identified hyposmia and cognitive deficit based on MoCA < 26 as exhibiting the strongest association with increased L1EV α-synuclein levels. Abbreviations: iRBD = isolated REM sleep behaviour disorder; DAT SPECT = dopamine transporter single-photon emission computed tomography; OH = orthostatic hypotension.

Lastly, I assessed the biomarker in relation to the presence of dopaminergic neurodegeneration as documented in subjects with available DaT SPECT. Nuclear imaging is the only available test to definitively demonstrate dopaminergic nerve loss in life. An abnormal DaT SPECT signifies progression of pathology and a higher risk of conversion to PD in subjects with iRBD or hyposmia.[54,66,252,253] I identified 47 iRBD subjects from Oxford, 50 iRBD subjects from Marburg, 22 iRBD subjects from Cologne, 27 iRBD subjects, 20 subjects with hyposmia, and 141 *GBA1*^{N409S} gene carriers from the PPMI cohort who had available DaT

SPECT results (n = 307 in total). In this comparison, L1EV α-synuclein levels were highest in subjects with an abnormal DaT SPECT (26.55 ± 18.31 pg/mL), intermediate in those with a normal DaT SPECT (18.92 ± 14.57 pg/mL), and lowest in healthy controls (12.60 ± 6.68 pg/mL), as shown in **Figure 4.6A**. ROC analyses revealed an improved differentiation from controls for those with an abnormal DaT SPECT (AUC = 0.90; 95% CI, 0.86 – 0.95) compared to those with a normal DaT SPECT (AUC = 0.71; 95% CI, 0.65 – 0.76), as shown in **Figure 4.6B**. This trend was also seen in each subgroup (*GBA1*^{N409S} gene carriers, iRBD, and hyposmics), as shown in **Figure S4.2**. There was no correlation between L1EV α-synuclein levels and MoCA or subthreshold parkinsonism scores when analysed across each condition (**Figure S4.3**) or each cohort (**Table S4.2**).

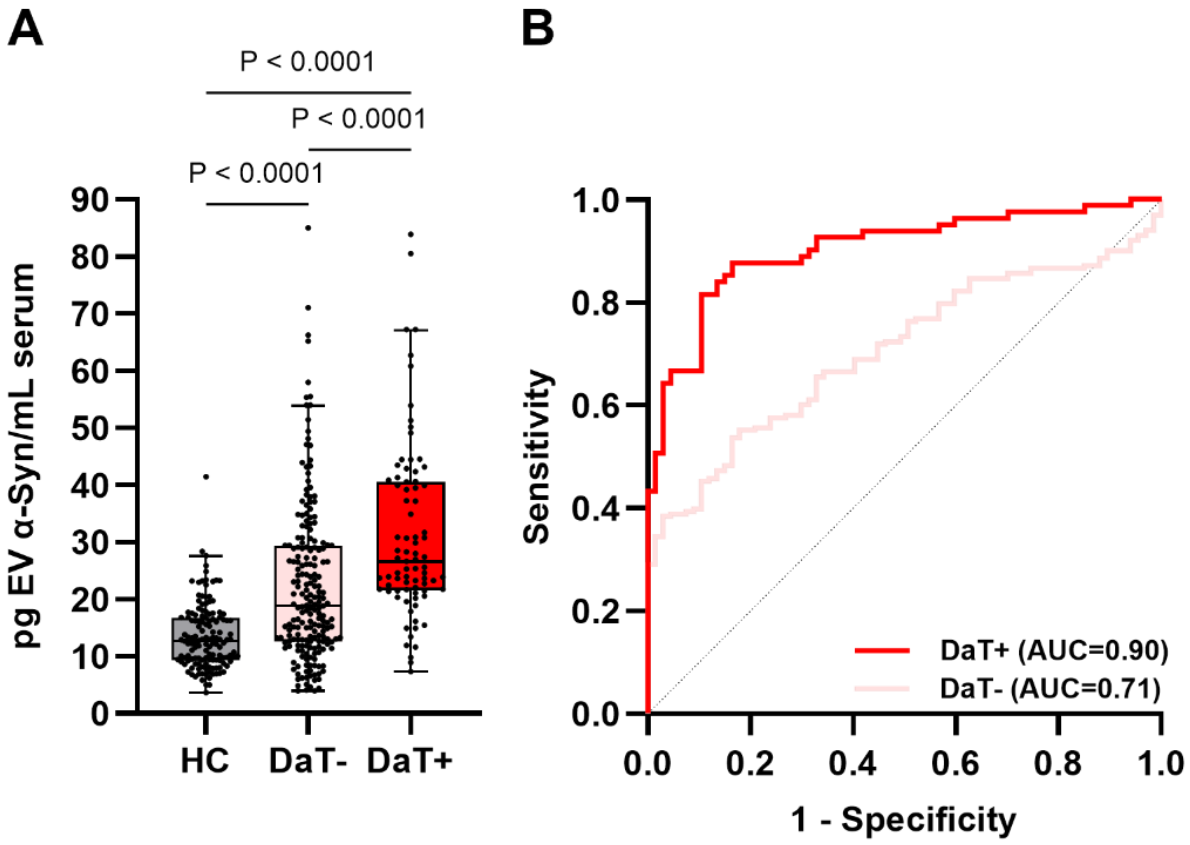


Figure 4.6: L1EV α-synuclein measurements in at-risk subjects with available DaT SPECT. (**A**) Boxplot of L1EV α-synuclein measurements and (**B**) corresponding ROC curves for healthy controls (HC) and at-risk subjects with a negative/normal (DaT-) or a positive/abnormal (DaT+) DaT SPECT. The midline of the box plots indicates the median, and the box indicates the 25th and 75th percentiles. Outliers and whiskers were plotted using the Tukey method. Statistical significance was determined by Kruskal-Wallis test.

4.4.5 L1EV α-synuclein differentiates those at-risk of developing PD from healthy control populations irrespective of initial diagnosis

I assessed L1EV α-synuclein across all at-risk subjects with any available prodromal markers (**Table 4.6**). I found that subjects (n = 190) who fulfilled the proposed criteria for prodromal PD (i.e. probability ≥ 80%; LR+; $P < 0.0001$) had higher serum L1EV α-synuclein levels compared to subjects with a negative LR (LR-; n = 175), as shown in **Figure 4.7A**. I also compared the levels of L1EV α-synuclein in LR+ and LR- subjects to our current (12.60 ± 6.68 pg/mL) and historic (11.12 ± 6.23 pg/mL) controls (**Figure S4.4**), pooled from multiple cohorts[94,95] (n = 282 in total), in order to obtain as accurate values as possible that would be applicable across populations. L1EV α-synuclein discriminated LR+ subjects from controls with an AUC of 0.90 (95% CI, 0.87 – 0.93), sensitivity of 0.81 (95% CI, 0.75 – 0.86), and specificity of 0.87 (95% CI, 0.83 – 0.91), but was less informative in LR- subjects compared to controls (AUC = 0.70; 95% CI, 0.65 – 0.76), as shown in **Figure 4.7B** and **Table S4.3**. There were no consistent differences in the generic EV marker syntenin-1 across these groups (**Figure 4.7C** and **Figure S4.5**).

No. (%)						
Cohort	**Oxford**	**Marburg**	**Cologne**	**PPMI**		
Diagnosis	**iRBD**				***GBA1*^{N409S} NMC**	**Hyposmics**
Total No.	97	51	24	27	146	20
PSG-proven iRBD	97 (100)	51 (100)	24 (100)	27 (100)	NA	NA
RBDSQ						
Positive	NA	NA	NA	NA	32 (13.0)	0
Negative	NA	NA	NA	NA	114 (87.0)	20 (100.0)
Missing data	NA	NA	NA	NA	0	0
DaT SPECT						
Abnormal	25 (25.8)	23 (45.1)	12 (50.0)	19 (70.4)	6 (4.1)	8 (40.0)
Normal	22 (22.7)	27 (52.9)	10 (41.7)	8 (29.6)	135 (92.5)	12 (60.0)
Missing data	50 (51.5)	1 (2.0)	2 (8.3)	0	5 (3.4)	0
Subthreshold parkinsonism						
Positive	27 (27.8)	0	1 (4.2)	4 (4.2)	12 (8.2)	4 (20.0)
Negative	63 (65.0)	50 (98.0)	23 (95.8)	23 (95.8)	134 (91.8)	16 (80.0)
Missing data	7 (7.2)	1 (2.0)	0	0	0	0
Olfaction						
Abnormal	61 (62.9)	44 (86.3)	21 (87.5)	22 (81.5)	19 (13.0)	20 (100.0)
Normal	25 (25.8)	7 (13.7)	3 (12.5)	4 (14.8)	126 (86.3)	0
Missing data	11 (11.3)	0	0	1 (3.7)	0	0
Constipation						
Yes	40 (41.2)	17 (33.3)	7 (29.2)	14 (51.9)	41 (28.1)	7 (35.0)
No	50 (51.6)	32 (62.7)	17 (70.8)	13 (48.1)	105 (71.9)	13 (65.0)
Missing data	7 (7.2)	2 (2.0)	0 (2.0)	0	0	
EDS						
Yes	56 (57.7)	9 (17.6)	5 (45.1)	20 (74.1)	81 (55.5)	14 (70.0)
No	33 (34.0)	16 (31.3)	19 (52.9)	7 (25.9)	65 (44.5)	6 (30.0)
Missing data	8 (8.3)	26 (50.1)	0	0	0	0
Symptomatic OH						
Yes	13 (13.4)	15 (29.4)	9 (37.5)	11 (40.7)	38 (24.7)	7 (35.0)

No	74 (76.3)	34 (66.7)	10 (41.7)	16 (59.3)	108 (75.3)	13 (65.0)
Missing data	10 (10.3)	2 (3.9)	5 (20.8)	0	0	0
Erectile dysfunction (in men)						
Yes	0 (23.0)	21 (43.8)	6 (28.6)	15 (68.2)	22 (26.0)	9 (56.3)
No	0 (24.7)	23 (47.9)	13 (61.9)	7 (31.8)	33 (74.0)	7 (43.7)
Missing data	92 (100)	4 (8.3)	2 (9.5)	0	0	0
Urinary dysfunction						
Yes	51 (52.6)	24 (47.1)	10 (41.7)	14 (51.9)	53 (36.3)	13 (65.0)
No	39 (40.2)	25 (49.0)	14 (58.3)	13 (48.1)	93 (63.7)	7 (35.0)
Missing data	7 (7.2)	2 (3.9)	0	0	0	0
Depression (± anxiety)						
Yes	27 (27.8)	12 (23.5)	9 (37.5)	4 (14.8)	27 (18.5)	5 (25.0)
No	63 (65.0)	38 (74.5)	15 (62.5)	23 (85.2)	119 (81.5)	15 (75.0)
Missing data	7 (7.2)	1 (2.0)	0	0	0	0
Cognitive deficit						
Yes	33 (34.0)	9 (17.6)	2 (8.3)	7 (25.9)	33 (22.6)	4 (20.0)
No	53 (54.7)	40 (78.5)	22 (91.7)	20 (74.1)	113 (77.4)	16 (80.0)
Missing data	11 (6.3)	2 (3.9)	0	0	0	0
Likelihood ratio						
Positive	73 (75.3)	48 (94.1)	20 (83.3)	25 (92.6)	13 (8.9)	9 (45.0)
Negative	24 (24.7)	3 (5.9)	4 (16.7)	2 (7.4)	133 (91.1)	11 (55.0)

Table 4.6: Summary of prodromal markers in each cohort. Data show number of subjects (n) and percentage (%) in brackets. Percentages were calculated based on the total number shown for each group. Abbreviations: PSG = polysomnography; iRBD = isolated REM sleep behaviour disorder; NMC = non-manifest carrier; RBDSQ = REM Sleep Behaviour Disorder Screening Questionnaire; DAT SPECT = dopamine transporter single-photon emission computed tomography; EDS = excessive daytime sleepiness; OH = orthostatic hypotension; NA = non-applicable. Likelihood ratio was positive (≥ 80% probability of having prodromal PD) or negative (< 80%) probability of having prodromal PD for the indicated numbers and percentages across each cohort.

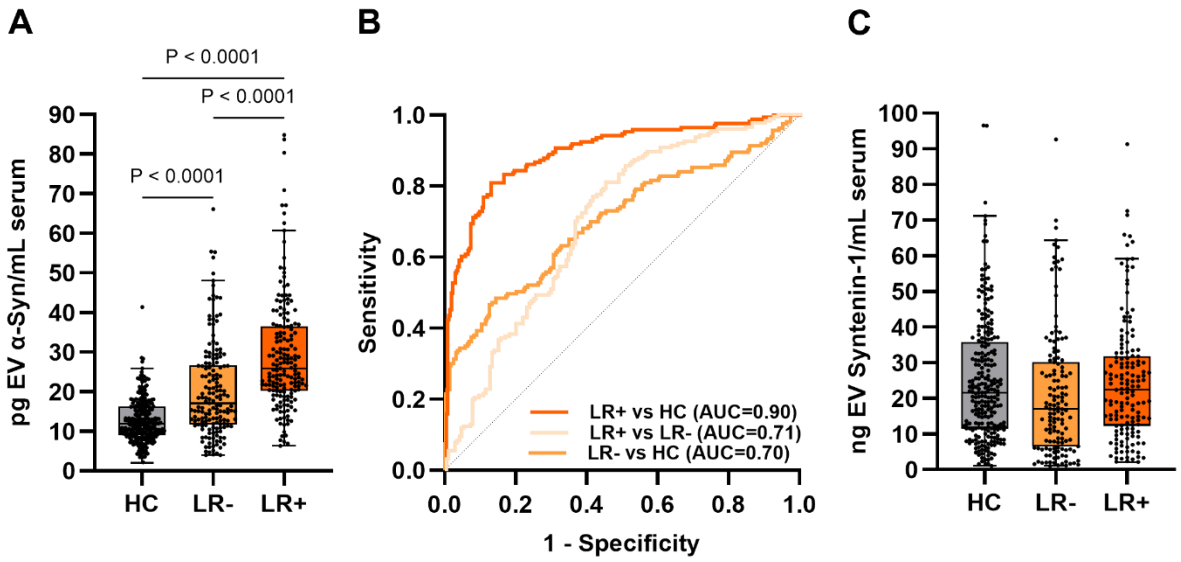


Figure 4.7: L1EV α-synuclein levels are increased in at-risk individuals with positive LR of developing PD. (**A**) Boxplot of L1EV α-synuclein measurements and (**B**) corresponding receiver operating characteristic (ROC) curves for those with a positive likelihood ratio (LR+) or a negative likelihood ratio (LR-) of prodromal PD based on the updated Movement Disorder Society prodromal research criteria, and current and historic healthy controls (HC). (**C**) Boxplot showing measurements for L1EV syntenin-1, which is a generic EV-associated marker. The midline of the box plots indicates the median and the box indicates the 25th and 75th percentiles. Outliers and whiskers were plotted using the Tukey method. Statistical significance was determined by Kruskal-Wallis test.

4.4.6 Association of serum L1EV α-synuclein levels with CSF pathology and phenoconversion

CSF α-synuclein SAA, which signifies the presence of brain pathology, was recently shown to detect a subgroup of at-risk subjects in the prodromal phase in the PPMI cohort.[155] To investigate the relevance of the biomarker to this readout of pathology, I analysed the SAA results for the PPMI subjects with hyposmia, iRBD, or *GBA1*^{N409S} (n = 157) in relation to L1EV α-synuclein levels and their probability of having prodromal PD. I found that those with a positive CSF SAA readout had higher L1EV α-synuclein in serum (26.41 ± 19.54 pg/mL) compared to those who were CSF SAA negative (15.88 ± 16.11 pg/mL), as shown in **Figures 4.8A** and **S4.6**. The SAA positive group primarily included those subjects with ≥ 80% probability of having prodromal PD who were also above the identified threshold derived from Oxford Discovery (17.75 pg/mL, shown as dotted blue line), as shown in **Figure 4.8B**. These

data showed that 68.3% of SAA negative, low risk subjects (< 5% probability) were also below the L1EV α-synuclein threshold derived (17.75 pg/mL) from the Oxford Discovery cohort, whereas 75.9% of SAA positive, high-risk subjects (≥ 80% probability) were above the threshold (**Figure 4.8B**). In the intermediate group (5 – 80% probability), 43.3% of SAA negative subjects were below the L1EV α-synuclein threshold and 50% of SAA positive subjects were above the threshold (**Figure 4.8B**).

Finally, across all cohorts, I identified 8 cases who converted to DLB, 32 cases who converted to PD and 1 case who converted to AD based on clinical diagnoses (**Figure 4.8C**). Of the 40 cases that phenoconverted to neuronal α-synucleinopathy, 32 (80.0% overall, 81.3% of PD, 75% of DLB) were above the threshold of 17.75 pg/mL, whereas the single AD case had L1EV α-synuclein below the threshold. In these clinically diagnosed cases, L1EV α-synuclein was lower in DLB phenoconverters (24.32 ± 14.53 pg/mL) than in the PD phenoconverters (30.59 ± 17.85 pg/mL), in line with our initial report in neuropathologically confirmed DLB cases.[94] In this small number of cases, I found a weak partial correlation after correcting for age and sex (r = 0.22, P = 0.25) between the levels of L1EV α-synuclein and time to phenoconversion (**Figure 4.8D**). However, complementary time-to-event analysis, using at-risk individuals who did not phenoconvert as the reference group, indicated that higher L1EV α-synuclein levels were not associated with the risk of phenoconversion to PD or DLB (**Figure 4.9**). I also found a weak inverse correlation between serum L1EV α-synuclein and total CSF α-synuclein in those who phenocoverted to PD (**Figure 4.10A**) and a significant inverse correlation in those with sporadic PD (**Figure 4.10B**). These data suggest that higher α-synuclein in L1EVs is associated with lower total α-synuclein in CSF and a longer time to conversion to PD.

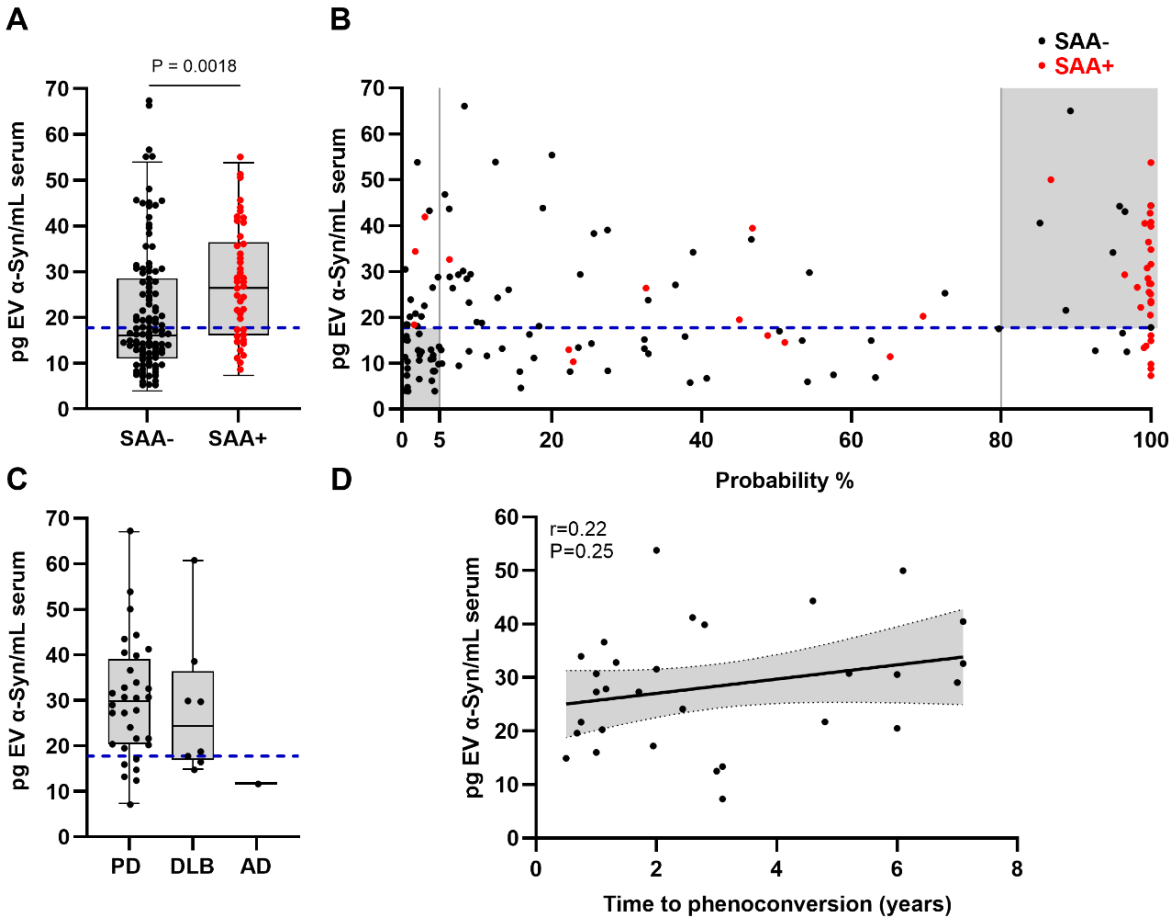


Figure 4.8: L1EV α-synuclein levels and CSF SAA or phenoconversion. (**A**) Serum L1EV α-synuclein levels were higher in subjects who were CSF α-synuclein SAA positive. The midline of the box plots indicates the median, and the box indicates the 25th and 75th percentiles. The horizontal dotted line represents the derived threshold (17.75 pg/mL) of L1EV α-synuclein. Outliers and whiskers were plotted using the Tukey method. Statistical significance was determined by Mann-Whitney test. (**B**) Relationship between serum L1EV α-synuclein levels, CSF α-synuclein SAA status and probability of having prodromal PD. The horizontal dotted line represents the derived threshold (17.75 pg/mL) of L1EV α-synuclein. The vertical lines represent the age and sex adjusted probability of having prodromal PD at 5% and 80%. (**C**) Boxplot of serum L1EV α-synuclein levels in at-risk subjects who phenoconverted to PD (*n* = 32), DLB (*n* = 8), and AD (*n* = 1). The horizontal dotted line represents the derived threshold (17.75 pg/mL) of L1EV α-synuclein. The midline of the box plots indicates the median, and the box indicates the 25th and 75th percentiles. Outliers and whiskers were plotted using the Tukey method. (**D**) Partial correlation between serum L1EV α-synuclein levels and time to phenoconversion to PD, adjusted for age and sex. Least squares regression line with 95% CI was plotted, Pearson coefficient r and corresponding P value were reported.

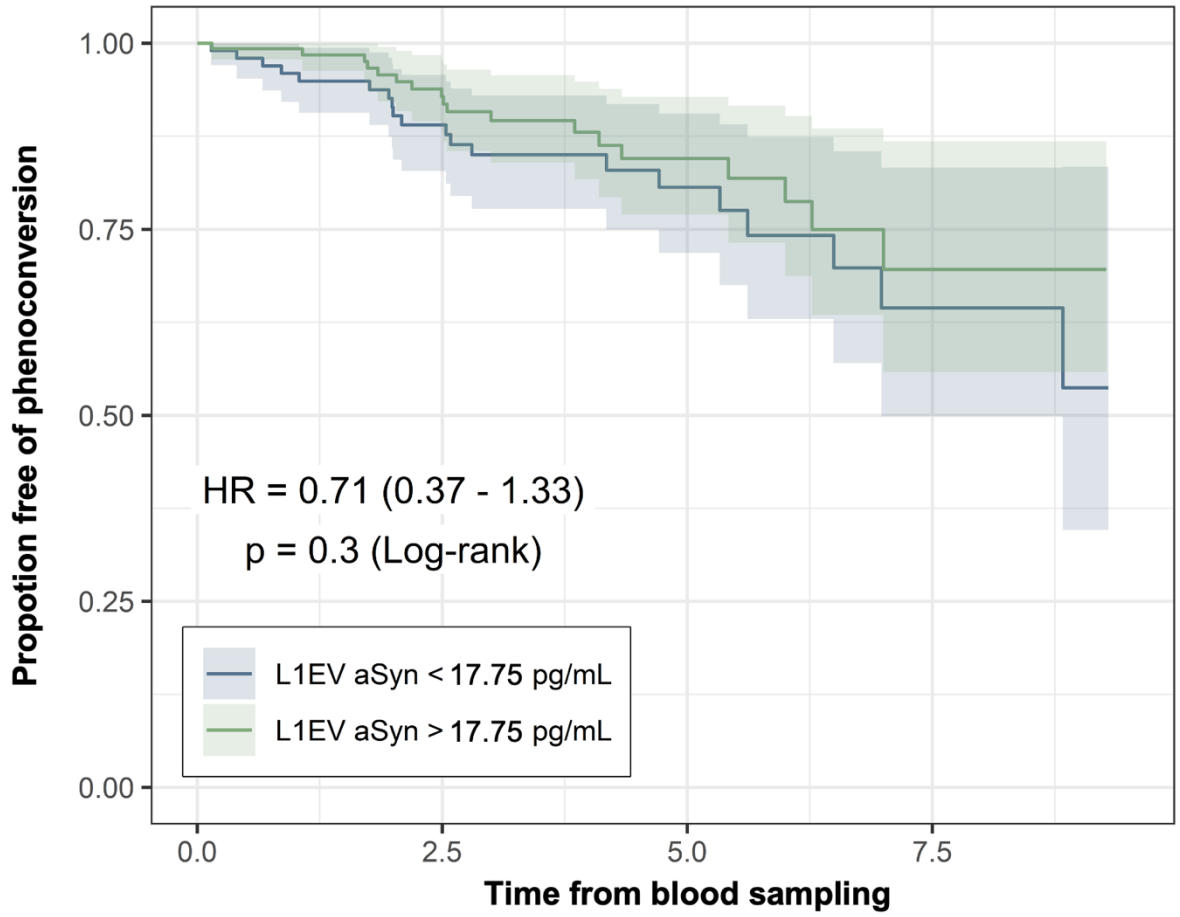


Figure 4.9: Kaplan-Meier survival curves for phenoconversion to PD or DLB as stratified by L1EV α-synuclein. Individuals stratified by L1EV α-synuclein above or below the optimal threshold (17.75 pg/mL) for differentiating individuals with iRBD from healthy controls derived from Oxford discovery cohort. Hazard ratio (HR) with 95% CI were derived from univariable Cox regression models, with phenoconverter group as a binary variable. This analysis was performed by Tanja Zerenner, University of Bristol.

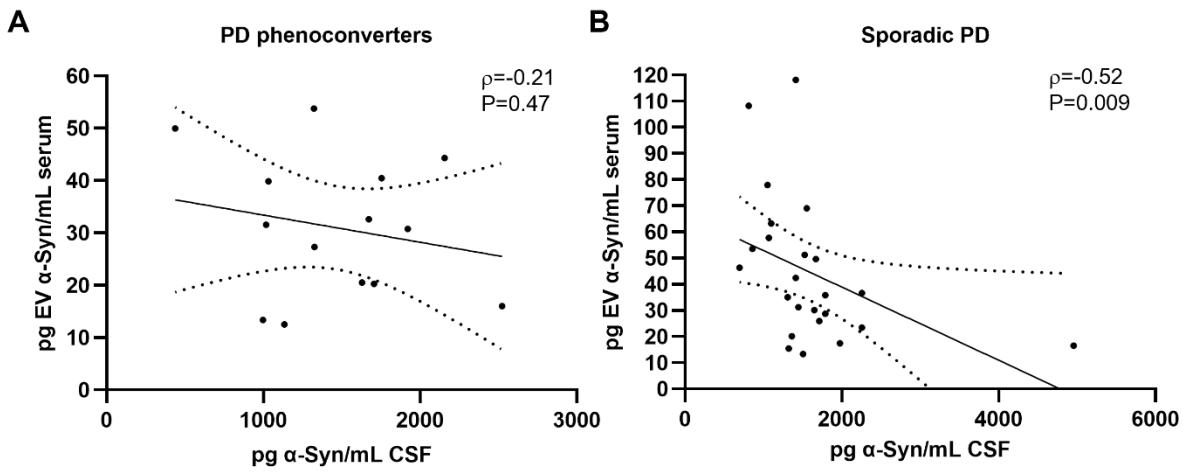


Figure 4.10: Correlation between serum L1EV α-synuclein and CSF total α-synuclein. Inverse correlation between serum L1EV α-synuclein and CSF total α-synuclein levels was (**A**) weak in a small number of at-risk subjects who phenoconverted to PD, and (**B**) significant in a larger group of patients with sporadic PD and available CSF measurements. Least squares regression line with 95% CI was plotted, Spearman coefficient ρ and corresponding P values were reported for each group.

4.4.7 Serum L1EV α-synuclein is increased in *LRRK2*^{G2019S} non-manifest carriers with additional prodromal markers and *LRRK2*^{G2019S} PD with CSF pathology

Carriers of the *LRRK2*^{G2019S} mutation have approximately a 10-fold increased risk of developing PD compared to non-carriers.[254] Unlike idiopathic PD, ~40% of *LRRK2* ^{G2019S} PD lack Lewy body pathology and are more likely to test negative for CSF α-synuclein SAA.[155,255] These findings suggest underlying heterogeneity in the core pathophysiology of *LRRK2* PD. To assess the potential of L1EV α-synuclein in the stratification of this group, I analysed *LRRK2*^{G2019S} NMC (*n* = 161) from the PPMI cohort (**Table 4.7**), focusing on those exhibiting pronounced prodromal markers beyond their genetic status. *LRRK2*^{G2019S} carriers with hyposmia (*n* = 16; 29.70 ± 23.14 pg/mL), an abnormal DaT SPECT (*n* = 18; 32.22 ± 29.11 pg/mL) or a positive SAA readout (*n* = 7; 23.96 ± 22.85 pg/mL) showed increased L1EV α-synuclein levels compared to those negative for the respective measures (20.98 ± 23.65 pg/mL, 20.36 ± 22.44 pg/mL, and 21.62 ± 22.34 pg/mL, respectively), as shown in **Figures 4.11A-C**.

I found that *LRRK2*^{G2019S} gene carriers with at least one of these markers (n = 38; 27.99 ± 25.46 pg/mL; *P* = 0.0059) exhibited higher L1EV α-synuclein levels than those without any of these markers (*n* = 123; 16.45 ± 20.88 pg/mL), as shown in **Figure 4.11D**. When stratified by estimated probability of developing PD, carriers with < 5% risk (*n* = 84), 5 – 80% risk (*n* = 65), and ≥ 80% risk (*n* = 12) exhibited overlapping L1EV α-synuclein levels. Unlike *GBA1*^{N409S} carriers, *LRRK2*^{G2019S} carriers at high risk (20.93 ± 19.12 pg/mL) did not show significant differences compared to those with a low (16.39 ± 22.65 pg/mL) or intermediate risk (26.74 ± 28.30 pg/mL), as shown in **Figure 4.11E**. This finding is consistent with previous finding showing only ~60% of *LRRK2*^{G2019S} PD exhibit Lewy body pathology.[255]

To investigate the relevance of L1EV α-synuclein in *LRRK2*^{G2019S} PD subjects (*n* = 144; **Table 4.7**), I examined L1EV α-synuclein levels in relation to CSF SAA and olfactory function. Unlike findings in iRBD, *LRRK2*^{G2019S} PD subjects with hyposmia (20.16 ± 17.98 pg/mL) exhibited similar L1EV α-synuclein levels to those with normal olfaction (19.57 ± 14.36 pg/mL), as shown in **Figure 4.11F**. However, those with a positive SAA readout (21.47 ± 19.52 pg/mL) had higher L1EV α-synuclein levels than SAA-negative subjects (15.79 ± 14.89 pg/mL), irrespective of olfactory function (**Figures 4.11G** and **4.11H**).

Lastly, I examined the association between L1EV α-synuclein and disease duration. *LRRK2*^{G2019S} PD positive for L1EV α-synuclein (≥ 17.75 pg/mL) had a longer disease duration (26.72 ± 33.42 months) compared to those who with lower levels (21.07 ± 20.34 pg/mL), regardless of their SAA status. However, no direct correlation was observed between L1EV α-synuclein levels and disease duration (**Figure 4.11I**).

	***LRRK2*^{G2019S} NMC**	***LRRK2*^{G2019S} PD**	**P-value**
No of individuals	161	144	NA
Gender, No. (%)			
Female	100	75	0.77
Male	61	69	
Age, mean (SD), y	61.43 (7.32)	63.85 (8.00)	0.063
MoCA, mean (SD)	26.93 (2.22)	26.15 (2.92)	0.04
L1EV α-Syn, median (IQR), pg/mL	20.47 (22.60)	20.10 (18.05)	0.55
CSF SAA, No. (%) [a]			
Positive	10 (7.7)	93 (66.4)	<0.0001
Negative	120 (92.3)	47 (33.6)	

Table 4.7: Demographic characteristics of subjects with *LRRK2*^{G2019S} from PPMI cohort. Data are number (%), mean (SD) or median (IQR). Abbreviations: iRBD = isolated REM sleep behaviour disorder; LRRK2 = Leucine-rich repeat kinase 2; NMC = non-manifest carriers; PD = Parkinson's Disease; MoCA = Montreal Cognitive Assessment; L1EV = L1CAM+ extracellular vesicles; α-Syn = α-synuclein. SAA = α-synuclein seed amplification assay. Student's t-test was used to compare age, Mann-Whitney U test was used to compare MoCA and L1EV α-Syn, and Pearson χ^2 test to compare gender and CSF SAA positivity frequency between groups.

[a] CSF SAA result was not available in *n* = 31 *LRRK2*^{G2019S} NMC and *n* = 4 *LRRK2*^{G2019S} PD.

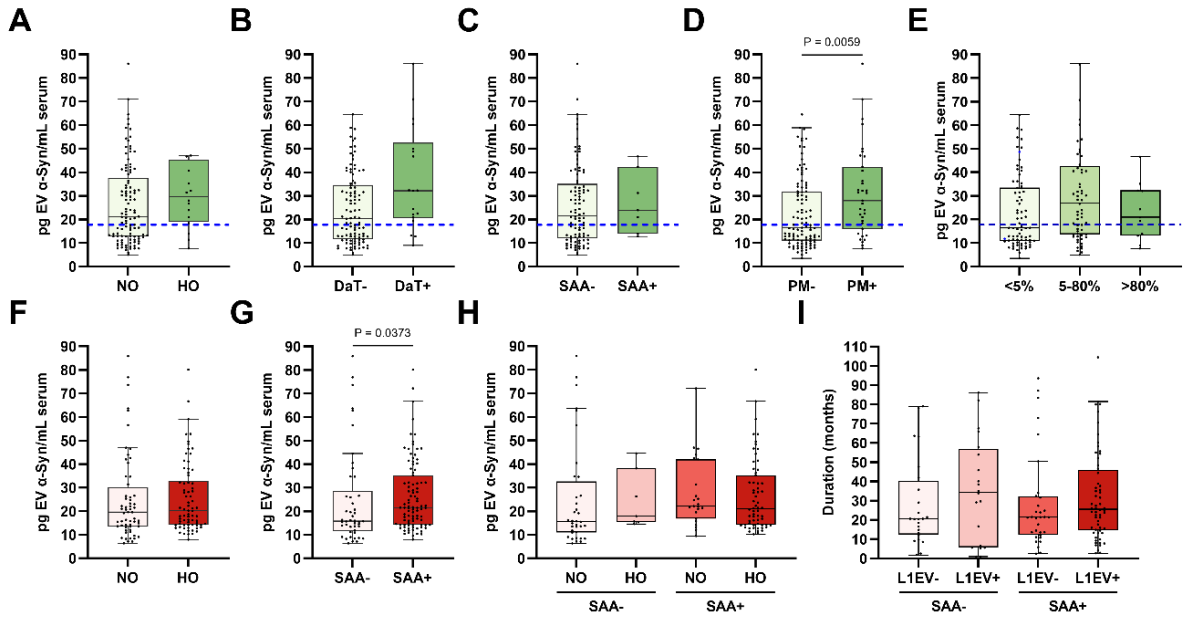


Figure 4.11: L1EV α-synuclein measurements in *LRRK2*^{G2019S} non-manifest gene carriers and *LRRK2*^{G2019S} PD subjects. Boxplot of L1EV α-synuclein measurements for *LRRK2*^{G2019S} non-manifest carriers (**A**) with normal (NO) or abnormal (HO) olfaction, (**B**) with a negative/normal (DaT-) or a positive/abnormal (DaT+) DaT SPECT, (**C**) with a negative (SAA-) or positive (SAA+) CSF α-synuclein SAA result, (**D**) without any of the following makers (PM-): HO, DaT+, or SAA+, and with at least one of these markers (PM+), and (**E**) with < 5%, or 5 – 80%, or ≥ 80% probability of having prodromal PD. Boxplot of L1EV α-synuclein measurements for *LRRK2*^{G2019S} PD (**F**) with NO or HO, (**G**) with SAA- or SAA+, (**H**) stratified by olfactory function and SAA status, and (**I**) stratified by a negative (< 17.75 pg/mL, L1EV-) or positive (≥ 17.75 pg/mL, L1EV+) L1EV α-synuclein measurement and SAA status. The midline of the box plots indicates the median, and the box indicates the 25th and 75th percentiles. Outliers and whiskers were plotted using the Tukey method. The horizontal dotted line represents the derived threshold (17.75 pg/mL) of L1EV α-synuclein. Statistical significance was determined by Mann-Whitney test (panels **D** and **G**).

4.5 Discussion

4.5.1 L1EV α-synuclein as a biomarker for subjects at risk of developing PD

In this study, I show that L1EV α-synuclein levels are increased in subjects at risk of developing PD and related dementia. iRBD subjects exhibit a 2-fold increase in L1EV α-synuclein levels compared to controls, as validated across independent iRBD groups. This is in line with our previous estimate of a ~2-fold increase in L1EV α-synuclein levels across multiple cohorts of sporadic PD compared to healthy controls[94,95] and consistent with the idea

that both conditions are α-synucleinopathies. Furthermore, a threshold derived from the largest iRBD group also differentiated subjects with ≥ 80% probability of having prodromal PD from those with a low risk (< 5% probability) in a further independent multicentre validation group (PPMI). This validation group consists of subjects with variable risk recruited across multiple sites in the USA, Europe, and Israel, which could explain the slightly reduced performance of the biomarker in this group. Nevertheless, these findings demonstrate the robustness of L1EV α-synuclein as a prodromal biomarker of α-synucleinopathy, irrespective of recruitment site or specific diagnosis.

4.5.2 Performance of L1EV α-synuclein in phenoconversion and subgroup stratification

The utility of L1EV α-synuclein as a prodromal biomarker is further supported by its ability to identify individuals who phenoconverted to α-synucleinopathy. In these cases, the biomarker correctly identified 80% of subjects who developed clinical PD or DLB, taken together with our previous reports that L1EV α-synuclein levels are increased in PD and DLB but not MSA,[94,95] the biomarker offers a blood-based measurement to identify prodromal neuronal α-synucleinopathy.

Across cohorts, subgroups with more than one prodromal marker exhibited higher L1EV α-synuclein levels. Thus, measurements of L1EV α-synuclein in combination with specific prodromal markers, such as olfactory, cognitive deficit, possible or definite RBD, and *GBA1* gene status, could be harnessed to aid the sub-stratification of those individuals with the highest probability of developing PD and related Lewy body diseases. Additive risk was previously observed with combination of other markers such as hyposmia, age, constipation, and abnormal DaT SPECT.[66] Measurement of L1EV α-synuclein could offer a cheaper and more accessible alternative means of screening at-risk individuals compared to a DaT SPECT

or labour-intensive clinical assessments. Notably, L1EV α-synuclein levels are also increased in DaT SPECT negative at-risk subjects, indicating that α-synuclein dyshomeostasis may be detectable in blood before overt dopaminergic neurodegeneration.

The variability in L1EV α-synuclein levels among *LRRK2*^{G2019S} carriers suggests heterogeneous disease mechanisms, where α-synuclein pathology is prominent in some but not all carriers.[157-159] The increase of L1EV α-synuclein in those with hyposmia, an abnormal DaT SPECT, or a positive SAA result indicates that certain subgroups exhibit α-synuclein-driven pathology even in the prodromal phase. However, the lack of differentiation between high- and low-risk carriers suggests that alternative mechanisms, such as *LRRK2*-driven neuroinflammation,[256] may also play a role in disease progression. These findings emphasise the importance of biomarker-based stratification to identify those most likely to develop α-synucleinopathy and guide targeted interventions.

4.5.3 Correlation of L1EV α-synuclein with CSF SAA

L1EV α-synuclein levels were higher in subjects with a positive CSF SAA result, and 76% of those subjects with both a positive CSF SAA result and ≥ 80% probability of having prodromal PD had L1EV α-synuclein above the derived threshold. Although none of these cases are neuropathologically confirmed, these data suggest that serum L1EV α-synuclein is a proxy biomarker of pathology based on this CSF assay, as previously found in a small number of neuropathologically confirmed DLB cases.[94]

It should be noted that those subjects with L1EV α-synuclein above the threshold but with a negative CSF SAA result in the intermediate group are still at-risk subjects based on the prodromal PD probability. At this stage, we do not know for certain whether the egress of α-synuclein in serum L1EV precedes pathology that is detectable by CSF SAA. Positive CSF SAA readouts were reported in 86% of subjects with iRBD or hyposmia,[155] which is similar to

the sensitivity of this blood-based assay in these groups. SAA of α-synuclein aggregates immunoprecipitated from serum was also positive in PD but only in 44% of iRBD.[257] The latter suggests that, at least in blood, egress of α-synuclein in L1EVs, which was above the threshold in 80.4 % (160 of 199) of the studied iRBD cases, may precede detection or formation of aggregates during the prodromal phase.

Because L1CAM is primarily expressed in neurons of both the central and peripheral nervous system, it is possible that L1EVs are partly derived from postganglionic autonomic nerves that are pathologically affected early in PD and related dementia. This supports a potential link to the "body-first" versus "brain-first" hypothesis of PD,[20] where peripheral α-synuclein pathology (e.g. in autonomic nerves) may precede CNS involvement in certain subtypes. Given this, L1EV α-synuclein could reflect early pathological changes in peripheral autonomic structures, aligning with the "body-first" trajectory. This raises the possibility that peripheral EV-derived biomarkers may help stratify patients by pathogenic subtype and disease initiation site. For instance, it would be interesting to investigate in the future whether skin SAA, which was recently reported in iRBD,[175] better correlates with the biomarker.

4.5.4 Potential mechanisms underlying increased L1EV α-synuclein

Because EVs are derived from within the cells, and α-synuclein is targeted to lysosomes[31] and released in EVs in response to lysosome inhibition,[258] these findings in patients suggest that increased L1EV secretion may reflect a fundamental defect in intracellular α-synuclein trafficking that occurs several years before clinical presentation. This mechanism would be consistent with the finding of an inverse correlation between L1EV α-synuclein and total CSF α-synuclein in those who went on to develop PD or had sporadic PD. I also observed that in those at-risk subjects who developed PD, higher L1EV α-synuclein at baseline was associated with longer interval to phenoconversion. One explanation for these observations is

the existence of an adaptive, likely protective, efflux of α-synuclein outside neuronal tissues in response to defective intraneuronal processing by lysosomes (e.g. due to *GBA1* gene mutations or polymorphisms in other lysosomal genes identified by genome-wide association studies in sporadic PD).

This assay measures total α-synuclein, and L1EVs may contain both physiological and pathogenic forms such as α-synuclein oligomers. For example, α-synuclein conformers with fibrillar appearance were amplified from plasma-derived L1EVs isolated from PD patients but not from controls.[199] Therefore, amplification assays or immunoassays with conformation specific antibodies, in combination with assay automation, could be applied to prodromal samples to further refine the performance of the biomarker.

4.5.5 Limitations and future directions

There are limitations to our findings. This is a cross-sectional study, and further validation of the biomarker in longitudinal cohorts will be an important future investigation that may identify other clinical correlates or more precise thresholds. Therefore, despite group validation across different cohorts, the clinical value of this biomarker at single-subject level for routine practice is not yet full established. The cut-off values may require further refinement ideally in neuropathologically confirmed cases when at-risk cohort participants eventually reach post-mortem examination. The cohorts were composed of clinical phenotypes highly predictive of α-synuclein pathology. Analyses of subgroups within these cohorts revealed associations with specific prodromal markers, despite the small subsets of patients. Future studies are needed to confirm these findings and extend their applicability to wider population cohorts. Where such data were available, most of the study participants self-identified as white, and this study was underpowered to test differences in analyte levels across racial and ethnic groups. Therefore, the results may not generalise to other populations.

A methodological limitation is that haemolysis was only assessed visually, and no systematic haemoglobin quantification was performed. Although rigorous protocols were used to minimise red blood cell contamination during sample preparation, low-level haemolysis could still affect α-synuclein readings, as red blood cells contain abundant α-synuclein. Future studies should incorporate haemoglobin measurement as part of pre-analytical quality control to reduce this potential confound and enhance data reliability.

4.5.6 Conclusion

In summary, this work demonstrates the value of L1EV α-synuclein in identifying subjects at-risk of developing neuronal α-synucleinopathy and offers patient-based measurements that support the existence of a fundamental shift in α-synuclein homeostasis that is detectable in blood at the early stages of the pathogenic cascade. Measurement of L1EV α-synuclein levels in serum could be used as a scalable screening test of Lewy body pathology in at-risk individuals and aid recruitment for disease-modifying trials.

4.6 Supplementary information

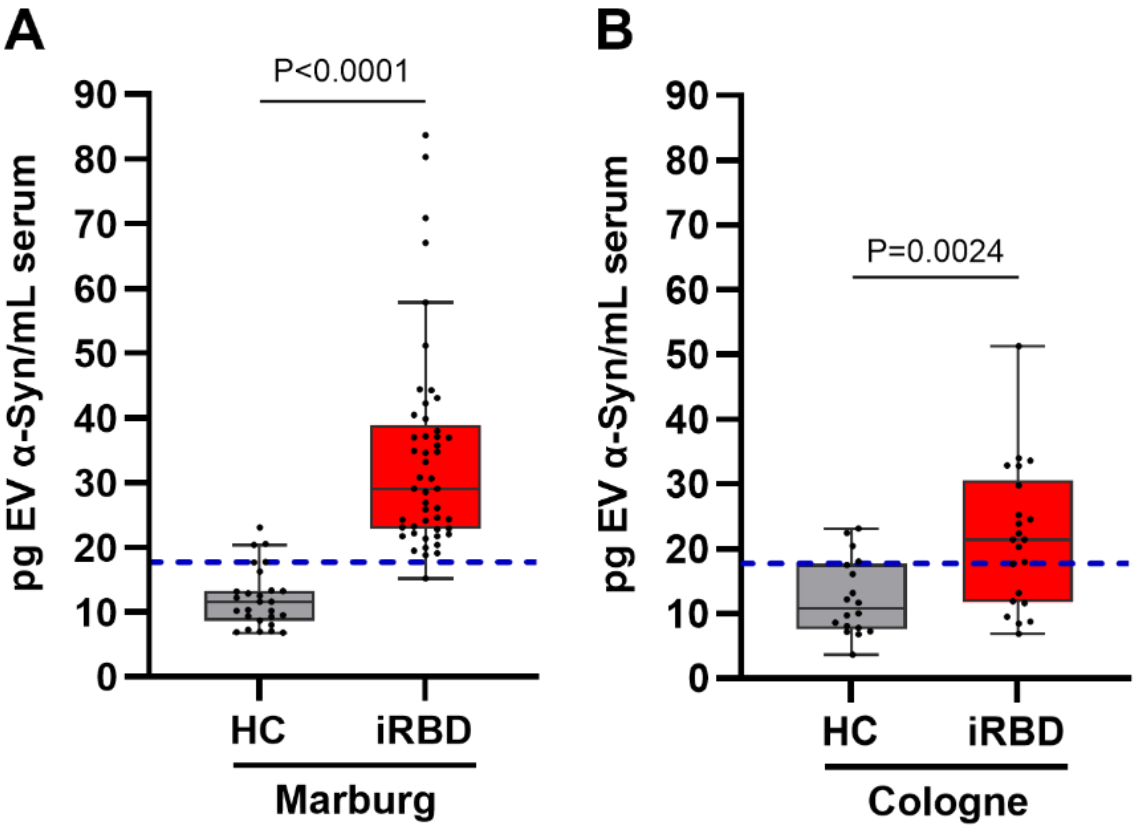


Figure S4.1: L1EV α-synuclein levels in Marburg and Cologne cohorts. Boxplots showing the distribution of L1EV α-synuclein for (**A**) Marburg cohort (**B**) Cologne cohort. The threshold derived from Oxford Discovery (17.75 pg/mL) is shown as a dotted blue line. The midline of the box plots indicates the median, and the box indicates the 25th and 75th percentiles. Outliers and whiskers were plotted using the Tukey method. Statistical significance was determined by Mann-Whitney test.

No. (%)			
Probability score	**< 5%**	**5 – 80%**	**≥ 80%**
Total No.	57	89	47
PSG-proven iRBD	0	2	25
RBDSQ			
Positive	4 (7.0)	22 (25.3)	7 (31.8)
Negative	53 (93.0)	65 (74.7)	15 (68.2)
Missing data	0	0	0
DaT SPECT			
Abnormal	0	3 (3.4)	30 (63.8)
Normal	57 (100)	83 (93.2)	15 (31.9)
Missing data	0	3 (3.4)	2 (4.3)
Subthreshold parkinsonism			
Positive	0	6 (6.8)	14 (29.8)
Negative	57 (100)	83 (93.2)	33 (70.2)
Missing data	0	0	0
Olfaction			
Abnormal	2 (3.5)	24 (27.0)	34 (72.3)
Normal	55 (96.5)	65 (73.0)	11 (23.4)
Missing data	0	0	2 (4.3)
Constipation			
Yes	5 (8.8)	27 (30.3)	30 (63.8)
No	52 (91.2)	62 (69.7)	17 (36.2)
Missing data	0	0	0
EDS			
Yes	20 (35.1)	58 (65.2)	37 (78.7)
No	37 (64.9)	31 (34.8)	10 (21.3)
Missing data	0	0	0
Symptomatic OH			

Yes	2 (3.5)	31 (34.8)	23 (48.9)
No	55 (96.5)	58 (65.2)	24 (51.1)
Missing data	0	0	0
Erectile dysfunction (in men)			
Yes	3 (4.8)	17 (45.9)	25 (71.4)
No	18 (95.2)	20 (54.1)	10 (28.6)
Missing data	0	0	0
Urinary dysfunction			
Yes	13 (22.8)	38 (42.7)	29 (61.7)
No	44 (77.2)	51 (57.3)	18 (38.3)
Missing data	0	0	0
Depression (± anxiety)			
Yes	6 (10.5)	17 (19.1)	13 (27.7)
No	51 (89.5)	72 (80.9)	34 (72.3)
Missing data	0	0	0
Cognitive deficit			
Yes	5 (8.8)	22 (24.7)	17 (36.2)
No	52 (91.2)	67 (75.3)	30 (63.8)
Missing data	0	0	0

Table S4.1: Summary of prodromal markers in the PPMI cohort. Data shown as number of subjects (n) and percentages (%) in brackets in subjects with < 5 %, 5 – 80%, and ≥ 80% probability of prodromal PD from PPMI cohort. Percentages were calculated based on the total number shown for each group. Abbreviations: PSG = polysomnography; iRBD = isolated REM Sleep Behaviour Disorder; RBDSQ = REM Sleep Behaviour Disorder Screening Questionnaire; DAT SPECT = dopamine transporter single-photon emission computed tomography; EDS = excessive daytime sleepiness; OH = orthostatic hypotension.

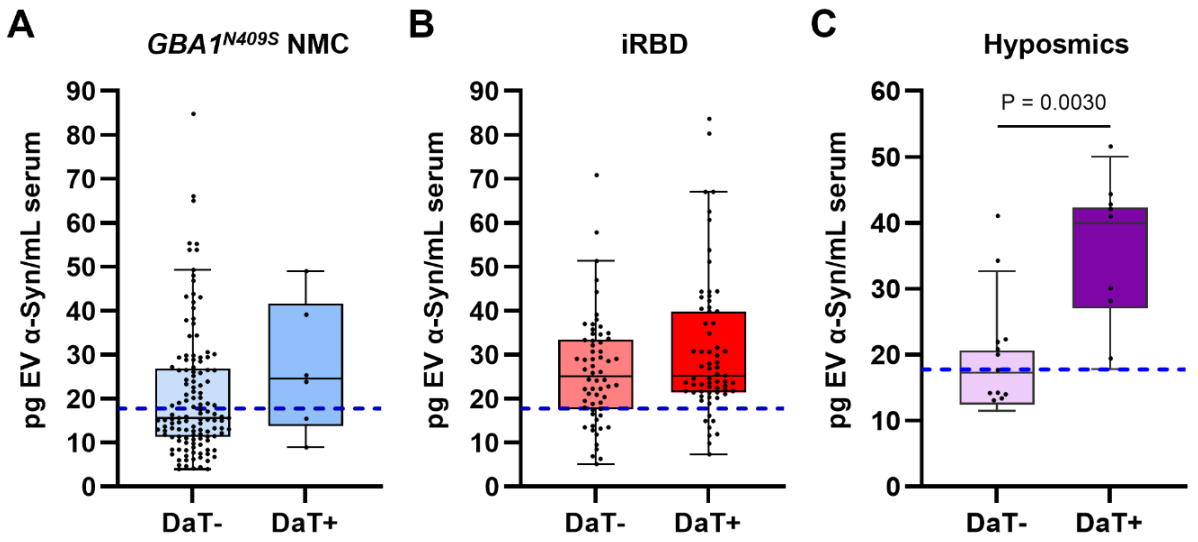


Figure S4.2: L1EV α-synuclein levels in prodromal groups with available DaT SPECT. Comparison between those with a negative (normal) and a positive (abnormal) DaT SPECT across individual prodromal groups of **(A)** *GBA1*^{N409S} non-manifest carrier (NMC), **(B)** iRBD, and **(C)** hyposmics. The threshold (17.75 pg/mL) derived from Oxford Discovery is shown as a dotted blue line. Analyses showed that 42% of *GBA1*^{N409S} NMC subjects, 74% of iRBD subjects, and 50% of hyposmics with a normal DaT SPECT had L1EV α-synuclein levels above the trained threshold. The midline of the box plots indicates the median, and the box indicates the 25th and 75th percentiles. Outliers and whiskers were plotted using the Tukey method. Statistical significance was determined by Mann-Whitney test.

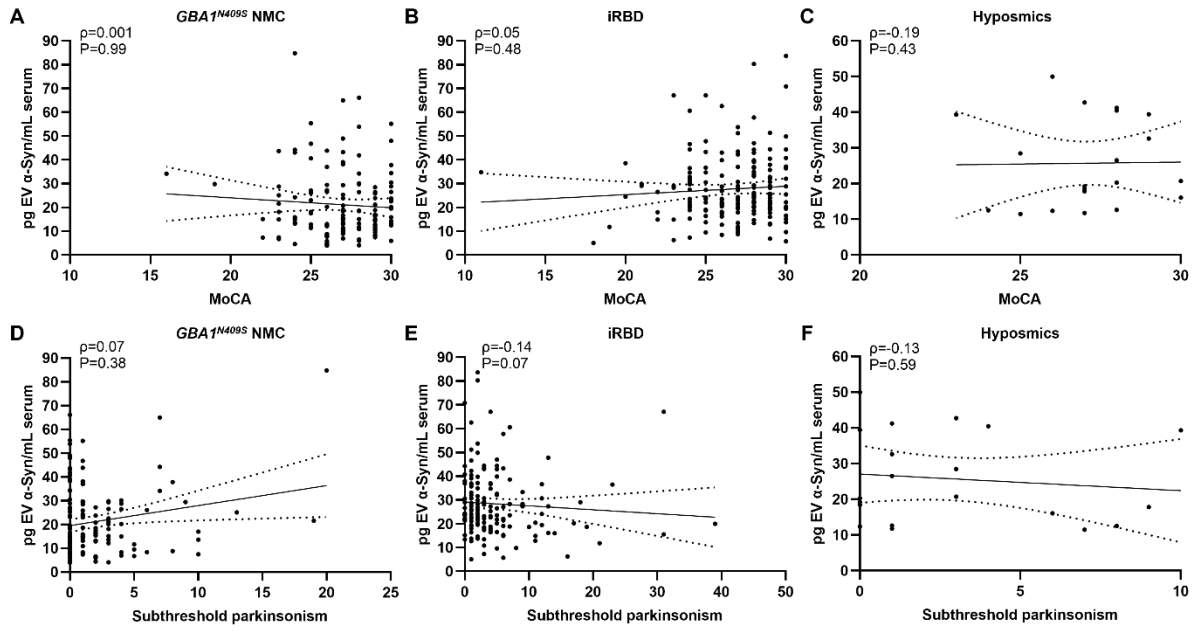


Figure S4.3: Correlation between L1EV α-synuclein levels and cognitive or motor scores. There was no correlation between (**A-C**) MoCA or (**D-F**) subthreshold parkinsonism as assessed by MDS-UPDRS-III and L1EV α-synuclein levels in any of the three prodromal conditions, including *GBA1*^{N409S} non-manifest carrier (NMC), iRBD, and hyposmics. Least squares regression line with 95% CI was plotted and Spearman coefficient ρ and corresponding P values were reported for each group.

Correlation coefficient r (p-value)							
Cohort		**HC**	**iRBD**	***GBA1*^{N409S} NMC**			**Hyposmics**
Oxford Discovery	Age	0.06 (0.65)	0.09 (0.42)	NA	NA	NA	NA
	MoCA	0.13 (0.36)	-0.01 (0.91)	NA	NA	NA	NA
	Subthreshold Parkinsonism	-0.08 (0.58)	-0.05 (0.66)	NA	NA	NA	NA
Marburg	Age	0.05 (0.79)	-0.07 (0.63)	NA	NA	NA	NA
	MoCA	0.74 (0.13)	0.03 (0.84)	NA	NA	NA	NA
	Subthreshold Parkinsonism	-0.12 (0.84)	-0.03 (0.81)	NA	NA	NA	NA
Cologne	Age	0.10 (0.70)	0.30 (0.18)				
	MoCA	0.20 (0.43)	0.04 (0.88)	NA	NA	NA	NA
	Subthreshold Parkinsonism	NA	NA	NA	NA	NA	NA
PPMI	Probability	NA	NA	< 5%	5 – 80%	≥ 80%	NA
	Age	-0.28 (0.23)	0.14 (0.52)	0.01 (0.93)	0.04 (0.72)	0.56 (0.05)	-0.12 (0.61)
	MoCA	-0.19 (0.41)	-0.04 (0.85)	0.23 (0.11)	0.06 (0.61)	-0.07 (0.83)	0.19 (0.43)
	Subthreshold Parkinsonism	-0.003 (0.99)	-0.22 (0.13)	0.19 (0.19)	-0.13 (0.26)	0.32 (0.28)	0.13 (0.59)

Table S4.2: Correlation analyses in each cohort. Correlations between the indicated clinical parameters and L1EV α-synuclein were calculated using Pearson correlation when data were normally distributed, or Spearman correlation when data were not normally distributed. Correlation coefficient r with corresponding P values in brackets were shown for each parameter.

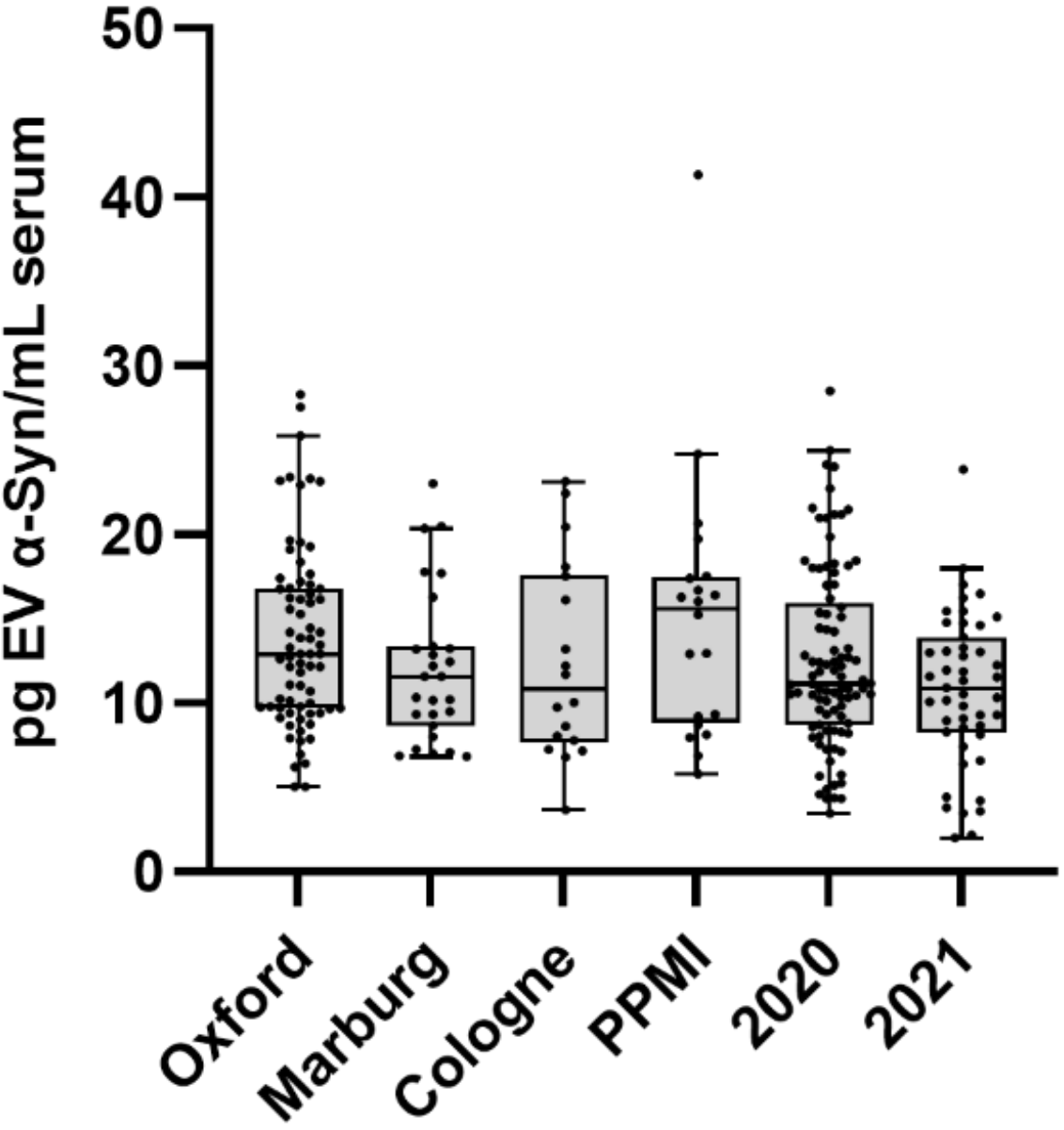


Figure S4.4: Comparison of L1EV α-synuclein levels between current and historic controls. There was no significant differences between current healthy control samples analysed in this study (Oxford, Marburg, Cologne, and PPMI) and historic control samples (analysed in 2020 and 2021). The midline of the box plots indicates the median, and the box indicates the 25th and 75th percentiles. Outliers and whiskers were plotted using the Tukey method. Statistical significance was determined by Kruskal-Wallis test.

	AUC (95% CI)	Threshold (pg/mL) [a]	Sensitivity (95% CI)	Specificity (95% CI)
HC vs LR+	0.90 (0.87 – 0.93)	18.54	0.81 (0.75 – 0.86)	0.87 (0.83 – 0.91)
HC vs LR-	0.70 (0.65 – 0.76)	18.09	0.48 (0.41 – 0.56)	0.86 (0.81 – 0.89)
LR+ vs LR-	0.71 (0.65 – 0.76)	18.65	0.81 (0.75 – 0.86)	0.55 (0.48 – 0.63)

Table S4.3: ROC analyses for stratifying at-risk subjects. Abbreviations: AUC = area under the Receiver Operating Characteristic curve; HC = healthy control; LR = likelihood ratio.

[a] Optimal threshold was determined by the Youden's index for each comparison and respective sensitivity and specificity were reported.

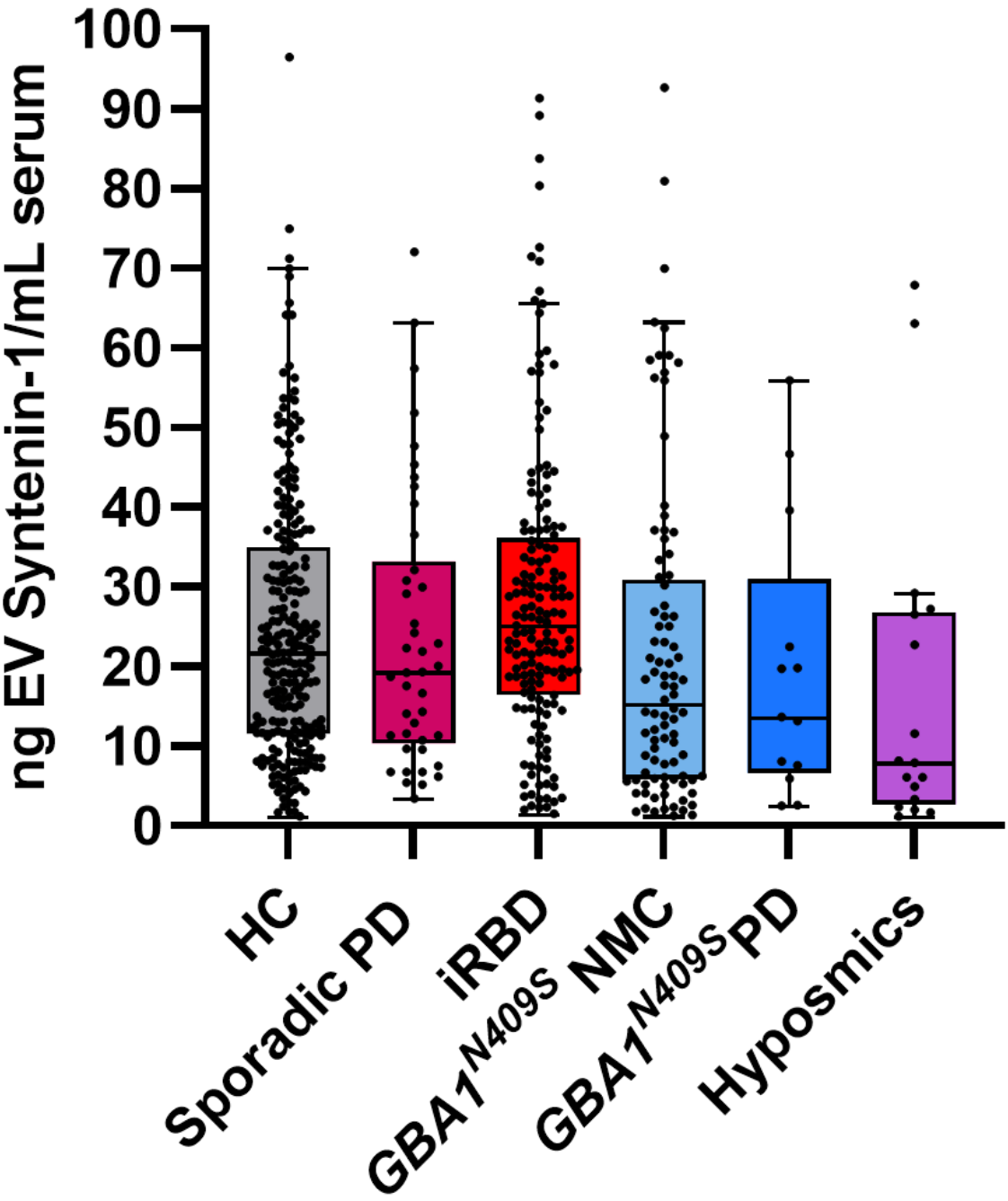


Figure S4.5: L1EV-associated syntenin-1 levels in each condition. No specific pattern was observed for this generic EV marker across groups with different conditions. The midline of the box plots indicates the median, and the box indicates the 25th and 75th percentiles. Outliers and whiskers were plotted using the Tukey method. Statistical significance was determined by Kruskal-Wallis test.

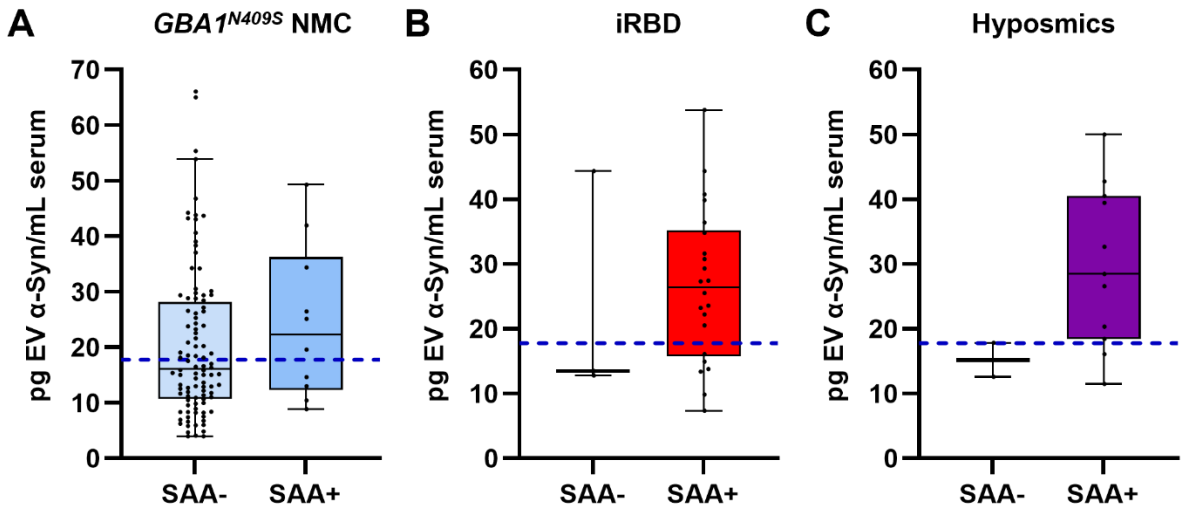


Figure S4.6: L1EV α-synuclein measurements in prodromal groups with available SAA. Comparison of those with a negative and a positive CSF SAA result across the individual prodromal groups of (**A**) *GBA1*^{N409S} non-manifest carrier (NMC), (**B**) iRBD, and (**C**) hyposmics. The threshold derived from Oxford Discovery (17.75 pg/mL) is shown with a dotted blue line. The midline of the box plots indicates the median, and the box indicates the 25th and 75th percentiles. Outliers and whiskers were plotted using the Tukey method. Statistical significance was determined by Mann-Whitney test.

Chapter 5

Single EV detection assay identifies membrane-associated α-synuclein as an early-stage biomarker in PD

Adapted from Yan et al. *Cell Reports Medicine* 2025; 6(3):101999

5. Single EV detection assay identifies membrane-associated α-synuclein as an early-stage biomarker in PD

5.1 Introduction

5.1.1 EVs as biomarkers for PD

Isolation of presumed neuronally-derived L1EVs, which mirror the homeostatic state of nerve cells, has shown promise as a biomarker for PD,[96,259,260] However, the detection of relevant proteins requires large sample input (typically > 200 μL) and specialised instruments, which may not always be easily accessible. Moreover, current analytical techniques often involve immunocapture, EV lysis, and bulk averaging, which obscure the heterogeneity of EV populations. These approaches also fail to resolve molecular features at the single-vesicle level and cannot distinguish between internalised and membrane-associated protein species.

Notably, recent studies have demonstrated that both total and pS129-α-synuclein are not only encapsulated within EVs, but also present on their external membrane surface, a form with distinct structural and immunological properties.[261] This underscores the need for more advanced analytical platforms capable of resolving such distinctions with adequate sensitivity.

5.1.2 Microfluidic-based EV analysis

Recent advances in single-EV analysis have demonstrated the potential of microfluidic technologies for high-resolution biomarker profiling. Among these, droplet microfluidic platforms offer a unique opportunity to analyse individual EVs in a high-throughput manner, enabling the detection of rare biomarkers with unprecedented sensitivity and specificity. Through sophisticated design of microchannels and precise manipulation of fluids at the microscale level, these platforms enable rapid and accurate detection of EV-based biomarkers

from complex biofluids. Furthermore, they allow for the simultaneous analysis of thousands of individual EVs, providing detailed quantitative resolution of EV heterogeneity.[220-223]

In addition to their sensitivity, droplet microfluidic platforms require minimal sample volumes (< 20 μL), making them ideal for analysing precious clinical samples.[212] The encapsulation of individual EVs also reduces cross-reactivity and non-specific binding, thus enhancing assay specificity and reproducibility. By preserving EV integrity throughout the assay, this technology ensures that detected signals originate exclusively from surface proteins, avoiding confounding from intraluminal or contaminating proteins. Together, these features make droplet microfluidic immunoassays a promising tool for the selective detection of EV membrane-associated biomarkers in PD.

5.2 Aims and objectives

This study aims to develop a droplet-based single-EV microfluidic assay for the ultrasensitive detection of membrane-associated protein on individual EVs, with a particular focus on L1EV membrane-associated α-synuclein. By integrating compartmentalisation of EVs droplet compartmentalisation, and enzyme-catalysed fluorescence amplification, the assay seeks to address current sensitivity constraints in EV-based biomarker detection (**Figure 5.1**). The assay would be further evaluated for its diagnostic potential in PD and prodromal individuals with iRBD. The specific objectives are to:

1. Develop a droplet-based microfluidic assay for high-throughput, single-EV detection and quantification of surface protein biomarkers.
2. Demonstrate that α-synuclein is present on the external membrane surface of serum-derived EVs.

3. Assess the pathological relevance of L1EV surface α-synuclein using conditioned media (CM) from neuroblastoma cells expressing PD-linked α-synuclein mutants or human iPSC-derived dopaminergic neurons from a patient with *SNCA* triplication.
4. Evaluate the diagnostic utility of the platform in detecting L1EV membrane-associated α-synuclein for distinguishing individuals with PD or iRBD from healthy controls.

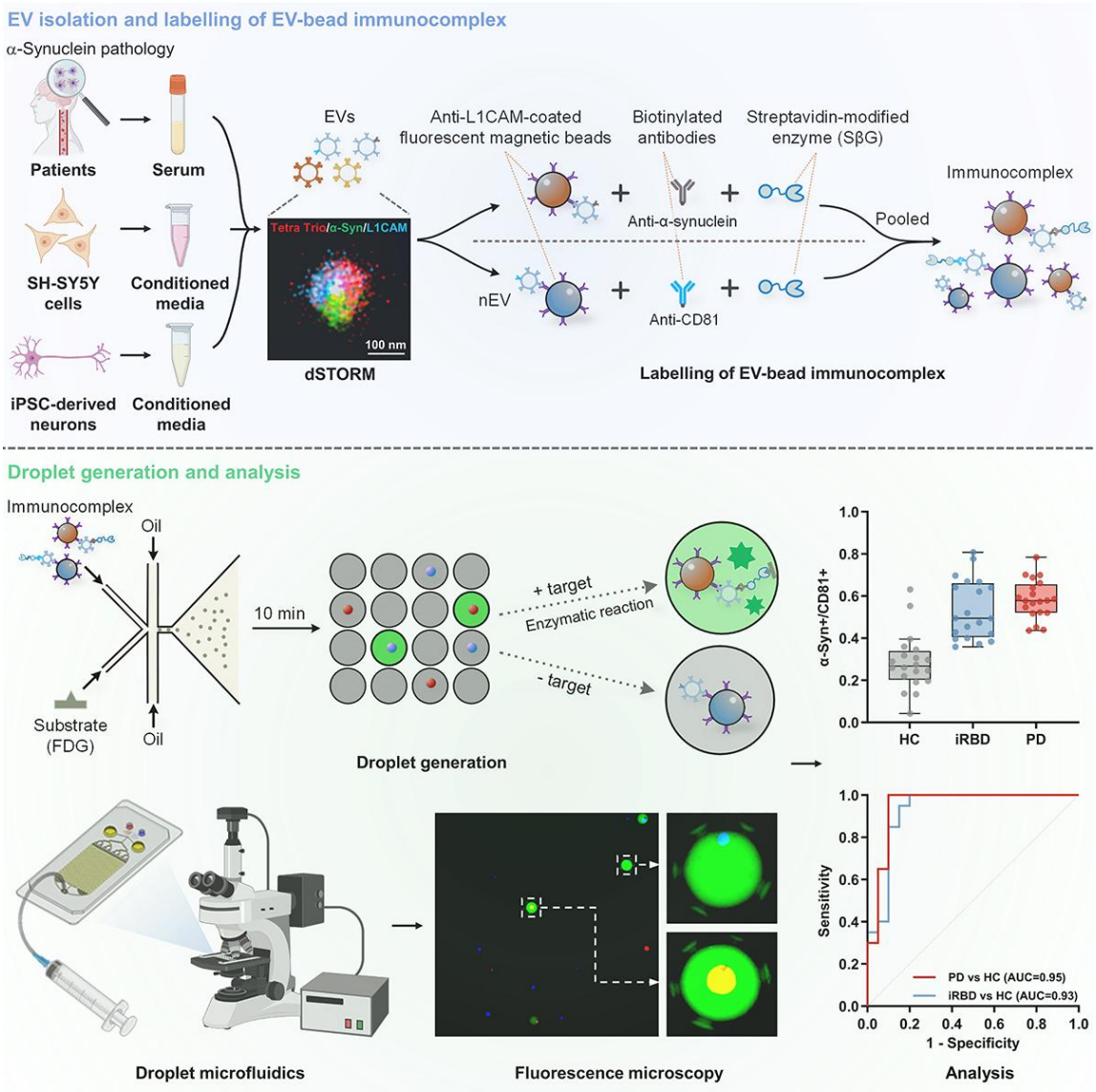


Figure 5.1: Graphic abstract. This study introduces a droplet-based microfluidic assay, which involves immunocapture of L1CAM+ EVs (L1EVs) using fluorescently encoded magnetic beads and droplet-confined enzymatic detection, enabling visualisation of membrane markers at single-EV resolution. Additionally, dSTORM was used to confirm α-synuclein localisation on L1EV membranes, and the assay was validated in serum samples from healthy controls, individuals with iRBD or PD, as well as cell models including neuroblastoma cells expressing PD-linked α-synuclein mutants and patient-derived induced pluripotent stem cells (iPSCs) dopaminergic neurons with α-synuclein gene triplication.

5.3 Material and methods

5.3.1 Clinical samples

Blood samples from the Oxford Discovery cohort were collected during the patient assessment, and the serum was isolated, aliquoted, and frozen at -80°C until further use. All samples were processed in a blinded to clinical information. A total of 60 subjects were included in this study. Serum samples and clinical data were collected from subjects with iRBD (n = 20) or PD (n = 20), and healthy controls (n = 20). The Oxford Parkinson's Disease Centre Discovery cohort is a prospective cohort of recently diagnosed patients with iRBD and PD who were recruited from 11 hospitals in the Thames Valley region between September 2010 and September 2023. Inclusion criteria for iRBD were confirmation by video-assisted PSG and availability of serum samples. Subjects were excluded if a secondary cause for RBD was identified. Patients with PD, and healthy controls without significant comorbidities or relevant family history were included. Full details of the discovery cohort and full inclusion and exclusion criteria have been published elsewhere.[247] There was no effect of age or sex on L1EV membrane-associated α-synuclein was observed in tested subjects.

5.3.2 Cell line cultures

SH-SY5Y neuroblastoma cells (human, female) were obtained from the European Collection of Authenticated Cell Cultures (RRID:CVCL_0019) and maintained in high-glucose DMEM (D5671, Sigma) supplemented with 10% (v/v) FBS (F7524, Sigma), 1X MEM non-essential amino acids (11140035, Thermo Fisher Scientific), 1X GlutaMAX (35050061, Thermo Fisher Scientific), and 1X Antibiotic-Antimycotic (15240062, Thermo Fisher Scientific). Cells were grown at 37°C in 5% CO_2 with 95% humidity, and detached using TrypLE (12605036, Thermo Fisher Scientific) for routine subculturing.

5.3.3 Generation of human iPSC-derived midbrain dopaminergic neurons

Dopaminergic neurons were derived from human iPSC lines using a previously published differentiation protocol optimised in-house.[262,263] The ND34391G iPSC line (obtained from the Coriell Institute, distributed through the NINDS Fibroblasts and iPSCs Collection) was derived from a 55-year-old white female PD patient carrying a triplication of a large 1.5 Mb region that includes the *SNCA* gene, and the corresponding *SNCA* isogenic clone was previously generated from this line (**Table 2.2)**.[264] Briefly, human iPSC lines were maintained in mTeSR1 media (85857, Stem Cell Technologies) and routinely screened for mycoplasma contamination prior to differentiation. The cells were passaged when reaching 90 – 95% confluency using Versene (15040066, Gibco) onto Geltrex (A1413202, Thermo Fisher Technologies)-coated plates until reaching appropriate morphology and confluency for differentiation. Human iPSCs were directed towards a midbrain floor plate lineage over 12 days using 100 nM LDN193189 (SML0559, Sigma), 2 μM A83-01 (2939, Tocris), 300 ng/mL Sonic Hedgehog (464-SH-200, R&D Systems), 2 μM purmorphamine (4551, Tocris), 200 ng/mL FGF8α (4745-F8, R&D Systems), and 3 μM CHIR99021 (4423, Tocris). Following this stage, the cells were further differentiated into a dopaminergic neuron lineage from day 21 onward using 20 ng/mL BDNF (450-02, PeproTech), 20 ng/mL GDNF (450-10, PeproTech), 1 ng/mL TGFß3 (PHG9305, Thermo Fisher Scientific), 10 μM DAPT (2634, Tocris), 200 μM ascorbic acid (A4403, Sigma), 500 μM db-cAMP (D0627, Sigma), and 1 μg/mL laminin (L2020, Sigma).

ID	Diagnosis	*SNCA* genotype	Sex	Biopsy age (years)	Original ID	Reprogramming method	iPSC clone characterisation	GEO
$SNCA^{TRIP}$	PD	Triplication/ WT	female	55	ND34 391G	Cytotune1	Heman-Ackah et al.[264]	GSE89886
$SNCA^{ISO}$	PD	Isogenic WT/WT	female	55	Clone 1-13	Cytotune1	Heman-Ackah et al.[264]	GSE89886

Table 5.1: iPSC clones used in this study. Abbreviations: PD=Parkinson's disease. iPSC-derived dopaminergic neurons were cultured by Chor Lai Lam in the lab.

5.3.4 EV isolation from serum

To isolate EVs from serum, a three-step sequential centrifugation (300 ×g for 10 min, 2,000 ×g for 20 min, and 10,000 ×g for 30 min) was applied to remove cellular debris, protein aggregates and fatty material from the sample. The resulting supernatant was transferred to protein low-binding tubes (0030108450, Eppendorf) for further processing as follows:

For multimodal chromatography, a HiScreen Capto Core 700 prepacked column (17548115, Cytiva) was used to separate EVs from the bulk of free serum proteins. In brief, 1 mL of pre-cleared serum was loaded onto the column and 10 fractions were collected in PBS at a flow rate of 1 mL/min.

Ten-fold excess of DAPI- (MEGB002, Bangs Laboratories) or Cy5- (MEFR002, Bangs Laboratories) labelled carboxylated magnetic encapsulated beads relative to the number of EVs, as determined by NTA, were transferred into a protein low-binding tube, and washed three times with 500 µL of 2-morpholinoethanesulfonic acid (MES, A8250, Sigma) buffer (50 mM, pH 5.5). Freshly prepared 10 mg of 1-ethyl-3-(3-(dimethylamino)propyl) carbodiimide hydrochloride (EDC, 03450, Sigma) and 10 mg of N-hydroxysuccinimide (NHS, 130672, Sigma) were reconstituted in 1 mL of MES buffer just prior to use. To activate the beads, 500 µL of the mixture was added to the beads and incubated for 1 h at room temperature with rotation. The activated beads were then washed twice with 500 µL of PBS, followed by adding 5 µg of capture antibody per mg beads. The capture antibodies against the following markers were conjugated to the beads: CD9 (CBL162, Millipore), L1CAM (UJ127: MA5-14140, Thermo Fisher Scientific), or α-synuclein (Syn1: 610787, BD Biosciences). Activated beads and antibodies were incubated for 1.5 h with rotation. The antibody-conjugated beads were then washed twice with 500 µL of PBS followed by blocking with 500 µL of 1% Bovine Serum Albumin (BSA, A7030, Sigma) in PBS for 1 h with rotation. Beads without antibody

conjugation (beads alone) were included as a negative control. The beads were washed twice with 500 µL of PBS and resuspended in 1 mL of PBS containing protease and phosphatase inhibitor cocktail (78444, Thermo Fisher Scientific). The antibody-coated beads were incubated with either 20 µL of precleared serum or 40 µL of EV-enriched Capto Core chromatography F3 and F4 at 4°C overnight with rotation. The supernatant of 20 µL of serum (i.e. EV-depleted serum), collected after UC (100,000 ×g for 90 min), was included as a negative control. The bead-EV complexes were collected by magnetic separation and washed successively with PBS containing 0.05% Tween-20 (P7949, Sigma) and PBS only for downstream analysis.

5.3.5 EV isolation from CM

For SH-SY5Y cells, 1 mL of culture media, conditioned for 48 h, was collected from a well of a 12-well plate (400,000 cells per well), aliquoted in protein low-binding tubes, and serially centrifuged at 300 ×g for 10 min, followed by 2,000 ×g for 10 min and 10,000 ×g for 30 min, all at 4°C. The resulting supernatant (i.e. precleared CM) was stored at -80°C. Thirty µL of precleared CM was processed for immunocapture of L1EVs as described above for serum, or subjected to NTA, and 1 mL of precleared CM was passed through polyethersulfone filters (0.22 µm, SLGP033RS, Millipore) before total EV isolation using ultracentrifugation.

For iPSC-derived cultures, 500 µL of neuronal media was conditioned from Day 52 to Day 60 and collected from a well of a 12-well plate (1.0×10^6 neurons per well). CM from one differentiation was pooled and considered as a single biological replicate. This time window was selected based on previously data from the lab showed that iPSC-derived dopaminergic neurons are electrophysiologically active from D45 onwards.[263] CM was precleared and stored as described above for SH-SY5Y cells. Thirty µL of precleared CM was processed for immunocapture with anti-L1CAM coated beads as described above or subjected to NTA. For

Capto Core multimodal chromatography, 4 mL precleared CM was passed through a HiScreen Capto Core 700 column, and EV-enriched fractions were collected.

5.3.6 Labelling of EV-bead immunocomplexes for surface marker analysis

To visualise relevant surface markers on the EV-bead immunocomplexes, 200 µL of 0.1 µg/mL biotinylated detection antibody was added to the EVs isolated using fluorescent beads and incubated for 1 h at room temperature with rotation. Biotinylated antibodies against the following markers were used: CD81 (ab239238, Abcam), CD11b (13-0118-82, Thermo Fisher Scientific), L1CAM (MA5-14137, Thermo Fisher Scientific), NCAM1 (13-0567-82, Thermo Fisher Scientific), α-synuclein (LB509: 807710, BioLegend), aggregated α-synuclein (A17183A: 864906, BioLegend), or syntenin-1 (PAB7132, Abnova). For anti-syntenin-1, antibody conjugation to biotin was performed using a commercial conjugation kit (21935, Thermo Fisher Scientific). The resulting EV-bead immunocomplexes were separated by a magnet and the supernatant was removed. Following three washes with PBS, 200 µL of 2 µg/mL SβG (S931, Thermo Fisher Scientific) was mixed with the bead-EV immunocomplexes and incubated for 30 min at room temperature with rotation. The enzyme-labelled immunocomplexes were washed three times with PBS and resuspended in PBS to a final concentration of 1.4×10^7 beads/mL for loading onto the microfluidic platform.

5.3.7 Microfluidic chip design and fabrication

Bowen Shu (Southern Medical University, China) designed a pump-free, syringe-vacuum-driven, droplet-based microfluidic chip with dual inlets for the independent introduction of pre-conjugated, enzyme-labelled immunocomplexes and fluorescein substrate (FDG). This design enables simple and high-throughput microdroplet generation, followed by the self-assembly of a high-density monolayer droplet array for *in situ* incubation and fluorescence imaging. The microfluidic chip comprises a pair of oil inlets, one inlet for the

introduction of the EV-bead immunocomplex and the other for the introduction of the fluorescein substrate solution, a flow-focusing structure for droplet generation, a Christmas tree-shaped network of distribution channels, and a collection chamber enabling self-assembly of the monolayer droplet array. Once the sample and the substrate are loaded into the inlet ports, fluid movement is driven by withdrawing the piston of the connected syringe to create a pre-determined pressure differential across the chip. The microfluidic chip is made of a single PDMS layer irreversibly bonded to a glass slide. The PDMS structure was fabricated using a refined soft lithography technique. The microchannel patterns (**Fig. S5.1**) were designed using AutoCAD software (Autodesk), which were then transferred to a high-resolution photomask. SU-8 (SU-8 3025, Kayaku) master moulds with a channel depth of 25 μm were fabricated adhering to manufacturer's guidelines. Post mould preparation, a 1:8 mixture of PDMS curing agent and elastomer (PDMS184, Dow-Corning) was degassed, poured over the SU-8/Si master (LY-118-A-1315, Youli Biotech), and cured in an oven at 120°C for 20 min. The cured PDMS was then peeled off, and its inlet and outlet holes were punched. The PDMS layer was then bonded to a standard glass slide (75 × 25 × 1.1 mm), or to a square glass substrate (70 mm × 70 mm × 1 mm) for devices with eight independent assay units, using oxygen plasma treatment for 20 seconds. The assembled droplet-based microfluidic chip was further cured in an oven overnight at 80°C to strengthen the bond.

5.3.8 Droplet generation

Prior to droplet generation, the microfluidic chip was filled with an oil phase (mineral oil [M5904, Sigma] containing the stabilising surfactants 3% ABIL EM 90 [Degussa] and 0.1% w/w Triton X-100 [T8787, Sigma]). A 5-mL single-use plastic syringe was then connected to the outlet of the chip with a length of Teflon tubing (0.46 mm × 0.76 mm, [i.d. × o.d.]). When the capillary force-driven oil flow reached the sample inlets, 10 μL of enzyme-labelled EV-bead immunocomplexes and 10 μL of FDG (F1179, Thermo Fisher Scientific) substrate

solution were individually loaded into the two sample inlets with a micropipette, ensuring no air bubbles were trapped. To initiate the droplet generation, the syringe piston was pulled outward and locked in place at an approximately 1-mL volume using a binder clip. Once the collection chamber was filled with microdroplets, the piston was gently pushed back to its starting position, and the tubing was cut off.

5.3.9 Fluorescence image acquisition

After incubation for 10 min at room temperature, the microfluidic chip was subjected to continuous imaging via an inverted fluorescence microscope (Eclipse Ti2, Nikon). This setup, equipped with a 10× objective, capture fields of 953 × 1432 μm² per frame, each containing approximately 2,500 – 3,500 microdroplets. Brightfield images were used to determine total droplet count, while fluorescence images (DS-Ri2, Nikon) identified fluorescently labelled beads and the fluorescein (green fluorescence)-positive droplets with a signal-to-noise ratio > 3. For detailed size analysis, three distinct regions were imaged at 10× magnification, and measurements were obtained for > 10,000 droplets using NIS-Elements (Nikon) software.

5.3.10 Image analysis

The number of droplets was counted using brightfield images, and a watershed algorithm was applied to separate any partially connected droplets. Each bead was identified, and by setting an intensity threshold, the number of fluorescently labelled beads (Cy5 or DAPI) was counted using the Find Maxima function. The number of positive droplets was counted using the fluorescent images captured in the FITC fluorescence channel. A background correction algorithm was then applied to the image to subtract the mean intensities of the droplets that did not contain a bead. If a fluorescent droplet was not colocalised with a bead, the droplet was excluded from analysis. Using this approach, the total number of fluorescent

droplets over the total number of beads was calculated. Twenty fields of view were acquired for quantitative analysis. Image analysis was performed using ImageJ 1.53t (Fiji) software.

5.3.11 Nano-flow cytometry

EV surface markers CD81 and CD9 were analysed by NanoFCM on a NanoAnalyzer U30 instrument (NanoFCM Inc.) equipped with dual 638 nm and 488 nm lasers. Total EVs isolated from 1 mL of serum using UC were resuspended in 1% BSA in PBS containing protease and phosphatase inhibitor cocktails. Isolated EVs were stained at 4°C overnight in the dark with an antibody cocktail consisting of Alexa Fluor 647-labelled anti-CD9 (A6-208-T100, EXBIO Praha) and FITC-labelled anti-CD81 (A15753, Thermo Fisher Scientific). Post-incubation, EV samples were diluted in PBS for immediate phenotypic analysis. Data acquisition and processing were performed using NanoFCM Professional Suite v2.0 software (NanoFCM Inc.).

5.3.12 Direct Stochastic Optical Reconstruction Microscopy

EVs isolated from serum using multimodal chromatography, or from CM using UC were resuspended in 0.5% BSA in HBSS buffer (88284, Thermo Fisher Scientific) containing protease and phosphatase inhibitor cocktails. Anti-α-synuclein (MJFR1: ab138501, Abcam) and anti-aggregated-α-synuclein (5G4: MABN389, Millipore) antibodies were conjugated to Alexa Fluor 647 using the Alexa Fluor 647 conjugation kit (ab269823, Abcam). Anti-L1CAM antibody (5G3: 14-1719-82, Thermo Fisher Scientific) was labelled with Alexa Fluor 488 using the Alexa Fluor 488 conjugation kit (ab236553, Abcam) following the manufacturer's protocol.

Serum EVs were stained overnight at 4°C in the dark with a cocktail of anti-α-synuclein-Alexa Fluor 647, anti-L1CAM-Alexa Fluor 488, and Tetraspanin Trio-Alexa 561 (800-00113, ONI). EVs from CM were stained with an antibody cocktail consisting of anti-aggregated-α-synuclein-Alexa Fluor 647 and Tetraspanin Trio-Alexa 561, under the same

condition. Following staining, EV samples were immobilized on 170 μm (#1.5H) thick glass slides pre-coated with 3% BSA for 1.5 h at 4°C in the dark. Slides were washed 10 to 12 times with PBS to remove any floating particles and free antibodies, followed by the addition of dSTORM imaging buffer (900-00083, ONI). Super-resolution images were acquired using ONI Nanoimager (Oxford Nanoimaging) equipped with a 100×, 1.4 numerical aperture oil immersion objective, and NimOS software (version 1.7). A total of 7,500 frames (2,500 per channel) were recorded for localisation mapping, using 30% laser power for each of the 488, 561, and 647 nm channels. Colocalisation analysis of different molecules on single EVs was analysed using the CODI online platform (https://alto.codi.bio/). Nine fields of view were acquired per sample for quantitation.

To identify single EVs on beads, L1EVs immunocaptured on DAPI-labelled beads from serially diluted serum (ratios of 1:10, 1:1, and 1:0.1 bead: EV). Samples were stained overnight at 4°C in the dark with anti-CD9-Alexa Fluor 647 or Tetraspanin Trio-Alexa Fluor 561. EV-depleted serum was included as a negative control. Following 3 washes with 1 mL of PBS, beads were mounted on 170 μm (#1.5H) thick glass slides, and images were acquired as described above. Seven fields of view were acquired per condition for quantitative analysis.

5.3.13 MSD electrochemiluminescence

L1EVs immunocaptured from 250 μL of precleared serum, or total EVs enriched in Capto Core multimodal chromatography F3 and F4 from 1 mL of serum or from 4 mL of CM, were lysed in PBS containing 1% Triton X-100, supplemented with protease and phosphatase inhibitor cocktail. The lysates were collected after incubation for 30 min at room temperature with shaking. α-Synuclein and CD81 levels in the lysates or 4-fold diluted serum were measured using MSD electrochemiluminescence U-PLEX assay (K151WKK-2, MSD) and R-PLEX assay (K1515NR-2, MSD), respectively.

5.3.14 Molecular cloning and lentivirus production

NEBuilder HiFi DNA Assembly Master Mix (NEB, E2621S) was used to combine two polymerase chain reaction fragments with homologous ends, one generated from pLV-eGFP (gift from Pantelis Tsoulfas; 36083, Addgene) and consisting of the blasticidin S deaminase coding sequence preceded by the UbC promoter, and the other generated from a pre-existing lentiviral transfer plasmid and consisting of the CMV promoter/enhancer, the *SNCA* coding sequence and sequences required for lentivirus production. The combined vector, pLenti-CMV-WTαSyn-BlastR, was used to generate additional A53T, E46K, G51D, A30P, 3K (E35K + E46K + E61K), and 3D (V40D + G51D + V66D) α-synuclein-encoding lentiviral transfer plasmids via HiFi Assembly with mutagenic primers. The correct DNA sequences were confirmed by Sanger sequencing. Lentiviruses were prepared by transfecting HEK293T cells with the packaging plasmid psPAX2 (gift from Didier Trono; 12260, Addgene), the envelope plasmid pMD2.G (gift from Didier Trono; 12259, Addgene) and a transfer plasmid were generated as described above (1:1:1 molar ratio), followed by medium replacement on the following day and CM collection after a further two days. CM was spun at 300 ×g for 5 min to pellet debris, and the supernatants were passed through polyethersulfone filters (0.22 μm; SLGP033RS, Millipore) before use.

5.3.15 Lentiviral transduction of SH-SY5Y cells and cell fractionation

SH-SY5Y cells were reverse transduced with lentiviruses in 12-well plates in a culture medium consisting of antibiotic-free high-glucose DMEM supplemented with 5% (v/v) FBS, 1X MEM non-essential amino acids, 1X GlutaMAX, and 5 μg/mL polybrene (sc-134220, Santa Cruz Biotechnology). The following day, the lentivirus-containing medium was aspirated, cells were rinsed once with PBS, and then incubated in fresh high-glucose DMEM supplemented

with 5% FBS, MEM non-essential amino acids, GlutaMAX and 1X Antibiotic-Antimycotic. After two additional days, the entire 1 mL of CM was collected.

Immediately after collecting the CM, cytosol-membrane fractionation was performed as described previously.[265] Briefly, the cell monolayer was rinsed with PBS before addition of 100 µL of cytosol extraction buffer (10 mM PIPES, pH 7.4, 300 mM sucrose, 100 mM NaCl, 5 mM $MgCl_2$, 5 mM EDTA, and protease and phosphatase inhibitors cocktail, supplemented with 900 µg/mL digitonin). After incubating for 15 min at 4°C with gentle agitation, the cytosolic fraction was collected into a 1.5 mL tube without disturbing the cell monolayer. Next, 100 µL of membrane extraction buffer was added (same as cytosol buffer except for supplementation with 0.5% Triton X-100 in place of the digitonin). After incubating for another 15 min at 4°C with gentle agitation, the membrane fraction was collected into a 1.5 mL tube, again without disturbing the cell monolayer. Cytosol and membrane fractions were both centrifuged at 1,000 ×g for 10 min at 4°C to pellet cell debris, and the supernatants were transferred to fresh tubes.

Separation of cell lysates into RIPA buffer (89901, Thermo Fisher Scientific)-soluble and -insoluble fractions was performed as follows. First, the cell monolayer was rinsed with ice-cold PBS and lysed in 100 µL of ice-cold RIPA lysis buffer containing protease and phosphatase inhibitors cocktails (78444, Thermo Fisher Scientific). After incubating for 15 min at 4°C with gentle rocking, cell lysates were scraped into tubes, processed with a handheld homogenizer, and centrifuged at 1,000 ×g for 10 min at 4°C to pellet cell debris. The supernatants were transferred to ultracentrifuge tubes and spun at 100,000 ×g for 1 h at 4°C. The soluble fractions were extracted and stored, while the RIPA-insoluble pellets were resuspended in the above lysis buffer with the sodium dodecyl sulfatepolyacrylamide concentration adjusted to 2% (v/v).

5.3.16 Immunofluorescence staining

iPSC-derived neurons were fixed in 4% paraformaldehyde (158127, Sigma) supplemented with 2% sucrose in PBS, then permeabilised in 0.1% Triton X-100 in PBS and blocked with 5% BSA in PBS. Cells were then incubated with primary antibodies, followed by fluorescently labelled secondary antibodies. The following primary antibodies were used: anti-α-synuclein (1:1000, 610787, BD Biosciences) and anti-MAP2 (1:2000, ab5392, Abcam). The following secondary antibodies were used: Alexa Fluor 568-labelled goat anti-mouse IgG (1:2000, A11004, Thermo Fisher Scientific) and Alexa Fluor 647-labelled goat anti-chicken IgY (1;2000, A21449, Thermo Fisher Scientific). Images were obtained using Zeiss LSM 980 Airyscan confocal microscope (Carl Zeiss AG). To quantify fluorescence intensity, 3 images were obtained per condition per differentiation, and 25 to 40 cells were quantified per image.

5.4 Results

5.4.1 Development of the microfluidic digital immunoassay for single EV detection

The microfluidic chip (**Figure S5.1**; design and fabricated by the Shu lab, Southern Medical University, China) generated picolitre-scale droplets containing a single immunocaptured EV, which was labelled with biotinylated antibodies against the target surface protein, conjugated to SβG, and visualised with fluorescein substrate FDG, as summarised in **Figures 5.2A-5.2C**. The chip facilitated sample mixing and droplet generation through differential pressure, driven by withdrawing the piston of a connecting syringe. This generated approximately 200,000 monodisperse picolitre-sized droplets with an average diameter of 27.9 μm in a high-throughput format (**Figures 5.2D** and **5.2E**), while consuming minimal sample at a piston withdrawal volume of 1 mL (**Figure S5.2**). In this way, approximately 10% of droplets contained a fluorescently encoded magnetic bead, with or without a single EV immunocomplex.

In the absence of an EV or the target EV membrane-associated protein, droplet-confined beads displayed solely the coded bead fluorescence and not green fluorescence. Therefore, the design enables the visualisation of a unique enzyme-labelled immunocomplex per bead targeting an EV membrane antigen that is amplified by the enzymatic reporter SβG. The assay sensitivity is determined by the ratio of green fluorescence-positive droplets to the total number of "bead only" containing droplet (red or blue), referred to as the percentage of EV positive beads (% EV+ beads). This readout can be converted to the percentage of EVs expressing the target per mL of biofluid, using the Poisson distribution.

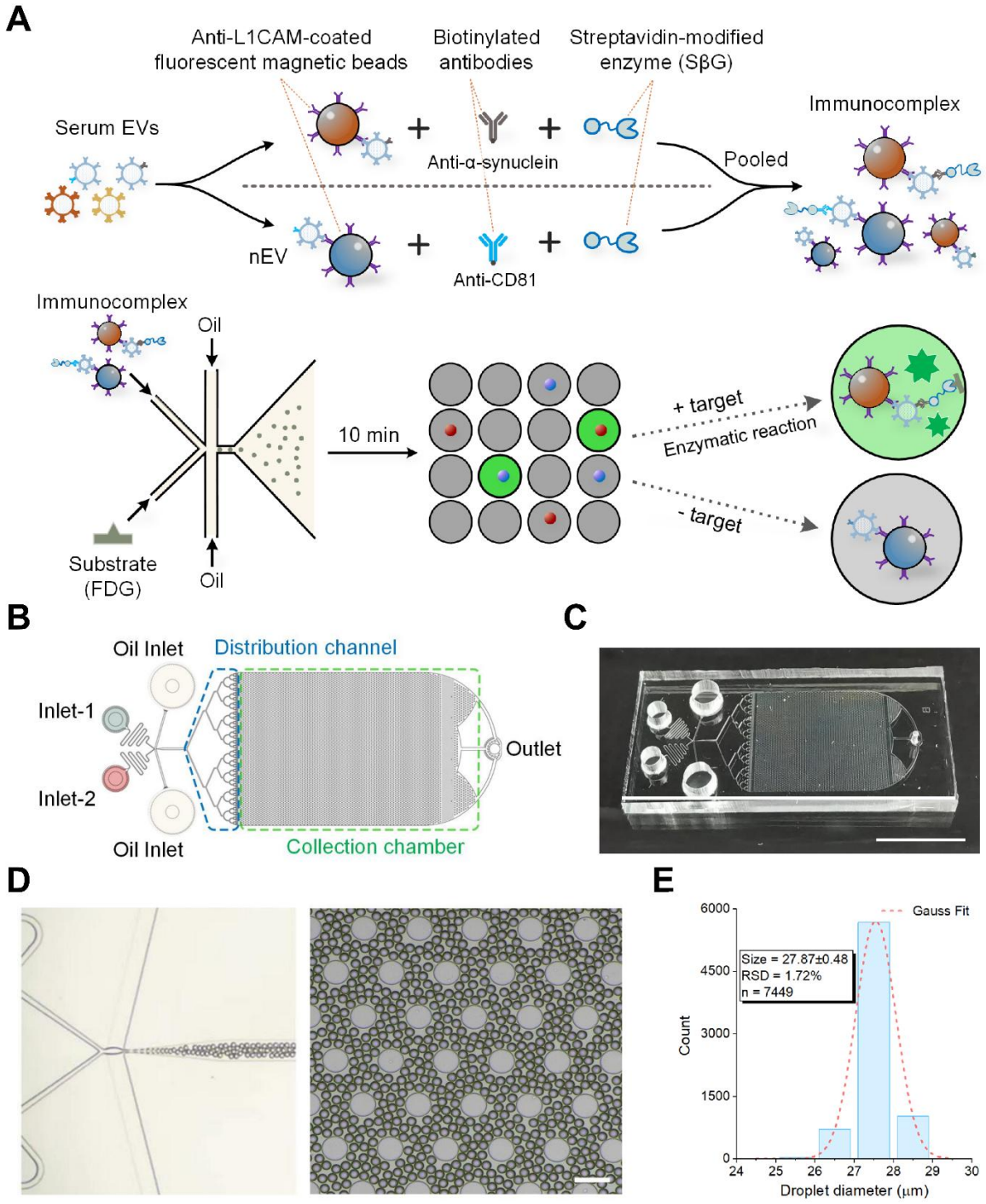


Figure 5.2: Droplet-based microfluidic EV digital immunoassay. (**A**) Workflow of the assay. (**B**) Schematic illustration of the droplet microfluidic device with further design details in **Figure S5.1**. (**C**) Photograph of the microfluidic device (75 × 25 × 1.1 mm); scale bar: 2 cm. (**D**) Representative images of the picolitre-sized droplets; scale bar: 100 μm. (**E**) Size distribution of the droplets averaging 27.9 μm in diameter. The microfluidic chip was provided by Xinying Li and Bowen Shu.

To confirm that the majority of droplets encapsulated no more than one bead, Wenjing Zhang (The Chinese University of Hong Kong, Shenzhen, China) and I performed serial dilutions of input beads (**Figure 5.3A**). At a concentration of 1.4×10^7 beads/mL, 9.8% of the

droplets contained a single bead, while 90.1% of did not contain a bead, consistent with the Poisson distribution prediction (**Figures 5.3B and 5.3C**). To optimise the reaction time for enzyme-mediated fluorescence at this optimal concentration, we monitored the time course of fluorescent signal generation. The enzymatic fluorescence peaked at 10 min, while no positive droplets were found in the absence of substrate (**Figure 5.4**).

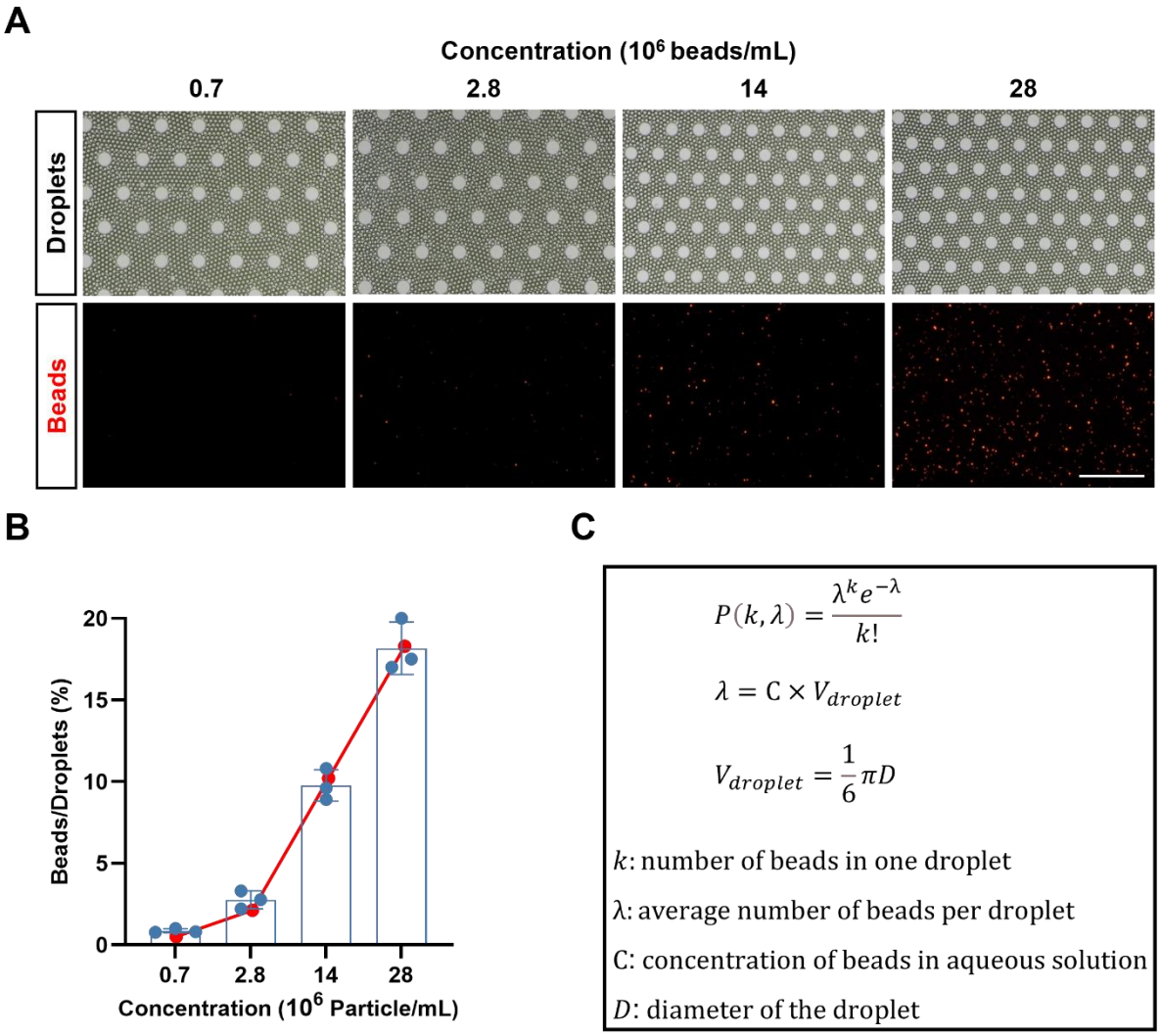


Figure 5.3: Quantification of bead-to-droplet ratio according to Poisson distribution. (**A**) Representative images and (**B**) quantification of serial dilutions of input beads. The Poisson distribution (red line) predicts that at a concentration of 1.4×10^7 beads/mL, ~10.2% of droplets contain only one bead, which aligns with our analysis showing that 9.8% of droplets contain a single bead (blue histogram). (**C**) Theoretical calculations of Poisson distribution. n = 3 independent experiments. Data are represented as mean ± SD. Experiments in panel **A** were performed by Wenjing Zhang.

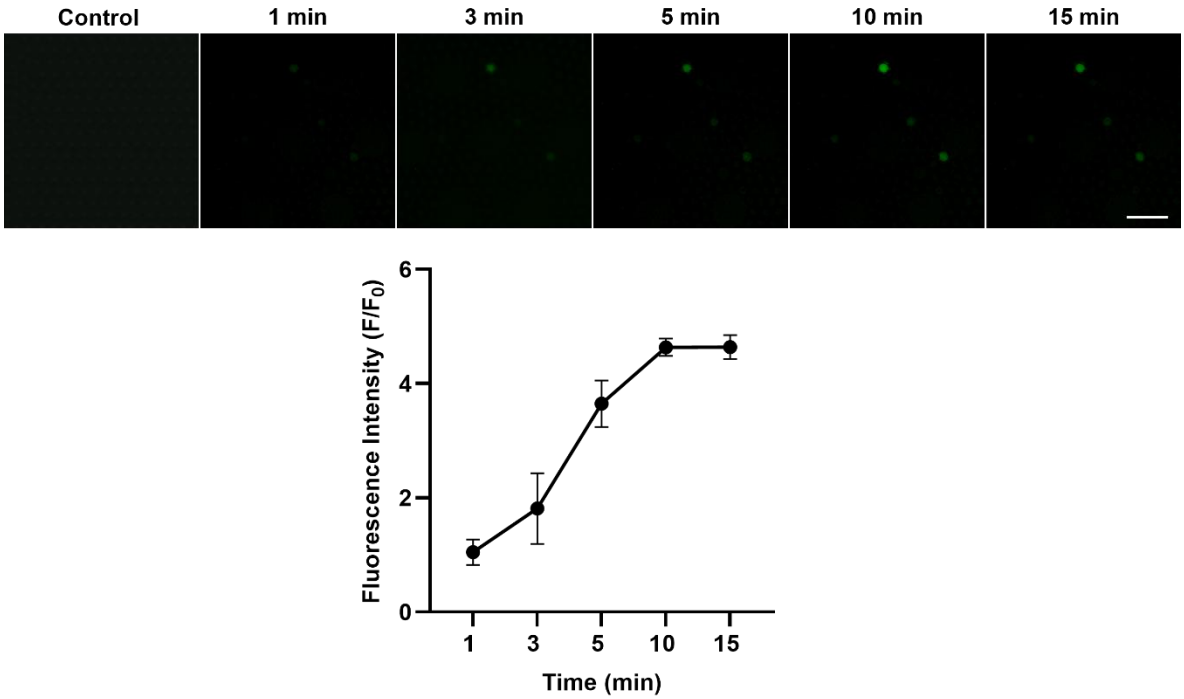


Figure 5.4: Time course of fluorescent signal generation through the microdroplet-confined enzymatic reaction. Representative images of fluorescent droplets and relative fluorescence intensity in the fluorescent droplets over time during the enzymatic reaction process. Scale bar:100 μm. Data are represented as mean ± SD. This experiment was performed by Wenjing Zhang.

To maximize the probability of capturing a single EV per bead per droplet, I introduced a 10-fold excess of beads relative to the number of EVs, as determined by NTA. To confirm that a single EV was captured per bead, Suman Dutta in the lab and I used fluorescence microscopy on serially diluted serum subjected to immunocapture with anti-L1CAM antibodies, followed by EV visualisation with Alexa 647-labelled anti-CD9 antibodies. We found that multiple EVs were captured per bead at 1:10 or 1:1 (bead: EV) ratio, whereas at 1:0.1 (bead: EV) ratio, only a single L1EV was captured per bead (**Figure 5.5A**). The suitability of 1:0.1 (bead: EV) ratio was further confirmed using Tetraspanin Trio (Tetra Trio) antibody cocktail (against CD9, CD63, CD81), which is more likely to label all EVs (**Figure 5.5B**). Thus, under these conditions, > 99.9% of the bead-positive droplets contained only one target EV, thereby enabling accurate single-EV membrane protein measurement. In control experiments, I tested and confirmed that no signal was detected in EV-depleted serum (**Figure**

5.5A). I further demonstrated successful EV immunocapture from serum with either anti-CD9 or anti-L1CAM antibodies-coated beads by immunoblotting, NTA, and TEM (**Figure 5.6**).

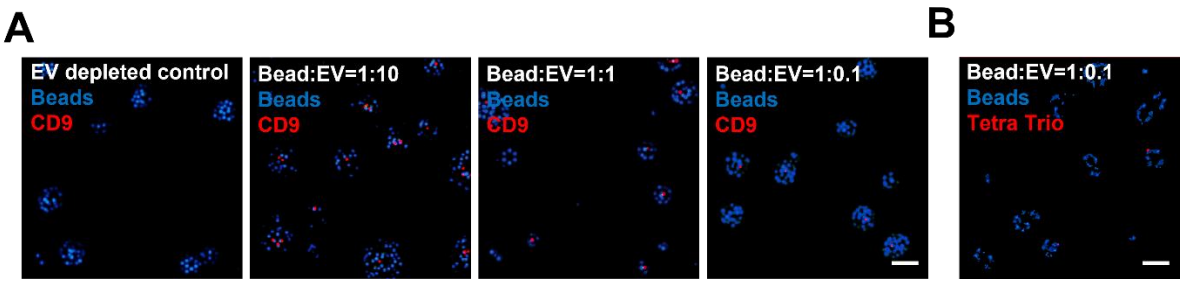


Figure 5.5: Single serum EVs captured on anti-L1CAM antibodies-coated beads. (**A**) Representative fluorescence microscopy images of L1EVs immunocaptured from serum using DAPI-labelled beads, followed by staining with Alexa-Fluor 647-labelled anti-CD9. EV-depleted serum was used as a control, and bead to serum EV ratio of 1:10, 1:1, or 1:0.1 were tested; scale bar: 2 μm. (**B**) Representative fluorescence microscopy image of L1EVs immunocaptured from serum using DAPI-labelled beads, followed by staining with Alexa-Fluor 561-labelled anti-Tetraspanin Trio (CD9, CD63, and CD81) using a bead to serum EV ratio of 1 to 0.1; scale bar: 2 μm. These experiments were performed by Suman Dutta.

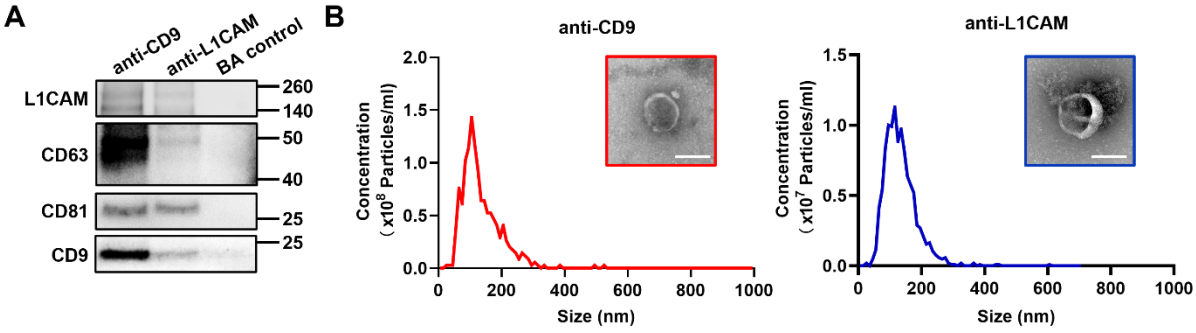


Figure 5.6: Confirmation of EV isolation from serum. (**A**) Immunocapture using anti-CD9 or anti-L1CAM from neat serum, followed by immunoblotting. Beads alone (BA) were used as a control. (**B**) Size distribution of eluted EVs after anti-CD9 (red) or anti-L1CAM (blue) immunocapture was confirmed by NTA, and the typical cup-shaped appearance was demonstrated by TEM; scale bar: 100 nm.

5.4.2 The assay enables parallel quantification of distinct EV subpopulations

Having optimised the conditions for single-EV detection, I performed direct serum EV immunocapture using Cy5-labelled beads conjugated to antibodies against the generic marker CD9, followed by on-chip detection of surface proteins that are either generic markers (e.g. CD81) or denote specific EV subpopulations (e.g. CD11b, NCAM1, L1CAM). Quantification throughout was performed by calculating the ratio of green fluorescence-positive droplets (denoting a target EV-bead immunocomplex) to red fluorescent beads (denoting the total

number of beads) and is referred as % of EV+ beads, as stated earlier. In control experiments, I included EV-depleted serum following UC or serum incubated with beads lacking antibody conjugation. These experiments confirmed that the signal generated by CD81 immunoreactivity arose specifically from CD9+ EVs, as no signal was seen in controls (**Figure 5.7A**). Quantification of the signal revealed that CD81 was detected in 7.2% EV+ beads (**Figure 5.7A**), corresponding to 80.0% of serum CD9+ EVs, as estimated by Poisson distribution, in agreement with previous measurements from the lab for these generic EV markers using immunoblotting.[228]

To further validate the accuracy of the droplet immunoassay, Suman Dutta and I used NanoFCM to analyse membrane-associated CD9 and CD81 expression on single serum EVs isolated using UC. This analysis revealed that CD81 was detected in 77.2% of serum CD9+ EVs (**Figures 5.7B** and **S5.3**), which aligns with the result obtained with the droplet-based platform. In control experiments, we tested and confirmed that negligible signal was detected in the antibody-only control without sample condition (**Figure S5.3**).

I then evaluated the performance of the platform in measuring the abundance of EV subpopulations using antibodies against neuronal (L1CAM or NCAM1) or immune (CD11b) markers after serum immunocapture with an antibody against CD9, a generic EV membrane marker. I found that the immune cell marker CD11b was detected in 5.3% EV+ beads, and the neuronal markers NCAM1 or L1CAM were detected in 1.2% and 0.7% EV+ beads, respectively (**Figure 5.7C**). These estimates correspond to 58.3% of CD9+ serum EVs for CD11b+ EVs, 13.2% for NCAM1+ EVs, and 8.0% for L1EVs.

To assess the multiplexing capability of the platform, I performed direct anti-CD9 immunocapture from serum using either DAPI-labelled or Cy5-labelled beads, followed by incubation with SβG-biotinylated detection antibodies against either CD11b (DAPI-labelled beads) or L1CAM (Cy5-labelled beads). The enzyme-labelled EV-bead immunocomplexes

were then mixed and loaded with FDG onto the platform for quantification. In this setup, I found that CD11b was detected in 5.0% EV+ beads and L1CAM was detected in 0.7% EV+ beads (**Figure 5.7D**). These estimates correspond to 54.8% of CD9+ serum EVs for CD11b+ EVs, and 8.2% for L1EVs, which concur with my singleplex measurements. These data show that this platform can be reliably used for the simultaneous multiplex assessment of target proteins on different EV subpopulations.

To further validate the efficacy of the platform in measuring signal arising from a single EV of low abundance, I focused subsequent experiments on L1EVs. Wenjing Zhang performed serial dilutions of serum followed by immunocapture with anti-L1CAM and quantified CD81 immunofluorescence. CD81+ L1EVs exhibited excellent correlation with NTA results (**Figure 5.7E**). I calculated the LOD as 3 standard deviations (SDs) above the background, and the limit of quantification (LOQ) as 10 SDs above the background for our assay. Based on these calculations, the LOD was 66 CD81+ L1EVs/μL, the LOQ was 112 CD81+ L1EVs/μL, and the dynamic range spanned from 66 to 8,307 CD81+ L1EVs/μL.

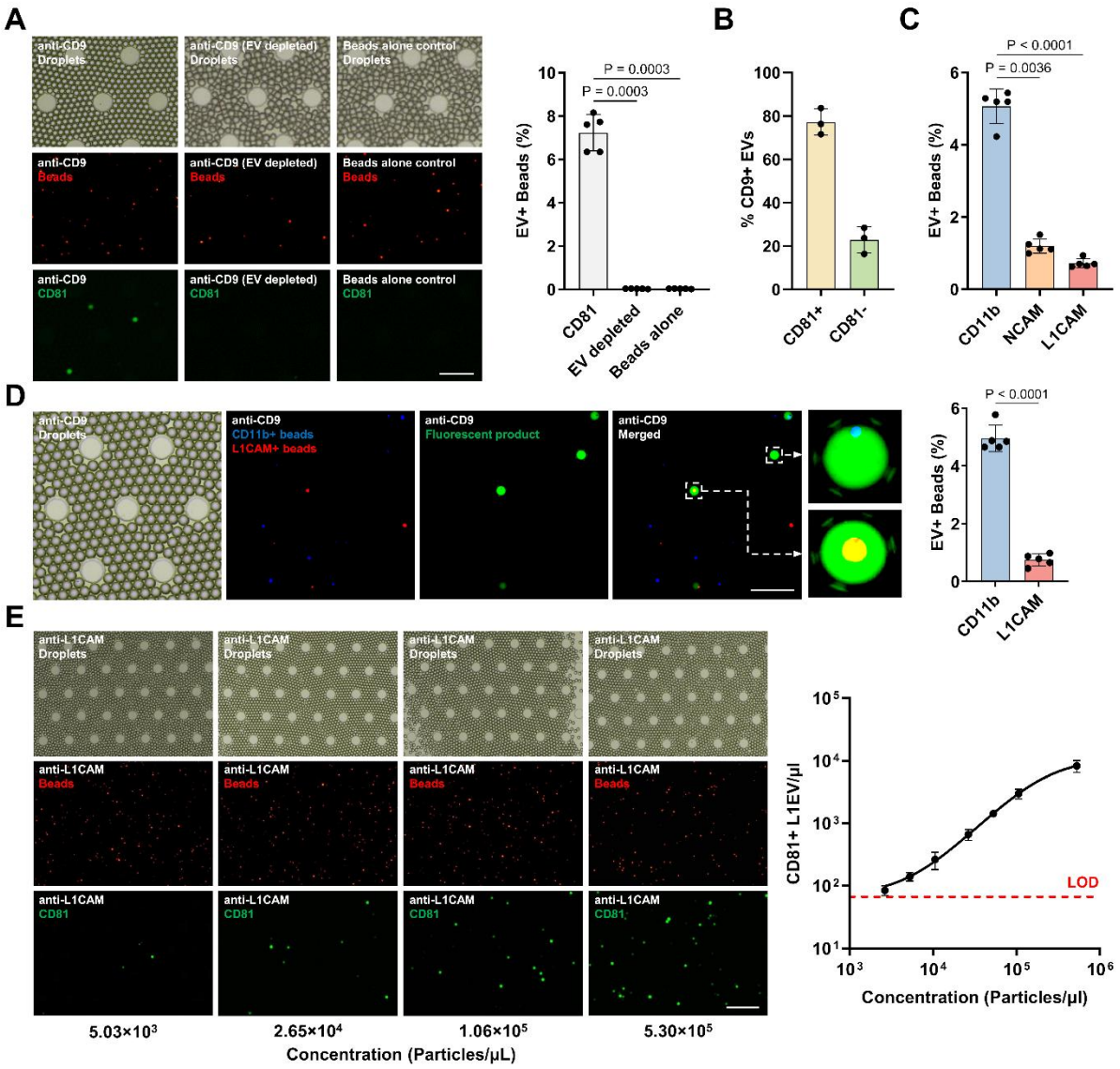


Figure 5.7: Singleplex and multiplex EV membrane protein detection. (**A**) Representative images and quantification of CD81 on CD9-immunocaptured EVs from human serum, EV-depleted serum, and beads alone control using Cy5-labelled beads, as measured by the droplet assay, *n* = 5 individuals with PD tested; scale bar: 150 µm. (**B**) Histogram showing the membrane-associated CD81 expression on single CD9+ EVs isolated from serum, as measured by Nano-flow cytometry; *n* = 3 individuals with PD tested, also see **Figure S5.3**. (**C**) Detection of CD11b, NCAM, and L1CAM on CD9-immunocaptured EVs from serum using the droplet assay; *n* = 5 individuals with PD tested. (**D**) Representative images and quantification of duplex CD11b (DAPI-labelled beads) and L1CAM (Cy5-labelled beads) on CD9-immunocaptured EVs from serum, as measured by the droplet assay; *n* = 5 individuals with PD tested; scale bar: 100 µm. (**E**) Representative images and calibration curve of CD81 detection on L1EVs using the droplet assay at various EV concentrations, as measured by NTA; *n* = 3 independent experiments; scale bar: 250 µm. Data are represented as mean ± SD. Statistical significance was determined by one way ANOVA (panels **A** and **C**) or Student's two-tailed t-test (panel **D**). Experiments in panel **B** were assisted by Suman Dutta and Dongnan Yan (Woods lab, University of Oxford). Images in panels **D** and **E** were taken by Wenjing Zhang.

5.4.3 Identification of α-synuclein as a serum EV membrane-associated protein

Since α-synuclein binds to lipid membranes either physiologically via its amphipathic helical conformation or pathologically when aggregated,[266] I asked whether it is detectable on the EV membrane. To this end, I mixed anti-CD9- or anti-L1CAM-immunocaptured EVs from PD patient serum with FDG substrate and two different SβG-labelled, biotinylated anti-α-synuclein antibodies: antibody clone A17183A, which recognises mainly the aggregated form of α-synuclein (Ab1),[267] or antibody clone LB509, which recognises an epitope in the C-terminal region spanning amino acids 115 – 125 of α-synuclein (Ab2).[268] Interestingly, potentially aggregated α-synuclein was detected in 1.3% CD9+ EV+ beads using Ab1, corresponding to 14.0% of CD9+ EVs (**Figure 5.8A**). Total α-synuclein was detected on 4.3% of L1CAM+ EV+ beads and 2.2% of CD9+ EV+ beads using Ab2, corresponding to 47.3% of L1EVs and 23.8% of CD9+ EVs, respectively. In control experiments, I tested and confirmed that under the same conditions, the internal EV protein syntenin-1 showed negligible signal (**Figure 5.8A**). These data indicate that physiological or aggregated forms of α-synuclein are associated with the EV membrane, and these conformers are enriched on L1EVs compared to CD9+ EVs.

To assess the performance of our droplet-based assay for detecting α-synuclein immunoreactive EVs, Wenjing Zhang quantified α-synuclein immunofluorescence in L1EVs isolated from serially diluted serum with either Ab1 (A17183A) or Ab2 (LB509), as shown in **Figures 5.8B** and **S5.4**. This analysis for Ab1 and Ab2 respectively, established a LOD of 79 or 103 α-synuclein+ L1EVs/μL, a LOQ of 131 or 176 α-synuclein+ L1EVs/μL, and a dynamic range from 79 to 4,328 or 103 to 5,759 α-synuclein+ L1EVs/μL (**Table S5.1**). The calculated minimum volume for the detection of L1EV membrane-associated α-synuclein is

approximately 3 µL of serum, outperforming other microfluidic EV detection platforms (**Table S5.2**). These are the estimated limits of the assay and further validation in patient samples was performed with 20 µL of serum as the starting volume.

To further validate this finding and exclude non-specific association of free α-synuclein, I separated the EVs from the bulk of free human serum proteins which includes free α-synuclein, using Capto Core multimodal chromatography. As I described previously in Chapter 3,[189] EVs were primarily eluted and enriched in fraction F3 and F4, as determined by MSD electrochemiluminescence detection of the EV marker CD81, and immunoblotting for the surface EV markers CD63, CD81, CD9 and the internal EV cargo protein Flotillin 1 (**Figure 5.8C**). In contrast, most α-synuclein in the serum was found in a free form in later fractions as measured by MSD electrochemiluminescence (**Figure 5.8C**). In neat serum, total α-synuclein as quantified by MSD was 5,294.1 ± 1,666.9 pg/mL (data shown as mean ± SD), whereas total α-synuclein in the combined F3 and F4 fractions was 92.0 ± 37.2 pg/mL, indicating that F3 and F4 are indeed depleted of excess free α-synuclein (**Figure 5.8D**). I then performed anti-L1CAM immunocapture from either neat serum or EV-enriched fractions F3 and F4 followed by duplex droplet-based measurements of total α-synuclein (LB509) or CD9 (n = 3). These experiments showed that α-synuclein and CD9 on L1EVs, as detected by our platform, were similar in neat serum and in the pooled F3 and F4 fractions, irrespective of the great excess of free α-synuclein in the former (**Figures 5.8E** and **S5.5**). Thus, free α-synuclein in the serum neither associate non-specifically with L1EVs during the isolation process, nor interfere with the specificity of the microfluidic assay. To further assess whether α-synuclein is on the EV surface, I performed immunocapture with anti-CD9, anti-L1CAM, or anti-α-synuclein (using antibody clone Syn1) from pooled F3 and F4, followed by immunoblotting. These experiments confirmed that the generic EV markers CD9, CD81, and Flotillin 1 were detected following anti-α-synuclein immunocapture, whereas no bands were observed in the beads-alone control

(**Figure 5.8F**). Direct detection of α-synuclein by immunoblotting is not possible as its abundance in EVs is below the LOD of this method.

I further confirmed these findings using dSTORM to visualise the colocalization of tetraspanins CD9, CD63, CD81 (Tetra Trio), L1CAM, and α-synuclein (antibody clone MJFR1) on serum EVs isolated by multimodal chromatography (dSTORM experiments were performed by Suman Dutta). These experiments identified individual EVs co-stained with fluorescently labelled antibodies against Tetra Trio (Alexa Fluor 561), L1CAM (Alexa Fluor 488), and α-synuclein (Alexa Fluor 647), as shown in **Figure 5.8G**. Quantification revealed that α-synuclein was detected on the surface of 11.99% of total EVs (8.99% α-synuclein+/L1CAM-/Tetra Trio+ and 3.00% α-synuclein+/L1CAM+/Tetra Trio+) and 24.27% of L1EVs (the ratio of 3.00% α-synuclein+/L1CAM+/Tetra Trio+ to 12.36% L1CAM+/Tetra Trio+), as shown in **Figure 5.8G**. Thus, membrane-associated α-synuclein is found on a subpopulation of serum EVs, and it is enriched in L1EVs, which are thought to originate from neurons, relative to total EVs.

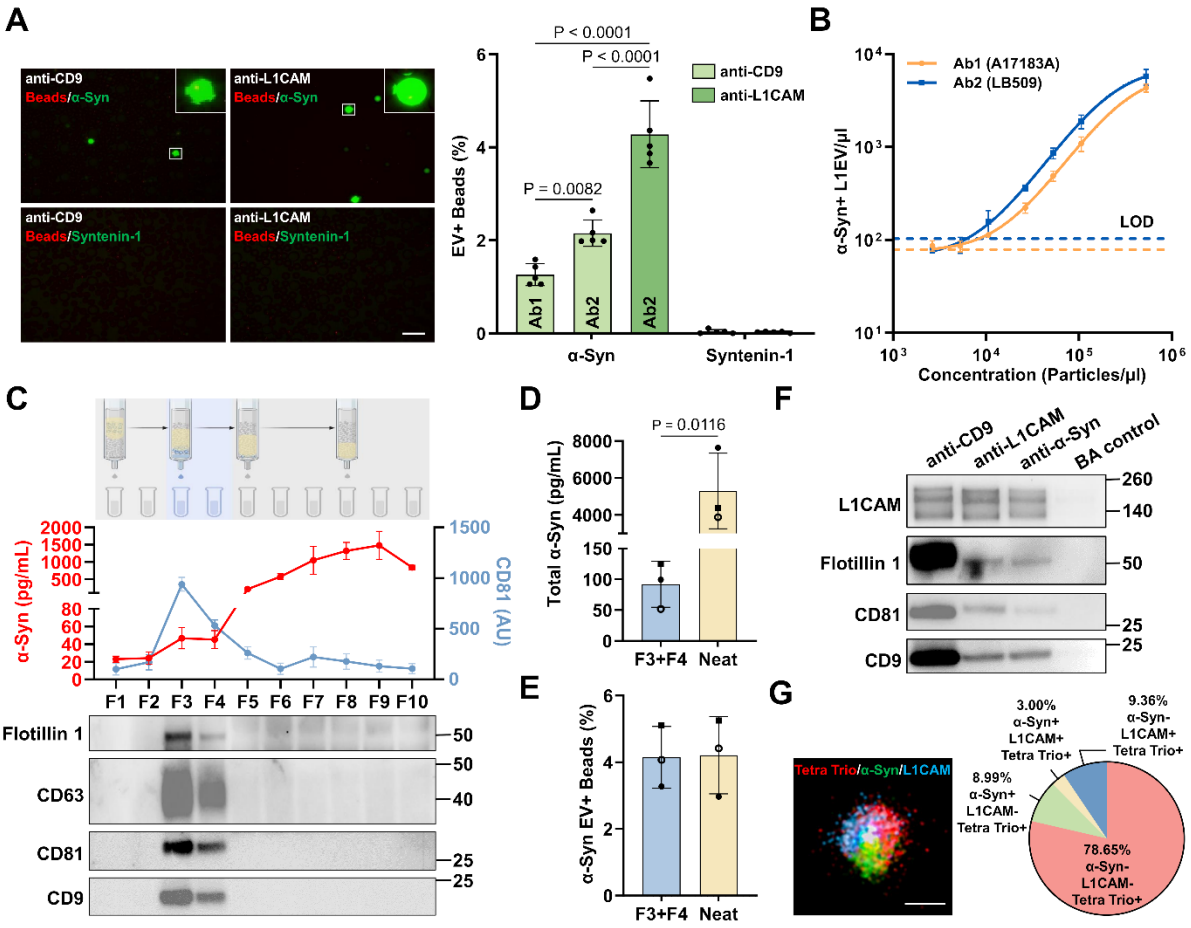


Figure 5.8: Identification of α-synuclein as a serum EV membrane-associated protein. (**A**) Representative images and quantification of membrane-associated α-synuclein (α-Syn) and the internal EV marker syntenin-1 on CD9+ EVs or L1EVs isolated from serum using the droplet assay. Anti-α-Syn antibody clone A17183A, which recognises mainly the aggregated forms of α-Syn under native conditions (Ab1), or clone LB509, which recognises a C-terminal region spanning amino acids 115 – 125 of total α-Syn (Ab2) were used; *n* = 5 individuals with PD tested; scale bar: 100 µm. (**B**) Assay calibration of L1EV membrane-associated α-Syn using Ab1 or Ab2 at various EV concentrations, as measured by NTA; *n* = 3 individuals with PD tested. LOD and LOQ values are summarised in **Table S5.2**. (**C**) Illustration of Capto Core multimodal chromatography, MSD electrochemiluminescence detection of α-Syn and the EV marker CD81, as well as immunoblotting of 10 eluted fractions (F) from 1 mL of serum. (**D**) MSD electrochemiluminescence detection of α-Syn in neat serum and chromatography pooled F3 and F4 fractions, and (**E**) detection of α-Syn on L1EVs immunocaptured from neat serum or chromatography pooled F3 and F4 fractions using the droplet assay, also see **Figure S5.5**; *n* = 3 individuals with PD tested. (**F**) Immunocapture using anti-CD9, anti-L1CAM, or anti-α-Syn from pooled F3 and F4 fractions followed by immunoblotting, with beads alone (BA) used as a control. (**G**) Representative image of a single EV obtained with dSTORM and corresponding quantification showing the percentages of colocalisation of L1CAM and α-Syn on Tetraspanin Trio+ EVs from chromatography pooled F3 and F4 fractions; pooled serum from 5 individuals with PD was tested; scale bar: 100 nm. Data are represented as mean ± SD. Statistical significance was determined by one-way ANOVA (panel **A**) or Student's two-tailed t-test (panel **D**). Experiments in panel **B** were performed by Wenjing Zhang, and dSTORM in panel **G** by Suman Dutta.

5.4.4 α-Synuclein L1EV membrane-association increases under pathological conditions

To investigate whether L1EV surface α-synuclein is a pathological association, Andrew Castle in the lab expressed either WT or PD-associated mutant α-synuclein (A53T, E46K, G51D, A30P) in SH-SY5Y cells, which endogenously express L1CAM. The culture media were conditioned for 48 h, and successful EV immunocapture with anti-L1CAM-coated beads from CM was confirmed (**Figure 5.9**). The cells were lysed in RIPA buffer and fractionated using UC into RIPA-soluble and RIPA-insoluble fractions. WT and mutant α-synuclein were detected in the RIPA-soluble fraction (**Figure 5.10A**), but not in the RIPA-insoluble fraction (**Figure S5.6A**). I then performed L1EV immunocapture, followed by on-chip duplex detection of either total α-synuclein (LB509 antibody) or CD81 (**Figures S5.6B** and **S5.6C**). Under these conditions, I found that intracellular α-synuclein levels are a critical determinant of L1EV membrane association (when compared to endogenous expression), based on EV membrane-associated α-synuclein to CD81 ratio (**Figure 5.10B**). In addition, I observed that the E46K mutation, which increases lipid binding,[269] further increased L1EV membrane association when expressed equally to the WT protein, whereas the G51D and A30P mutations, which are known to decrease lipid binding,[270,271] were associated with L1EV membrane similar to WT protein (**Figure 5.10B**), even though their intracellular expression was higher than that of the WT protein (**Figure 5.10A**). These data suggest that L1EV membrane-association is, at least partly, also determined by the effect of the pathogenic mutations on lipid binding.

To further corroborate this observation, Andrew Castle generated α-synuclein mutants that were previously shown to exacerbate the lipid binding affinity of single point mutations. Specifically, the engineered mutant 3K (E35K + E46K + E61K) enhances, whereas the

engineered mutant 3D (V40D + G51D + V66D) reduces the membrane association of their corresponding single PD-associated mutations (E46K vs. G51D).[272] α-Synuclein WT, 3K, and 3D were expressed in SH-SY5Y cells, and the media were conditioned for 48 h and collected for L1EV isolation, while the cells were subjected to subcellular fractionation into digitonin-soluble (cytosol) and Triton X-100-soluble (membrane) fractions, according to a previously published α-synuclein fractionation protocol.[265] Immunoblotting confirmed that expression of the 3K mutant α-synuclein increased the membrane to cytosol ratio compared to WT, whereas expression of 3D mutant α-synuclein decreased the membrane to cytosol ratio (**Figure 5.10C**). L1EVs immunocaptured from corresponding CM were followed by on-chip duplex detection of either total α-synuclein (LB509) or CD81 (**Figures S5.6D** and **S5.6E**). I found that expression of the 3K mutant, which binds more avidly to membranes inside the cells, also led to increased L1EV membrane association, as quantified by the α-synuclein to CD81 ratio relative to WT or 3D (**Figure 5.10D**). It is noteworthy that under these conditions, the 3K expression was associated with weak pS129-α-synuclein (**Figure 5.10C**), suggesting that this L1EV membrane association reflects a pathological form of α-synuclein, as demonstrated previously inside the cells. This was further corroborated by dSTORM, using Tetra Trio to visualise all EVs and the clone 5G4 α-synuclein antibody, which recognises primarily aggregated α-synuclein under native conditions.[18] In this experiment conducted by Suman Dutta, EVs were isolated from CM using UC. Quantification showed that the percentage of Tetra Trio+ (Alexa Fluor 561) and α-synuclein+ (Alexa Fluor 647) EVs was increased in 3K- compared to 3D-expressing cells (**Figure 5.10E**).

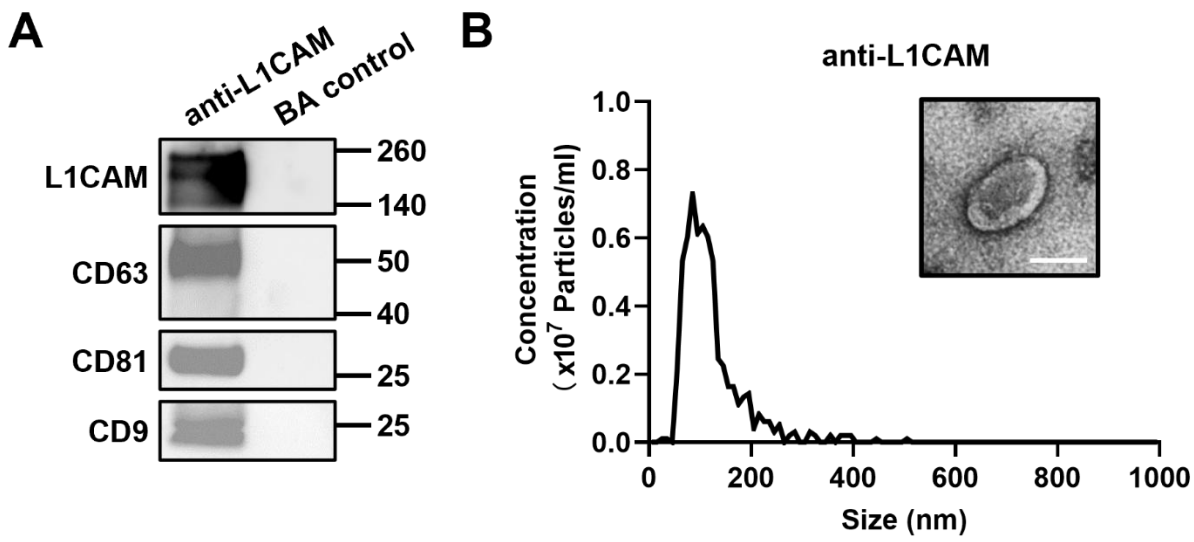


Figure 5.9: Confirmation of EV isolation from conditioned media. (**A**) Immunocapture using anti-L1CAM from conditioned media of SH-SY5Y cells expressing WT α-synuclein, followed by immunoblotting, with beads alone (BA) used as a control. (**B**) Size distribution of eluted EVs after anti-L1CAM immunocapture was confirmed by NTA and the typical cup-shaped appearance was demonstrated by TEM; scale bar: 100 nm.

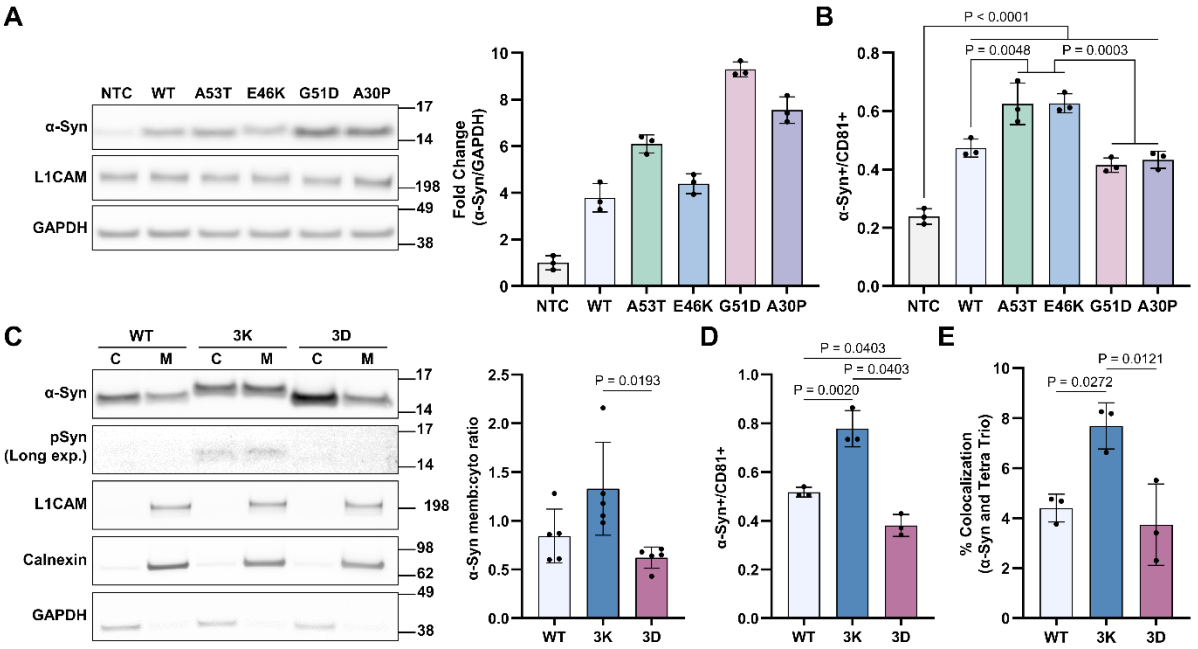


Figure 5.10: L1EV membrane-associated α-synuclein is increased under pathological conditions. (**A**) Immunoblotting of RIPA-soluble fraction from SH-SY5Y cells expressing PD-associated α-synuclein (α-Syn) mutations A53T, E46K, G51D, and A30P. (**B**) A53T and E46K mutant α-Syn increased the L1EV membrane-associated α-Syn to CD81 ratio compared to non-transduced control (NTC), wild-type (WT), G51D, and A30P, as measured by the droplet assay. (**C**) Expression of the 3K mutant α-Syn in SH-SY5Y cells increased the membrane (memb) to cytosol (cyto) ratio compared to expression of the 3D mutant α-Syn; *n* = 5 independent experiments. (**D**) The 3K mutant α-Syn had increased membrane-associated α-Syn to CD81 ratio compared to WT and 3D, whereas expression of the 3D mutant α-Syn decreased L1EV membrane association, as measured by the droplet assay. (**E**) Quantification by dSTORM of membrane-associated α-Syn on individual EVs using antibody clone 5G4, which recognises mainly the aggregated forms of α-Syn under native conditions. *n* = 3 independent experiments unless stated otherwise. Data are represented as mean ± SD. Statistical significance was determined by Kruskal-Wallis test (panel **C**) or one-way ANOVA (panels **B, D,** and **E**). Experiments in panel **A** and **C** were performed by Andrew Castle.

To confirm that membrane-associated α-synuclein is present on EVs released by human neurons and is increased under pathological conditions detectable by the droplet-based assay, I isolated L1EVs from CM collected from patient-derived iPSC dopaminergic neuronal cultures. An iPSC line from a patient with α-synuclein gene (*SNCA*) triplication (*SNCA*^{TRIP}), which is associated with higher α-synuclein expression and more severe disease, and its isogenic iPSC clone (*SNCA*^{ISO}; **Table 5.1**), were differentiated into dopaminergic neurons by Chor Lai Lam in the lab. I confirmed an approximately 2-fold increase in intracellular α-

synuclein levels in *SNCA*^{TRIP} compared to *SNCA*^{ISO} neuronal cultures,[262] as evidenced by α-synuclein immunostaining (**Figure 5.11A**) and immunoblotting (**Figure 5.11B**), without any significant difference in the neuronal markers L1CAM and Tuj1 across the two lines (**Figure 5.11B**). Culture media conditioned from Day 52 to Day 60 were similarly enriched in EVs, as measured by NTA (**Figure 5.11C**). L1EV immunocapture from CM was then performed, followed by on-chip detection of either total α-synuclein (LB509) or CD81 (**Figure 5.11D**). I found that membrane-associated α-synuclein was increased in L1EVs isolated from *SNCA*^{TRIP} neurons compared to *SNCA*^{ISO} control L1EVs (**Figure 5.11E**). In agreement with the NTA measurements, CD81 quantification was similar between the two conditions (**Figure 5.11F**). The α-synuclein to CD81 ratio also differentiated *SNCA*^{TRIP} from *SNCA*^{ISO} neuronal cultures (**Figure 5.11G**). To further corroborate these findings, Anis Sahoo in the lab used Capto Core multimodal chromatography followed by MSD electrochemiluminescence to quantify α-synuclein and CD81 levels in EV-enriched fractions isolated from neuronal CM. This experiment further confirmed an increase in the α-synuclein to CD81 ratio in EVs from *SNCA*^{TRIP} neurons compared to its isogenic control (**Figure S5.6F**). Thus, L1EVs released from human neurons with *SNCA*^{TRIP} exhibit a 2-fold increase in EV membrane-associated α-synuclein levels compared to *SNCA*^{ISO} L1EVs, which reflects the increased α-synuclein expression in *SNCA*^{TRIP} neurons.[262] Collectively, these data show that membrane-associated α-synuclein is, at least in part, present on the surface of EVs and that this phenomenon is increased by pathogenic protein mutations or overexpression.

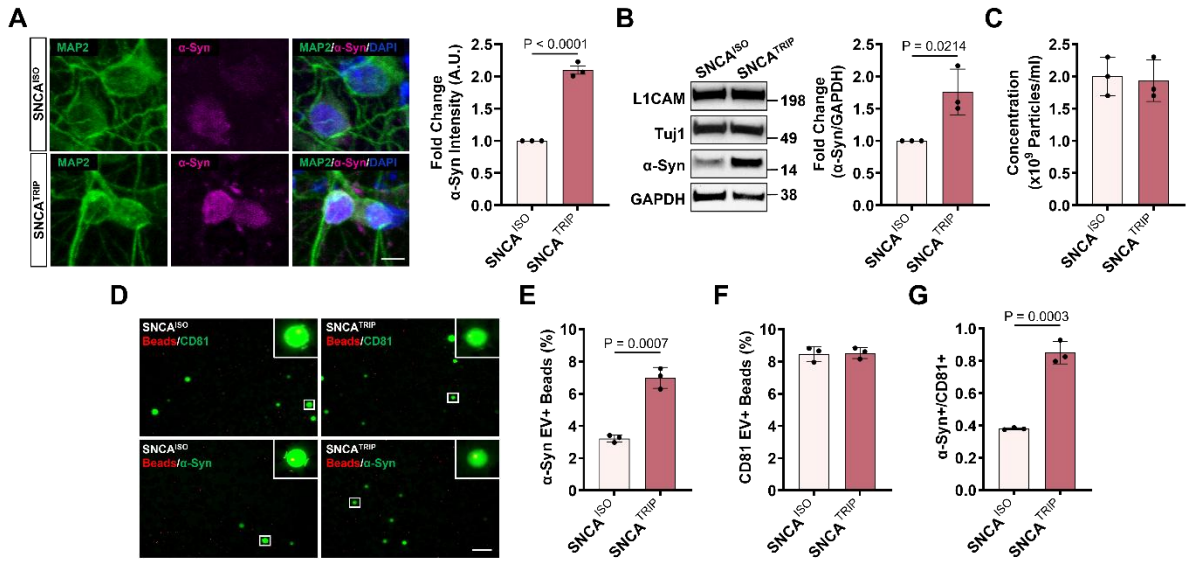


Figure 5.11: L1EV membrane-associated α-synuclein is increased in iPSC-derived *SNCA^{TRIP}* dopaminergic neurons. (**A**) Confocal images and corresponding quantification of iPSC-derived *SNCA^{ISO}* and *SNCA^{TRIP}* dopaminergic neurons stained with MAP2 and α-synuclein (α-Syn), showing an approximately 2-fold increase in α-Syn immunofluorescence in the *SNCA^{TRIP}* line; scale bar: 5 μm. (**B**) Immunoblotting showed an approximately 2-fold increase in endogenous α-Syn expression when normalised to GAPDH in *SNCA^{TRIP}* neuronal lysates compared to its isogenic controls. (**C**) NTA of the neuronal CM showed that the total EV concentration was similar between the two lines and was not affected by pathological α-Syn expression. (**D**) Representative images of membrane-associated α-Syn and CD81 detection on L1EVs from neuronal CM, as measured by the droplet assay; scale bar: 100 μm. (**E**) Membrane-associated α-Syn was increased in L1EVs isolated from *SNCA^{TRIP}* neurons compared to *SNCA^{ISO}* L1EVs, as measured by the droplet assay. (**F**) No difference in membrane-associated CD81 in L1EVs from *SNCA^{TRIP}* neurons compared to *SNCA^{ISO}* L1EVs, as measured by the droplet assay, in agreement with the NTA results. (**G**) L1EV membrane-associated α-Syn to CD81 ratio was increased by approximately 2-fold in *SNCA^{TRIP}* compared to *SNCA^{ISO}* L1EVs, as measured by the droplet assay. n = 3 independent differentiations (iPSC-derived neurons). Data are represented as mean ± SD. Statistical significance was determined by Student's two-tailed t-test. Experiments in panels **A** and **B** were performed by Chor Lai Lam.

5.4.5 Serum L1EV membrane-associated α-synuclein is increased in individuals with iRBD or PD compared to healthy controls

To investigate the clinical utility of this platform and the potential of L1EV membrane-associated α-synuclein as a biomarker in patients, I assessed serum samples from age- and sex-matched individuals with the diagnosis of iRBD (n = 20) or PD (n = 20), and healthy controls

(*n* = 20) from the Oxford Discovery cohort (**Table 5.2**). All sample processing and analyses were performed blinded to the diagnosis.

	HC	**iRBD**	**Sporadic PD**	**P-value**
No of individuals	20	20	20	NA
Sex, No. (%)				
Female	5 (25.0)	3 (15.0)	5 (25.0)	0.68
Male	15 (75.0)	17 (85.0)	15 (75.0)	
Age, mean (SD), y	65.28 (12.53)	66.35 (6.15)	66.49 (8.39)	0.91
MoCA, mean (SD)	27.05 (2.04)	26.50 (2.88)	25.68 (2.56)	0.17
L1EV α-Syn, median (IQR), pg/mL[a]	10.03 (5.96)	19.78 (12.78)	28.36 (8.21)	<0.0001
α-Syn EV+ beads, median (IQR), %[b]	1.98 (1.16)	3.72 (1.29)	3.85 (0.75)	<0.0001
CD81 EV+ beads, median (IQR), %[b]	7.50 (1.55)	7.65 (1.85)	6.87 (1.41)	0.64
α-Syn+/CD81+, median (IQR), [b]	0.26 (0.11)	0.49 (0.24)	0.56 (0.09)	<0.0001

Table 5.2: Demographic characteristics. Data are number (%), mean (SD), or median (IQR). Abbreviations: HC = healthy controls; iRBD = isolated REM sleep behaviour disorder; PD = Parkinson's Disease; MoCA = Montreal Cognitive Assessment; L1EV = L1CAM positive extracellular vesicles; α-Syn = α-synuclein. One way ANOVA was used to compare age and MoCA, Kruskal-Wallis one-way analysis of variance was used to compare L1EV α-Syn, α-Syn EV+ beads, CD81 EV+ beads, and α-Syn+/CD81+ ratio, and Pearson $\chi 2$ test was used to compare sex frequency between groups.

[a] Measurements of total α-Syn in L1EV using MSD electrochemiluminescence.

[b] Quantification of L1EV membrane-associated α-Syn and CD81 using the droplet assay.

I found that patients with iRBD or PD exhibited increased L1EV membrane-associated α-synuclein compared to healthy controls (**Figure 5.12A**). Individuals with iRBD were differentiated from controls with an AUC of 0.89 (**Figure 5.12B**). Similarly, patients with sporadic PD were differentiated from controls with an AUC of 0.89 (**Figure 5.12B**). There was no significant difference in CD81 quantification across these groups (**Figure 5.12C**). I also assessed the α-synuclein to CD81 ratio, which adjusts for the number of EVs detected across groups. Interestingly, L1EV α-synuclein to CD81 ratio exhibited an improved performance in differentiating individuals with either iRBD or PD from controls, compared to the

measurements of α-synuclein alone (**Figure 5.12D**). Specifically, the α-synuclein to CD81 ratio differentiated individuals with iRBD from controls with an AUC of 0.93, and PD patients from controls with an AUC of 0.95 (**Figure 5.12E**).

To further evaluate the clinical potential of L1EV membrane-associated α-synuclein as a biomarker, I assessed the reproducibility of the assay by examining the same sample in triplicate or two separate samples from the same individual (n = 3). I estimated the inter-assay coefficient of variation to be 4.45% (**Figure 5.13A**). I also found that L1EV membrane-associated α-synuclein, as measured by the droplet-based assay (**Figures 5.13B-5.13D**), and total L1EV α-synuclein levels, as measured by MSD electrochemiluminescence (**Figure S5.13E**), remained consistent across two samples from the same individual, despite variability in total, free serum α-synuclein, as determined by MSD electrochemiluminescence (**Figure 5.13F**). I thus asked whether single-EV measurements of membrane-associated α-synuclein correlate with our previous quantification of total α-synuclein in bulk lysates of L1EVs using MSD electrochemiluminescence.[93,94] This analysis revealed a correlation (ρ = 0.44, P = 0.0004) between L1EV membrane-associated α-synuclein to CD81 ratio and L1EV total α-synuclein levels (**Figure 5.12F**).

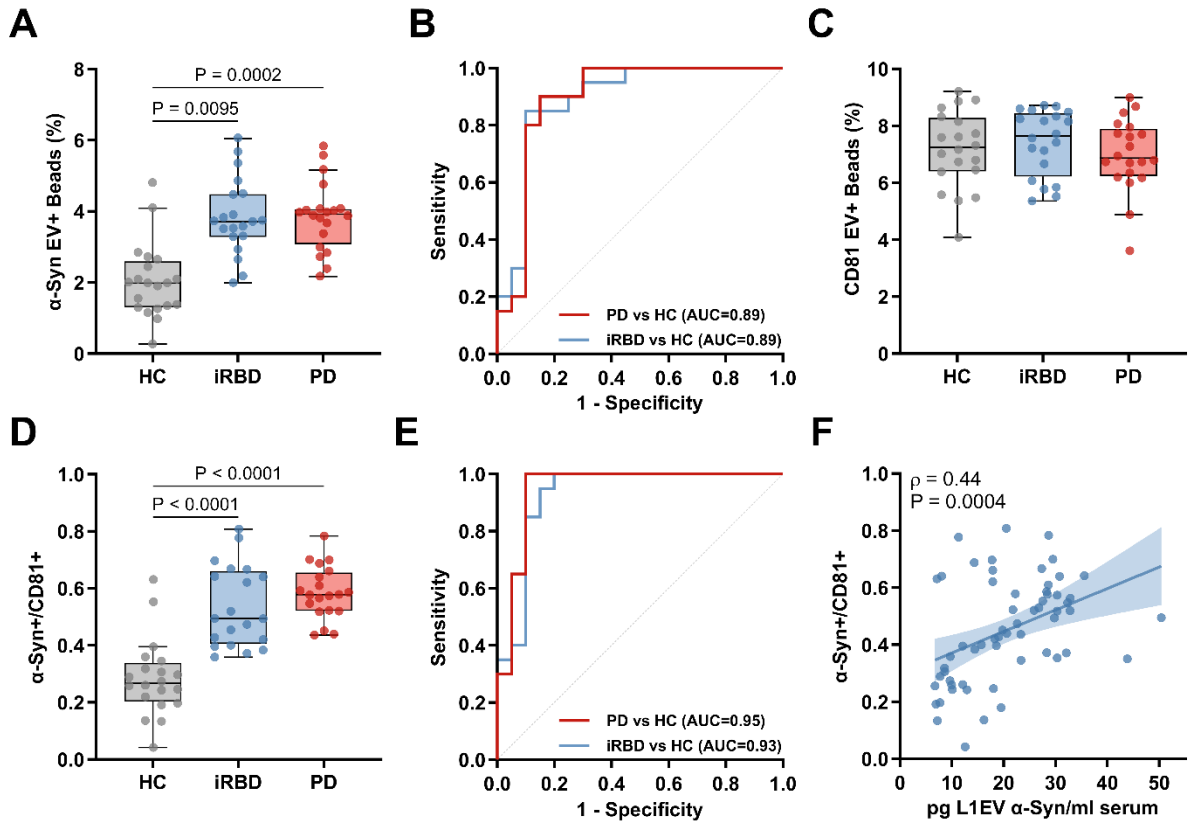


Figure 5.12: Serum L1EV membrane-associated α-synuclein is increased in individuals with iRBD or PD. (**A**) Boxplot and (**B**) corresponding Receiver Operating Characteristic (ROC) curves of L1EV membrane-associated α-synuclein (α-Syn) measurements using the LB509 antibody for healthy controls (HC) and individuals with iRBD or PD. (**C**) Boxplot of L1EV membrane-associated CD81 measurements for HC and individuals with iRBD or PD. (**D**) Boxplot and (**E**) corresponding ROC curves of L1EV membrane-associated α-Syn to CD81 ratio for HC and individuals with iRBD or PD. (**F**) Correlation between total α-Syn levels in serum L1EV lysates, as measured by MSD electrochemiluminescence, and L1EV membrane-associated α-Syn to CD81 ratio, as measured by the droplet-based immunoassay. *n* = 20 individuals per group. The midline of the box plots indicates the median and the box indicates the 25th and 75th percentiles (panels **A, C,** and **D**). Statistical significance was determined by Kruskal-Wallis test (panels **A, C,** and **D**). Least squares regression line with 95% CI was plotted and Spearman coefficient was reported (panel **F**).

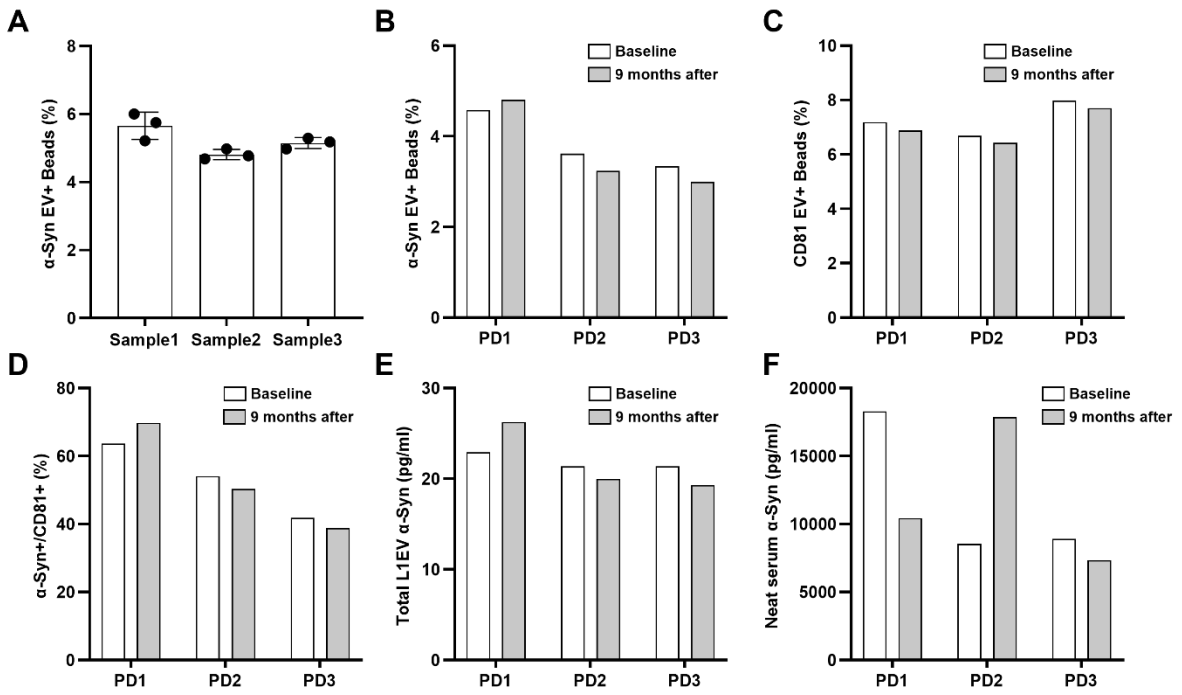


Figure 5.13: Reproducibility of the assay in detecting L1EV membrane-associated α-synuclein. (**A**) L1EV membrane-associated α-synuclein (α-Syn) was measured in triplicate from the same sample by the droplet assay, demonstrating the high reproducibility of the assay (*n* = 3 individuals). (**B**) Membrane-associated α-Syn or (**C**) CD81 on serum L1EVs from the same patient, collected 9 months apart, as measured by the droplet assay. (**D**) L1EV membrane-associated α-Syn to CD81 ratio detected by the droplet assay and (**E**) total L1EV α-Syn levels measured by the MSD electrochemiluminescence were stable between serum samples collected 9 months apart, despite variability in (**F**) soluble, free α-Syn in neat serum measured by the MSD electrochemiluminescence. Data are represented as mean ± SD. Experiments in panel **A** were performed by Wenjing Zhang.

5.5 Discussion

5.5.1 Droplet-based assay for precise multiplexed quantification of EV membrane proteins

In this study, I describe an improved analytical platform designed for the ultrasensitive detection and quantification of EV membrane-associated proteins at single-EV resolution. By compartmentalising individual EVs captured on magnetic beads into tens of thousands of microdroplets, the assay enables the detection of low-abundance EV subtypes, such as nEVs, with an estimated LOD of 66 CD81+ L1EVs/μL, surpassing the detection limit of previously reported nanoplasmonic[273] or nanosensor-based[274] EV detection techniques, as well as standard

ELISA measurements by several orders of magnitude. Our assay offers a number of advantages over previously reported droplet-based EV prototypes applied in cancer,[220] such as speed (approximately 10 min) and simplicity. It can be implemented by a syringe-vacuum-driven microfluidic droplet chip and a standard fluorescence microscope, while maintaining analytical performance comparable to those performed by exclusive equipment such as a fluorescence spectrophotometer.

Importantly, unlike other microfluidic EV detection platforms,[220,221] this assay enables multiplexed detection of diverse EV membrane-associated proteins at single-EV resolution from an estimated minimum volume of ~3 μL of serum, which is well within the blood volume (~35 μL) required for "pin-prick" tests. These features are highly desirable for potential clinical use in point-of-care settings. Thus, this technology offers a more detailed representation of EV heterogeneity and enables a more comprehensive understanding of individual EV changes from minimal sample volumes. This is especially useful for the detection of rare neuronally relevant EV biomarkers that are diluted in the massive excess of serum proteins.

In addition to binary detection (positive/negative) of EV subtypes per droplet, this platform can be adapted through assay modifications to quantify levels of EV-associated proteins and to distinguish membrane-associated from cytosolic fractions, functioning similarly to a digital droplet ELISA.[275] This quantitative potential allows not only the enumeration of EVs carrying specific markers but also estimation of antigen abundance per EV population, expanding its utility in both clinical and mechanistic studies.

5.5.2 α-Synuclein is a L1EV membrane-associated protein

An important discovery enabled by the assay is the identification of membrane-associated α-synuclein as a biomarker that is detected already in individuals with iRBD, preceding the clinical diagnosis of PD. Interestingly, membrane-associated α-synuclein was

detected in the minority of the total (CD9+) EV population in PD but was especially enriched in neuronally-derived (L1EVs), based on two complementary methods and confirmed in neuronal CM. This finding suggests that the membrane-associated fraction of α-synuclein, and the capability to measure it by this platform, offer a more sensitive assay of neuronal homeostasis. Accordingly, I found that L1EV membrane-associated α-synuclein was increased under pathological conditions in cell culture and that it exhibited an improved performance (AUC = 0.95 for PD), when compared to previously reported (AUC = 0.86 for PD) bulk measurements in lysed EVs.[94]

In solution, α-synuclein adopts an α-helical conformation in its N-terminal domain in the presence of membranes with acidic phospholipids or high curvature,[266] as in the case of EVs,[111] but binding to membranous vesicles isolated from human samples has not been systematically evaluated in patients or demonstrated on EVs. The interaction of α-synuclein with membranes was shown to promote the formation of physiological multimers[276] or, under certain conditions, to induce aggregation.[277-279] *In vitro*, membrane-associated α-synuclein acquires a "pathological" conformation depending on the lipid composition and the α-synuclein-to-lipid ratio,[280] but to what extent such changes occur in patient-derived EVs requires further investigation. Therefore, it is presently unknown how much of the signal detected in patients reflects increased mislocalisation of physiological α-synuclein on the EV surface, or its assembly into a pathological conformation with differential antibody binding affinity. The assay utilised the LB509 antibody (BioLegend), which binds to amino acids 115 – 125 of α-synuclein[268] and has a higher affinity for monomeric than fibrillar α-synuclein.[229] α-Synuclein was also detectable on EVs with antibodies (clone A17183A and 5G4) that reportedly recognise primarily oligomeric or aggregated forms of α-synuclein under native conditions, and at concentrations higher than those used in this assay.[267] The latter suggests that a fraction of α-synuclein on the L1EV membrane exhibits a pathological assembly or

conformation, and that refinement of the assay using conformation-specific antibodies could further enhance the sensitivity and specificity of the biomarker.

5.5.3 α-Synuclein and L1EV membrane association increases under pathological conditions

The results in cells expressing PD-associated α-synuclein mutations and in iPSC-derived dopaminergic neuronal cultures with *SNCA*^{TRIP} suggest that the association of α-synuclein with EV membranes reflects, at least partly, a pathological state. The mechanisms regulating α-synuclein binding to EV membrane is currently unclear and requires further investigation. These cell-based experiments show that intracellular α-synuclein levels and the lipid binding affinity of α-synuclein, as determined by disease-associated and engineered mutations, are two critical determinants of incorporation into the EV membrane. We propose that α-synuclein on the EV membrane could signify the formation of a conformer of α-synuclein that may accumulate in close vicinity to membranous organelles during EV biogenesis or is induced by changes in their lipid composition. The comparative analysis of L1EV membrane-associated α-synuclein in neat and Capto Core multimodal chromatography-processed serum suggests that neither a potential protein corona that has been reported in some EV preparations[281] nor free α-synuclein confound the reproducibility of the results when measurements are performed at single-EV resolution.

5.5.4 L1EV membrane associated α-synuclein is an improved biomarker for early PD diagnostics

Although further validation is required in larger cohorts, our results suggest that L1EV membrane-associated α-synuclein may serve as an improved predictive biomarker for PD compared to bulk measurements in EV lysates.[93,94] Alongside previous work from our lab,[94,95]

including those reported in Chapter 4,[93] these findings reinforce the notion that L1EVs isolated from serum exhibit altered composition in neurodegenerative diseases well before the onset of disabling symptoms, thus offering a promising means of developing clinical screening tests that are pertinent to specific brain pathologies. In this regard, the capability afforded by our platform for precise quantification of EV subpopulations signifies a substantial progress towards this goal.

5.5.5 Limitations and future directions

The sensitivity demonstrated in this experimental setup does not fully reflect the inherent potential of this detection method, primarily due to throughput restrictions. The speed limitations in acquiring and processing fluorescent images resulted in the analysis of only approximately 10% of the input beads, which compromises the assay sensitivity. Future improvements could integrate automated video-based image acquisition and quantification[282] or on-chip EV immunocapture, such as the one recently described.[137] A device incorporating such elements could facilitate rapid EV biomarker detection in a form not dissimilar to current "pin-prick" tests for other indications and clinical use in point-of-care settings.

5.5.6 Conclusion

In summary, this work describes on-chip droplet-confined fluorescence reporting assay that identified α-synuclein on the membrane of L1EVs immunocaptured from human serum and corroborated this finding by super-resolution dSTORM. Using CM from neuroblastoma cells expressing α-synuclein mutants or patient-derived iPSC neurons with α-synuclein gene triplication, I found that association of α-synuclein with the L1EV surface is increased under pathological conditions. Accordingly, this readout, combined with membrane-associated CD81, as measured by the droplet-based assay, is an improved predictive biomarker in the prodromal phase (AUC = 0.93) or diagnostic biomarker in the clinical phase (AUC = 0.95) of PD. More

broadly, this platform will simplify the assessment of EV membrane proteins and facilitate their application as diagnostic biomarkers across diverse clinical indications.

5.6 Supplementary information

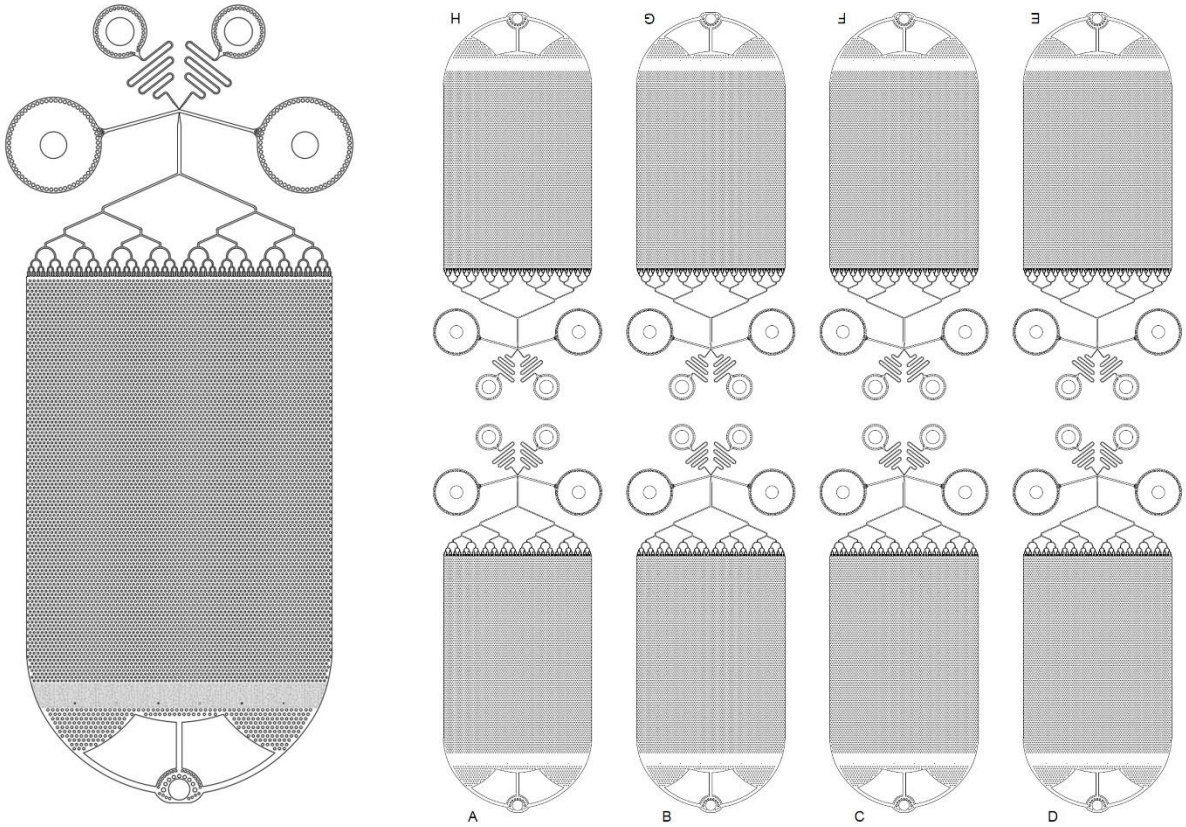


Figure S5.1: Detailed mask design of the microfluidic chip. The chip was designed by Bowen Shu.

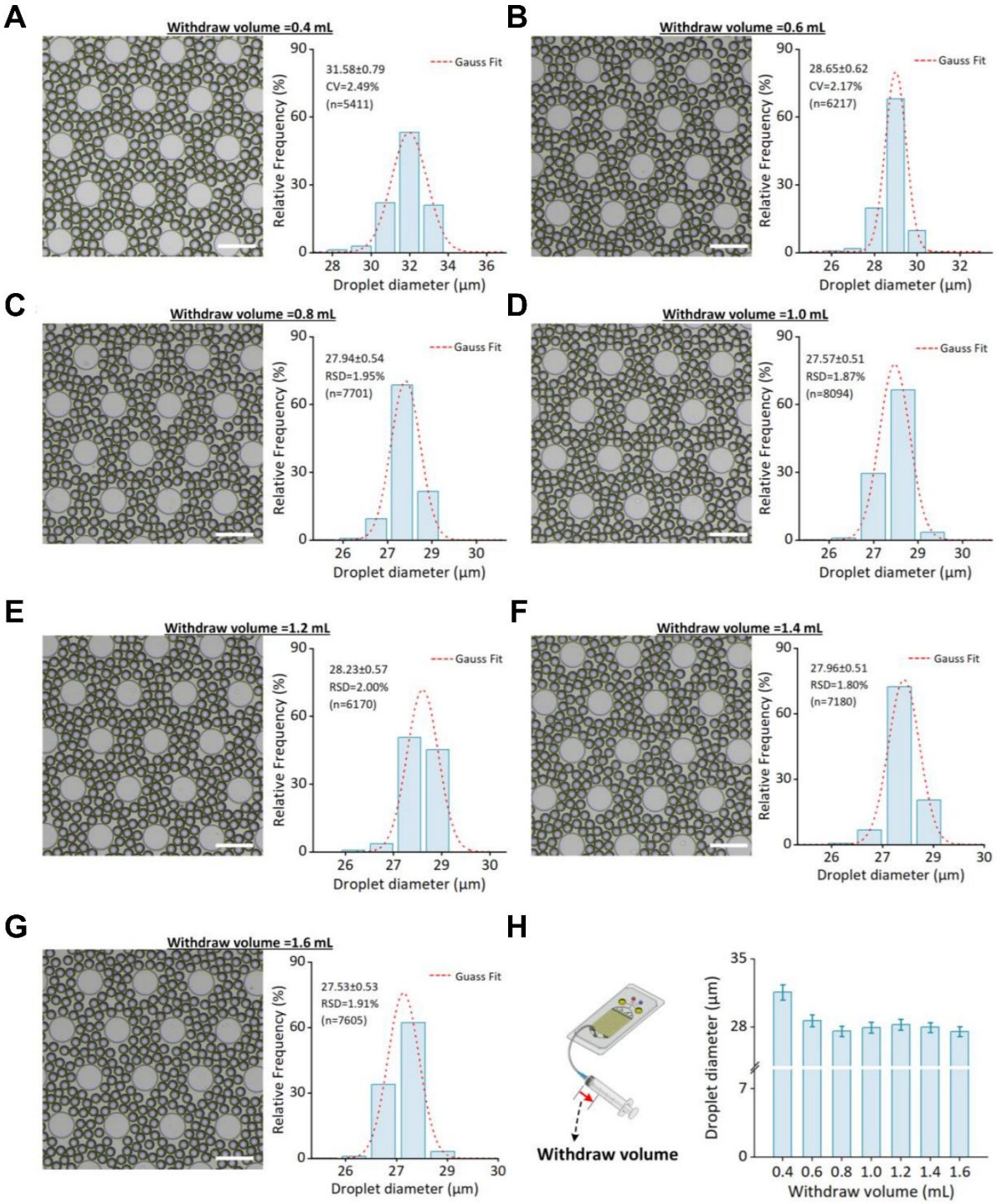


Figure S5.2: Robust droplet generation by syringe-vacuum-driven microfluidic device. (**A-G**) Microscopic images of droplets and corresponding size distributions under different negative pressures, initiated by withdrawing and locking the piston of a 5-mL plastic syringe at volumes ranging from 0.4 mL to 1.6 mL; scale bar: 100 μm. (**H**) Schematic and summary of the device, demonstrating its ability to generate highly uniform picolitre-sized droplets for a robust and user friendly digital assay. Microfluidic chip characterisation was performed by Xinying Li and Bowen Shu.

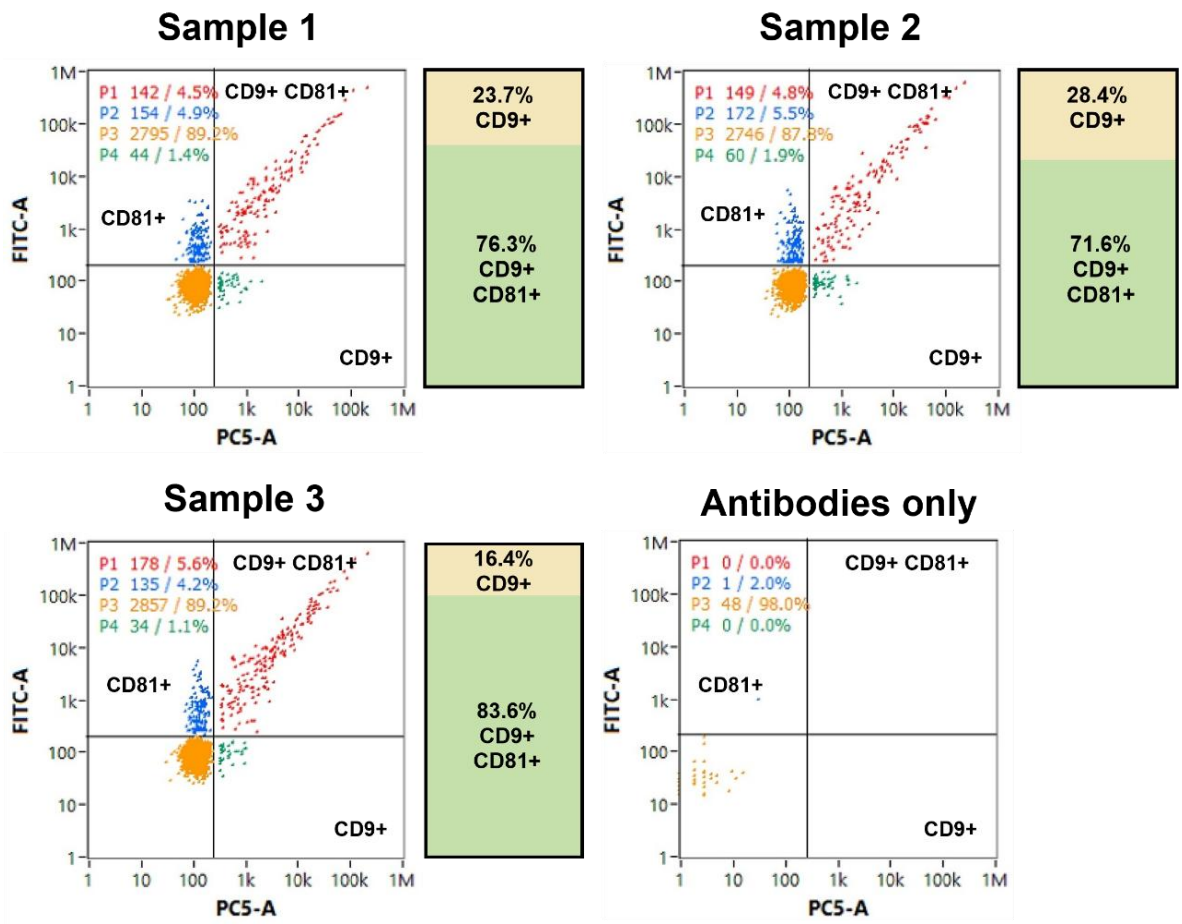


Figure S5.3: NanoFCM analysis of membrane-associated CD9 and CD81 expression on single serum EVs. Following ultracentrifugation, EVs (*n* = 3 individuals with PD tested) were stained with Alexa Fluor-647-labelled anti-CD9 and FITC-labelled anti-CD81. Antibodies only (without sample) was included as a control. The majority of EVs were unlabelled (orange) or not recognised as such by this method. Focusing on the labelled particles, an average of 77.2% of CD9+ EVs were also CD81+, in agreement with estimates from the droplet-based assay (as summarised in **Figures 5.7A** and **5.7B**). This experiment was assisted by Suman Dutta and Dongnan Yan.

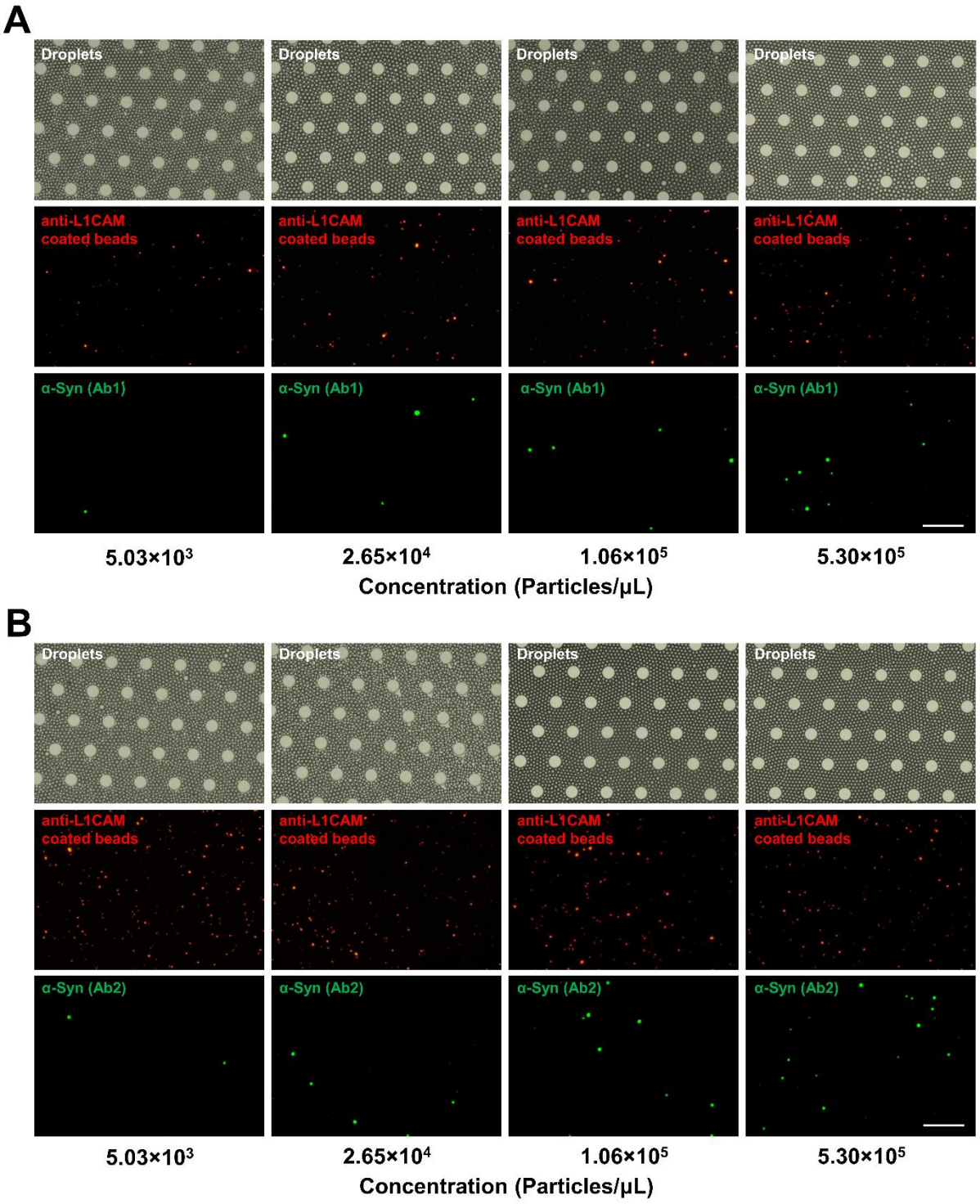


Figure S5.4: Representative images of α-synuclein detection on L1EVs using the droplet assay at various EV concentrations. Detection of serum L1EV membrane-associated α-synuclein using (**A**) antibody clone A17183A and (**B**) antibody clone LB509 across various starting EV concentrations, as measured by NTA. Scale bar: 250 μm. These experiments were performed by Wenjing Zhang.

	CD81	**α-Syn (A17183A)**	**α-Syn (LB509)**
LOD (L1EVs/μL)	66.6	78.9	103.2
LOQ (L1EVs/μL)	111.6	131.4	175.9
Dynamic Range (L1EVs/μL)	66.6 to 8306.7	78.9 to 4328.0	103.2 to 5758.7
Estimated minimal volume based on LOD (μL)	0.8	2.6	2.4

Table S5.1: Performance of the assay in detecting serum L1EV membrane-associated α-synuclein and CD81. The assay supports reliable detection of membrane associated CD81 or α-synuclein with < 3 μL of serum. Abbreviations: α-Syn = α-synuclein; LOD = limit of detection; LOQ = limit of quantification, L1EV = L1CAM positive EV. Experiments were performed by Wenjing Zhang.

Target	Multiplex capability	Sample	LOD	Application	Readout equipment	Ref
PD-L1	Singleplex	270 μL biofluids	158 EVs/μL	Cancer	Microplate reader	[283]
EpCAM, CA-125, CD24	Triplex	10 μL to 10 mL plasma	750 EVs/μL	Ovarian cancer	Fluorescence microscope	[140]
CD63	Singleplex	8mL CM or urine	10 AU/mL	Bladder cancer	Smart phone	[284]
CD63	Singleplex	10 μL CM or serum	160 EVs/μL	Cancer	Fluorescence spectrophotometer	[285]
CD63	Singleplex	80 μL plasma	65.6 EVs/μL	Cancer	Fluorescence spectrophotometer	[274]
Aβ42	Singleplex	CM or plasma	200 EVs	Alzheimer's disease	Spectrometer	[286]
GPC-1	Singleplex	Plasma	10 EVs/μL	Breast cancer	Inverted epifluorescent microscope	[220]
PD-L1, GZMB, TCF7	Multiplex	CM or plasma	38 EVs/μL	Cancer	Fluorescence microscope	[222]
CD81	Singleplex	CM or plasma	9 EVs/μL	/	Machine vision camera	[221]
CD9, F4/80, CD11b, CD63, CD45, CD81	Multiplex	CM or plasma	/	/	Next generation sequencing sequencer	[223]
LRG1	Singleplex	500 μL urine	~1 EV/μL	Lung cancer	Dark field microscope	[287]
PD-L1	Singleplex	CM or plasma	10.76 EVs/μL	Cancer	Fluorescence microscope	[288]
CD63	Singleplex	2 μL blood	100 EVs/μL	/	Fluorescence microscope	[289]
PD-L1	Singleplex	90 μL plasma	/	Cancer	Total internal reflective fluorescence microscopy	[290]
CD81, EphA2, CA19-9	Triplex	CM or plasma	16 EVs/μL	Pancreatic cancer	Confocal laser scanning microscopy	[291]
α-Syn, aggregated α-Syn, L1CAM, NCAM, CD11b, CD81	Duplex	3 μL CM or serum	66 EVs/μL	Parkinson's disease	Fluorescence microscope	This work[292]

Table S5.2: Comparison of current microfluidic assays for EV protein detection. Abbreviations: LOD = limit of detection; Ref = reference; CM = conditioned media; α-Syn = α-synuclein.

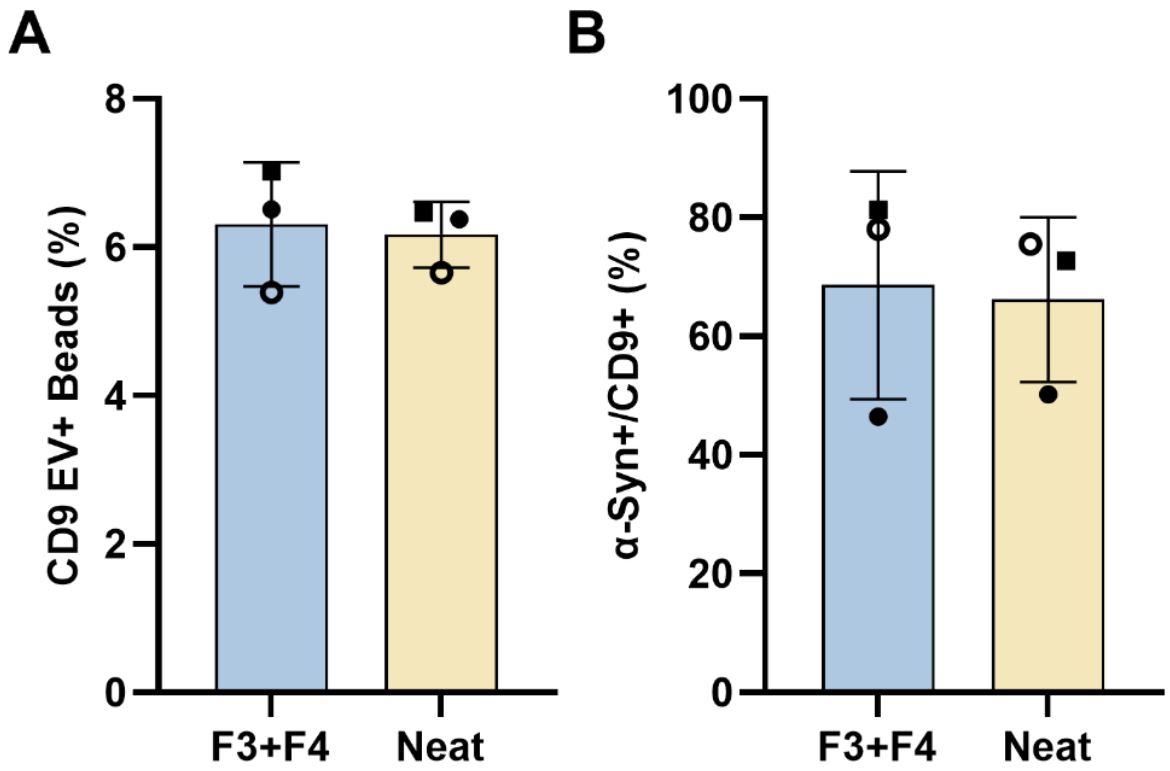


Figure S5.5: Detection of α-synuclein and CD9 on serum L1EVs. (**A**) L1EV membrane-associated CD9 levels and (**B**) the α-synuclein (α-Syn) to CD9 ratio, as measured by the droplet assay, were similar in neat serum and Capto Core multimodal chromatography pooled EV-enriched F3 and F4 fractions. *n* = 3 individuals with PD. Data are represented as mean ± SD. Statistical significance was determined by Mann-Whitney test.

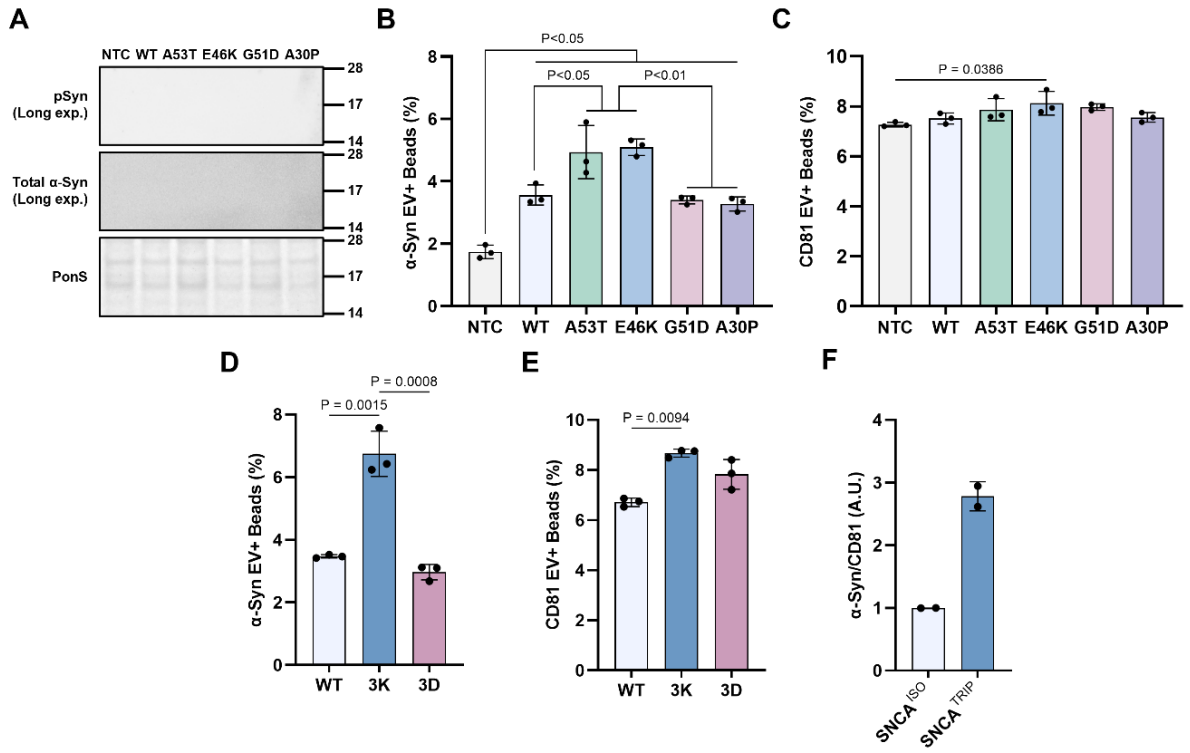


Figure S5.6: Detection of L1EV membrane-associated α-synuclein and CD81 under pathological conditions. (**A**) Neither pS-129-α-synuclein (sin) nor total α-synuclein (α-Syn) was detected in the RIPA-insoluble 100,000 ×g fraction of non-transduced SH-SY5Y cells (NTC) or cells expressing α-Syn WT, A53T, E46K, G51D, and A30P. (**B**) Quantification of α-Syn-EV-positive beads and (**C**) CD81-EV-positive beads following anti-L1CAM immunocapture from conditioned media (CM) of the above cell lines by the droplet assay (*n* = 3 independent experiments). (**D**) Quantification of α-Syn and (**E**) CD81 on L1EVs immunocaptured from CM of SH-SY5Y cells expressing α-Syn WT, 3D, and 3K by the droplet assay (*n* = 3 independent experiments). (**F**) The α-Syn to CD81 ratio in the Capto Core multimodal chromatography pooled EV-enriched F3 and F4 fractions isolated from CM of iPSC-derived dopaminergic neuronal cultures was increased in *SNCA*^{TRIP} neurons compared to *SCNA*^{ISO} control, as measured by MSD electrochemiluminescence (*n* = 2 independent differentiations). Data are represented as mean ± SD. Statistical significance was determined by one-way ANOVA (panels **B-E**). The experiments in panels **A** and **F** were performed by Andrew Castle and Anis Sahoo, respectively.

Chapter 6

Serum p-tau217 predicts cognitive impairment in iRBD

6. Serum p-tau217 predicts cognitive impairment in iRBD

6.1 Introduction

6.1.1 Co-pathologies and cognitive decline in iRBD

iRBD is a well-established prodrome of synucleinopathies, with many individuals eventually developing PD, PDD, DLB, or MSA.[54] While α-synuclein aggregation is the main neuropathological hallmark, this pattern of pathology *per se* is not sufficient to explain the clinical heterogeneity observed across disease subtypes.[293] It is therefore likely that co-pathologies, especially of Alzheimer's type, contribute to the cognitive decline and may also influence disease trajectory more broadly.

Post-mortem and biomarker studies have identified tau pathology, especially in limbic and neocortical regions, in individuals with PDD and DLB.[294,295] Recent studies demonstrated that p-tau isoform (p-tau181) can predict DLB outcome in iRBD.[296] However, among tau species, plasma p-tau217 has shown remarkable diagnostic specificity and sensitivity, outperforming other p-tau isoforms in differentiating AD from non-AD dementias and predicting amyloid-β positivity across multiple cohorts.[297-299] Despite these promising findings, the role of p-tau217 in iRBD remains underexplored.

6.1.2 Serum NfL as a biomarker for diffuse neurodegeneration

Serum NfL has gained attention as a sensitive, albeit generic marker of neurodegeneration. Serum or CSF NfL levels are increased in conditions with accelerated or diffuse neurodegeneration, such as motor neuron disease[300] and dementias.[301,302] In synucleinopathies, NfL levels are most prominently increased in MSA, and to a lesser extent in DLB, but not in idiopathic PD.[303,304] However, in PD, serum NfL levels were shown to

correlate with disease severity and motor deterioration.[305] In a small prospective study, elevated baseline NfL levels in individuals with iRBD who later developed PD or DLB suggest a potential role for NfL as a risk-marker of phenoconversion.[306] The relevance of NfL has not been validated in large iRBD cohorts and its clinical utility in prodromal synucleinopathies remains unclear.

6.1.3 Multimodal biomarker strategies in prodromal PD

We previously identified L1EV α-synuclein as a serum biomarker for iRBD, PD, and DLB.[93,94] Given the underlying neuropathological heterogeneity in synucleinopathies, reliance on a single biomarker may not be sufficient to provide adequate diagnostic or prognostic value. A multimodal strategy that integrates multiple serum biomarkers may improve risk stratification and guide the optimal timing of intervention with precision therapies.

6.2 Aims and objectives

Given the neuropathological heterogeneity of iRBD, this chapter aims to evaluate the performance of p-tau217 *vis-à-vis* NfL in predicting risk of cognitive or motor impairment, as well as disease phenoconversion in individuals with iRBD. The specific aims are to:

1. Examine the associations between biomarkers levels and key prodromal markers.
2. Assess whether these biomarkers distinguish participants with MCI from cognitively normal participants.
3. Determine whether serum p-tau217 and NfL levels identify iRBD participants who phenoconvert to PD-MCI or DLB.
4. Evaluate the potential of serum p-tau217 and NfL as prognostic biomarkers in iRBD for predicting time to phenoconversion.

6.3 Material and methods

6.3.1 Study design

This is a retrospective cross-sectional study of four cohorts that followed the STORBE guidelines. The study profile is shown in **Figure 6.1**. Inclusion criteria for iRBD were confirmation by video-assisted PSG and availability of serum samples. Participants were excluded if a secondary cause for RBD was present. Participants were recruited from July 2013 through February 2024, and samples were analysed from May 2024 through April 2025. Oxford iRBD participants ($n = 186$) were recruited from the Discovery cohort.[247] The Marburg iRBD cohort ($n = 62$) were recruited nationwide from the German RBD registry project and followed annually for at least 4 years.[249] iRBD participants from Cologne ($n = 37$) were identified through structured population-based screening process.[250] The PPMI iRBD cohort ($n = 15$) were recruited across sites in the US, Europe, or Israel (https://www.ppmi-info.org/). Subgroup analyses were performed to assess biomarker performance in individuals with additional prodromal markers. Where such results were available, the associations between biomarker levels and phenoconversion were assessed. Healthy controls without significant comorbidities or relevant family history were included from Oxford ($n = 5$) and Marburg ($n = 2$) as a reference group.

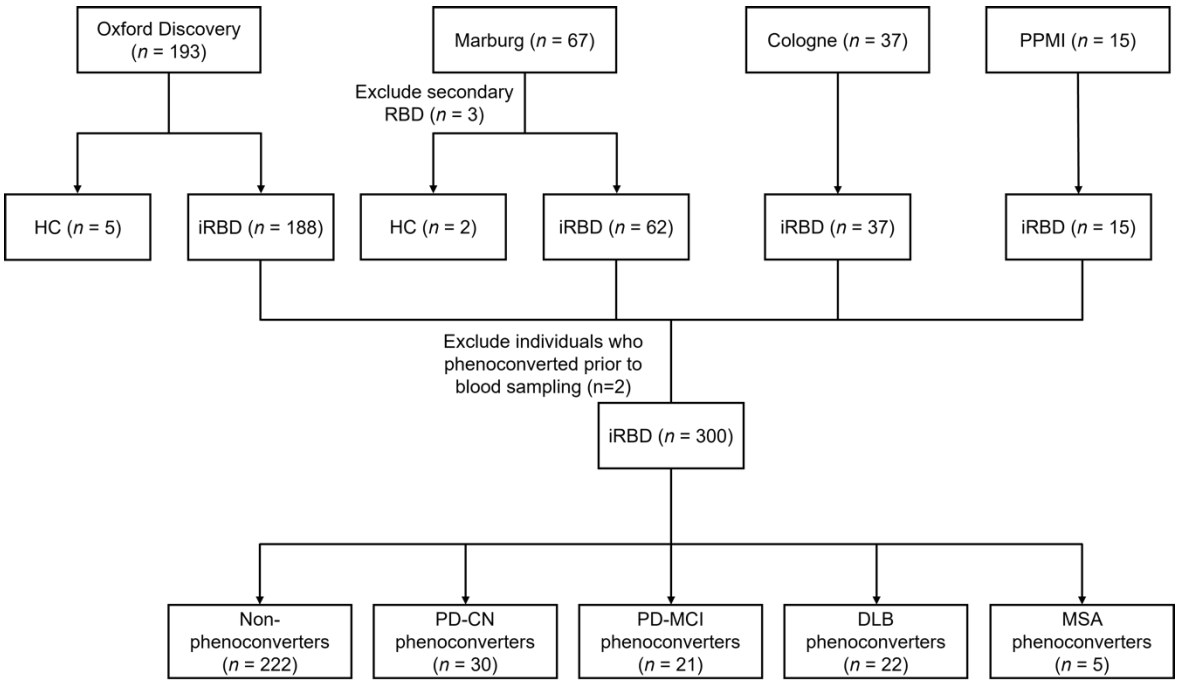


Figure 6.1: Study selection criteria and design.

6.3.2 Biomarker measurements

Blood samples from all the centres were collected during the patient assessment. Serum was isolated, aliquoted, and stored at -80˚C until further use. All samples were sent on dry ice and processed in a blinded manner at Oxford. Serum p-tau217 and NfL levels were measured using the MSD electrochemiluminescence S-PLEX human Tau kit (K151APFS-2, MSD) and the R-PLEX human NfL antibody set (F217X-3, MSD) in 96-well R-Plex plates (L45SA-2, MSD), respectively, following the manufacturer's protocols. All samples were visually inspected before analysis, and haemolysed samples were excluded. Undiluted serum was used for the p-tau217 assay, whereas a 4-fold dilution was applied for the NfL assay.

6.4 Results

6.4.1 Demographic characteristics

Among the 307 participants included, the mean (SD) age was 66.59 (8.32) years, 268 were male (87.3%), and 39 were female (12.7%), as summarized in the **Table 6.1**. In the Oxford

Discovery cohort, 191 participants (mean [SD] age, 66.70 [9.08] years; 164 male [85.9%] and 27 female [14.1%]) were included, and the mean (SD) time between blood sampling and last visit was 2.92 (2.70) years. In the Marburg cohort, 64 participants (67.75 [6.76] years; 60 male [93.8%] and 4 female [6.2%]) were included, and the mean time between blood sampling and last visit was 3.48 (2.09) years. In the Cologne cohort, 37 participants (66.59 [7.80] years; 31 male [83.8%] and 6 female [16.2%]) were included, and the mean time between blood sampling and last visit was 1.88 (1.35) years. In the PPMI cohort, 15 participants (70.80 [5.66] years; 13 male [86.7%] and 2 female [13.3%]) were included, and the mean time between blood sampling and last visit was 4.03 (3.54) years. Higher serum p-tau217 was associated with older age and male sex, while no effects of age or sex were observed on serum NfL in iRBD (**Table S6.1**).

	Characteristic	HC	iRBD non-converter	PD-CN converter	PD-MCI converter	DLB converter	MSA converter	P-value[a]
Oxford Discovery	No of individuals	5	128	16	19	18	5	NA
	Sex, No (%)							
	Female	0 (0.0)	21 (16.4)	4 (25.0)	1 (5.3)	1 (5.6)	0 (0.0)	0.01
	Male	5 (100.0)	107 (83.6)	12 (75.0)	18 (94.7)	17 (94.4)	5 (100.0)	
	Age, mean (SD), years	55.73 (2.35)	65.23 (9.32)	67.51 (6.52)	70.33 (7.16)	67.92 (8.08)	62.86 (9.09)	0.018
	MoCA, mean (SD)	27.00 (2.35)	25.11 (3.08)	26.93 (1.79)	24.26 (2.33)	23.41 (3.30)	23.60 (2.19)	0.007
	Follow-up after sampling, mean (SD), years	NA	3.47 (2.92)	3.46 (2.38)	2.81 (2.14)	3.29 (2.11)	2.14 (1.50)	0.74
	P-tau217, median (IQR), pg/mL	0.35 (0.38)	0.67 (0.68)	0.57 (0.43)	1.05 (0.54)	1.33 (1.19)	0.36 (0.70)	<0.0001
	NfL, median (IQR), pg/mL	93.51 (206.77)	221.95 (357.63)	186.96 (288.87)	185.57 (243.22)	60.44 (117.17)	602.55 (90.34)	0.008
Marburg	No of individuals	2	45	12	2	3	NA	NA
	Sex, No (%)							
	Female	0 (0.0)	4 (8.9)	0 (0.0)	0 (0.0)	0 (0.0)	NA	NA
	Male	2 (100.0)	41 (91.1)	12 (100.0)	2 (100.0)	3 (100.0)	NA	
	Age, mean (SD), y	68.49 (—)	67.70 (7.28)	68.11 (5.52)	61.23 (—)	70.80 (3.16)	NA	NA
	MoCA, mean (SD)	28.50 (—)	28.00 (1.70)	27.00 (2.78)	23.00 (—)	23.00 (2.83)	NA	NA
	Follow-up after sampling, mean (SD), years	NA	3.56 (2.01)	3.27 (2.56)	1.77 (—)	4.29 (1.34)	NA	NA
	P-tau217, median (IQR), pg/mL	0.62 (—)	0.50 (0.42)	0.49 (0.31)	1.04 (—)	1.12 (1.24)	NA	NA
	NfL, median (IQR), pg/mL	75.42 (—)	114.67 (247.18)	293.20 (73.81)	264.64 (—)	124.34 (215.83)	NA	NA
Cologne	No of individuals	NA	36	1	NA	NA	NA	NA
	Sex, No (%)							
	Female	NA	5 (13.9)	1 (100.0)	NA	NA	NA	NA
	Male	NA	31 (86.1)	0 (0.0)	NA	NA	NA	
	Age, mean (SD), years	NA	66.29 (6.64)	77.38 (—)	NA	NA	NA	NA
	MoCA, mean (SD)	NA	27.08 (2.36)	27.00 (—)	NA	NA	NA	NA
	Follow-up after sampling, mean (SD), years	NA	1.88 (1.37)	1.96 (—)	NA	NA	NA	NA

	P-tau217, median (IQR), pg/mL	NA	0.26 (0.44)	0.14 (—)	NA	NA	NA	NA
	NfL, median (IQR), pg/mL	NA	93.92 (89.74)	62.60 (—)	NA	NA	NA	NA
PPMI	No of individuals	NA	13	1	NA	1	NA	NA
	Sex, No (%)							
	Female	NA	1 (7.7)	1 (100.0)	NA	0 (0.0)	NA	NA
	Male	NA	12 (92.3)	0 (0.0)	NA	1 (100.0)	NA	
	Age, mean (SD), years	NA	70.94 (5.94)	66.40 (—)	NA	73.20 (—)	NA	NA
	MoCA, mean (SD)	NA	25.46 (4.74)	30.00 (—)	NA	30.00 (—)	NA	NA
	Follow-up after sampling, mean (SD), years	NA	4.93 (3.28)	10.06 (—)	NA	10.18 (—)	NA	NA
	P-tau217, median (IQR), pg/mL	NA	0.46 (0.82)	0.19 (—)	NA	0.60 (—)	NA	NA
	NfL, median (IQR), pg/mL	NA	63.75 (67.39)	724.51 (—)	NA	265.11 (—)	NA	NA

Table 6.1: Demographic, clinical, and biomarker characteristics of the iRBD cohorts. Data are shown as number (%), mean (SD) or median (IQR), as appropriate. Abbreviations: iRBD = isolated REM sleep behaviour disorder; PD-CN = Parkinson's disease with normal cognition; PD-MCI = Parkinson's disease with mild cognitive impairment; DLB = dementia with Lewy bodies; MSA = multiple system atrophy; NA = not applicable; MoCA = Montreal Cognitive Assessment; P-tau217 = Phosphorylated tau 217; NfL = Neurofilament light.
For groups with $n < 3$, only raw values or limited statistics are reported.
[a] P values show within-cohort comparisons where group sizes were sufficient for statistical testing. One-way ANOVA was used for age, MoCA, and follow-up after blood sampling, the $\chi 2$ test for sex distribution, and the Kruskal-Wallis test for p-tau217 and NfL levels between groups.

6.4.2 Serum p-tau217 is a better predictor of cognitive and motor impairment than NfL in individuals with iRBD

Plasma p-tau217 has recently emerged as a promising biomarker for predicting cognitive decline.[307] I first confirmed the diagnostic utility of serum p-tau217 for AD, and assessed whether it is enriched in EV isolated by UC or found free in serum. In a small cohort ($n = 3$ per group), p-tau217 levels distinguished AD patients from controls as shown in **Figure 6.2A**. With an estimated LOD of this assay at ~0.3 pg/mL (**Figure S6.1**), p-tau217 was not

detectable in EVs, suggesting that it is predominantly circulates in the free serum fraction (**Figure 6.2B**).

To evaluate early co-pathology in individuals with iRBD, Anis and I measured serum p-tau217, which is the best proxy biomarker of AD pathology,[297] and NfL across four cohorts (**Table 6.1**). I first assessed whether these biomarkers are increased in iRBD individuals with ≥ 80% probability of being in the prodromal phase of PD (n = 250), as defined by the updated MDS prodromal research criteria.[59] Neither p-tau217 nor NfL were *per se* reliable independent predictors of prodromal PD (**Figures S6.2**). To determine whether any of the prodromal markers is individually associated with p-tau217 or NfL, I performed multiple linear regression analysis in an iRBD subgroup where complete clinical data were available (n = 187). This analysis revealed that MCI (β = 0.53 [SE = 0.12]; $P < 0.0001$) and excessive daytime sleepiness (β = 0.34 [SE = 0.12]; P = 0.006) were the strongest independent predictors of increased serum p-tau217 levels (**Table 6.2**), whereas lower NfL levels were associated with hyposmia (β = -186.35 [SE = 70.21]; P = 0.009), as shown in **Table 6.3**.

Variable	β	SE	P-value
Intercept	-0.17	0.46	0.71
Age	0.01	0.007	0.08
Sex [Male]	0.09	0.17	0.61
Mild cognitive impairment [Yes]	0.53	0.12	<0.0001
Subthreshold parkinsonism [Positive]	0.13	0.14	0.33
Olfaction [Abnormal]	-0.09	0.14	0.51
Excessive daytime sleepiness [Yes]	0.34	0.12	0.006
Constipation [Yes]	-0.08	0.12	0.51
Urinary dysfunction [Yes]	-0.17	0.12	0.15
Symptomatic OH [Yes]	0.12	0.15	0.41
Depression [Yes]	-0.21	0.13	0.12

Table 6.2: Association between serum p-tau217 levels and prodromal markers in iRBD. Multiple linear regression modelling identified mild cognitive impairment based on MoCA < 26 and excessive daytime sleepiness as having the strongest association with increased p-tau217 levels. Abbreviations: OH = orthostatic hypotension.

Variable	β	SE	P-value
Intercept	411.91	258.90	0.11
Age	2.03	3.63	0.58
Sex [Male]	-76.86	78.03	0.33
Mild cognitive impairment [Yes]	17.13	61.44	0.78
Subthreshold parkinsonism [Positive]	10.22	66.78	0.88
Olfaction [Abnormal]	-186.35	70.21	0.009
Excessive daytime sleepiness [Yes]	-65.39	59.58	0.27
Constipation [Yes]	-5.41	56.69	0.92
Urinary dysfunction [Yes]	-79.09	56.02	0.16
Symptomatic OH [Yes]	-56.07	75.09	0.46
Depression [Yes]	-37.97	61.97	0.54

Table 6.3: Association between serum NfL levels and prodromal markers in iRBD. Multiple linear regression modelling identified hyposmia as having the strongest association with lower serum NfL levels. Abbreviations: OH = orthostatic hypotension.

In further subgroup analysis, iRBD individuals with MCI, defined as a MoCA score < 26 (iRBD-MCI; n = 114) had increased serum p-tau217 levels (data shown as median ± IQR: 0.92 ± 0.81 pg/mL; $P < 0.0001$) compared to cognitively normal iRBD participants (iRBD-CN; n = 176; 0.51 ± 0.50 pg/mL). Serum p-tau217 also exhibited an inverse partial correlation with MoCA scores after adjusting for age and sex (r = -0.31, $P < 0.001$), as shown in **Figure 6.3A**. Interestingly, p-tau217 levels were also increased in iRBD individuals with SP (SP+; n = 66; 0.85 ± 0.87 pg/mL; P = 0.0134) relative to SP- individuals (n = 227; 0.58 ± 0.64 pg/mL), and positively correlated with SP scores (r = 0.18, P = 0.004) as shown in **Figure 6.3B**. However, p-tau217 levels were similar in iRBD individuals with an abnormal DaT SPECT (n = 47) compared to those with a normal DaT SPECT (n = 42), where this information was available (**Figure S6.3A**). ROC curve analyses of the aforementioned comparisons revealed

modest discriminative power (**Table S6.1**). In contrast, NfL levels did not differ between iRBD subgroups stratified by cognitive status, SP, or DaT SPECT (**Figures S6.3B-D**). However, NfL levels were lower in iRBD individuals with hyposmia (*n* = 183; 154.22 ± 202.08 pg/mL; *P* = 0.0480) compared to normosmic individuals (*n* = 113; 231.21 ± 376.94 pg/mL), and positively correlated Sniffin' Sticks test scores (*r* = 0.23, *P* = 0.002) where available (Oxford and Cologne cohorts, combined *n* = 220), as shown in **Figure 6.3C**. No correlation was found between NfL and MoCA (*r* = -0.05, *P* = 0.48) or SP scores (*r* = 0.10, *P* = 0.88). Collectively, these analyses identify p-tau217, but not NfL, as a useful adjunct biomarker when assessing individuals with iRBD at risk of cognitive impairment.

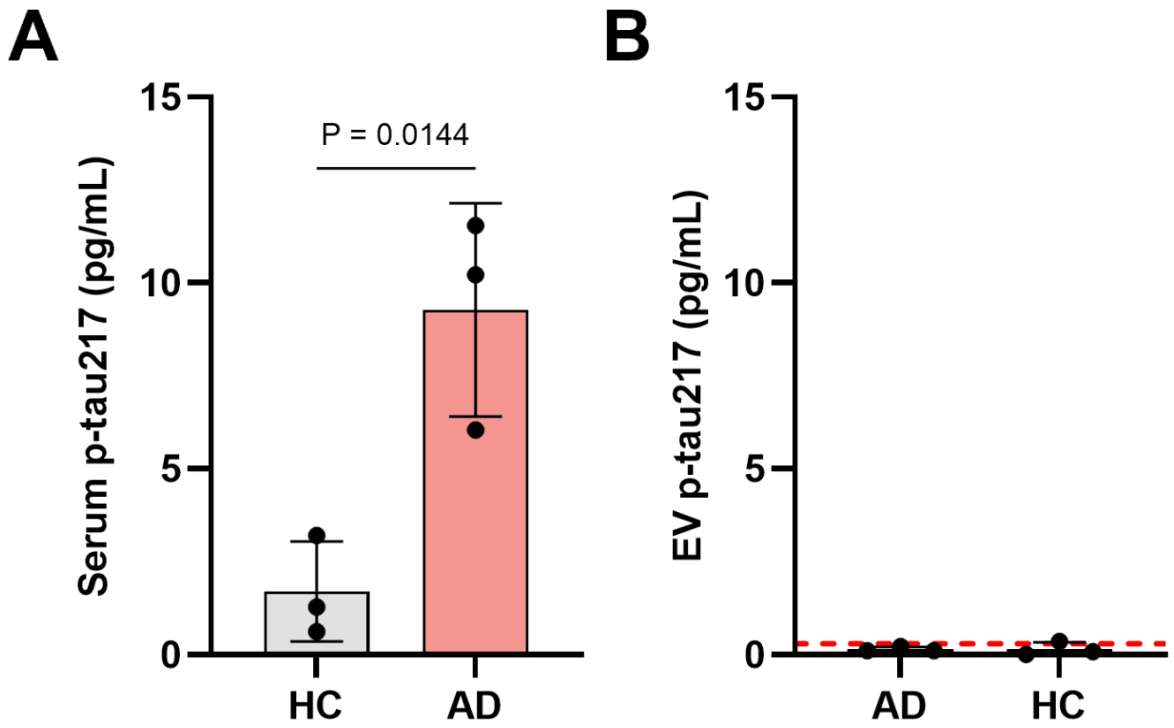


Figure 6.2: Serum and EV-associated p-tau217 levels in AD and healthy controls. (**A**) Serum p-tau217 levels were increased in AD patients compared to healthy controls (HC). (**B**) p-tau217 was not detectable in EVs isolated from serum using UC. *n* = 3 participants per group. Data are represented as mean ± SD. Statistical significance was determined by Student's two-tailed t-test.

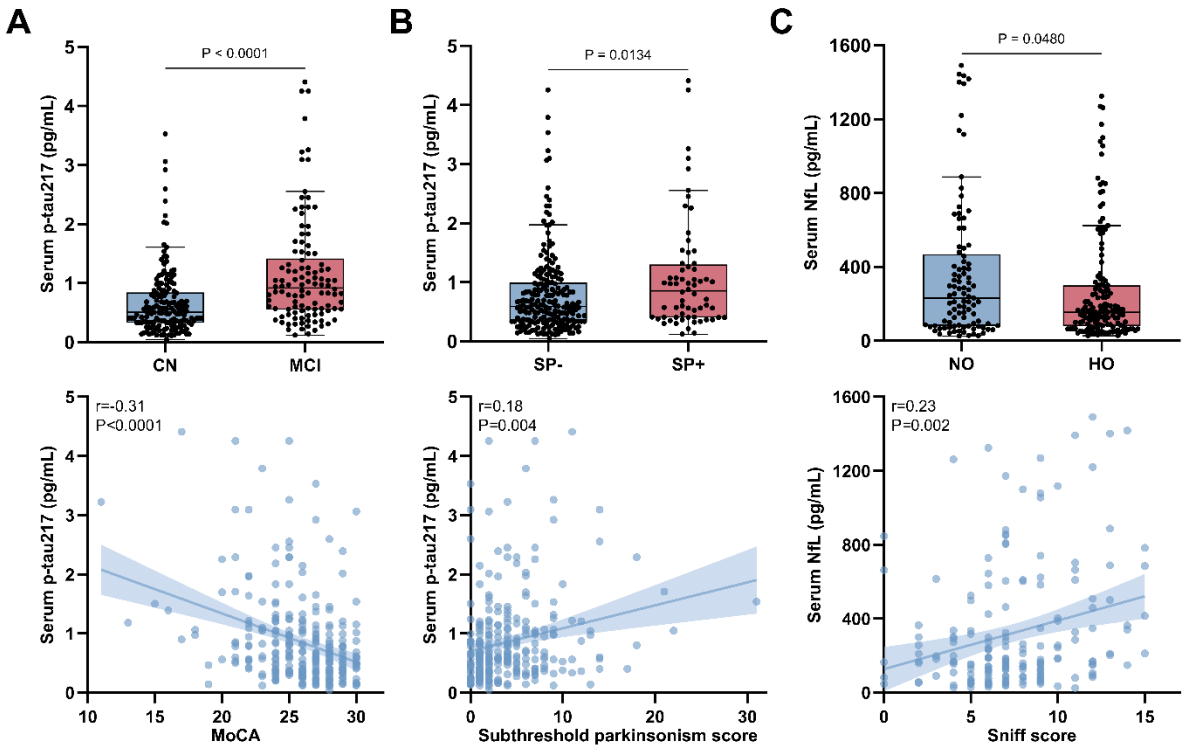


Figure 6.3: Serum p-tau217 and NfL in iRBD with additional prodromal markers. (**A**) *Top*: Boxplot of p-tau217 levels in individuals with iRBD and normal cognition (CN; *n* = 176) or mild cognitive impairment (MCI; *n* = 114). *Bottom*: Scatter plot showing an inverse partial correlation between p-tau217 and MoCA scores, adjusted for age and sex. (**B**) *Top*: Boxplot of p-tau217 levels in iRBD individuals with (SP+; *n* = 66) or without (SP-; *n* = 227) subthreshold parkinsonism (SP). *Bottom*: Scatter plot showing a positive partial correlation between p-tau217 and SP scores, adjusted for age and sex. (**C**) *Top*: Boxplot of NfL levels in iRBD individuals with normosmia (NO; *n* = 113) or hyposmia (HO; *n* = 183). *Bottom*: Scatter plot showing a positive partial correlation between NfL and Sniffin' Sticks test scores, adjusted for age and sex. Boxes represent the interquartile range from the 25th to 75th percentiles, the midline indicates the median, and whiskers and outliers are plotted using the Tukey method. Statistical significance was determined by the Mann-Whitney U test. Least squares regression lines with 95% CI were shown, with Pearson correlation coefficients and corresponding P values reported. NfL measurements were partially performed by Anis Sahoo.

6.4.3 Serum p-tau217 predicts phenoconversion to PD with cognitive impairment or DLB

To further evaluate the clinical potential of serum biomarkers for dementia prediction, I identified 30 individuals with iRBD who phenoconverted to PD with normal cognition (PD), 21 to PD with MCI (PD-MCI), 22 to DLB, and 5 to MSA across cohorts. I found that serum p-tau217 levels were higher in individuals who developed PD-MCI (1.05 ± 0.46 pg/mL) and

DLB (1.17 ± 1.45 pg/mL) compared to PD phenoconverters (0.50 ± 0.50 pg/mL) who exhibited levels similar to healthy controls (0.50 ± 0.38 pg/mL), as shown in **Figure 6.4A**. In contrast, NfL levels were notably increased in those who phenoconverted to MSA (663.11 ± 85.74 pg/mL), as shown in **Figure 6.4B**. There was no correlation (r = 0.06, P = 0.39) between p-tau217 and NfL levels (**Figure S6.4A**).

In further logistic regression adjusted for age and sex, I found that serum p-tau217 differentiated those who phenoconverted to PD-MCI or DLB from non-converters without MCI, with an AUC of 0.83 (95% CI, 0.77 – 0.89), sensitivity of 0.81 (95% CI, 0.67 – 0.90), and specificity of 0.74 (95% CI, 0.66 – 0.81). In contrast, NfL exhibited only modest discriminative value (AUC = 0.67; 95% CI, 0.57 – 0.77), and its combination with p-tau217 only marginally improved the discrimination (AUC = 0.85; 95% CI, 0.78 – 0.92), as shown in **Figure 6.4C**. Serum p-tau217, but not NfL, also differentiated phenoconverters to PD-MCI and DLB from those who phenoconverted to PD with AUC of 0.82 (95% CI, 0.70 – 0.93), as shown in **Figure S6.4B**.

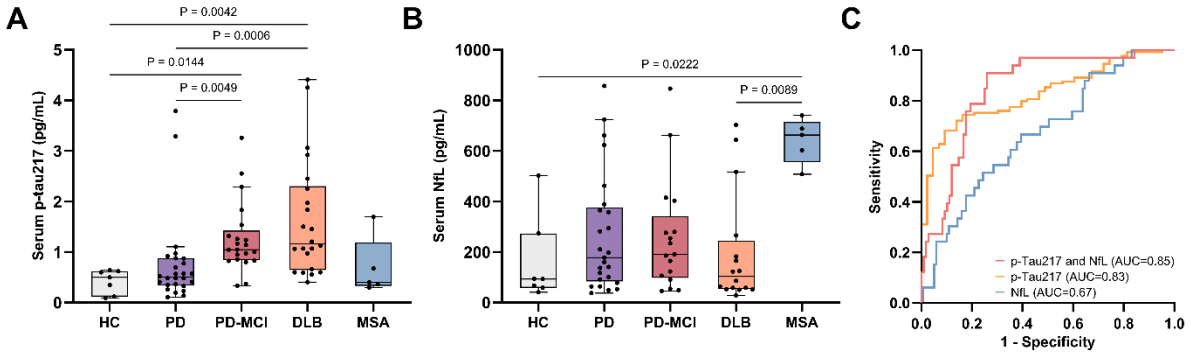


Figure 6.4: Serum p-tau217 and NfL levels in individuals with iRBD who phenoconverted. (**A**) Boxplot of p-tau217 and (**B**) NfL levels in healthy controls (HC; n = 7), phenoconverters to PD with normal cognition (PD; n = 30), PD with mild cognitive impairment (PD-MCI; n = 21), dementia with Lewy bodies (DLB; n = 22), or multiple system atrophy (MSA; n = 5). (**C**) Logistic regression adjusted for age and sex, evaluating the performance of p-tau217, NfL, and their combination in distinguishing individuals who phenoconverted to PD-MCI or DLB from iRBD non-phenoconverters with normal cognition. Boxes represent the interquartile range from the 25th to 75th percentiles, the midline indicates the median, and whiskers and outliers are plotted using the Tukey method. Statistical significance was determined by Kruskal-Willis test (panels **A** and **B**). NfL measurements were partially performed by Anis Sahoo.

6.4.4 Time to event analysis

We then assessed the potential of serum p-tau217 and/or NfL as prognostic biomarkers in iRBD for predicting time to phenoconversion to PD-MCI or DLB (these analyses were performed by Tanja Zerenner, University of Bristol). Stratification based on the optimal cut-off for differentiating iRBD-MCI from iRBD-CN revealed that individuals with p-tau217 > 0.78 pg/mL were ~5 times (HR = 5.33; 95% CI, 2.54 – 11.57) more likely to phenoconvert to PD-MCI or DLB than individuals with p-tau217 below this threshold (**Figure 6.5A**). Stratification based on quantiles showed that individuals with p-tau217 in the top quartile were ~8 times (HR = 8.30; 95% CI, 2.49 – 27.65) more likely to phenoconvert to PD-MCI or DLB compared to those in the bottom quartile (**Figure 6.5B**). Cox regression considering p-tau217 as a continuous variable, showed that a 1 pg/mL increase in p-tau217 was associated with a ~2-fold increased risk of phenoconversion to PD-MCI or DLB (**Tables S6.2** and **S6.3**). In contrast, serum NfL levels were not associated with risk of phenoconversion to PD-MCI or DLB (**Figure S6.5** and **Tables S6.2** and **S6.3**). Complementary time-to-event analyses for phenoconversion to DLB alone, using non-phenoconverters without MCI as the reference group, revealed a similar association (**Figure S6.6**).

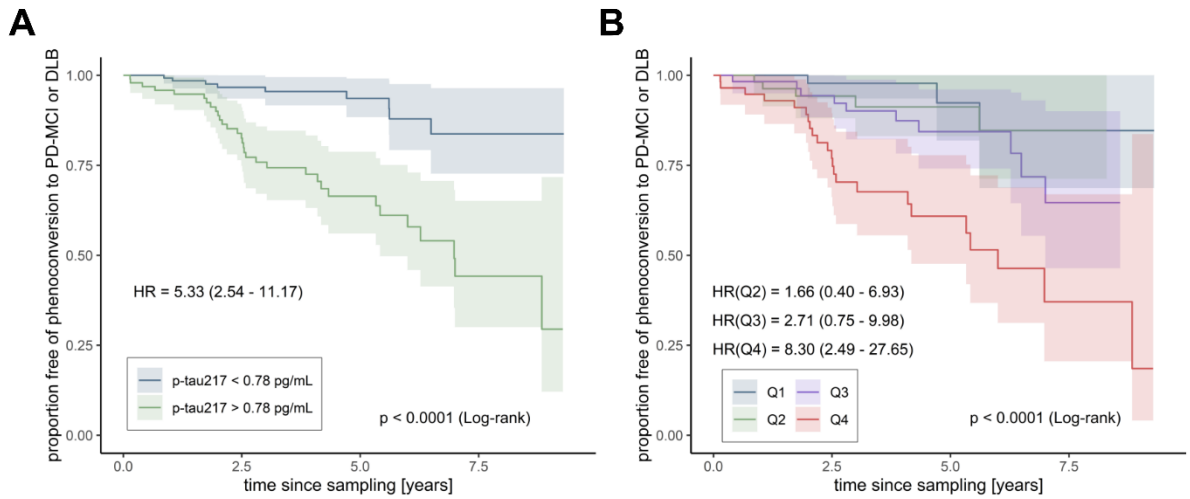


Figure 6.5: Kaplan-Meier survival curves for phenoconversion to PD-MCI or DLB as stratified by serum p-tau217. (**A**) Individuals stratified by p-tau217 levels above or below the optimal threshold (0.78 pg/mL) for differentiating iRBD individuals with and without MCI. (**B**) Individuals stratified by p-tau217 quartiles (Q1: < 0.361, Q2: 0.361 – 0.605, Q3: 0.605 – 1.047, Q4: > 1.047). Hazard ratios (HR) with 95% CI were derived from univariable Cox regression models, with patient group as a binary variable (panel **A**) or factor variable with quartiles (panel **B**). These analyses were performed by Tanja Zerenner, University of Bristol.

6.5 Discussion

6.5.1 Serum p-tau217 reflects early cognitive and motor changes in iRBD

In this study, I showed that serum p-tau217 levels are significantly increased in iRBD individuals with cognitive impairment and correlate inversely with MoCA scores, suggesting that tau pathology may already be present during the prodromal phase of PD. This observation is in line with growing neuropathological and biomarker-based evidence that tau pathology contributes to the clinical heterogeneity in synucleinopathies.[296,308] Mechanistically, this is likely to involve distinct processes, as α-synuclein aggregates rarely co-exist in the same neuron with tau hyperphosphorylation,[309] or alternatively, may signify a shared underpinning failure in proteostasis networks.

Increased p-tau217 also correlated weakly with SP scores but was not increased in iRBD individuals with abnormal DaT SPECT, suggesting that the effect of tau pathology on movement may be due to involvement of cortical regions of motor control rather than basal

ganglia dysfunction. In agreement with this interpretation, neuropathological studies in iRBD have not reported neuronal tau pathology in the brainstem, although astrocytic tau has occasionally been detected.[310]

6.5.2 Serum p-tau217 stratifies cognitive risk in iRBD

The discriminatory performance of serum p-tau217 in distinguishing iRBD-MCI participants from iRBD-CN participants remained modest, indicating that while biologically meaningful, its diagnostic utility in isolation is limited. Our analysis shows that p-tau217 is most useful clinically in predicting progression to MCI or dementia phenotypes in individuals with iRBD with a HR of 8.3. These findings are consistent with recent reports of increased p-tau217 levels in clinically diagnosed DLB[311] and elevated plasma p-tau181 levels in iRBD individuals who later developed DLB.[296] Importantly, and in contrast to p-tau181,[296] our data demonstrate that p-tau217 also predicts PD-MCI in iRBD.

Interestingly, serum p-tau217 levels even associate with the presence of excessive daytime sleepiness, which was previously reported to correlate with tau pathology in AD.[312] Thus, greater subjective daytime sleepiness in iRBD may be a harbinger of progression to dementia. Although the optimal p-tau species in prodromal α-synucleinopathies will require *vis-à-vis* comparisons in longitudinal cohorts, p-tau217 is known to exhibit superior specificity compared to p-tau181, at least in prodromal AD.[299]

Given the established interplay between tau and Aβ in AD, the inclusion of Aβ biomarkers may further refine risk stratification in iRBD. Plasma Aβ42/40 ratio has demonstrated utility in identifying early Aβ pathology and may serve as a complementary marker to p-tau217 in capturing mixed pathology or incipient AD-type co-pathology in prodromal synucleinopathies.[296] Integrating Aβ into a multimodal biomarker panel could therefore help distinguish iRBD individuals more likely to develop DLB rather than PD.

6.5.3 Serum NfL identifies rapidly progressive iRBD trajectories

Despite the promise of serum NfL in prodromal AD,[301] this biomarker was neither increased in iRBD participants with MCI, nor did it predict phenoconversion to DLB or PD-MCI. It is noteworthy that serum p-tau217 and NfL levels did not correlate, suggesting that tau pathology may not be the main driver of neurodegeneration in iRBD, as reflected by serum NfL levels. Although limited by numbers, these data suggest that markedly elevated NfL levels in iRBD most likely signify progression to MSA, which is consistent with prior findings of increased NfL levels in clinically diagnosed MSA cases.[303] Thus, NfL measurements in iRBD could be most useful clinically as a prognostic indicator in this context. The observed association between olfactory dysfunction and lower NfL levels requires further investigation, but may suggest that hyposmic iRBD individuals represent a disease subtype that is associated with less neuronal degeneration.

6.5.4 Limitations and Future Directions

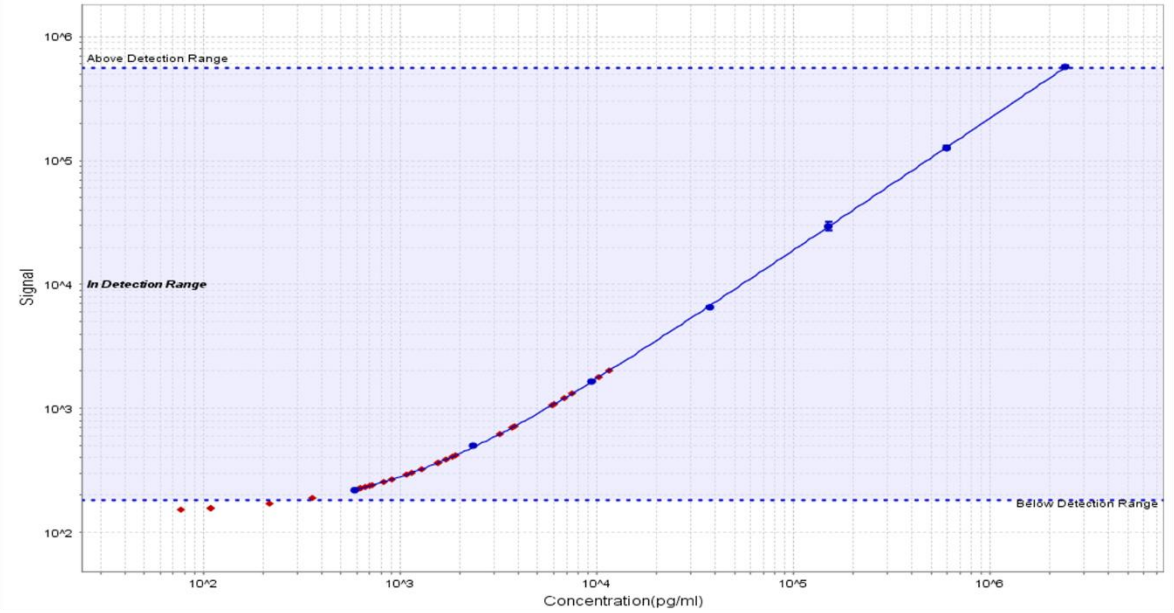
Several limitations of this study warrant consideration. First, phenoconversion is based on clinical diagnosis without neuropathological examination, and it is possible that some of these diagnoses might be incorrect. Second, although this is the largest iRBD group for p-tau blood biomarker assessment to date, the number of individuals who phenoconverted was relatively small, which may preclude definitive estimation of sensitivity and specificity. Third, where such data were available, most iRBD participants self-identified as white, and this work was underpowered to test differences across racial or ethnic groups.

6.5.5 Conclusion

In conclusion, these findings identify serum p-tau217 as a prognostic indicator for cognitive impairment in iRBD and a potential stratification biomarker when designing clinical trials for precision disease-modifying therapies in this condition. Validation of these results in

longitudinal cohorts incorporating additional co-pathology biomarkers, will provide deeper insights into the temporal dynamics of pathological trajectories relative to clinical progression.

6.6 Supplementary information



P-tau217 (fg/mL)	Signal 1	Signal 2	Signal mean	CV	% Recovery mean	Calculated concentration mean (fg/mL)	Calculated concentration CV
2400000	564292	575538	569915	1.40	101.66	2439951	1.31
600000	128993	122931	125962	3.40	98.74	592416.4	3.19
150000	31107	27727	29417	8.12	100.77	151150.1	7.65
37500	6550	6556	6556	0.12	97.21	36455.6	0.11
9375	1642	1660	1651	0.77	100.19	9392.6	0.79
2343.75	496	508	502	1.69	104.27	2443.7	2.22
585.9375	218	221	220	0.97	96.96	568.1	2.63
0	139	149	144	4.91	NA	NA	NA

Figure S6.1: Validation of the MSD p-tau217 assay. The calibration curve and dynamic range are shown for the MSD p-tau217 assay. Dynamic range: 295-2400000 fg/mL, limit of detection: 295 fg/mL.

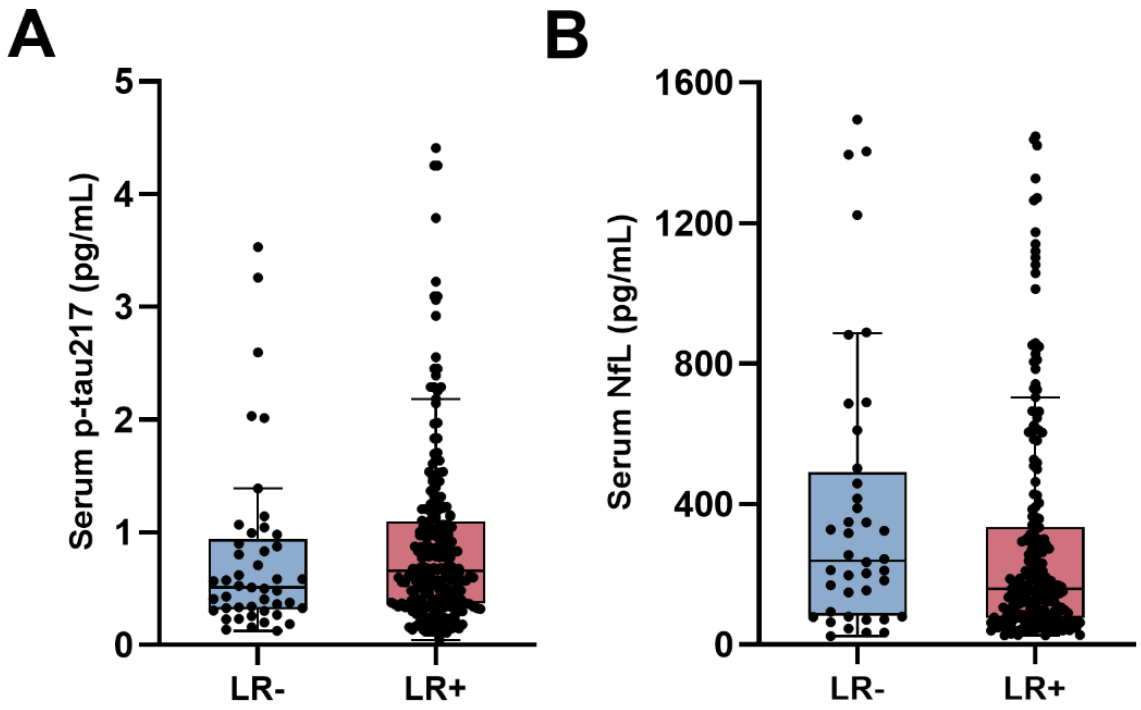


Figure S6.2: Serum p-tau217 and NfL levels in iRBD stratified by likelihood ratio of prodromal PD. (**A**) Boxplot of p-tau217 and (**B**) NfL measurements in iRBD subjects with a positive likelihood ratio (i.e. ≥ 80% probability of prodromal PD; LR+; *n* = 250) or negative likelihood ratio (i.e. < 80% probability of prodromal PD; LR-; *n* = 50) of prodromal PD, based on the updated Movement Disorder Society prodromal research criteria. Boxes represent the interquartile range from the 25th to 75th percentiles, the midline indicates the median, and whiskers and outliers are plotted using the Tukey method. Statistical comparisons were performed using the Mann-Whitney U test.

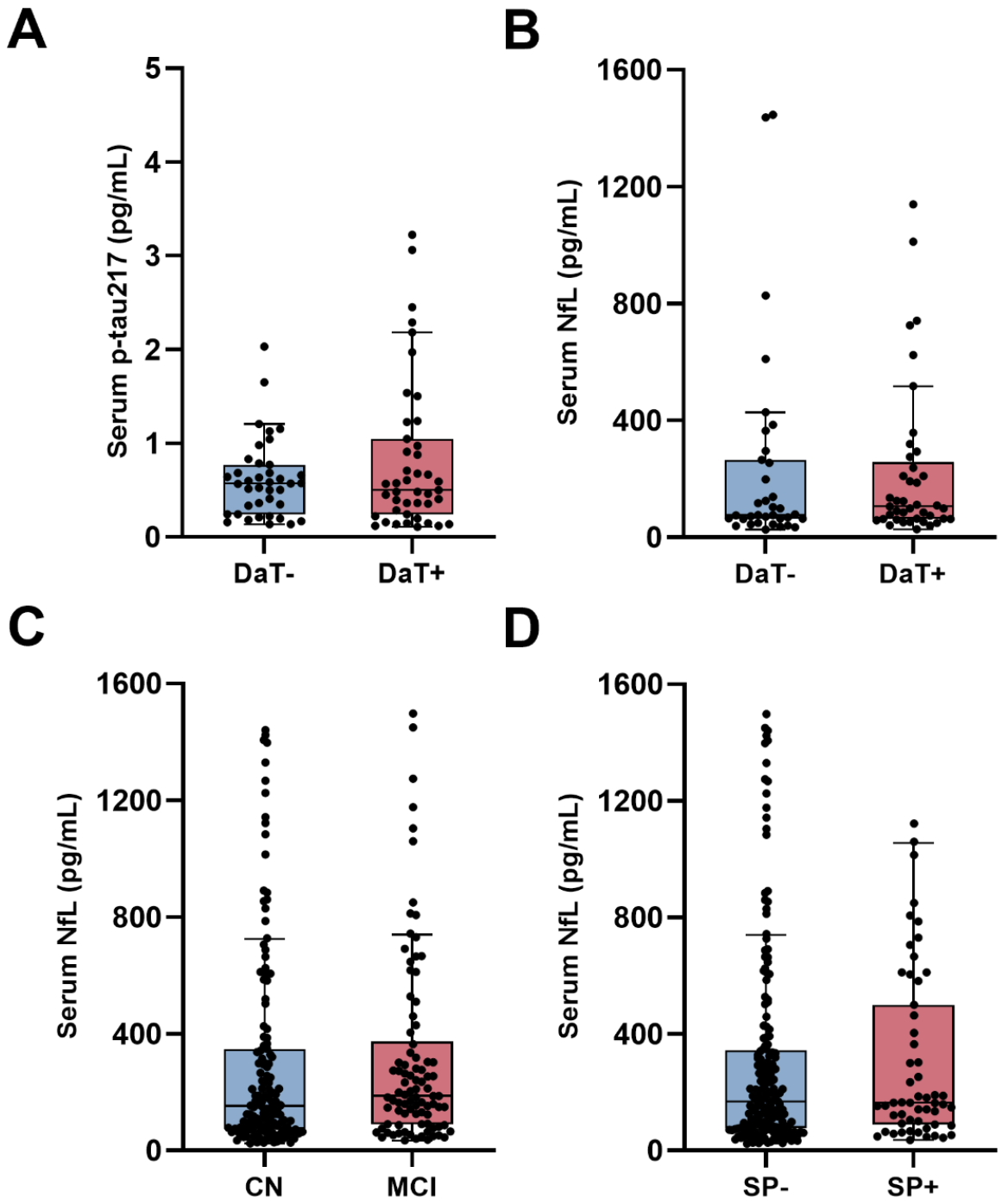


Figure S6.3: Serum p-tau217 and NfL levels in iRBD with additional prodromal marker. (**A**) Boxplot of p-tau217 and (**B**) NfL measurements in iRBD subjects with a negative/normal (DaT-; *n* = 42) or positive/abnormal (DaT+; *n* = 47) DAT SPECT. (**C**) Boxplot of NfL measurements in iRBD subjects with normal cognition (CN; *n* = 176) or mild cognitive impairment (MCI; *n* = 114). (**D**) Boxplot of NfL levels in iRBD individuals with (SP+; *n* = 66) or without (SP-; *n* = 227) subthreshold parkinsonism (SP), defined as MDS-UPDRS-III > 6 excluding postural and action tremor. Boxes represent the interquartile range from the 25th to 75th percentiles, the midline indicates the median, and whiskers and outliers are plotted using the Tukey method. Statistical comparisons were performed using the Mann-Whitney U test.

	CN vs MCI	SP- vs SP+
AUC (95% CI)	0.70 (0.64 – 0.76)	0.60 (0.52 – 0.68)
Optimal threshold (pg/mL)[a]	0.78	0.94
Sensitivity (95% CI)	0.62 (0.52 – 0.70)	0.48 (0.37 – 0.60)
Specificity (95% CI)	0.72 (0.65 – 0.79)	0.73 (0.66 – 0.78)

Table S6.1: ROC analyses of p-tau217 in the iRBD subgroup comparisons. Abbreviations: AUC = area under the receiver operating characteristic curve; MCI = mild cognitive impairment; CN = cognitively normal; SP = subthreshold parkinsonism.

[a] Optimal threshold was determined by the Youden's index for each comparison and the respective sensitivity and specificity were reported.

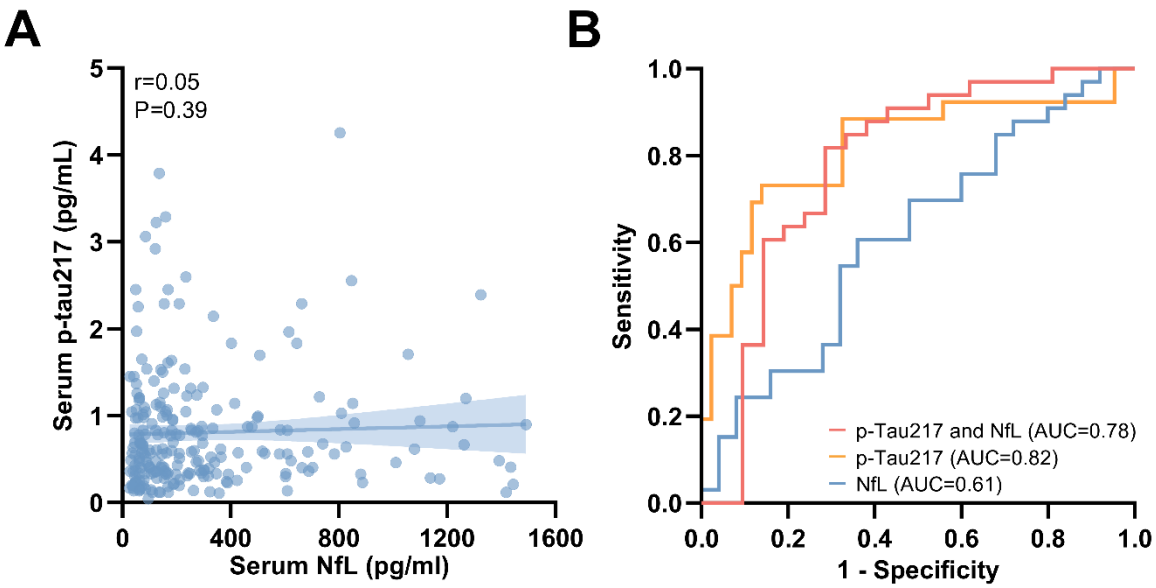


Figure S6.4: Correlation between serum p-tau217 and NfL levels, and logistic regression analysis of their performance in distinguishing phenoconversion to PD-MCI or DLB from PD with normal cognition. (**A**) Scatter plot showing no significant partial correlation between serum p-tau217 and NfL levels, adjusted for age and sex. (**B**) Logistic regression analysis controlling for age and sex, assessing the performance of p-tau217, NfL, and their combination in distinguishing individuals who phenoconverted to PD-MCI or DLB from PD with normal cognition. Least squares regression line with 95% CI is shown. Pearson correlation coefficient and corresponding P value are reported.

Variable	HR (95% CI)	P-value	N (obs)	N (events)
p-tau217 (pg/mL)	1.92 (1.47 - 2.51)	2.04×10^{-6}	234	42
NfL (10 pg/mL)	1.00 (0.98 – 1.01)	0.56	210	32

Table S6.2: Cox regression for time to phenoconversion to PD-MCI or DLB. Cox proportional hazards models were fitted for each marker and adjusted for age and sex. The hazard ratios for reflect the increase in phenoconversion risk associated with a 1 pg/mL in p-tau217 and a 10 pg/mL increase in NfL, respectively. Abbreviations: HR = hazard ratio; obs = observations.

Variable	HR (95% CI)	P-value
p-tau217 (pg/mL)	2.12 (1.43 – 3.13)	0.0002
NfL (10 pg/mL)	0.99 (0.98 - 1.01)	0.45

Table S6.3: Mutually adjusted Cox regression for time to phenoconversion to PD-MCI or DLB. Cox proportional hazards models were fitted including both serum p-tau217 and NfL as covariates, mutually adjusted and additionally controlled for age and sex. Model was fitted to n = 194 observations including 32 cases who phenoconverted to PD-MCI or DLB. Abbreviations: HR = hazard ratio.

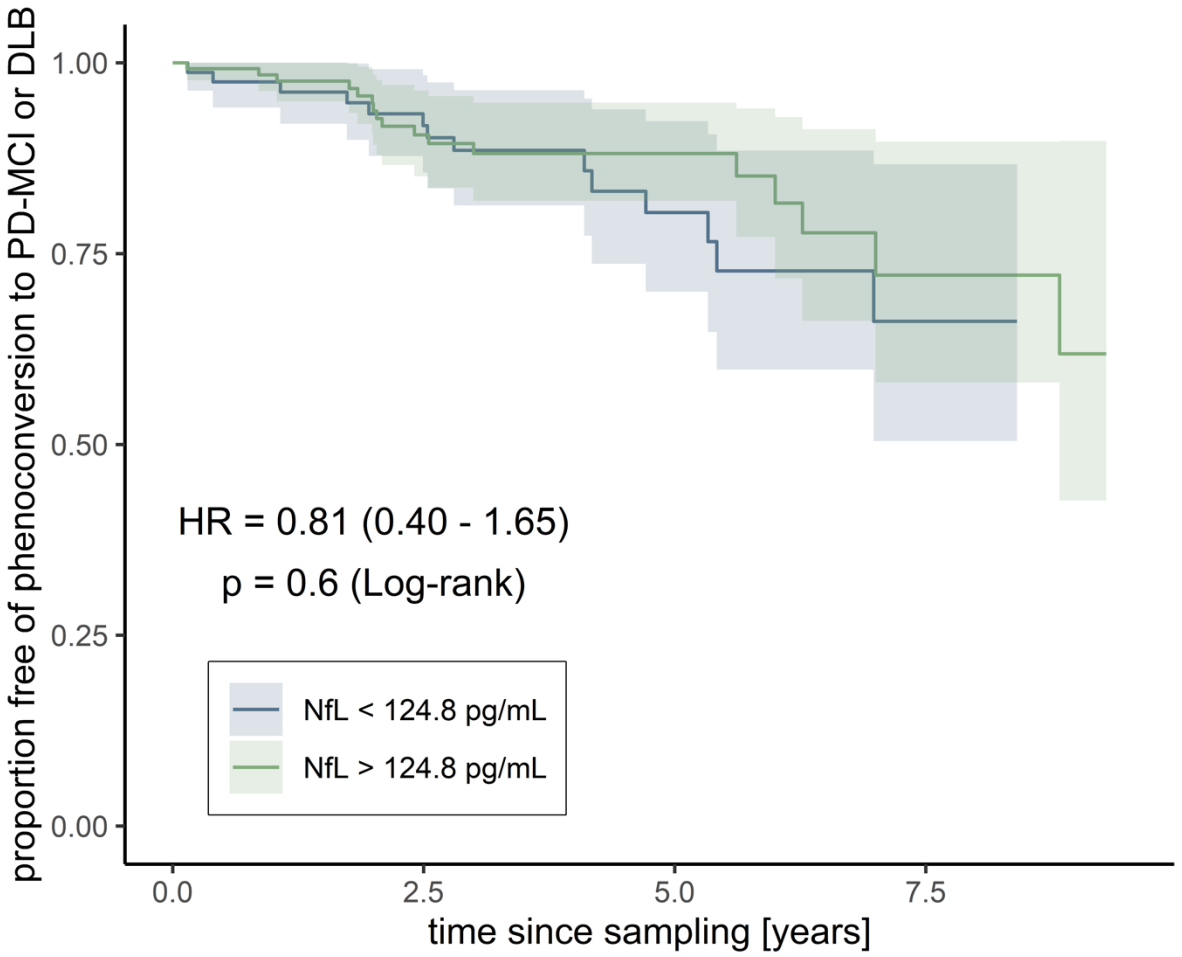


Figure S6.5: Kaplan-Meier survival curves for phenoconversion to PD-MCI or DLB with subjects stratified by NfL. Individuals stratified by NfL levels above or below the optimal threshold (124.8 pg/mL), as determined by the Youden's index for differentiating iRBD individuals with and without MCI. The reference group included iRBD individuals who did not phenoconvert and who phenoconverted to other diagnoses. Hazard ratio (HR) with 95% CI was derived from univariable Cox regression models with patient group as a binary variable. See also **Table S6.2**.

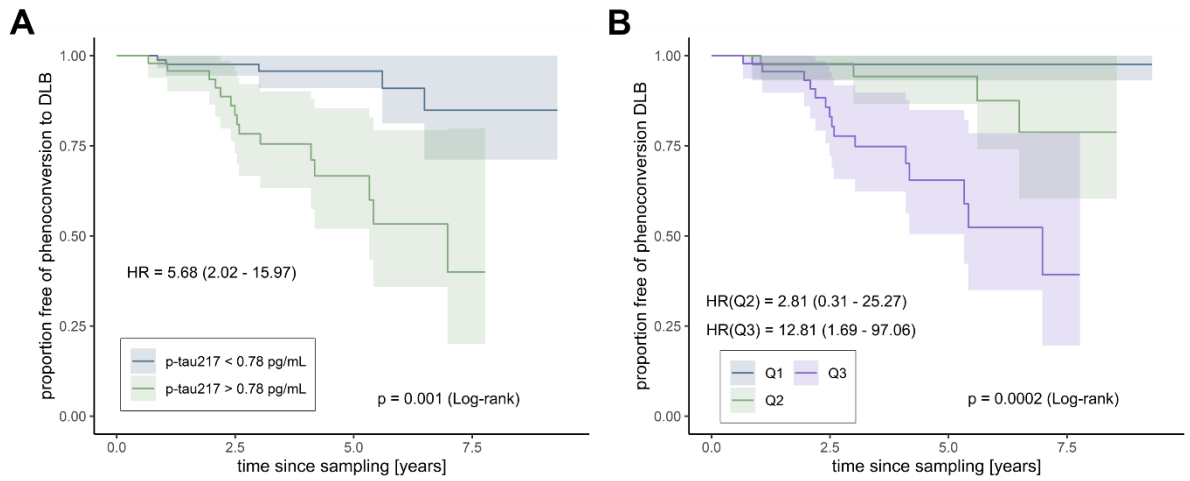


Figure S6.6: Kaplan-Meier survival curves for phenoconversion to DLB with subjects stratified by p-tau217 using non-phenoconverters without MCI as the reference group. (**A**) Individuals stratified by p-tau217 levels above or below the optimal threshold (0.78 pg/mL) for differentiating iRBD individuals with and without MCI. (**B**) Individuals stratified by p-tau217 tertiles (Q1: < 0.405, Q2: 0.405 – 0.810, Q3: > 0.810). Hazard ratios (HR) with 95% CI were derived from univariable Cox regression models, with patient group as a binary variable (panel **A**) or factor variable with 3 levels (panel **B**).

Chapter 7

Discussion and conclusions

7. Discussion and conclusions

7.1 Summary of key findings

This thesis advances the identification and characterisation of serum L1EV as a source of biomarkers for PD and related α-synucleinopathies. By integrating rigorous EV isolation methods with high-resolution analytical techniques and cross-cohort clinical validation, the work refines both the biological and technical framework for the blood-based early diagnosis of α-synucleinopathies.

A fundamental step was the establishment of Capto Core multimodal chromatography as a reliable method for isolating serum EVs with minimal contamination from soluble proteins, alongside the validation of L1CAM as a robust EV marker. The purity of EV fractions enriched by Capto Core multimodal chromatography provided a clean analytical background for the specific assessment of EV-associated targets. This was particularly important in the context of α-synuclein biomarkers, as the majority of which are predominantly found in soluble form in serum, with only a small fraction associated with EVs. Quantitative characterisation confirmed that L1EVs comprise a small but distinct subset of serum EVs, accounting for approximately 8% of the total, and that their α-synuclein content represents a measurable and biologically meaningful fraction of EV-associated α-synuclein.

Across multiple independent cohorts, elevated levels of L1EV α-synuclein were consistently observed in individuals at high risk of developing PD, including those with iRBD, hyposmia, and *GBA1*^{N409S} gene mutation. This increase was detected even in the absence of nigrostriatal deficits on DaT SPECT, suggesting that alterations in α-synuclein trafficking may precede dopaminergic degeneration. Importantly, correlations between the biomarker and other disease-relevant parameters, including cognitive deficit, CSF α-synuclein SAA positivity, and

eventual phenoconversion, support its potential utility in risk stratification and early pathological detection.

To overcome the limitations of bulk EV analysis, a droplet-based microfluidic immunoassay was developed. This platform enabled multiplexed quantification of EV membrane proteins, including α-synuclein, at single-vesicle resolution, using minimal sample volumes (as low as 3 μL). The increase of membrane-associated α-synuclein in L1EVs under pathological conditions, validated by dSTORM imaging and supported by findings in cells expressing PD-linked mutants and iPSC-derived neurons, suggested that this membrane association may reflect a functionally relevant conformation of the protein. Importantly, this readout achieved strong diagnostic performance, with AUCs > 0.9 in both prodromal and clinical PD cohorts, suggesting its utility as an early-stage biomarker.

Complementary analyses of serum p-tau217 and NfL further expanded the biomarker landscape in iRBD. Serum p-tau217, but not NfL, was significantly associated with cognitive impairment and predicted phenoconversion to PD-MCI or DLB. Elevated p-tau217 levels correlated inversely with MoCA scores and positively with prodromal features such as subthreshold parkinsonism and excessive daytime sleepiness, implicating early tauopathy in cognitive vulnerability. Although NfL levels were notably increased in individuals converting to MSA, they did not correlate with cognitive decline or enhance prediction of PD-MCI or DLB. These findings support a model in which stage-specific biomarkers, particularly serum p-tau217, improve risk stratification by capturing tau co-pathology early in the disease course.

7.2 Broader implications and applications

The findings presented in this thesis highlight the diagnostic and mechanistic relevance of L1EV-associated α-synuclein as a biomarker of preclinical PD, and demonstrate the technical feasibility of deploying single-EV assays within scalable, clinically relevant

frameworks. The detection of both total and membrane-associated α-synuclein in serum nEVs provides a peripheral readout of central synucleinopathy, offering an alternative or complement to more invasive or resource-intensive measures such as CSF SAA or DaT SPECT.

The ability of L1EV α-synuclein to stratify high-risk individuals provides a compelling rationale for its use in early-phase clinical trials. Importantly, it can identify patients prior to dopaminergic neurodegeneration and clinical presentations, allowing for targeted enrolment in clinical trials for disease-modifying therapies targeting α-synuclein, including antisense oligonucleotides and immunotherapies.[313] In this context, L1EV α-synuclein could serve both as a screening tool and as a pharmacodynamic marker for target engagement.

The droplet-based assay redefines EV biomarker detection by resolving rare neuronal subpopulations with high sensitivity and clinical practicality. Its ability to quantify EV membrane-associated proteins from minimal sample volumes could catalyse the development of multi-parametric diagnostic panels, not only in PD but also in other conditions where EVs can serve as biomarkers.

Beyond diagnosis, these findings offer mechanistic value. The inverse correlation between L1EV and CSF α-synuclein in phenoconverters supports a lysosome-linked clearance pathway, likely reflecting an adaptive EV-mediated efflux of toxic proteins. This suggests that EV-associated export could represent a protective mechanism in early disease, with membrane-associated α-synuclein acting not merely as a by-product but as an indicator of altered protein trafficking. Further investigation into EV biogenesis under lysosomal stress could reveal therapeutic targets for modulating α-synuclein release.

Finally, the association of serum p-tau217 with cognitive decline and its predictive value for phenoconversion to MCI- or dementia-related synucleinopathies underscores the relevance of AD-type co-pathology in iRBD. These findings suggest that p-tau217 may reflect a critical inflection point where tau-driven cortical dysfunction emerges independently or in

synergy with α-synuclein pathology. Notably, individuals in the top quartile of p-tau217 exhibited an 8-fold increased risk of developing PD-MCI or DLB, highlighting its translational utility as a staging biomarker for stratifying phenoconversion risk. Although NfL lacked specificity, its marked elevation in MSA phenoconverters indicates potential utility in distinguishing divergent phenoconversion trajectories. Collectively, these biomarkers offer a foundation for precision diagnostics by integrating tau, NfL and α-synuclein signatures in prodromal stratification of synucleinopathies.

7.3 Future prospects for clinical translation

The clinical translation of L1EV-based biomarkers will require coordinated advances across methodological standardisation, technological scalability, and population-level validation. Although the microfluidic assay developed in this thesis offers a compelling proof of concept, the next step involves adapting the system to a high-throughput, regulatory-compliant format compatible with routine diagnostics. This will require improvements in chip design, EV isolation, and automation, enabling widespread deployment across clinical and research settings. These efforts could ultimately yield portable, point-of-care devices that allow low-cost, rapid, and decentralised screening for prodromal PD and related disorders.

A critical milestone will be the establishment of standardised workflows for sample collection, EV isolation, and assay calibration. Current variability in protocols such as centrifugation speed, clotting time, and storage conditions, limits reproducibility and hampers biomarker comparability across studies.[314] Collaborative guidelines, such as those proposed by ISEV, may serve as a framework, but broader adoption and context-specific adaptation will be required for establishing cross-laboratory consensus.[75,82]

Parallel to standardisation, expansion of assay scope is necessary. The integration of L1EV α-synuclein with broader clinical, imaging, and genetic data holds promise for

enhancing risk stratification. Incorporating such biomarkers into digital health records or trial eligibility algorithms may enable staging systems to evolve from static thresholds to dynamic, multi-parameter decision tools.

Furthermore, while assays employed in this thesis mainly focus on the total α-synuclein, pathogenic conformers (e.g. oligomers, fibrils) detectable using conformation-specific antibodies, such as A17183 and 5G4 used in Chapter 5, may offer greater specificity. Future assay development could integrate multiplexed detection of additional disease-relevant proteins, such as inflammatory cytokines and lysosomal enzymes, offering a broader and more dynamic picture of disease biology. Such panels may be especially useful in identifying mechanistic subtypes of PD or distinguishing cognitive from motor-dominant trajectories. Combined with EV proteomics, lipidomics, or miRNA profiling, this approach could enable a systems-level view of disease progression grounded in cell-type-specific biology.

Longitudinal studies will be critical for refining biomarker thresholds for risk stratification and treatment response. In particular, time-resolved profiling of L1EV α-synuclein and its relation to phenoconversion milestones, such as motor symptom onset or cognitive decline, will help clarify its temporal dynamics and prognostic scope. Parallel evaluation of assay performance across diverse ethnic and clinical subgroups will be equally important in supporting broader application.

Looking forward, the integration of L1EV-based assays into prospective stratified trial designs will be essential. Partnerships with diagnostic companies could accelerate the development of standardised, cost-effective kits for clinical deployment. This will not only help establish temporal validity and biological consistency but also enable benchmarking against existing standards of care. In doing so, EV-based diagnostics may contribute to reshape PD management, shifting from late-stage clinical reaction to preclinical intervention guided by dynamic, peripheral molecular cues.

7.4 Concluding remarks

This thesis demonstrates that serum L1EV-associated α-synuclein, holds considerable promise as a biomarker for early PD detection. The integration of nEV isolation with the advanced high-resolution droplet-based microfluidic platform described in this thesis has enhanced diagnostic sensitivity while offering mechanistic insight into α-synuclein dysregulation. Collectively, these advances support new approaches to disease stratification, biomarker-guided trial design, and longitudinal monitoring, marking a potential shift from symptom-based diagnosis to molecularly defined, pre-symptomatic detection.

Although challenges remain in standardisation, clinical validation, and commercialisation, the work described herein establishes a foundation for the clinical implementation of EV-based diagnostics in neurodegeneration, providing both technical rigour and biological relevance. Future efforts should prioritise the refinement and validation of these biomarkers to enable accessible, reproducible, and cost-effective tools capable of informing therapeutic pathways and improving outcomes for individuals at risk of PD and beyond.

References

8. References

1. Dorsey ER, Sherer T, Okun MS, Bloem BR. The emerging evidence of the Parkinson pandemic. *J Parkinsons Dis*. 2018;8:S3-S8.
2. Kowal SL, Dall TM, Chakrabarti R, Storm MV, Jain A. The current and projected economic burden of Parkinson's disease in the United States. *Mov Disord*. 2013;28:311-318.
3. Pringsheim T, Jette N, Frolkis A, Steeves TD. The prevalence of Parkinson's disease: a systematic review and meta-analysis. *Mov Disord*. 2014;29:1583-1590.
4. Rajan R, Holla VV, Kamble N, Yadav R, Pal PK. Genetic heterogeneity of early onset Parkinson disease: The dilemma of clinico-genetic correlation. *Parkinsonism Relat Disord*. 2024;129:107146.
5. Blauwendraat C, Nalls MA, Singleton AB. The genetic architecture of Parkinson's disease. *Lancet Neurol*. 2020;19:170-178.
6. Collaborators GBDPsD. Global, regional, and national burden of Parkinson's disease, 1990-2016: a systematic analysis for the Global Burden of Disease Study 2016. *Lancet Neurol*. 2018;17:939-953.
7. Wright Willis A, Evanoff BA, Lian M, Criswell SR, Racette BA. Geographic and ethnic variation in Parkinson disease: a population-based study of US Medicare beneficiaries. *Neuroepidemiology*. 2010;34:143-151.
8. Lesage S, Dürr A, Tazir M, *et al*. LRRK2 G2019S as a cause of Parkinson's disease in North African Arabs. *N Engl J Med*. 2006;354:422-423.
9. Ozelius LJ, Senthil G, Saunders-Pullman R, *et al*. LRRK2 G2019S as a cause of Parkinson's disease in Ashkenazi Jews. *N Engl J Med*. 2006;354:424-425.
10. Aharon-Peretz J, Rosenbaum H, Gershoni-Baruch R. Mutations in the glucocerebrosidase gene and Parkinson's disease in Ashkenazi Jews. *N Engl J Med*. 2004;351:1972-1977.
11. Smith KM, Dahodwala N. Sex differences in Parkinson's disease and other movement disorders. *Exp Neurol*. 2014;259:44-56.
12. Dorsey ER, Zafar M, Lettenberger SE, *et al*. Trichloroethylene: An invisible cause of Parkinson’s disease? *J Parkinsons Dis*. 2023;13:203-218.
13. Guilarte TR. Manganese and Parkinson’s disease: a critical review and new findings. *Environ Health Perspect*. 2010;118:1071-1080.
14. Currie LJ, Harrison MB, Trugman JM, Bennett JP, Wooten GF. Postmenopausal estrogen use affects risk for Parkinson disease. *Arch Neurol*. 2004;61:886-888.
15. Chen J-F, Schwarzschild MA. Do caffeine and more selective adenosine A2A receptor antagonists protect against dopaminergic neurodegeneration in Parkinson's disease? *Parkinsonism Relat Disord*. 2020;80:S45-S53.
16. Grandinetti A, Morens DM, Reed D, MacEachern D. Prospective study of cigarette smoking and the risk of developing idiopathic Parkinson's disease. *Am J Epidemiol*. 1994;139:1129-38.
17. Spillantini MG, Schmidt ML, Lee VM-Y, Trojanowski JQ, Jakes R, Goedert M. α-Synuclein in Lewy bodies. *Nature*. 1997;388:839-840.
18. Braak H, Del Tredici K, Rüb U, De Vos RA, Steur ENJ, Braak E. Staging of brain pathology related to sporadic Parkinson’s disease. *Neurobiol Aging*. 2003;24:197-211.
19. Dickson DW, Fujishiro H, Orr C, *et al*. Neuropathology of non-motor features of Parkinson disease. *Parkinsonism Relat Disord*. 2009;15:S1-S5.
20. Horsager J, Andersen KB, Knudsen K, *et al*. Brain-first versus body-first Parkinson's disease: a multimodal imaging case-control study. *Brain*. 2020;143:3077-3088.

21. Lashuel HA, Overk CR, Oueslati A, Masliah E. The many faces of α-synuclein: from structure and toxicity to therapeutic target. *Nat Rev Neurosci*. 2013;14:38-48.
22. Masuda-Suzukake M, Nonaka T, Hosokawa M, *et al*. Prion-like spreading of pathological alpha-synuclein in brain. *Brain*. 2013;136:1128-38.
23. Ngolab J, Trinh I, Rockenstein E, *et al*. Brain-derived exosomes from dementia with Lewy bodies propagate alpha-synuclein pathology. *Acta Neuropathol Commun*. 2017;5:46.
24. Guo JL, Lee VM. Cell-to-cell transmission of pathogenic proteins in neurodegenerative diseases. *Nat Med*. 2014;20:130-8.
25. Ostrerova-Golts N, Petrucelli L, Hardy J, Lee JM, Farer M, Wolozin B. The A53T alpha-synuclein mutation increases iron-dependent aggregation and toxicity. *J Neurosci*. 2000;20:6048-54.
26. Lemkau LR, Comellas G, Kloepper KD, Woods WS, George JM, Rienstra CM. Mutant protein A30P alpha-synuclein adopts wild-type fibril structure, despite slower fibrillation kinetics. *J Biol Chem*. 2012;287:11526-32.
27. Lashuel HA, Petre BM, Wall J, *et al*. Alpha-synuclein, especially the Parkinson's disease-associated mutants, forms pore-like annular and tubular protofibrils. *J Mol Biol*. 2002;322:1089-102.
28. Burre J, Sharma M, Tsetsenis T, Buchman V, Etherton MR, Sudhof TC. Alpha-synuclein promotes SNARE-complex assembly in vivo and in vitro. *Science*. 2010;329:1663-7.
29. Anderson JP, Walker DE, Goldstein JM, *et al*. Phosphorylation of Ser-129 is the dominant pathological modification of alpha-synuclein in familial and sporadic Lewy body disease. *J Biol Chem*. 2006;281:29739-52.
30. Ma MR, Hu ZW, Zhao YF, Chen YX, Li YM. Phosphorylation induces distinct alpha-synuclein strain formation. *Sci Rep*. 2016;6:37130.
31. Zenko D, Marsh J, Castle AR, Lewin R, Fischer R, Tofaris GK. Monitoring alpha-synuclein ubiquitination dynamics reveals key endosomal effectors mediating its trafficking and degradation. *Sci Adv*. 2023;9:eadd8910.
32. Pedersen CC, Maple-Grodem J, Lange J. A systematic review of biofluid phosphorylated alpha-synuclein in Parkinson's disease. *Parkinsonism Relat Disord*. 2025;132:107240.
33. Wallace JN, Crockford ZC, Roman-Vendrell C, *et al*. Excess phosphoserine-129 alpha-synuclein induces synaptic vesicle trafficking and declustering defects at a vertebrate synapse. *Mol Biol Cell*. 2024;35:ar10.
34. Hara S, Arawaka S, Sato H, *et al*. Serine 129 phosphorylation of membrane-associated alpha-synuclein modulates dopamine transporter function in a G protein-coupled receptor kinase-dependent manner. *Mol Biol Cell*. 2013;24:1649-60, S1-3.
35. Henrich MT, Oertel WH, Surmeier DJ, Geibl FF. Mitochondrial dysfunction in Parkinson's disease - a key disease hallmark with therapeutic potential. *Mol Neurodegener*. 2023;18:83.
36. Kitada T, Asakawa S, Hattori N, *et al*. Mutations in the parkin gene cause autosomal recessive juvenile parkinsonism. *Nature*. 1998;392:605-608.
37. Morais VA, Verstreken P, Roethig A, *et al*. Parkinson's disease mutations in PINK1 result in decreased Complex I activity and deficient synaptic function. *EMBO Mol Med*. 2009;1:99-111.
38. Xiao B, Goh J-Y, Xiao L, Xian H, Lim K-L, Liou Y-C. Reactive oxygen species trigger Parkin/PINK1 pathway–dependent mitophagy by inducing mitochondrial recruitment of Parkin. *J Biol Chem*. 2017;292:16697-16708.

39. Betarbet R, Sherer TB, MacKenzie G, Garcia-Osuna M, Panov AV, Greenamyre JT. Chronic systemic pesticide exposure reproduces features of Parkinson's disease. *Nat Neurosci*. 2000;3:1301-1306.
40. Gordon R, Albornoz EA, Christie DC, *et al*. Inflammasome inhibition prevents alpha-synuclein pathology and dopaminergic neurodegeneration in mice. *Sci Transl Med*. 2018;10:
41. Fan Z, Pan Y-T, Zhang Z-Y, *et al*. Systemic activation of NLRP3 inflammasome and plasma α-synuclein levels are correlated with motor severity and progression in Parkinson's disease. *Journal of neuroinflammation*. 2020;17:1-10.
42. Liddelow SA, Guttenplan KA, Clarke LE, *et al*. Neurotoxic reactive astrocytes are induced by activated microglia. *Nature*. 2017;541:481-487.
43. Tansey MG, Goldberg MS. Neuroinflammation in Parkinson's disease: its role in neuronal death and implications for therapeutic intervention. *Neurobiology of disease*. 2010;37:510-518.
44. Devi L, Raghavendran V, Prabhu BM, Avadhani NG, Anandatheerthavarada HK. Mitochondrial import and accumulation of α-synuclein impair complex I in human dopaminergic neuronal cultures and Parkinson disease brain. *J Biol Chem*. 2008;283:9089-9100.
45. Braak H, Ghebremedhin E, Rüb U, Bratzke H, Del Tredici K. Stages in the development of Parkinson's disease-related pathology. *Cell Tissue Res*. 2004;318:121-134.
46. Braak H, Rüb U, Gai W, Del Tredici K. Idiopathic Parkinson's disease: possible routes by which vulnerable neuronal types may be subject to neuroinvasion by an unknown pathogen. *J Neural Transm*. 2003;110:517-536.
47. Burke RE, Dauer WT, Vonsattel JPG. A critical evaluation of the Braak staging scheme for Parkinson's disease. *Ann Neurol*. 2008;64:485-491.
48. Braak H, Rüb U, Del Tredici K. Cognitive decline correlates with neuropathological stage in Parkinson's disease. *J Neurol Sci*. 2006;248:255-258.
49. Bologna M, Paparella G, Fasano A, Hallett M, Berardelli A. Evolving concepts on bradykinesia. *Brain*. 2020;143:727-750.
50. Berg D, Adler CH, Bloem BR, *et al*. Movement disorder society criteria for clinically established early Parkinson's disease. *Mov Disord*. 2018;33:1643-1646.
51. Chen W, Hopfner F, Becktepe JS, Deuschl G. Rest tremor revisited: Parkinson's disease and other disorders. *Transl Neurodegener*. 2017;6:1-8.
52. Pantall A, Suresparan P, Kapa L, *et al*. Postural dynamics are associated with cognitive decline in Parkinson's disease. *Front Neurol*. 2018;9:1044.
53. Schapira AH, Chaudhuri KR, Jenner P. Non-motor features of Parkinson disease. *Nat Rev Neurosci*. 2017;18:435-450.
54. Postuma RB, Iranzo A, Hu M, *et al*. Risk and predictors of dementia and parkinsonism in idiopathic REM sleep behaviour disorder: a multicentre study. *Brain*. 2019;142:744-759.
55. Cersosimo MG, Benarroch EE. Autonomic involvement in Parkinson's disease: pathology, pathophysiology, clinical features and possible peripheral biomarkers. *J Neurol Sci*. 2012;313:57-63.
56. Politis M, Wu K, Loane C, *et al*. Depressive symptoms in PD correlate with higher 5-HTT binding in raphe and limbic structures. *Neurology*. 2010;75:1920-7.
57. Compta Y, Parkkinen L, O'Sullivan SS, *et al*. Lewy- and Alzheimer-type pathologies in Parkinson's disease dementia: which is more important? *Brain*. 2011;134:1493-1505.
58. Berg D, Postuma RB, Adler CH, *et al*. MDS research criteria for prodromal Parkinson's disease. *Mov Disord*. 2015;30:1600-11.
59. Heinzel S, Berg D, Gasser T, *et al*. Update of the MDS research criteria for prodromal Parkinson's disease. *Mov Disord*. 2019;34:1464-1470.

60. Sidransky E, Nalls MA, Aasly JO, *et al*. Multicenter analysis of glucocerebrosidase mutations in Parkinson's disease. *N Engl J Med*. 2009;361:1651-61.
61. Nalls MA, Blauwendraat C, Vallerga CL, *et al*. Identification of novel risk loci, causal insights, and heritable risk for Parkinson's disease: a meta-analysis of genome-wide association studies. *Lancet Neurol*. 2019;18:1091-1102.
62. Paul KC, Krolewski RC, Lucumi Moreno E, *et al*. A pesticide and iPSC dopaminergic neuron screen identifies and classifies Parkinson-relevant pesticides. *Nat Commun*. 2023;14:2803.
63. Ross GW, Petrovitch H, Abbott RD, *et al*. Association of olfactory dysfunction with risk for future Parkinson's disease. *Ann Neurol*. 2008;63:167-73.
64. Goetz CG, Tilley BC, Shaftman SR, *et al*. Movement Disorder Society-sponsored revision of the Unified Parkinson's Disease Rating Scale (MDS-UPDRS): scale presentation and clinimetric testing results. *Mov Disord*. 2008;23:2129-70.
65. Hinkle JT, Pontone GM. Psychomotor processing and functional decline in Parkinson's disease predicted by the Purdue Pegboard test. *Int J Geriatr Psychiatry*. 2021;36:909-916.
66. Jennings D, Siderowf A, Stern M, *et al*. Conversion to Parkinson Disease in the PARS Hyposmic and Dopamine Transporter-Deficit Prodromal Cohort. *JAMA Neurol*. 2017;74:933-940.
67. Marsili L, Rizzo G, Colosimo C. Diagnostic Criteria for Parkinson's Disease: From James Parkinson to the Concept of Prodromal Disease. *Front Neurol*. 2018;9:156.
68. Postuma RB, Berg D, Stern M, *et al*. MDS clinical diagnostic criteria for Parkinson's disease. *Mov Disord*. 2015;30:1591-601.
69. Beach TG, Adler CH. Importance of low diagnostic Accuracy for early Parkinson's disease. *Mov Disord*. 2018;33:1551-1554.
70. di Biase L, Pecoraro PM, Di Lazzaro V. Validating the Accuracy of Parkinson's Disease Clinical Diagnosis: A UK Brain Bank Case-Control Study. *Ann Neurol*. 2025;
71. Rizzo G, Copetti M, Arcuti S, Martino D, Fontana A, Logroscino G. Accuracy of clinical diagnosis of Parkinson disease: A systematic review and meta-analysis. *Neurology*. 2016;86:566-76.
72. Cheng HC, Ulane CM, Burke RE. Clinical progression in Parkinson disease and the neurobiology of axons. *Ann Neurol*. 2010;67:715-25.
73. Arora S, Baig F, Lo C, *et al*. Smartphone motor testing to distinguish idiopathic REM sleep behavior disorder, controls, and PD. *Neurology*. 2018;91:e1528-e1538.
74. Zhang J, Zhou W, Yu H, *et al*. Prediction of Parkinson's Disease Using Machine Learning Methods. *Biomolecules*. 2023;13:
75. Welsh JA, Goberdhan DCI, O'Driscoll L, *et al*. Minimal information for studies of extracellular vesicles (MISEV2023): From basic to advanced approaches. *J Extracell Vesicles*. 2024;13:e12404.
76. Emmanouilidou E, Melachroinou K, Roumeliotis T, *et al*. Cell-produced alpha-synuclein is secreted in a calcium-dependent manner by exosomes and impacts neuronal survival. *J Neurosci*. 2010;30:6838-51.
77. Colombo M, Moita C, van Niel G, *et al*. Analysis of ESCRT functions in exosome biogenesis, composition and secretion highlights the heterogeneity of extracellular vesicles. *J Cell Sci*. 2013;126:5553-65.
78. Trajkovic K, Hsu C, Chiantia S, *et al*. Ceramide triggers budding of exosome vesicles into multivesicular endosomes. *Science*. 2008;319:1244-7.
79. Atkin-Smith GK, Tixeira R, Paone S, *et al*. A novel mechanism of generating extracellular vesicles during apoptosis via a beads-on-a-string membrane structure. *Nat Commun*. 2015;6:7439.

80. Jeppesen DK, Fenix AM, Franklin JL, *et al*. Reassessment of Exosome Composition. *Cell*. 2019;177:428-445 e18.
81. Crescitelli R, Lasser C, Szabo TG, *et al*. Distinct RNA profiles in subpopulations of extracellular vesicles: apoptotic bodies, microvesicles and exosomes. *J Extracell Vesicles*. 2013;2:
82. Thery C, Witwer KW, Aikawa E, *et al*. Minimal information for studies of extracellular vesicles 2018 (MISEV2018): a position statement of the International Society for Extracellular Vesicles and update of the MISEV2014 guidelines. *J Extracell Vesicles*. 2018;7:1535750.
83. Andreu Z, Yanez-Mo M. Tetraspanins in extracellular vesicle formation and function. *Front Immunol*. 2014;5:442.
84. Kowal J, Arras G, Colombo M, *et al*. Proteomic comparison defines novel markers to characterize heterogeneous populations of extracellular vesicle subtypes. *Proc Natl Acad Sci U S A*. 2016;113:E968-77.
85. Skog J, Wurdinger T, van Rijn S, *et al*. Glioblastoma microvesicles transport RNA and proteins that promote tumour growth and provide diagnostic biomarkers. *Nat Cell Biol*. 2008;10:1470-6.
86. Thery C, Boussac M, Veron P, *et al*. Proteomic analysis of dendritic cell-derived exosomes: a secreted subcellular compartment distinct from apoptotic vesicles. *J Immunol*. 2001;166:7309-18.
87. Wang Y, Cella M, Mallinson K, *et al*. TREM2 lipid sensing sustains the microglial response in an Alzheimer's disease model. *Cell*. 2015;160:1061-71.
88. Su H, Rustam YH, Masters CL, *et al*. Characterization of brain-derived extracellular vesicle lipids in Alzheimer's disease. *J Extracell Vesicles*. 2021;10:e12089.
89. Fabbiano F, Corsi J, Gurrieri E, Trevisan C, Notarangelo M, D'Agostino VG. RNA packaging into extracellular vesicles: An orchestra of RNA-binding proteins? *J Extracell Vesicles*. 2020;10:e12043.
90. Valcz G, Ujvari B, Buzas EI, *et al*. Small extracellular vesicle DNA-mediated horizontal gene transfer as a driving force for tumor evolution: Facts and riddles. *Front Oncol*. 2022;12:945376.
91. Solana-Balaguer J, Campoy-Campos G, Martin-Flores N, *et al*. Neuron-derived extracellular vesicles contain synaptic proteins, promote spine formation, activate TrkB-mediated signalling and preserve neuronal complexity. *J Extracell Vesicles*. 2023;12:e12355.
92. Hernandez P, Rackles E, Alboniga OE, *et al*. Metabolic Profiling of Brain Tissue and Brain-Derived Extracellular Vesicles in Alzheimer's Disease. *J Extracell Vesicles*. 2025;14:e70043.
93. Yan S, Jiang C, Janzen A, *et al*. Neuronally Derived Extracellular Vesicle alpha-Synuclein as a Serum Biomarker for Individuals at Risk of Developing Parkinson Disease. *JAMA Neurol*. 2024;81:59-68.
94. Jiang C, Hopfner F, Katsikoudi A, *et al*. Serum neuronal exosomes predict and differentiate Parkinson's disease from atypical parkinsonism. *J Neurol Neurosurg Psychiatry*. 2020;91:720-729.
95. Jiang C, Hopfner F, Berg D, *et al*. Validation of alpha-Synuclein in L1CAM-Immunocaptured Exosomes as a Biomarker for the Stratification of Parkinsonian Syndromes. *Mov Disord*. 2021;36:2663-2669.
96. Hornung S, Dutta S, Bitan G. CNS-Derived Blood Exosomes as a Promising Source of Biomarkers: Opportunities and Challenges. *Front Mol Neurosci*. 2020;13:38.
97. Wang H, Moyano AL, Ma Z, *et al*. miR-219 Cooperates with miR-338 in Myelination and Promotes Myelin Repair in the CNS. *Dev Cell*. 2017;40:566-582 e5.
98. Fruhbeis C, Frohlich D, Kuo WP, *et al*. Neurotransmitter-triggered transfer of exosomes mediates oligodendrocyte-neuron communication. *PLoS Biol*. 2013;11:e1001604.

99. Zhao S, Sheng S, Wang Y, *et al*. Astrocyte-derived extracellular vesicles: A double-edged sword in central nervous system disorders. *Neurosci Biobehav Rev*. 2021;125:148-159.
100. Aires ID, Ribeiro-Rodrigues T, Boia R, *et al*. Microglial Extracellular Vesicles as Vehicles for Neurodegeneration Spreading. *Biomolecules*. 2021;11:
101. Muraoka S, DeLeo AM, Sethi MK, *et al*. Proteomic and biological profiling of extracellular vesicles from Alzheimer's disease human brain tissues. *Alzheimers Dement*. 2020;16:896-907.
102. Sardar Sinha M, Ansell-Schultz A, Civitelli L, *et al*. Alzheimer's disease pathology propagation by exosomes containing toxic amyloid-beta oligomers. *Acta Neuropathol*. 2018;136:41-56.
103. Saman S, Kim W, Raya M, *et al*. Exosome-associated tau is secreted in tauopathy models and is selectively phosphorylated in cerebrospinal fluid in early Alzheimer disease. *J Biol Chem*. 2012;287:3842-9.
104. Fiandaca MS, Kapogiannis D, Mapstone M, *et al*. Identification of preclinical Alzheimer's disease by a profile of pathogenic proteins in neurally derived blood exosomes: A case-control study. *Alzheimers Dement*. 2015;11:600-7 e1.
105. Gagliardi D, Bresolin N, Comi GP, Corti S. Extracellular vesicles and amyotrophic lateral sclerosis: from misfolded protein vehicles to promising clinical biomarkers. *Cell Mol Life Sci*. 2021;78:561-572.
106. Pasetto L, Callegaro S, Corbelli A, *et al*. Decoding distinctive features of plasma extracellular vesicles in amyotrophic lateral sclerosis. *Mol Neurodegener*. 2021;16:52.
107. Loov C, Scherzer CR, Hyman BT, Breakefield XO, Ingelsson M. alpha-Synuclein in Extracellular Vesicles: Functional Implications and Diagnostic Opportunities. *Cell Mol Neurobiol*. 2016;36:437-48.
108. Holmes BB, DeVos SL, Kfoury N, *et al*. Heparan sulfate proteoglycans mediate internalization and propagation of specific proteopathic seeds. *Proc Natl Acad Sci U S A*. 2013;110:E3138-47.
109. Hansen C, Angot E, Bergstrom AL, *et al*. alpha-Synuclein propagates from mouse brain to grafted dopaminergic neurons and seeds aggregation in cultured human cells. *J Clin Invest*. 2011;121:715-25.
110. Desplats P, Lee HJ, Bae EJ, *et al*. Inclusion formation and neuronal cell death through neuron-to-neuron transmission of alpha-synuclein. *Proc Natl Acad Sci U S A*. 2009;106:13010-5.
111. Grey M, Dunning CJ, Gaspar R, *et al*. Acceleration of alpha-synuclein aggregation by exosomes. *J Biol Chem*. 2015;290:2969-82.
112. Cerri S, Ghezzi C, Ongari G, *et al*. GBA Mutations Influence the Release and Pathological Effects of Small Extracellular Vesicles from Fibroblasts of Patients with Parkinson's Disease. *Int J Mol Sci*. 2021;22:
113. Scheiblich H, Bousset L, Schwartz S, *et al*. Microglial NLRP3 Inflammasome Activation upon TLR2 and TLR5 Ligation by Distinct alpha-Synuclein Assemblies. *J Immunol*. 2021;207:2143-2154.
114. Chi X, Yin S, Sun Y, *et al*. Astrocyte-neuron communication through the complement C3-C3aR pathway in Parkinson's disease. *Brain Behav Immun*. 2025;123:229-243.
115. Shippey LE, Campbell SG, Hill AF, Smith DP. Propagation of Parkinson's disease by extracellular vesicle production and secretion. *Biochem Soc Trans*. 2022;50:1303-1314.
116. Wang L, Zhang X, Yang Z, *et al*. Extracellular vesicles: biological mechanisms and emerging therapeutic opportunities in neurodegenerative diseases. *Transl Neurodegener*. 2024;13:60.

117. He S, Wang Q, Chen L, He YJ, Wang X, Qu S. miR-100a-5p-enriched exosomes derived from mesenchymal stem cells enhance the anti-oxidant effect in a Parkinson's disease model via regulation of Nox4/ROS/Nrf2 signaling. *J Transl Med*. 2023;21:747.
118. Narbute K, Pilipenko V, Pupure J, *et al*. Intranasal Administration of Extracellular Vesicles Derived from Human Teeth Stem Cells Improves Motor Symptoms and Normalizes Tyrosine Hydroxylase Expression in the Substantia Nigra and Striatum of the 6-Hydroxydopamine-Treated Rats. *Stem Cells Transl Med*. 2019;8:490-499.
119. Kojima R, Bojar D, Rizzi G, *et al*. Designer exosomes produced by implanted cells intracerebrally deliver therapeutic cargo for Parkinson's disease treatment. *Nat Commun*. 2018;9:1305.
120. Izco M, Blesa J, Schleef M, *et al*. Systemic Exosomal Delivery of shRNA Minicircles Prevents Parkinsonian Pathology. *Mol Ther*. 2019;27:2111-2122.
121. Li P, Kaslan M, Lee SH, Yao J, Gao Z. Progress in Exosome Isolation Techniques. *Theranostics*. 2017;7:789-804.
122. Sidhom K, Obi PO, Saleem A. A Review of Exosomal Isolation Methods: Is Size Exclusion Chromatography the Best Option? *Int J Mol Sci*. 2020;21:
123. Thery C, Amigorena S, Raposo G, Clayton A. Isolation and characterization of exosomes from cell culture supernatants and biological fluids. *Curr Protoc Cell Biol*. 2006;Chapter 3:Unit 3 22.
124. Van Deun J, Mestdagh P, Sormunen R, *et al*. The impact of disparate isolation methods for extracellular vesicles on downstream RNA profiling. *J Extracell Vesicles*. 2014;3:
125. Abramowicz A, Widlak P, Pietrowska M. Proteomic analysis of exosomal cargo: the challenge of high purity vesicle isolation. *Mol Biosyst*. 2016;12:1407-19.
126. Lobb RJ, Becker M, Wen SW, *et al*. Optimized exosome isolation protocol for cell culture supernatant and human plasma. *J Extracell Vesicles*. 2015;4:27031.
127. Witwer KW, Buzas EI, Bemis LT, *et al*. Standardization of sample collection, isolation and analysis methods in extracellular vesicle research. *J Extracell Vesicles*. 2013;2:
128. Nogueras-Ortiz CJ, Eren E, Yao P, *et al*. Single-extracellular vesicle (EV) analyses validate the use of L1 Cell Adhesion Molecule (L1CAM) as a reliable biomarker of neuron-derived EVs. *J Extracell Vesicles*. 2024;13:e12459.
129. Liangsupree T, Multia E, Riekkola ML. Modern isolation and separation techniques for extracellular vesicles. *J Chromatogr A*. 2021;1636:461773.
130. Zhao Z, Wijerathne H, Godwin AK, Soper SA. Isolation and analysis methods of extracellular vesicles (EVs). *Extracell Vesicles Circ Nucl Acids*. 2021;2:80-103.
131. Vergauwen G, Dhondt B, Van Deun J, *et al*. Confounding factors of ultrafiltration and protein analysis in extracellular vesicle research. *Sci Rep*. 2017;7:2704.
132. Boing AN, van der Pol E, Grootemaat AE, Coumans FA, Sturk A, Nieuwland R. Single-step isolation of extracellular vesicles by size-exclusion chromatography. *J Extracell Vesicles*. 2014;3:
133. Gamez-Valero A, Campdelacreu J, Vilas D, *et al*. Exploratory study on microRNA profiles from plasma-derived extracellular vesicles in Alzheimer's disease and dementia with Lewy bodies. *Transl Neurodegener*. 2019;8:31.
134. Zhang H, Freitas D, Kim HS, *et al*. Identification of distinct nanoparticles and subsets of extracellular vesicles by asymmetric flow field-flow fractionation. *Nat Cell Biol*. 2018;20:332-343.
135. Bonner SE, van de Wakker SI, Phillips W, *et al*. Scalable purification of extracellular vesicles with high yield and purity using multimodal flowthrough chromatography. *J Extracell Biol*. 2024;3:e138.

136. Kanwar SS, Dunlay CJ, Simeone DM, Nagrath S. Microfluidic device (ExoChip) for on-chip isolation, quantification and characterization of circulating exosomes. *Lab Chip*. 2014;14:1891-900.
137. Sharafeldin M, Yan S, Jiang C, Tofaris GK, Davis JJ. Alternating Magnetic Field-Promoted Nanoparticle Mixing: The On-Chip Immunocapture of Serum Neuronal Exosomes for Parkinson's Disease Diagnostics. *Anal Chem*. 2023;95:7906-7913.
138. Wunsch BH, Smith JT, Gifford SM, *et al*. Nanoscale lateral displacement arrays for the separation of exosomes and colloids down to 20 nm. *Nat Nanotechnol*. 2016;11:936-940.
139. Wu M, Ouyang Y, Wang Z, *et al*. Isolation of exosomes from whole blood by integrating acoustics and microfluidics. *Proc Natl Acad Sci U S A*. 2017;114:10584-10589.
140. Zhao Z, Yang Y, Zeng Y, He M. A microfluidic ExoSearch chip for multiplexed exosome detection towards blood-based ovarian cancer diagnosis. *Lab Chip*. 2016;16:489-96.
141. Rider MA, Hurwitz SN, Meckes DG, Jr. ExtraPEG: A Polyethylene Glycol-Based Method for Enrichment of Extracellular Vesicles. *Sci Rep*. 2016;6:23978.
142. Lee H, He X, Ni K, Carnino JM, Jin Y. Low concentration of polyethylene glycol facilitates separation of extracellular vesicles from bronchoalveolar lavage fluid. *Am J Physiol Lung Cell Mol Physiol*. 2021;320:L522-L529.
143. Xiang C, Cong S, Tan X, *et al*. A meta-analysis of the diagnostic utility of biomarkers in cerebrospinal fluid in Parkinson's disease. *NPJ Parkinsons Dis*. 2022;8:165.
144. Majbour NK, Vaikath NN, van Dijk KD, *et al*. Oligomeric and phosphorylated alpha-synuclein as potential CSF biomarkers for Parkinson's disease. *Mol Neurodegener*. 2016;11:7.
145. Katayama T, Sawada J, Takahashi K, Yahara O. Cerebrospinal Fluid Biomarkers in Parkinson's Disease: A Critical Overview of the Literature and Meta-Analyses. *Brain Sci*. 2020;10:466.
146. Henderson MX, Sengupta M, Trojanowski JQ, Lee VMY. Alzheimer's disease tau is a prominent pathology in LRRK2 Parkinson's disease. *Acta Neuropathol Commun*. 2019;7:183.
147. Morenas-Rodriguez E, Alcolea D, Suarez-Calvet M, *et al*. Different pattern of CSF glial markers between dementia with Lewy bodies and Alzheimer's disease. *Sci Rep*. 2019;9:7803.
148. Kou W, Li S, Yan R, Zhang J, Wan Z, Feng T. Cerebrospinal fluid and blood neurofilament light chain in Parkinson's disease and atypical parkinsonian syndromes: a systematic review and Bayesian network meta-analysis. *J Neurol*. 2025;272:311.
149. Magdalinou NK, Paterson RW, Schott JM, *et al*. A panel of nine cerebrospinal fluid biomarkers may identify patients with atypical parkinsonian syndromes. *J Neurol Neurosurg Psychiatry*. 2015;86:1240-7.
150. Concha-Marambio L, Pritzkow S, Shahnawaz M, Farris CM, Soto C. Seed amplification assay for the detection of pathologic alpha-synuclein aggregates in cerebrospinal fluid. *Nat Protoc*. 2023;18:1179-1196.
151. Fairfoul G, McGuire LI, Pal S, *et al*. Alpha-synuclein RT-QuIC in the CSF of patients with alpha-synucleinopathies. *Ann Clin Transl Neurol*. 2016;3:812-818.
152. Shahnawaz M, Tokuda T, Waragai M, *et al*. Development of a Biochemical Diagnosis of Parkinson Disease by Detection of alpha-Synuclein Misfolded Aggregates in Cerebrospinal Fluid. *JAMA Neurol*. 2017;74:163-172.
153. Orru CD, Ma TC, Hughson AG, *et al*. A rapid alpha-synuclein seed assay of Parkinson's disease CSF panel shows high diagnostic accuracy. *Ann Clin Transl Neurol*. 2021;8:374-384.
154. Russo MJ, Orru CD, Concha-Marambio L, *et al*. High diagnostic performance of independent alpha-synuclein seed amplification assays for detection of early Parkinson's disease. *Acta Neuropathol Commun*. 2021;9:179.
155. Siderowf A, Concha-Marambio L, Lafontant DE, *et al*. Assessment of heterogeneity among participants in the Parkinson's Progression Markers Initiative cohort using alpha-synuclein seed amplification: a cross-sectional study. *Lancet Neurol*. 2023;22:407-417.

156. Concha-Marambio L, Weber S, Farris CM, *et al*. Accurate Detection of alpha-Synuclein Seeds in Cerebrospinal Fluid from Isolated Rapid Eye Movement Sleep Behavior Disorder and Patients with Parkinson's Disease in the DeNovo Parkinson (DeNoPa) Cohort. *Mov Disord*. 2023;38:567-578.
157. Kalia LV, Lang AE, Hazrati LN, *et al*. Clinical correlations with Lewy body pathology in LRRK2-related Parkinson disease. *JAMA Neurol*. 2015;72:100-5.
158. Sekiya H, Franke L, Hashimoto Y, *et al*. Widespread distribution of alpha-synuclein oligomers in LRRK2-related Parkinson's disease. *Acta Neuropathol*. 2025;149:42.
159. Jensen NM, Vitic Z, Antorini MR, Viftrup TB, Parkkinen L, Jensen PH. Abundant non-inclusion alpha-synuclein pathology in Lewy body-negative LRRK2-mutant cases. *Acta Neuropathol*. 2025;149:41.
160. Zubelzu M, Morera-Herreras T, Irastorza G, Gomez-Esteban JC, Murueta-Goyena A. Plasma and serum alpha-synuclein as a biomarker in Parkinson's disease: A meta-analysis. *Parkinsonism Relat Disord*. 2022;99:107-115.
161. Wang X, Yu S, Li F, Feng T. Detection of alpha-synuclein oligomers in red blood cells as a potential biomarker of Parkinson's disease. *Neurosci Lett*. 2015;599:115-9.
162. El-Agnaf OM, Salem SA, Paleologou KE, *et al*. Detection of oligomeric forms of alpha-synuclein protein in human plasma as a potential biomarker for Parkinson's disease. *FASEB J*. 2006;20:419-25.
163. Foulds PG, Mitchell JD, Parker A, *et al*. Phosphorylated alpha-synuclein can be detected in blood plasma and is potentially a useful biomarker for Parkinson's disease. *FASEB J*. 2011;25:4127-37.
164. Hansson O, Janelidze S, Hall S, *et al*. Blood-based NfL: A biomarker for differential diagnosis of parkinsonian disorder. *Neurology*. 2017;88:930-937.
165. Oeckl P, Weydt P, Steinacker P, *et al*. Different neuroinflammatory profile in amyotrophic lateral sclerosis and frontotemporal dementia is linked to the clinical phase. *J Neurol Neurosurg Psychiatry*. 2019;90:4-10.
166. Pedersen CC, Ushakova A, Alves G, *et al*. Serum neurofilament light at diagnosis: a prognostic indicator for accelerated disease progression in Parkinson’s Disease. *NPJ Parkinsons Dis*. 2024;10:162.
167. Gu L, Zhang P, Gao R, Shu H, Wang P. Predictive value of serum neurofilament light chain for cognitive impairment in Parkinson's disease. *Front Aging Neurosci*. 2024;16:1465016.
168. Liu M, Cai Y, Pan J, *et al*. Serum neurofilament light chain as a diagnostic and prognostic biomarker in multiple system atrophy: a prospective cohort study. *J Neurol*. 2024;272:74.
169. Mollenhauer B, Dakna M, Kruse N, *et al*. Validation of Serum Neurofilament Light Chain as a Biomarker of Parkinson's Disease Progression. *Mov Disord*. 2020;35:1999-2008.
170. Tang Y, Han L, Li S, *et al*. Plasma GFAP in Parkinson's disease with cognitive impairment and its potential to predict conversion to dementia. *NPJ Parkinsons Dis*. 2023;9:23.
171. Guevremont D, Roy J, Cutfield NJ, Williams JM. MicroRNAs in Parkinson's disease: a systematic review and diagnostic accuracy meta-analysis. *Sci Rep*. 2023;13:16272.
172. Gibbons CH, Levine T, Adler C, *et al*. Skin Biopsy Detection of Phosphorylated alpha-Synuclein in Patients With Synucleinopathies. *JAMA*. 2024;331:1298-1306.
173. Gibbons CH, Freeman R, Bellaire B, Adler CH, Moore D, Levine T. Synuclein-One study: skin biopsy detection of phosphorylated alpha-synuclein for diagnosis of synucleinopathies. *Biomark Med*. 2022;16:499-509.
174. Wang Z, Becker K, Donadio V, *et al*. Skin alpha-Synuclein Aggregation Seeding Activity as a Novel Biomarker for Parkinson Disease. *JAMA Neurol*. 2020;78:1-11.

175. Iranzo A, Mammana A, Munoz-Lopetegi A, *et al*. Misfolded alpha-Synuclein Assessment in the Skin and CSF by RT-QuIC in Isolated REM Sleep Behavior Disorder. *Neurology*. 2023;100:e1944-e1954.
176. Chahine LM, Beach TG, Brumm MC, *et al*. In vivo distribution of alpha-synuclein in multiple tissues and biofluids in Parkinson disease. *Neurology*. 2020;95:e1267-e1284.
177. Lebouvier T, Neunlist M, Bruley des Varannes S, *et al*. Colonic biopsies to assess the neuropathology of Parkinson's disease and its relationship with symptoms. *PLoS One*. 2010;5:e12728.
178. Shannon KM, Keshavarzian A, Mutlu E, *et al*. Alpha-synuclein in colonic submucosa in early untreated Parkinson's disease. *Mov Disord*. 2012;27:709-15.
179. Pouclet H, Lebouvier T, Coron E, Des Varannes SB, Neunlist M, Derkinderen P. A comparison between colonic submucosa and mucosa to detect Lewy pathology in Parkinson's disease. *Neurogastroenterol Motil*. 2012;24:e202-5.
180. Shin C, Park SH, Yun JY, *et al*. Fundamental limit of alpha-synuclein pathology in gastrointestinal biopsy as a pathologic biomarker of Parkinson's disease: Comparison with surgical specimens. *Parkinsonism Relat Disord*. 2017;44:73-78.
181. Kuzkina A, Rossle J, Seger A, *et al*. Combining skin and olfactory alpha-synuclein seed amplification assays (SAA)-towards biomarker-driven phenotyping in synucleinopathies. *NPJ Parkinsons Dis*. 2023;9:79.
182. Manne S, Kondru N, Jin H, *et al*. alpha-Synuclein real-time quaking-induced conversion in the submandibular glands of Parkinson's disease patients. *Mov Disord*. 2020;35:268-278.
183. Kharel S, Ojha R, Bist A, Joshi SP, Rauniyar R, Yadav JK. Salivary alpha-synuclein as a potential fluid biomarker in Parkinson's disease: A systematic review and meta-analysis. *Aging Med (Milton)*. 2022;5:53-62.
184. Wang Z, Gilliland T, Kim HJ, *et al*. A minimally invasive biomarker for sensitive and accurate diagnosis of Parkinson's disease. *Acta Neuropathol Commun*. 2024;12:167.
185. Bai JH, Zheng YL, Yu YP. Urinary kynurenine as a biomarker for Parkinson's disease. *Neurol Sci*. 2021;42:697-703.
186. Kumari S, Kumaran SS, Goyal V, *et al*. Identification of potential urine biomarkers in idiopathic parkinson's disease using NMR. *Clin Chim Acta*. 2020;510:442-449.
187. Habibzadeh A, Ostovan VR, Keshavarzian O, *et al*. Volatile organic compounds analysis as promising biomarkers for Parkinson's disease diagnosis: A systematic review and meta-analysis. *Clin Neurol Neurosurg*. 2023;235:108022.
188. Norman M, Ter-Ovanesyan D, Trieu W, *et al*. L1CAM is not associated with extracellular vesicles in human cerebrospinal fluid or plasma. *Nat Methods*. 2021;18:631-634.
189. Yan S, Jiang C, Davis JJ, Tofaris GK. Methodological considerations in neuronal extracellular vesicle isolation for alpha-synuclein biomarkers. *Brain*. 2023;146:e95-e97.
190. Faure J, Lachenal G, Court M, *et al*. Exosomes are released by cultured cortical neurones. *Mol Cell Neurosci*. 2006;31:642-8.
191. Kapogiannis D, Mustapic M, Shardell MD, *et al*. Association of Extracellular Vesicle Biomarkers With Alzheimer Disease in the Baltimore Longitudinal Study of Aging. *JAMA Neurol*. 2019;76:1340-1351.
192. Eitan E, Thornton-Wells T, Elgart K, *et al*. Synaptic proteins in neuron-derived extracellular vesicles as biomarkers for Alzheimer's disease: novel methodology and clinical proof of concept. *Extracell Vesicles Circ Nucl Acids*. 2023;4:133-150.
193. You Y, Zhang Z, Sultana N, *et al*. ATP1A3 as a target for isolating neuron-specific extracellular vesicles from human brain and biofluids. *Sci Adv*. 2023;9:eadi3647.
194. Shi M, Liu C, Cook TJ, *et al*. Plasma exosomal alpha-synuclein is likely CNS-derived and increased in Parkinson's disease. *Acta Neuropathol*. 2014;128:639-650.

195. Xylaki M, Chopra A, Weber S, Bartl M, Outeiro TF, Mollenhauer B. Extracellular Vesicles for the Diagnosis of Parkinson's Disease: Systematic Review and Meta-Analysis. *Mov Disord*. 2023;38:1585-1597.
196. Stuendl A, Kraus T, Chatterjee M, *et al*. alpha-Synuclein in Plasma-Derived Extracellular Vesicles Is a Potential Biomarker of Parkinson's Disease. *Mov Disord*. 2021;36:2508-2518.
197. Sharma M, Burre J. alpha-Synuclein in synaptic function and dysfunction. *Trends Neurosci*. 2023;46:153-166.
198. Kluge A, Schaeffer E, Bunk J, *et al*. Detecting Misfolded alpha-Synuclein in Blood Years before the Diagnosis of Parkinson's Disease. *Mov Disord*. 2024;39:1289-1299.
199. Kluge A, Bunk J, Schaeffer E, *et al*. Detection of neuron-derived pathological alpha-synuclein in blood. *Brain*. 2022;145:3058-3071.
200. Bernhardt AM, Nemati M, Boros FA, *et al*. alpha-Synuclein Seed Amplification Assays from Blood-Based Extracellular Vesicles in Parkinson's Disease: An Evaluation of the Evidence. *Mov Disord*. 2024;39:1269-1271.
201. Rocha DAS, Santos LE, Da Fonseca PB, De Felice FG. Prospects and challenges in using neuronal extracellular vesicles in biomarker research. *Alzheimers Dement*. 2024;20:6632-6638.
202. Chan L, Chung CC, Chen JH, Yu RC, Hong CT. Cytokine Profile in Plasma Extracellular Vesicles of Parkinson's Disease and the Association with Cognitive Function. *Cells*. 2021;10:
203. Wang S, Kojima K, Mobley JA, West AB. Proteomic analysis of urinary extracellular vesicles reveal biomarkers for neurologic disease. *EBioMedicine*. 2019;45:351-361.
204. Fraser KB, Rawlins AB, Clark RG, *et al*. Ser(P)-1292 LRRK2 in urinary exosomes is elevated in idiopathic Parkinson's disease. *Mov Disord*. 2016;31:1543-1550.
205. Ho DH, Yi S, Seo H, Son I, Seol W. Increased DJ-1 in urine exosome of Korean males with Parkinson's disease. *Biomed Res Int*. 2014;2014:704678.
206. Shi M, Kovac A, Korff A, *et al*. CNS tau efflux via exosomes is likely increased in Parkinson's disease but not in Alzheimer's disease. *Alzheimers Dement*. 2016;12:1125-1131.
207. Gualerzi A, Picciolini S, Bedoni M, Guerini FR, Clerici M, Agliardi C. Extracellular Vesicles as Biomarkers for Parkinson's Disease: How Far from Clinical Translation? *Int J Mol Sci*. 2024;25:
208. Gui Y, Liu H, Zhang L, Lv W, Hu X. Altered microRNA profiles in cerebrospinal fluid exosome in Parkinson disease and Alzheimer disease. *Oncotarget*. 2015;6:37043-53.
209. Yao YF, Qu MW, Li GC, Zhang FB, Rui HC. Circulating exosomal miRNAs as diagnostic biomarkers in Parkinson's disease. *Eur Rev Med Pharmacol Sci*. 2018;22:5278-5283.
210. Dutta S, Hornung S, Kruayatidee A, *et al*. alpha-Synuclein in blood exosomes immunoprecipitated using neuronal and oligodendroglial markers distinguishes Parkinson's disease from multiple system atrophy. *Acta Neuropathol*. 2021;142:495-511.
211. Dutta S, Hornung S, Taha HB, *et al*. Development of a Novel Electrochemiluminescence ELISA for Quantification of alpha-Synuclein Phosphorylated at Ser(129) in Biological Samples. *ACS Chem Neurosci*. 2023;14:1238-1248.
212. Shami-Shah A, Norman M, Walt DR. Ultrasensitive Protein Detection Technologies for Extracellular Vesicle Measurements. *Mol Cell Proteomics*. 2023;22:100557.
213. Norman M, Shami-Shah A, D'Amaddio SC, *et al*. Toward Identification of Markers for Brain-Derived Extracellular Vesicles in Cerebrospinal Fluid: A Large-Scale, Unbiased Analysis Using Proximity Extension Assays. *J Extracell Vesicles*. 2025;14:e70052.

214. Ellegaard Nielsen J, Sofie Pedersen K, Vestergard K, *et al*. Novel Blood-Derived Extracellular Vesicle-Based Biomarkers in Alzheimer's Disease Identified by Proximity Extension Assay. *Biomedicines*. 2020;8:
215. Rissin DM, Kan CW, Campbell TG, *et al*. Single-molecule enzyme-linked immunosorbent assay detects serum proteins at subfemtomolar concentrations. *Nat Biotechnol*. 2010;28:595-9.
216. Cohen L, Walt DR. Highly Sensitive and Multiplexed Protein Measurements. *Chem Rev*. 2019;119:293-321.
217. Boken D, Xia Z, Lam JYL, *et al*. Ultrasensitive Protein Aggregate Quantification Assays for Neurodegenerative Diseases on the Simoa Platform. *Anal Chem*. 2025;97:290-299.
218. Gilboa T, Ter-Ovanesyan D, Wang SC, *et al*. Measurement of alpha-synuclein as protein cargo in plasma extracellular vesicles. *Proc Natl Acad Sci U S A*. 2024;121:e2408949121.
219. Guix FX, Corbett GT, Cha DJ, *et al*. Detection of Aggregation-Competent Tau in Neuron-Derived Extracellular Vesicles. *Int J Mol Sci*. 2018;19:
220. Liu C, Xu X, Li B, *et al*. Single-Exosome-Counting Immunoassays for Cancer Diagnostics. *Nano Lett*. 2018;18:4226-4232.
221. Yang Z, Atiyas Y, Shen H, *et al*. Ultrasensitive Single Extracellular Vesicle Detection Using High Throughput Droplet Digital Enzyme-Linked Immunosorbent Assay. *Nano Lett*. 2022;22:4315-4324.
222. Ko J, Wang Y, Carlson JCT, *et al*. Single Extracellular Vesicle Protein Analysis Using Immuno-Droplet Digital Polymerase Chain Reaction Amplification. *Adv Biosyst*. 2020;4:e1900307.
223. Ko J, Wang Y, Sheng K, Weitz DA, Weissleder R. Sequencing-Based Protein Analysis of Single Extracellular Vesicles. *ACS Nano*. 2021;15:5631-5638.
224. Chen C, Zong S, Liu Y, *et al*. Profiling of Exosomal Biomarkers for Accurate Cancer Identification: Combining DNA-PAINT with Machine- Learning-Based Classification. *Small*. 2019;15:e1901014.
225. Salmond N, Khanna K, Owen GR, Williams KC. Nanoscale flow cytometry for immunophenotyping and quantitating extracellular vesicles in blood plasma. *Nanoscale*. 2021;13:2012-2025.
226. Dayarathna T, Roseborough AD, Gomes J, *et al*. Nanoscale flow cytometry-based quantification of blood-based extracellular vesicle biomarkers distinguishes MCI and Alzheimer's disease. *Alzheimers Dement*. 2024;20:6094-6106.
227. Janzen A, Vadasz D, Booij J, *et al*. Progressive Olfactory Impairment and Cardiac Sympathetic Denervation in REM Sleep Behavior Disorder. *J Parkinsons Dis*. 2022;12:1921-1935.
228. Fu Y, Jiang C, Tofaris GK, Davis JJ. Facile Impedimetric Analysis of Neuronal Exosome Markers in Parkinson's Disease Diagnostics. *Anal Chem*. 2020;92:13647-13651.
229. Graef JD, Hoque N, Polson C, *et al*. Characterization of pathology-inducing α-synuclein species from human diseased brain tissue. *bioRxiv*. 2019;588335.
230. Youssef P, Kim WS, Halliday GM, Lewis SJG, Dzamko N. Comparison of Different Platform Immunoassays for the Measurement of Plasma Alpha-Synuclein in Parkinson's Disease Patients. *J Parkinsons Dis*. 2021;11:1761-1772.
231. Barbour R, Kling K, Anderson JP, *et al*. Red blood cells are the major source of alpha-synuclein in blood. *Neurodegener Dis*. 2008;5:55-9.
232. Gomes DE, Witwer KW. L1CAM-associated extracellular vesicles: A systematic review of nomenclature, sources, separation, and characterization. *J Extracell Biol*. 2022;1:e35.

233. Cerri S, Ghezzi C, Sampieri M, *et al*. The Exosomal/Total alpha-Synuclein Ratio in Plasma Is Associated With Glucocerebrosidase Activity and Correlates With Measures of Disease Severity in PD Patients. *Front Cell Neurosci*. 2018;12:125.
234. Niu M, Li Y, Li G, *et al*. A longitudinal study on alpha-synuclein in plasma neuronal exosomes as a biomarker for Parkinson's disease development and progression. *Eur J Neurol*. 2020;27:967-974.
235. Zhao ZH, Chen ZT, Zhou RL, Zhang X, Ye QY, Wang YZ. Increased DJ-1 and alpha-Synuclein in Plasma Neural-Derived Exosomes as Potential Markers for Parkinson's Disease. *Front Aging Neurosci*. 2018;10:438.
236. Mustapic M, Eitan E, Werner JK, Jr., *et al*. Plasma Extracellular Vesicles Enriched for Neuronal Origin: A Potential Window into Brain Pathologic Processes. *Front Neurosci*. 2017;11:278.
237. Blommer J, Pitcher T, Mustapic M, *et al*. Extracellular vesicle biomarkers for cognitive impairment in Parkinson's disease. *Brain*. 2023;146:195-208.
238. Danzer KM, Kranich LR, Ruf WP, *et al*. Exosomal cell-to-cell transmission of alpha synuclein oligomers. *Mol Neurodegener*. 2012;7:42.
239. Lee HJ, Suk JE, Patrick C, *et al*. Direct transfer of alpha-synuclein from neuron to astroglia causes inflammatory responses in synucleinopathies. *J Biol Chem*. 2010;285:9262-72.
240. Stoyanova, II, Lutz D. Functional Diversity of Neuronal Cell Adhesion and Recognition Molecule L1CAM through Proteolytic Cleavage. *Cells*. 2022;11:
241. Si X, Tian J, Chen Y, Yan Y, Pu J, Zhang B. Central Nervous System-Derived Exosomal Alpha-Synuclein in Serum May Be a Biomarker in Parkinson's Disease. *Neuroscience*. 2019;413:308-316.
242. Chung CC, Chan L, Chen JH, Hung YC, Hong CT. Plasma Extracellular Vesicle alpha-Synuclein Level in Patients with Parkinson's Disease. *Biomolecules*. 2021;11:
243. Jiang C, Fu Y, Liu G, Shu B, Davis J, Tofaris GK. Multiplexed Profiling of Extracellular Vesicles for Biomarker Development. *Nanomicro Lett*. 2021;14:3.
244. Yan YQ, Pu JL, Zheng R, *et al*. Different patterns of exosomal alpha-synuclein between Parkinson's disease and probable rapid eye movement sleep behavior disorder. *Eur J Neurol*. 2022;29:3590-3599.
245. Hong Z, Shi M, Chung KA, *et al*. DJ-1 and alpha-synuclein in human cerebrospinal fluid as biomarkers of Parkinson's disease. *Brain*. 2010;133:713-26.
246. Mollenhauer B, Caspell-Garcia CJ, Coffey CS, *et al*. Longitudinal analyses of cerebrospinal fluid alpha-Synuclein in prodromal and early Parkinson's disease. *Mov Disord*. 2019;34:1354-1364.
247. Liu Y, Lawton MA, Lo C, *et al*. Longitudinal Changes in Parkinson's Disease Symptoms with and Without Rapid Eye Movement Sleep Behavior Disorder: The Oxford Discovery Cohort Study. *Mov Disord*. 2021;36:2821-2832.
248. Barber TR, Lawton M, Rolinski M, *et al*. Prodromal Parkinsonism and Neurodegenerative Risk Stratification in REM Sleep Behavior Disorder. *Sleep*. 2017;40:
249. Janzen A, Kogan RV, Meles SK, *et al*. Rapid Eye Movement Sleep Behavior Disorder: Abnormal Cardiac Image and Progressive Abnormal Metabolic Brain Pattern. *Mov Disord*. 2022;37:624-629.
250. Seger A, Ophey A, Heitzmann W, *et al*. Evaluation of a Structured Screening Assessment to Detect Isolated Rapid Eye Movement Sleep Behavior Disorder. *Mov Disord*. 2023;38:990-999.
251. Rana HQ, Balwani M, Bier L, Alcalay RN. Age-specific Parkinson disease risk in GBA mutation carriers: information for genetic counseling. *Genet Med*. 2013;15:146-9.

252. Iranzo A, Santamaria J, Valldeoriola F, *et al*. Dopamine transporter imaging deficit predicts early transition to synucleinopathy in idiopathic rapid eye movement sleep behavior disorder. *Ann Neurol*. 2017;82:419-428.
253. Arnaldi D, Chincarini A, Hu MT, *et al*. Dopaminergic imaging and clinical predictors for phenoconversion of REM sleep behaviour disorder. *Brain*. 2021;144:278-287.
254. Kmiecik MJ, Micheletti S, Coker D, *et al*. Genetic analysis and natural history of Parkinson's disease due to the LRRK2 G2019S variant. *Brain*. 2024;147:1996-2008.
255. Attems J, Toledo JB, Walker L, *et al*. Neuropathological consensus criteria for the evaluation of Lewy pathology in post-mortem brains: a multi-centre study. *Acta Neuropathol*. 2021;141:159-172.
256. Wang Q, Liu Y, Zhou J. Neuroinflammation in Parkinson's disease and its potential as therapeutic target. *Translational neurodegeneration*. 2015;4:1-9.
257. Okuzumi A, Hatano T, Matsumoto G, *et al*. Propagative alpha-synuclein seeds as serum biomarkers for synucleinopathies. *Nat Med*. 2023;29:1448-1455.
258. Alvarez-Erviti L, Seow Y, Schapira AH, *et al*. Lysosomal dysfunction increases exosome-mediated alpha-synuclein release and transmission. *Neurobiol Dis*. 2011;42:360-7.
259. Dutta S, Hornung S, Taha HB, Bitan G. Biomarkers for parkinsonian disorders in CNS-originating EVs: promise and challenges. *Acta Neuropathol*. 2023;145:515-540.
260. Tofaris GK. A Critical Assessment of Exosomes in the Pathogenesis and Stratification of Parkinson's Disease. *J Parkinsons Dis*. 2017;7:569-576.
261. Zheng H, Xie Z, Zhang X, *et al*. Investigation of alpha-Synuclein Species in Plasma Exosomes and the Oligomeric and Phosphorylated alpha-Synuclein as Potential Peripheral Biomarker of Parkinson's Disease. *Neuroscience*. 2021;469:79-90.
262. Tanudjojo B, Shaikh SS, Fenyi A, *et al*. Phenotypic manifestation of alpha-synuclein strains derived from Parkinson's disease and multiple system atrophy in human dopaminergic neurons. *Nat Commun*. 2021;12:3817.
263. Jonikas M, Madill M, Mathy A, *et al*. Stem cell modeling of mitochondrial parkinsonism reveals key functions of OPA1. *Ann Neurol*. 2018;83:915-925.
264. Heman-Ackah SM, Manzano R, Hoozemans JJM, *et al*. Alpha-synuclein induces the unfolded protein response in Parkinson's disease SNCA triplication iPSC-derived neurons. *Hum Mol Genet*. 2017;26:4441-4450.
265. Ramalingam N, Dettmer U. Temperature is a key determinant of alpha- and beta-synuclein membrane interactions in neurons. *J Biol Chem*. 2021;296:100271.
266. Tofaris GK. Initiation and progression of alpha-synuclein pathology in Parkinson's disease. *Cell Mol Life Sci*. 2022;79:210.
267. Kumar ST, Jagannath S, Francois C, Vanderstichele H, Stoops E, Lashuel HA. How specific are the conformation-specific alpha-synuclein antibodies? Characterization and validation of 16 alpha-synuclein conformation-specific antibodies using well-characterized preparations of alpha-synuclein monomers, fibrils and oligomers with distinct structures and morphology. *Neurobiol Dis*. 2020;146:105086.
268. Jakes R, Crowther RA, Lee VM, Trojanowski JQ, Iwatsubo T, Goedert M. Epitope mapping of LB509, a monoclonal antibody directed against human alpha-synuclein. *Neurosci Lett*. 1999;269:13-6.
269. Choi W, Zibaee S, Jakes R, *et al*. Mutation E46K increases phospholipid binding and assembly into filaments of human alpha-synuclein. *FEBS Lett*. 2004;576:363-8.
270. Fares MB, Ait-Bouziad N, Dikiy I, *et al*. The novel Parkinson's disease linked mutation G51D attenuates in vitro aggregation and membrane binding of alpha-synuclein, and enhances its secretion and nuclear localization in cells. *Hum Mol Genet*. 2014;23:4491-509.

271. Jensen PH, Nielsen MS, Jakes R, Dotti CG, Goedert M. Binding of alpha-synuclein to brain vesicles is abolished by familial Parkinson's disease mutation. *J Biol Chem*. 1998;273:26292-4.
272. Tripathi A, Alnakhala H, Terry-Kantor E, *et al*. Pathogenic Mechanisms of Cytosolic and Membrane-Enriched alpha-Synuclein Converge on Fatty Acid Homeostasis. *J Neurosci*. 2022;42:2116-2130.
273. Zhu L, Wang K, Cui J, *et al*. Label-free quantitative detection of tumor-derived exosomes through surface plasmon resonance imaging. *Anal Chem*. 2014;86:8857-64.
274. Li B, Pan W, Liu C, *et al*. Homogenous Magneto-Fluorescent Nanosensor for Tumor-Derived Exosome Isolation and Analysis. *ACS Sens*. 2020;5:2052-2060.
275. Cohen L, Cui N, Cai Y, *et al*. Single Molecule Protein Detection with Attomolar Sensitivity Using Droplet Digital Enzyme-Linked Immunosorbent Assay. *ACS Nano*. 2020;14:9491-9501.
276. Burre J, Sharma M, Sudhof TC. alpha-Synuclein assembles into higher-order multimers upon membrane binding to promote SNARE complex formation. *Proc Natl Acad Sci U S A*. 2014;111:E4274-83.
277. Dettmer U, Ramalingam N, von Saucken VE, *et al*. Loss of native alpha-synuclein multimerization by strategically mutating its amphipathic helix causes abnormal vesicle interactions in neuronal cells. *Hum Mol Genet*. 2017;26:3466-3481.
278. Comellas G, Lemkau LR, Zhou DH, George JM, Rienstra CM. Structural intermediates during alpha-synuclein fibrillogenesis on phospholipid vesicles. *J Am Chem Soc*. 2012;134:5090-9.
279. Lee HJ, Choi C, Lee SJ. Membrane-bound alpha-synuclein has a high aggregation propensity and the ability to seed the aggregation of the cytosolic form. *J Biol Chem*. 2002;277:671-8.
280. Galvagnion C, Brown JW, Ouberai MM, *et al*. Chemical properties of lipids strongly affect the kinetics of the membrane-induced aggregation of alpha-synuclein. *Proc Natl Acad Sci U S A*. 2016;113:7065-70.
281. Wolf M, Poupardin RW, Ebner-Peking P, *et al*. A functional corona around extracellular vesicles enhances angiogenesis, skin regeneration and immunomodulation. *J Extracell Vesicles*. 2022;11:e12207.
282. Yelleswarapu V, Buser JR, Haber M, Baron J, Inapuri E, Issadore D. Mobile platform for rapid sub-picogram-per-milliliter, multiplexed, digital droplet detection of proteins. *Proc Natl Acad Sci U S A*. 2019;116:4489-4495.
283. Zhao L, Wang H, Fu J, *et al*. Microfluidic-based exosome isolation and highly sensitive aptamer exosome membrane protein detection for lung cancer diagnosis. *Biosens Bioelectron*. 2022;214:114487.
284. Liang LG, Kong MQ, Zhou S, *et al*. An integrated double-filtration microfluidic device for isolation, enrichment and quantification of urinary extracellular vesicles for detection of bladder cancer. *Sci Rep*. 2017;7:46224.
285. Jin D, Yang F, Zhang Y, *et al*. ExoAPP: Exosome-Oriented, Aptamer Nanoprobe-Enabled Surface Proteins Profiling and Detection. *Anal Chem*. 2018;90:14402-14411.
286. Lim CZJ, Zhang Y, Chen Y, *et al*. Subtyping of circulating exosome-bound amyloid beta reflects brain plaque deposition. *Nat Commun*. 2019;10:1144.
287. Yang Q, Cheng L, Hu L, *et al*. An integrative microfluidic device for isolation and ultrasensitive detection of lung cancer-specific exosomes from patient urine. *Biosens Bioelectron*. 2020;163:112290.
288. Lu Y, Ye L, Jian X, *et al*. Integrated microfluidic system for isolating exosome and analyzing protein marker PD-L1. *Biosens Bioelectron*. 2022;204:113879.

289. Chen YS, Chen CC, Lai CPK, Lee GB. Isolation and digital counting of extracellular vesicles from blood via membrane-integrated microfluidics. *Sensor Actuat B-Chem*. 2022;358:131473.
290. Zhou J, Wu Z, Hu J, *et al*. High-throughput single-EV liquid biopsy: Rapid, simultaneous, and multiplexed detection of nucleic acids, proteins, and their combinations. *Sci Adv*. 2020;6:
291. Zhou SS, Hu T, Han GH, *et al*. Accurate Cancer Diagnosis and Stage Monitoring Enabled by Comprehensive Profiling of Different Types of Exosomal Biomarkers: Surface Proteins and miRNAs. *Small*. 2020;16:2004492.
292. Yan S, Zhang W, Li X, *et al*. Single extracellular vesicle detection assay identifies membrane-associated alpha-synuclein as an early-stage biomarker in Parkinson's disease. *Cell Rep Med*. 2025;6:101999.
293. De Pablo-Fernandez E, Lees AJ, Holton JL, Warner TT. Prognosis and Neuropathologic Correlation of Clinical Subtypes of Parkinson Disease. *JAMA Neurol*. 2019;76:470-479.
294. Colloby SJ, McAleese KE, Walker L, *et al*. Patterns of tau, amyloid and synuclein pathology in ageing, Alzheimer's disease and synucleinopathies. *Brain*. 2025;148:1562-1576.
295. Hall S, Janelidze S, Londos E, *et al*. Plasma Phospho-Tau Identifies Alzheimer's Co-Pathology in Patients with Lewy Body Disease. *Mov Disord*. 2021;36:767-771.
296. Delva A, Pelletier A, Somerville E, *et al*. Plasma pTau181 and amyloid markers predict conversion to dementia in idiopathic REM sleep behaviour disorder. *Brain*. 2025;
297. Ashton NJ, Brum WS, Di Molfetta G, *et al*. Diagnostic Accuracy of a Plasma Phosphorylated Tau 217 Immunoassay for Alzheimer Disease Pathology. *JAMA Neurol*. 2024;81:255-263.
298. Mattsson-Carlgren N, Janelidze S, Palmqvist S, *et al*. Longitudinal plasma p-tau217 is increased in early stages of Alzheimer's disease. *Brain*. 2020;143:3234-3241.
299. Janelidze S, Bali D, Ashton NJ, *et al*. Head-to-head comparison of 10 plasma phospho-tau assays in prodromal Alzheimer's disease. *Brain*. 2023;146:1592-1601.
300. Bridel C, van Wieringen WN, Zetterberg H, *et al*. Diagnostic Value of Cerebrospinal Fluid Neurofilament Light Protein in Neurology: A Systematic Review and Meta-analysis. *JAMA Neurol*. 2019;76:1035-1048.
301. Preische O, Schultz SA, Apel A, *et al*. Serum neurofilament dynamics predicts neurodegeneration and clinical progression in presymptomatic Alzheimer's disease. *Nat Med*. 2019;25:277-283.
302. Ye R, Locascio JJ, Goodheart AE, Quan M, Zhang B, Gomperts SN. Serum NFL levels predict progression of motor impairment and reduction in putamen dopamine transporter binding ratios in de novo Parkinson's disease: An 8-year longitudinal study. *Parkinsonism Relat Disord*. 2021;85:11-16.
303. Singer W, Schmeichel AM, Shahnawaz M, *et al*. Alpha-Synuclein Oligomers and Neurofilament Light Chain in Spinal Fluid Differentiate Multiple System Atrophy from Lewy Body Synucleinopathies. *Ann Neurol*. 2020;88:503-512.
304. Ashton NJ, Janelidze S, Al Khleifat A, *et al*. A multicentre validation study of the diagnostic value of plasma neurofilament light. *Nat Commun*. 2021;12:3400.
305. Sampedro F, Perez-Gonzalez R, Martinez-Horta S, Marin-Lahoz J, Pagonabarraga J, Kulisevsky J. Serum neurofilament light chain levels reflect cortical neurodegeneration in de novo Parkinson's disease. *Parkinsonism Relat Disord*. 2020;74:43-49.
306. Zhang X, Ma L, Liang D, *et al*. Neurofilament Light Protein Predicts Disease Progression in Idiopathic REM Sleep Behavior Disorder. *J Parkinsons Dis*. 2023;13:485-499.

307. Mattsson-Carlgren N, Salvadó G, Ashton NJ, *et al*. Prediction of longitudinal cognitive decline in preclinical Alzheimer disease using plasma biomarkers. *JAMA Neurol*. 2023;80:360-369.
308. Coughlin DG, Hurtig HI, Irwin DJ. Pathological Influences on Clinical Heterogeneity in Lewy Body Diseases. *Mov Disord*. 2020;35:5-19.
309. Kramer ML, Schulz-Schaeffer WJ. Presynaptic alpha-synuclein aggregates, not Lewy bodies, cause neurodegeneration in dementia with Lewy bodies. *J Neurosci*. 2007;27:1405-10.
310. Maya G, Iranzo A, Gaig C, *et al*. Post-mortem neuropathology of idiopathic rapid eye movement sleep behaviour disorder: a case series. *Lancet Neurol*. 2024;23:1238-1251.
311. Hannaway N, Zarkali A, Bhome R, *et al*. Neuroimaging and plasma biomarker differences and commonalities in Lewy body dementia subtypes. *Alzheimers Dement*. 2025;21:e70274.
312. Lucey BP, McCullough A, Landsness EC, *et al*. Reduced non-rapid eye movement sleep is associated with tau pathology in early Alzheimer's disease. *Sci Transl Med*. 2019;11:
313. Pagano G, Taylor KI, Anzures-Cabrera J, *et al*. Trial of Prasinezumab in Early-Stage Parkinson's Disease. *N Engl J Med*. 2022;387:421-432.
314. Nieuwland R, Siljander PR. A beginner's guide to study extracellular vesicles in human blood plasma and serum. *J Extracell Vesicles*. 2024;13:e12400.

Appendix

9. Appendix

9.1 Manuscripts accepted for publication

Yan S, Zhang W, Li X, et al. Single extracellular vesicle detection assay identifies membrane-associated α-synuclein as an early-stage biomarker in Parkinson's disease. *Cell Reports Medicine*. 2025, 6(3):101999. doi:10.1016/j.xcrm.2025.101999

Yan S, Jiang C, Janzen A, et al. Neuronally derived extracellular vesicle α-synuclein as a serum biomarker for individuals at risk of developing Parkinson disease. *JAMA Neurol.* 2024;81(1):59-68. doi:10.1001/jamaneurol.2023.4398

Zhou Y, **Yan S**, Dong W, et al. Biosensing strategies for amyloid-like protein aggregates. *BMEMat*. 2024;2(1):e12053. doi:10.1002/bmm2.12053

Yan S, Jiang C, Davis JJ, Tofaris GK. Methodological considerations in neuronal extracellular vesicle isolation for α-synuclein biomarkers. *Brain*. 2023;146(11):e95-e97. doi:10.1093/brain/awad169

Sharafeldin M, **Yan S**, Jiang C, Tofaris GK, Davis JJ. Alternating Magnetic Field-Promoted Nanoparticle Mixing: The On-Chip Immunocapture of Serum Neuronal Exosomes for Parkinson's Disease Diagnostics. Anal Chem. 2023;95(20):7906-7913. doi:10.1021/acs.analchem.3c00357

9.2 Attended conferences

April 2025

Synuclein 2025 Conference, Cambridge, UK. Oral presentation: Single Extracellular Vesicle Detection Assay Identifies Membrane-Associated α-Synuclein as an Early-stage Biomarker in Parkinson's Disease.

March 2024

Oxford Neuroscience Symposium, Oxford, UK. Oral Presentation: Neuronally-Derived Extracellular Vesicle α-Synuclein as a Serum Biomarker for Individuals at Risk of Developing Parkinson's Disease.

January 2024

ARUK Thames Valley Network ECR Day, Oxford, UK. Oral Presentation: Neuronally-Derived Extracellular Vesicle α-Synuclein as a Serum Biomarker for Individuals at Risk of Developing Parkinson's Disease (**Best Scientific Talk**).

November 2023

Kavli INsD Scientific Advisory Board Meeting, Oxford, UK. Poster Presentation: α-Synuclein in Serum L1CAM-Positive Extracellular Vesicles as a Predictive Biomarker for Parkinson's Disease Pathology.

November 2023

Oxosome annual meeting (The Oxford Extracellular Vesicle Group), Oxford, UK. Oral presentation: Neuronally-Derived Extracellular Vesicle α-Synuclein as a Serum Biomarker for Individuals at Risk of Developing Parkinson's Disease.

June 2023

NDCN Thomas Willis Day, Oxford, UK. Poster presentation: α-Synuclein in Serum L1CAM-Positive Extracellular Vesicles as a Predictive Biomarker for Parkinson's Disease Pathology.

March 2023

Oxford Neuroscience Symposium, Oxford, UK. Poster presentation: α-Synuclein in Serum L1CAM-Positive Extracellular Vesicles as a Predictive Biomarker for Parkinson's Disease Pathology.

November 2022

Oxford Parkinson's Disease Research Day, Oxford, UK. Poster presentation: α-Synuclein in Serum L1CAM-Positive Extracellular Vesicles as a Predictive Biomarker for Parkinson's Disease Pathology (**Best Poster Award**).